PROGRESS IN RESEARCH

April 1, 2009 - March 31, 2010

CYCLOTRON INSTITUTE

Texas A&M University

College Station, Texas

PROGRESS IN RESEARCH

APRIL 1, 2009- MARCH 31, 2010

Prepared By

The Cyclotron Institute Staff

Texas A&M University

College Station, TX 77843-3366

Phone: (979) 845-1411
Fax: (979) 845-1899

Web: http://cyclotron.tamu.edu

June 2010

TABLE OF CONTENTS

SECTION II: HEAVY ION REACTIONS

SECTION III: NUCLEAR THEORY

SECTION IV: ATOMIC, MOLECULAR AND MATERIALS SCIENCE

SECTION V: SUPERCONDUCTING CYCLOTRON, INSTRUMENTATION AND RIB UPGRADE

SECTION VI: PUBLICATIONS

SECTION VII: APPENDIX

Introduction
April 1, 2009 – March 31, 2010

Progress in research and operations at the Texas A&M Cyclotron Institute is summarized in this report for the period April, 1, 2009 through March 31, 2010. The format follows that of previous years. Sections I through IV contain reports from individual research projects. Operation and technical developments are given in Section V. Section VI lists the publications with Cyclotron Institute authors and the Appendix gives additional information including talks presented by members of the Institute during the past year. Once again, the full volume of this year's Progress in Research is available only on our web site (http://cyclotron.tamu.edu). *Since most of the contributions presented here are truly reports on progress in research, results and conclusions should not be quoted from the report without the consent of the authors.*

We have now completed 5 1/2 years of the Upgrade Project which ultimately will give us accelerated radioactive beams at intermediate energies. The progress on the project continues to be good. The K150 cyclotron is operational for both positive-ion and negative-ion beams. As of mid June, the new radiation monitoring system has been installed and is waiting on a short schedule break to be implemented. We expect to have limited operation of the machine to experiments before the end of the summer.

During the past year, two decisions made by the TAMU administration will impact the Cyclotron Institute in the near future. A request to develop a new multi-disciplinary research effort involving basic and applied nuclear science and nuclear non-proliferation policy issues was approved. A new institute—the Nuclear Solutions Institute—will be established as an umbrella institute to coordinate the activities of several departments and institutes that will form this program. The Cyclotron Institute will be one of the principle components of the NSI. In September, 2009, TAMU approved our plan to add a second floor of offices onto the existing building. In June, an architect firm will be awarded the contract to develop a final design for the addition. Construction should begin before the end of the current calendar year.

As in previous reports, I have pulled out some highlights of work over the past year. Those that are noteworthy are given below.

Research highlights:
 (1) A review article on the evaluation of V_{ud} and its impact on the unitarity of the Cabibbo-Kobayashi-Maskawa (CKM) quark-mixing matrix was published this past year. The value for V_{ud} can be obtained from four different classes of beta-decay measurement: superallowed $0^+ \rightarrow 0^+$ nuclear transitions, neutron decay, mirror nuclear transitions and pion decay. All four results are consistent with one another, but the nuclear superallowed value has an uncertainty that is at least a factor of six smaller than the others, and it thus dominates the average. Currently V_{ud} is the most precisely known element of the CKM matrix (by a factor of nearly 20). The sum of squares of the top row elements of the CKM matrix now equals 0.9999(6), confirming the matrix's unitarity to unprecedented precision.

(2) A new proton resonance has been found for ^{22}Na+p by measuring the beta-delayed proton decay of ^{23}Al. The new resonance is the lowest energy one observed and it dominates the reaction rate for ^{22}Na(p,γ)^{23}Mg.

(3) A unified description of heavy-quarkonium spectral functions and heavy-quark transport properties in the quark-gluon plasma (QGP) has been established using a thermodynamic T-matrix approach based on model independent input potentials including relativistic corrections, paving the way for quantitative analysis of the QGP as produce in high-energy heavy-ion collisions.

(4) Recent work at TAMU has demonstrated that a quantum statistical model of nuclear matter that includes formation of clusters at densities below nuclear saturation describes quite well the low-density symmetry energy, which was extracted from the analysis of heavy-ion collisions. Within such a theoretical approach the composition and the thermodynamic quantities of nuclear matter can be modeled in a large region of densities, temperatures, and asymmetries that are required in models such as supernova simulations.

(5) The beta asymmetry parameter measurement using ultra-cold neutrons has been improved, using data obtained by the UCNA collaboration in 2008 and 2009, to 1.3% of its value. The result is in good agreement with the most recent result for the asymmetry parameter.

(6) The heavy element group completed its characterization of the MARS velocity filter for low-velocity ions using a ^{241}Am source. With this information, the excitation function of the ^{40}Ar + ^{165}Ho reaction for the production of At isotopes was determined.

(7) The transverse collective flow of isotopically identified particles was observed to depend on both the neutron concentration of the particle of interest as well as the reacting system. The first experimental evidence isolating the dependence of the transverse flow on the charge of the system, and thus the Coulomb force, was found. In comparison to theory, the data favors a stiff form of the symmetry energy.

(8) Using an empirically constrained isospin- and momentum-dependent nuclear interaction, a better understanding of the properties of neutron stars, such as the relation between their masses and radii as well as the transition density and pressure at the boundary between their inner crust and liquid core, has been obtained.

(9) Two Institute theorists (Fries and Ko) are founding members and co-PI's of the newly established JET collaboration. The multi-institutional 'Collaboration on Jet and Electromagnetic Tomography of Extreme Phases of Matter in Heavy-Ion Collisions' will systematically study various probes of the quark-gluon plasma and hot hadronic matter. The JET collaboration is one of the topical collaborations being supported by DOE.

(10) The theory of reactions leading to resonance excitation in the Trojan Horse Method (THM) has been completed and is now the main tool for analysis of important astrophysical processes that are studied by the THM.

(11) The STAR collaboration has observed charge-dependent azimuthal correlations in ultra-relativistic Au+Au and Cu+Cu collisions that may arise from local strong parity violation.

(12) By including the effect of the medium on the binding energies of light clusters, the symmetry energy of low-density nuclear matter at low temperature is significantly larger than that obtained from the commonly used mean-field approximation.

As in the past, Institute scientists remain active in a number of collaborative research efforts around the world. Major programs include: a measurement of Michel parameters in normal μ^+ decay at TRIUMF in Vancouver, B.C.; mass measurements using the Penning Traps at Argonne National Laboratory and the University of Jyväskylä; continued work with the STAR collaboration at RHIC; and the measurement of neutron beta decay with the UCNA collaboration.

Once again, I am indebted to Dr. Y.-W. Lui for assembling this report.

R.E. Tribble
June 18, 2010

SECTION I

NUCLEAR STRUCTURE, FUNDAMENTAL INTERACTIONS, AND ASTROPHYSICS

Superallowed beta decay

J. C. Hardy, I. S. Towner, V. E. Iacob, N. Nica, L. Chen, V. Horvat, H. I. Park,
J. Goodwin, L. Trache, and R. E. Tribble

Superallowed $0^+ \rightarrow 0^+$ beta decay between T=1 analogue states has been a subject of continuous and often intense study for five decades. The *ft* values of such transitions are nearly independent of nuclear-structure ambiguities and depend uniquely on the vector part of the weak interaction. Their measurement gives us access to clean tests of some of the fundamental precepts of weak-interaction theory, and, over the years, this strong motivation has led to very high precision being achieved in both the experiments and the theory used to interpret them. We have a major program at the Cyclotron Institute to study superallowed beta decay.

To obtain the *ft* value for any transition, three quantities must be measured: the half life of the parent, the Q_{EC} value for the transition of interest and the branching ratio for that transition. This year, our complete new survey of existing data on these superallowed decays was published [1]. It replaced our previous one [2], which was already out of date. Although the latter was published as recently as 2005, there had been an avalanche of new measurements – some from our group and some from a variety of other groups worldwide – that had been published in the intervening time.

As in all our surveys, the new one provides a critical evaluation of all the experimental data and obtains final *ft* values from the averaged results, to which improved radiative and isospin-symmetry-breaking corrections [3] have been applied in order to derive a final set of "corrected ft values", denoted F*t*. One of the new features added this time was that we calculated the radial-overlap correction, δ_{C2}, with Hartree-Fock radial wave functions as well as the Saxon-Woods wave functions we have used before. The differences in the results from these two methods are used as a measure of the systematic uncertainty to be applied to the theoretical corrections. These differences also offer the possibility that measured *ft* values with the highest precision could actually distinguish between the two methods and thereby reduce the systematic uncertainty.

With the updated world data and improved corrections the F*t* values are completely consistent with one another, thus demonstrating the constancy of G_V to 1.3 parts in 10^4. Not only is this an important confirmation of the Conserved Vector Current (CVC) hypothesis but it sets the stage for using the average value of G_V to test a fundamental principle of the electroweak standard model: the unitarity of the Cabibbo-Kobayashi-Maskawa (CKM) matrix. The up-down quark mixing element of that matrix, V_{ud}, is given by $V_{ud} = G_V / G_F$, where G_F is the weak interaction constant for the purely leptonic muon decay. The value of V_{ud} is a key component of the most demanding test available for the unitarity of the CKM matrix, the sum of squares of its top-row elements [1]. As elaborated in our recent review article on the evaluation of V_{ud} [4], superallowed nuclear beta decays provide by far the most precise and reliable value for V_{ud} and, in fact, that element is also the most precisely known one in the CKM matrix – by an order of magnitude! Its current value [1,4] is 0.97425(22), a result that yields a CKM unitarity sum

of 0.99990(60) [4], in full agreement with the standard-model expectation, and carrying the smallest uncertainty yet obtained.

This result is not only a significant verification of the standard model but the uncertainty quoted on the sum provides a tight limit on any possible new physics beyond the standard model, such as right-hand currents, extra Z bosons or supersymmetric models. In short, superallowed $0^+ \rightarrow 0^+$ beta decay provides a high-profile application of nuclear-physics measurements to the study of fundamental symmetries, a subject of vital interest to both nuclear and particle physicists. Although much has already been achieved in this field by nuclear physicists, improvements are still possible. Reducing the uncertainty on the unitarity sum – and, with it, the scope for new physics – remains the primary goal of our research program.
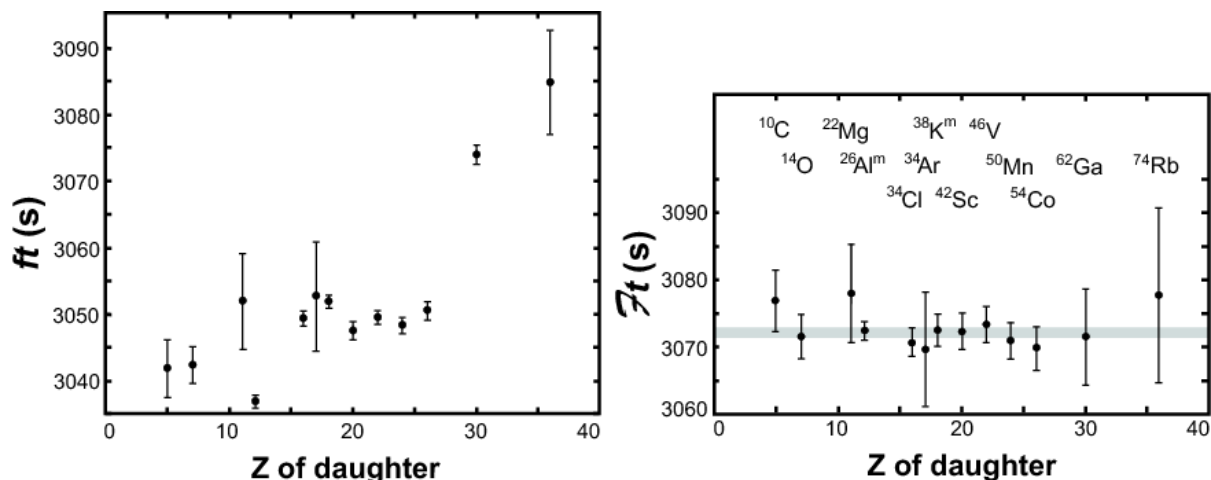
FIG. 1. Results from the 2009 survey [1]. The uncorrected *ft* values for the thirteen best known superallowed decays (left) are compared with the same results after corrections have been applied (right). The grey band in the right-hand panel is the average F*t* value, including its uncertainty.

Our approach follows from the observation [1,4] that the second largest contributor to the uncertainty in V_{ud} is the theoretical uncertainty in the nuclear-structure-dependent corrections, δ_{NS} and δ_C, used in the derivation of the F*t* values. Though these corrections are only of order 1%, their effect is very significant: Fig. 1, which is taken from our 2009 survey [1], shows the result of applying δ_{NS} and δ_C (together with δ'_R, which is nearly independent of *Z*). Obviously they act very well to remove the considerable "scatter" in *ft* values apparent in the left panel, replacing it with the consistent set of corrected F*t* values appearing in the right panel. Since these corrections were determined [3] completely independently of the superallowed decay data, this consistency in F*t* values is already a powerful validation of these calculated corrections, but obviously the remaining uncertainty still influences the final result for V_{ud}.

Even though the 2009 survey [1] included more than 145 individual measurements relating to 13 precisely known *ft* values, it is still possible for well selected experiments to make real improvements in

the validation tests of the nuclear-structure-dependent correction terms. At TAMU we are currently focusing on adding to the *ft*-value list new superallowed transitions, selected from amongst those with *large* calculated corrections. If the *ft* values measured for cases with large calculated corrections also turn into corrected F*t* values that are consistent with the others, then this must verify the calculations' reliability for the existing cases, which have smaller corrections. We are studying decays from $T_z = -1$ parent nuclei, which consistently have higher predicted structure-dependent correction terms than the well known $T_z = 0$ cases. In that context, during this past year we have continued to work on half-life measurements for the decays of ^{26}Si [5] and ^{38}Ca [6]. A manuscript describing the former has now been submitted to Physical Review C, while the latter is nearing completion and has been reported on at the Washington APS Meeting. At the same time, we have been exploring from a theoretical perspective [7] what else can be learned from a more exact experimental characterization of the nuclear-structure-dependent correction terms.

There are also compelling reasons to confirm and improve the *ft* values for the $T_z = 0$ cases as well. After all, these are the transitions that principally determine the value of V_{ud}. Since ^{46}V was a key transition that led to important improvements in the structure-dependent corrections when its Q_{EC} value was found to have been incorrectly measured by reaction studies in the past, we have been re-measuring its half-life [8] to be sure that no errors are lurking there. In addition we have extended Penning-trap measurements of Q_{EC} values to ^{34}Cl and ^{38}K^m [9], which has significantly improved the precision on these two values and has effectively eliminated the possibility of there being systematic differences between reaction-based and Penning-trap-based Q_{EC} value measurements.

We also endeavor to improve our data acquisition techniques for half-life measurements by a variety of means, from x-ray analysis of possible contaminant activities [10] and a new TDC-based data-acquisition system [11] to digital pulse analysis for the signals from our 4π proportional gas counter [12]. We are working to eliminate spurious pulses and to reduce our system dead time. Since we limit our count rate to avoid too large a dead-time correction, any reduction in the dead time itself will translate directly into improved statistical uncertainties on our measurements. Improvements have also been made to the equipment we use to measure branching ratios [13].

[1] J.C. Hardy and I.S. Towner, Phys. Rev. C **79**, 055502 (2009).
[2] J.C. Hardy and I.S. Towner, Phys. Rev. C **71**, 055501 (2005).
[3] I.S. Towner and J.C. Hardy, Phys. Rev. C **77**, 025501 (2008).
[4] I.S. Towner and J.C. Hardy, *Progress in Research,* Cyclotron Institute, Texas A&M University (2009 -2010), p. III-17; I.S. Towner and J.C. Hardy, Rep. Prog. Phys. **73**, in press.
[5] V.E. Iacob, J.C. Hardy, A. Banu, L. Chen, V.V. Golovko, J. Goodwin, V. Horvat, N. Nica, H.I. Park, L. Trache and R.E. Tribble, *Progress in Research,* Cyclotron Institute, Texas A&M University (2009-2010), p. I-5; submitted to Phys. Rev. C .
[6] H.I. Park, J.C. Hardy, V.E. Iacob, L. Chen, J. Goodwin, V. Horvat, N. Nica, L. Trache and R.E. Tribble, *Progress in Research,* Cyclotron Institute, Texas A&M University (2009-2010), p. I-9

[7] I.S. Towner and J.C. Hardy, *Progress in Research,* Cyclotron Institute, Texas A&M University (2009-2010), p. III-18.

[8] H.I. Park, J.C. Hardy, V.E. Iacob, L. Chen, J. Goodwin, V. Horvat, N. Nica, E. Simmons, L. Trache and R.E. Tribble, *Progress in Research,* Cyclotron Institute, Texas A&M University (2009-2010), p. I-10.

[9] T. Eronen, V.-V Elomaa, J. Hakala, J.C. Hardy, A. Jokinen, I.D. Moore, M. Reponen, J. Rissanen, A. Saastamoinen, C. Weber and J. Aysto, Phys. Rev. Lett. **103**, 252501 (2009); J.C. Hardy, *Progress in Research,* Cyclotron Institute, Texas A&M University (2009-2010), p. I-11.

[10] V. Horvat and J.C. Hardy, *Progress in Research,* Cyclotron Institute, Texas A&M University (2009-2010), p. V-27.

[11] V. Horvat and J.C. Hardy, *Progress in Research,* Cyclotron Institute, Texas A&M University (2009-2010), p. V-24.

[12] L. Chen and J.C. Hardy, *Progress in Research,* Cyclotron Institute, Texas A&M University (2009-2010), p. V-22.

[13] L. Chen and J.C. Hardy, *Progress in Research,* Cyclotron Institute, Texas A&M University (2009-2010), p. V-29.

Precise half-life measurement of the superallowed β^{+} emitter ^{26}Si

V. E. Iacob, J. C. Hardy, A. Banu, L. Chen, V. V. Golovko, J. Goodwin, V. Horvat, N. Nica,

H. I. Park, L. Trache, and R. E. Tribble

We have measured the half-life of the superallowed beta emitter ^{26}Si as part of our program to test the three-generation electroweak Standard Model via the unitarity of the Cabibbo-Kobayashi-Maskawa (CKM) matrix [1]. The half life, branching ratio and Q_{EC} value are the three measured parameters that define a β-decay ft value, and all three must be measured precisely for the $0^{+} \rightarrow 0^{+}$ superallowed decays that are used for the test. The precision required by this test is, in fact, very demanding, as a measurement becomes meaningful only if its precision is better than 0.1 %. Recently the Q_{EC} value for the superallowed branch in the decay of ^{26}Si has been measured to 0.0025 % accuracy [2], thus taking the first step in permitting this nucleus to join the group of superallowed emitters with ft values determined precisely enough to be used for the unitarity test. It is a particularly interesting case because its isospin symmetry-breaking correction ($\delta_{C} - \delta_{NS}$), though not particularly large compared to most of the well-measured cases, is more than double the size of the correction for the superallowed transition from ^{26}Al^{m}, which is its mirror transition. Experimental verification of this predicted mirror asymmetry would be a valuable test of the calculations.

We followed essentially the same procedure we used previously in our ^{34}Ar half-life experiment [3] since this case exhibits the same challenge: ^{26}Si decays to a daughter, ^{26}Al^{m}, which is itself radioactive with a comparable half-life. As already noted, ^{26}Al^{m} is another superallowed emitter.

We produced a ^{26}Si radioactive beam via the p(^{27}Al,2n)^{26}Si reaction, with a 30 A-MeV ^{27}Al primary beam impinging on a H$_2$ cryogenic gas-target kept at a pressure of 2 atm and at liquid-nitrogen temperature. A high purity ^{26}Si beam with 25.2 A MeV was then selected with the Momentum Achromat Recoil Separator (MARS) [4]. The ^{26}Si beam intensity was about 10^{4} ions per second. Similarly to the ^{34}Ar half-life experiment [3], the radioactive beam was extracted into air, then passed through a thin plastic scintillator, a series of Al degraders, and eventually implanted in the 76-μm-thick mylar tape of our fast tape-transport system. The thickness of the Al degraders was experimentally tuned to optimize the implantation and purity of the ^{26}Si beam.

Data were collected in cycles: After ^{26}Si nuclei had been implanted for a pre-selected time interval (of the same order as the ^{26}Si half-life), the beam was turned off and the tape-transport system moved the sample in ~175 ms to a well-shielded location 90 cm away, stopping it in the center of a 4π proportional gas counter. The decay positrons were then detected for twenty half-lives (45 s), with signals from the detector being multiscaled into a 500-channel time spectrum. These collect-move-detect cycles were computer controlled and their timing was continuously monitored on-line. They were repeated, with a separate decay spectrum recorded for each, until the desired overall statistics had been achieved. In its shielded location, the gas counter had a background rate of about 0.5 counts/s, which was 3-4 orders of magnitude lower than the initial count rate for each collected sample.

For this experiment we accumulated data from 5,000 cycles split into 55 separate runs, which yielded a total of 2×10^{8} counts. The total time-decay spectrum obtained from the combined runs is

presented in Fig. 1, where we also show the separate contributions from the decays of the [26]Si parent and the [26]Al[m] daughter.
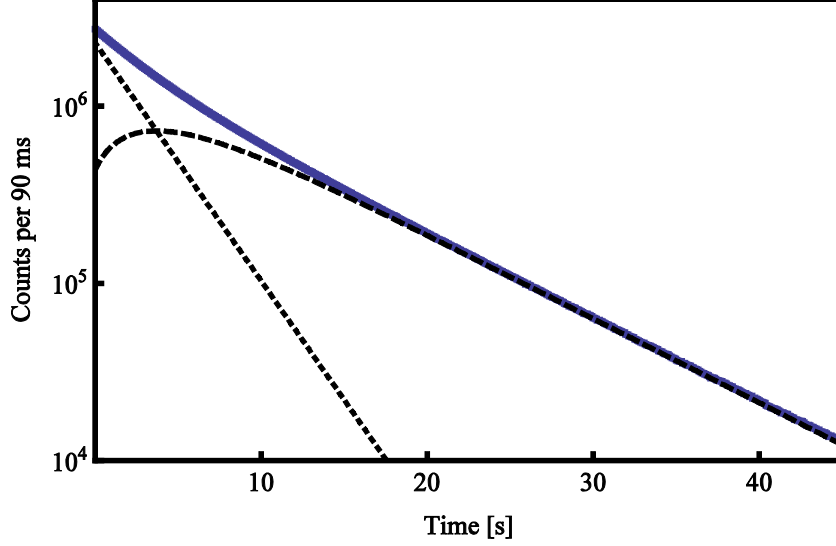
FIG. 1. Measured time-decay spectrum (solid line) obtained for the β^+ decay of [26]Si and its daughter [26]Al[m]. The dotted/dashed lines represent the derived [26]Si/[26]Al[m] contributions.

As our detection system does not disentangle the two components, the only information that can be processed is the combined parent-daughter decay. A detailed analysis of the coupled [26]Si and [26]Al[m] decay equations gives for the total detected rate

$$\Delta_{tot} = C_1 e^{-\lambda_1 t} + C_2 e^{\lambda_1 t}, \tag{1}$$

with

$$C_1 = N_1 \varepsilon_2 \lambda_1 \left(\frac{\varepsilon_1}{\varepsilon_2} - \frac{\lambda_2}{\lambda_1 - \lambda_2} \right) \tag{2}$$

$$C_2 = N_1 \varepsilon_2 \lambda_2 \left(\frac{N_2}{N_1} + \frac{\lambda_1}{\lambda_1 - \lambda_2} \right), \tag{3}$$

where t is the time elapsed after the end of the collect period; $N_{1,2}$ are the numbers of [26]Si and [26]Al[m] nuclei present in the sample at $t = 0$; $\varepsilon_{1,2}$ are the experimental efficiencies for detecting the positrons from the respective decays; and $\lambda_{1,2}$ are the corresponding decay constants. Note that if $\varepsilon_1 = \varepsilon_2$ and $\lambda_1 = 2\lambda_2$, the coefficient C_1 vanishes and the total decay rate is fully determined by $C_2 e^{-\lambda_2 t}$. While the half-lives of [26]Si and [26]Al[m] are actually related by a factor of 2.8, this is close enough to 2 for the total decay spectrum to

be dominated by the daughter's half life. This can easily be observed in Fig. 1, where the total spectrum deviates very little from a one-component decay curve with the daughter's decay-constant. This is similar to the situation we encountered for our [34]Ar experiment [3].

Thus, even with high accumulated statistics, the required precision can barely be obtained in a free two-component fit, which in the present case gives a half-life result for [26]Si of 2243.2(22) ms. Much better precision can be obtained if a parent-daughter link is imposed in the fit. In this case, the two coefficients $C_{1,2}$ are interconnected and dependent on the decay constants as shown in Eqns. 1-3. While more computation intensive, since in each iteration of the fitting process the two coefficients had to be recalculated, the effort is rewarded by a considerably improved precision. An important requirement in this linked procedure is the value of $\varepsilon_1/\varepsilon_2$, the relative parent/daughter detection efficiency. From a Monte Carlo analysis of our experimental setup we determined this ratio to be $\varepsilon_1/\varepsilon_2 = 1.00143(25)$.

The electronic scheme used to process the data was identical to the one used in the [34]Ar experiment [3]. To test the robustness of our results, each run was obtained with a different combination of critical detection settings: detector bias, discriminator threshold and major dead-time combination. As seen in Fig. 2, the half-life results show no systematic dependence on detector bias or discriminator threshold.
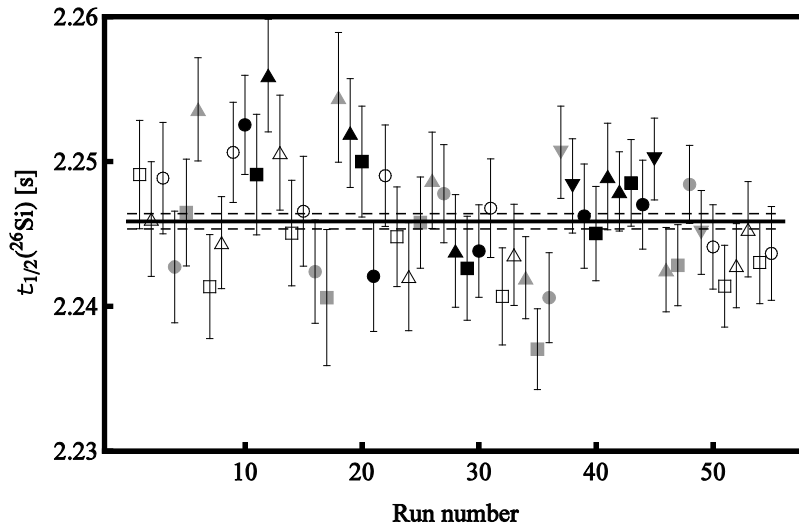
FIG. 2. Test for possible systematic bias in the [26]Si half-life measurement due to discriminator threshold or detector voltage. Open/grey/black symbols represent the three discriminator settings, 150 mV/200 mV/250 mV; the four detector biases, 2550 V, 2650 V, 2750 V and 2850 V are represented by the symbol shapes $\triangle$, $\square$, O and ∇, respectively. The average value for the half-life is 2245.26(51) ms (statistical uncertainty only) with $\chi^2/ndf = 70.6/54$. The average value appears as the solid line, with dashed lines as uncertainty limits.

Although not illustrated, the results were also found to be independent of both the imposed circuit dead time and the length of time for which the sample was collected.

Further tests of the half-life stability versus undetected short-lived impurities or rate-dependent counting losses were performed by the standard "front-channel-chopping" technique, which involves

separate fits to subsets of the data with successively longer time periods removed from the beginning of the counting cycle. Here too the derived half-life proved to be stable: no statistically significant change was observed as the starting time for the fit was systematically changed.

Our new precise result for the ^{26}Si half-life, 2245.3(7) ms, is considerably different from the average value quoted in the most recent survey of world data for superallowed $0^+\to0^+$ β-decay transitions [5].   However, that average is dominated by a measurement [6] that followed a somewhat similar analysis procedure to ours but neglected to deal properly with the correction for parent-daughter detection-efficiency differences.

With our half-life result for ^{26}Si decay having 0.03% precision, and the Q_{EC} value for its superallowed branch being recently determined to 0.0025% [2], the *ft* value for the branch can in principle be determined to sub-0.1% precision once the branching ratio can be measured to that level. We plan to measure the branching ratio in the near future.

[1] J.C. Hardy, I.S. Towner, V.E. Iacob, N. Nica, L. Chen, V. Horvat, H.I. Park, J. Goodwin, L. Trache and R.E. Tribble, *Progress in Research,* Cyclotron Institute, Texas A&M University (2009-2010), p. I-1.

[2] T. Eronen, V.-V. Elomaa, U. Hager, J. Hakala, A. Jokinen, A. Kankainen, T. Kessler, I.D. Moore, S. Rahaman, J. Rissanen, C. Weber and J. Aysto, Phys. Rev. C **79**, 032802(R) (2009).

[3] V.E. Iacob, J.C. Hardy, J.F. Brinkley, C.A. Gagliardi, V.E. Mayes, N. Nica, M. Sanchez-Vega, G. Tabacaru, L. Trache and R.E. Tribble, Phys. Rev. C **74,** 055502 (2006).

[4] R.E. Tribble, A. Azhari, C.A. Gagliardi, J.C. Hardy, A. Mukhamedzhanov, X. Tang, L. Trache and S.J. Yennello, Nucl. Phys. **A701,** 278 (2002).

[5] J.C. Hardy and I.S. Towner, Phys. Rev. C **79**, 055502 (2009). .

[6] I. Matea, J. Souin, J. Aysto, B. Blank, P. Delahaye, V.-V. Elomaa, T. Eronen, J. Giovinazzo, U. Hager, J. Hakala, J. Huikari, A. Jokinen, A. Kankainen, I.D. Moore, J.-L. Pedroza, S. Rahaman, J. Rissanen, J. Ronkainen, A. Saastamoinen, T. Sonoda and C. Weber, Eur. Phys. J. A **37**, 151 (2008).

High precision half-life measurement of the superallowed β-emitter ^{38}Ca

H. I. Park, J. C. Hardy, V. E. Iacob, L. Chen, J. Goodwin, V. Horvat, N. Nica, L.Trache,
and R. E. Tribble

Previously we made two measurements of the half-life of ^{38}Ca [1,2], the first an exploratory one and the second a higher-statistics one that suffered from an unusually unstable – and high (up to ~3%) – contamination from ^{35}Ar ($t_{1/2}$ = 1.77 s) in the ^{38}Ca beam at the focal plane of MARS. Since the range difference between ^{38}Ca and ^{35}Ar is less than half the thickness of our mylar collection tape, our positioning of the stopped ^{38}Ca ions mid-way through the tape resulted in the simultaneous deposit of some ^{35}Ar near the back of the tape. Although the contribution of ^{35}Ar could be accounted for when we extracted the half-life of ^{38}Ca, we believed that the precision of our result could be further improved by better control of the impurities and optimized positioning of the collected sample in the tape.

We performed the final half-life measurement of ^{38}Ca in September 2009 using the same ^{1}H(^{39}K, $2n$)^{38}Ca reaction at a primary beam energy of 30A MeV. Our experimental arrangement was the same as described before [1]. The Momentum Achromat Recoil Separator (MARS) produced a secondary ^{38}Ca beam that was better than 99% pure. Moreover, we further minimized the ^{35}Ar contaminant by depositing ^{38}Ca near the back of the mylar tape, thus ensuring that much of the ^{35}Ar passed entirely through it. During a daily routine check of MARS beam, no change was observed this time in the amount of ^{35}Ar relative to ^{38}Ca. Approximately, 200 million β events were recorded under various different settings of the experimental parameters – bias voltage of the 4π proportional gas counter, discriminator threshold, and dominant dead times – in order to check for possible systematic effects. The analysis is close to completion. This will lead to our final result for the half-life of ^{38}Ca and its associated error budget.

[1] H. I. Park *et al*., *Progress in Research*, Cyclotron Institute, Texas A&M University (2006- 2007), p. I-58; H. I. Park *et al*., *Progress in Research*, Cyclotron Institute, Texas A&M University (2007-2008), p. I-30.

[2] H. I. Park *et al*., *Progress in Research*, Cyclotron Institute, Texas A&M University (2008- 2009), p. I-33.

Half-life of the superallowed β-emitter ^{46}V

H. I. Park, J. C. Hardy, V. E. Iacob, L. Chen, J. Goodwin, V. Horvat, N. Nica,
E. Simmons, L. Trache, and R. E. Tribble

After making concerted efforts over several years to develop a useful ^{47}Ti beam [1], we completed a successful measurement of the half-life of ^{46}V with up to 50 nA of beam in June 2009. We used the ^{1}H(^{47}Ti, $2n$)^{46}V reaction at a primary beam energy of 32A MeV. Our experimental arrangement was the same as described before [1].

The main contaminant for this measurement was ^{42}Sc, another superallowed β-emitter with $t_{1/2} =$ 680.72 ms, which is rather similar to the 422.50 ms half-life of ^{46}V. Because of this potentially serious problem, we carefully adjusted the distribution of implanted ^{46}V in the mylar tape by setting the thickness of Al degraders to minimize the number of ^{42}Sc ions stopping in the tape; and then we routinely measured the purity of the beam with a position-sensitive silicon detector inserted at the focal plane of the Momentum Achromat Recoil Separator (MARS) on a daily basis throughout the whole experiment. Finally, the subsequent data analysis has included a detailed impurity analysis based on the range differences among all possible impurities, including ^{42}Sc, in the collected ^{46}V samples. The amount of ^{42}Sc present in the samples relative to that of ^{46}V was determined to be 0.1%, an amount for which we can satisfactorily correct.

Approximately 95 million β events were recorded under the various combinations of different bias voltages for the 4π proportional gas counter, discriminator thresholds, and dominant dead times. Currently, we are finalizing our analysis to extract the precise half-life for ^{46}V with an associated error budget.

[1] H.I. Park *et al*., *Progress in Research*, Cyclotron Institute, Texas A&M University (2008-2009), p. I-34.

JYFLTRAP : Q_{EC}-values of the superallowed decays of ^{34}Cl and ^{38}K^m

J. C. Hardy

We have now completed and published three successful measurements of the Q_{EC} values for superallowed $0^+ \rightarrow 0^+$ transitions from $T_z = 0$ nuclei using the JYFLTRAP Penning-trap mass spectrometer at the University of Jyvaskyla cyclotron facility in Finland. The first comprised the results for ^{26}Al^m, ^{42}Sc and ^{46}V [1] and the second, ^{50}Mn and ^{54}Co [2]. In the most recent [3], our collaboration determined the Q_{EC} values for the superallowed decays of ^{34}Cl and ^{38}K^m. The Q_{EC} values for these two transitions had previously been determined to a claimed high precision with (p,n) threshold measurements, and combined (p,γ) and (n,γ) Q-value measurements, the methods used in the past before Penning traps became available for on-line measurements. They had never been measured with a Penning trap. These two cases thus provided an excellent means to test carefully for any systematic discrepancies between reaction-based and trap-based measurements, a subject of some concern [4] when one combines both types of measurement in the determination of a world average.

As we did in our previous experiments, we produced ^{34}Cl and ^{38}K^m via (p,n) reactions. A powerful advantage of this approach is that, not only were the superallowed emitters of interest produced in the primary reactions but ions from the target material itself – the beta-decay daughters of these emitters – were also released by elastic scattering of the cyclotron beam. As explained in Ref. [1], with the JYFLTRAP system we can isolate a specific nuclide from the reaction products and measure the cyclotron frequency of its ions in the Penning trap. For each determination of a Q_{EC} value, the cyclotron frequency measurements were interleaved: first we recorded a frequency scan for the daughter, then for the mother, then for the daughter and so on. This way, most potential systematic effects could be reduced to a minimum or eliminated. For each measurement, data were collected in several sets, each comprising ~10 pairs of parent-daughter frequency scans taken under the same conditions.

Our results for the Q_{EC} values of ^{34}Cl and ^{38}K^m were 5491.662(47) keV and 6044.223(41) keV respectively. The uncertainties, 47 and 41 eV, are the smallest ever obtained for any superallowed Q_{EC} value. Penning-trap results for four transitions, including these two, are compared with reaction-based results in Fig. 1. There is no evidence for any systematic difference between the two types of measurement, although there is an obvious error in the (p,n) measurement of the ^{26}Al^m Q_{EC} value. Excluding this result, the weighted average difference (reaction result minus Penning-trap result) is 15(85) eV. Any systematic difference between reaction and trap measurements, if it exists at all, must be below 100 eV, which is below – and usually well below – the uncertainties quoted on the reaction-based measurements themselves.

These new Q_{EC}-value results leave the uncertainties in the *ft* values for the ^{34}Cl and ^{38}K^m transitions totally dependent on the uncertainties of their half-lives. The *ft*-value uncertainties would now be reduced by nearly an order of magnitude if the half-life measurements were to be improved by that factor.

We plan to complete our measurements on the "traditional nine" superallowed transitions by measuring the Q_{EC} values for ^{10}C and ^{14}O in an experiment scheduled for May 2010.
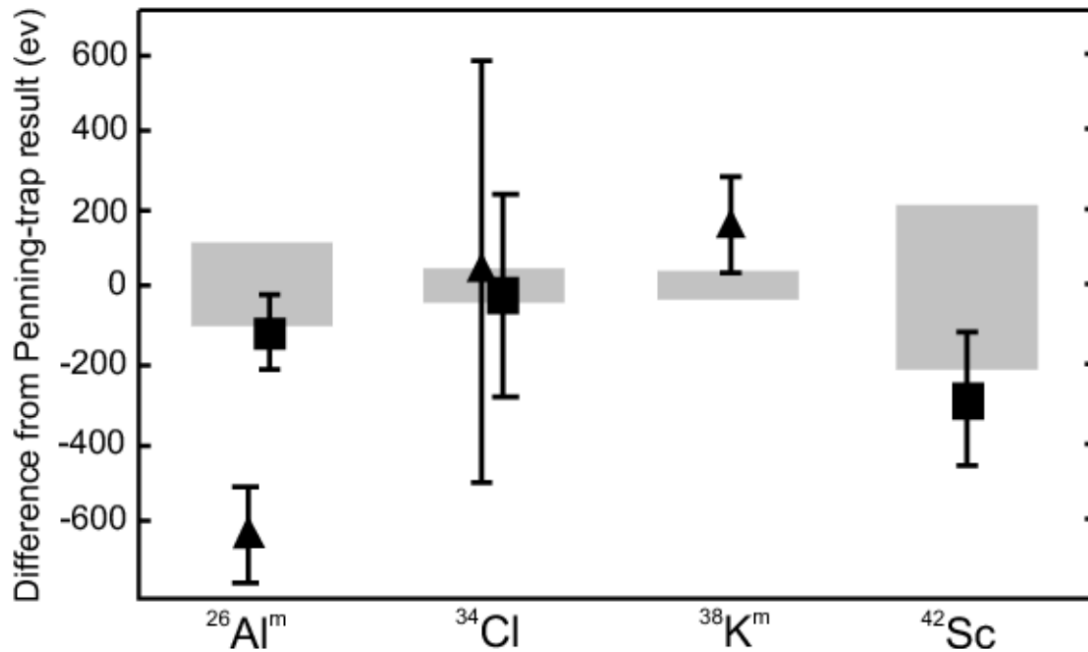
FIG. 1. Differences between precise reaction-based and Penning-trap QEC value measurements for ^{26}Al^m, ^{34}Cl, ^{38}K^m and ^{42}Sc. The (p,n)-threshold measurements are shown as triangles and the (p,γ)+(n,γ) measurements appear as squares. The grey bands about the zero line represent the uncertainty of the Penning-trap measurements. (Experimental references are given in [3].)

[1] T. Eronen, V. Elomaa, U. Hager, J. Hakala, A. Jokinen, A. Kankainen, I. Moore, H. Penttilä, S. Rahaman, A. Saastamoinen, T. Sonoda, J. Äystő, J.C. Hardy and V. Kolhinen, Phys. Rev. Lett. 97, 232501 (2006).

[2] T. Eronen, V.-V. Elomaa, U. Hager, J. Hakala, J.C. Hardy, A. Jokinen, A. Kankainen, I.D. Moore, H. Penttila, S. Rahaman, S. Rinta-Antila, J. Rissanen, A. Saastamoinen, T. Sonoda, C. Weber and J Aysto, Phys. Rev. Lett. **100**, 132502 (2008).

[3] T. Eronen, V.-V Elomaa, J. Hakala, J.C. Hardy, A. Jokinen, I.D. Moore, M. Reponen, J. Rissanen, A. Saastamoinen, C. Weber and J. Aysto, Phys. Rev. Lett. **103**, 252501 (2009).

[4] J.C. Hardy, I.S. Towner and G. Savard, Int. J. Mass Spectrometry **251**, 95 (2006).

Tests of internal-conversion theory with precise γ- and x-ray spectroscopy

J. C. Hardy, N. Nica, V. E. Iacob and M. B. Trzhaskovskaya[1]

[1]*Petersburg Nuclear Physics Institute, Gatchina RU-188300, Russia*

Internal conversion plays an important role in most nuclear decay schemes yet, until recently, the accuracy of calculated internal conversion coefficients (ICCs) was, at best, ill defined. Not only were there very few precise measurements of ICCs in existence but, for many years, there appeared to be a systematic difference between experiment and theory. In 1973 Raman compared "precisely measured" ICCs for fifteen *E*3 and *M*4 transitions with the tabulated Hager and Seltzer calculations and concluded that the theoretical values were systematically higher by 2-3%. However, even this select group of transitions included only five with measured ICCs that were known with a precision of 2% or better, so the apparent discrepancy was hardly definitive. Even so, this is where the matter remained for 30 years.

By 2002, Raman *et al.* [1] had 100 experimental ICCs to compare with tabulated values, but even at that recent date only 20 of the measured ICCs had a precision of 2% or better. Their results still indicated that all previous tables of ICCs exhibited a 3% systematic bias but the authors found much better agreement (within ~1%) for a new table by Band *et al.* [2], which was calculated in the framework of the Dirac-Fock method, with the exchange between electrons treated exactly. Yet, even though the average agreement was now much better, some of the individual ICCs disagreed significantly with the calculated values and, even more troubling, the data appeared to show a surprising preference for one particular model in which the final-state electron wave function was computed in a field that did not include the atomic subshell vacancy caused by the conversion process.

The first experiment that definitively established the need to include the atomic vacancy was our precise 2004 measurement ($\pm$ 0.8%) of the *K*-shell conversion coefficient, α_K, for the 80.2-keV *M*4 transition in ^{193}Ir [3]. However, this measurement was for a single high-*Z* nucleus and certainly needed to be confirmed for lower-*Z* cases. Furthermore, among the other transitions whose ICC's had been measured with a precision claimed to be under 2%, several disagreed significantly with both types of calculations, *i.e.* whether or not the vacancy was included. Since 2004 we have addressed three of these latter cases, ^{134}Cs^{m} [4], ^{137}Ba [4] and ^{197}Pt^{m} [5], and have shown that the apparent discrepancies were due entirely to flawed experiments. With the case of ^{134}Cs^{m}, we also extended our experimental verification of the need to include the atomic vacancy down to $Z = 55$.

The impact of our results so far is illustrated in Fig. 1, where we plot differences between 21 experimental ICCs and two versions of the Dirac-Fock theory [1,2], one that ignores the atomic vacancy and the other that includes it via the "frozen orbital" approximation. In addition to our four results, the figure includes the twenty cases with better than 2% precision, which were listed by Raman *et al.* [1] in 2002. Note that three of the Raman results were improved and supplanted by our new measurements.

There is one more viable case that would allow us to extend our test to even lower Z, and would discriminate more definitively than ^{134}Cs^{m} between the vacancy and no-vacancy prescriptions. This is the 293.1-day isomeric state, ^{119}Sn^{m}, which decays 100% by cascade via a 66-keV *M*4 and a 24-keV *M*1/*E*2 transition. Since the latter cannot convert in the *K* shell, the *K* x rays in the measured photon spectrum

from this decay scheme will be exclusively from the *M*4 transition. Consequently the *K* conversion coefficient for the *M*4 transition can be determined from the equation

$$\alpha_K \omega_K = \frac{N_K}{N_\gamma} \frac{\varepsilon_\gamma}{\varepsilon_K},$$

where ω_K is the fluorescence yield; N_K and N_γ are the total numbers of observed *K* x rays and 66-keV γ rays, respectively; and ε_K and ε_γ are the corresponding detector efficiencies. This is our standard method for making such measurements and, although our detector efficiency in the 25-29 keV *K*-x-ray energy range is not as well established as it is at higher energies, we still anticipate being able to measure the ICC to ~1% precision. Since the difference between the calculated ICC values with and without the atomic vacancy is 4.9%, this precision will be more than adequate for us to distinguish definitively between them.

These measurements are generally carried out in the summer when an REU student can be involved. The student becomes a co-author of the paper that results.
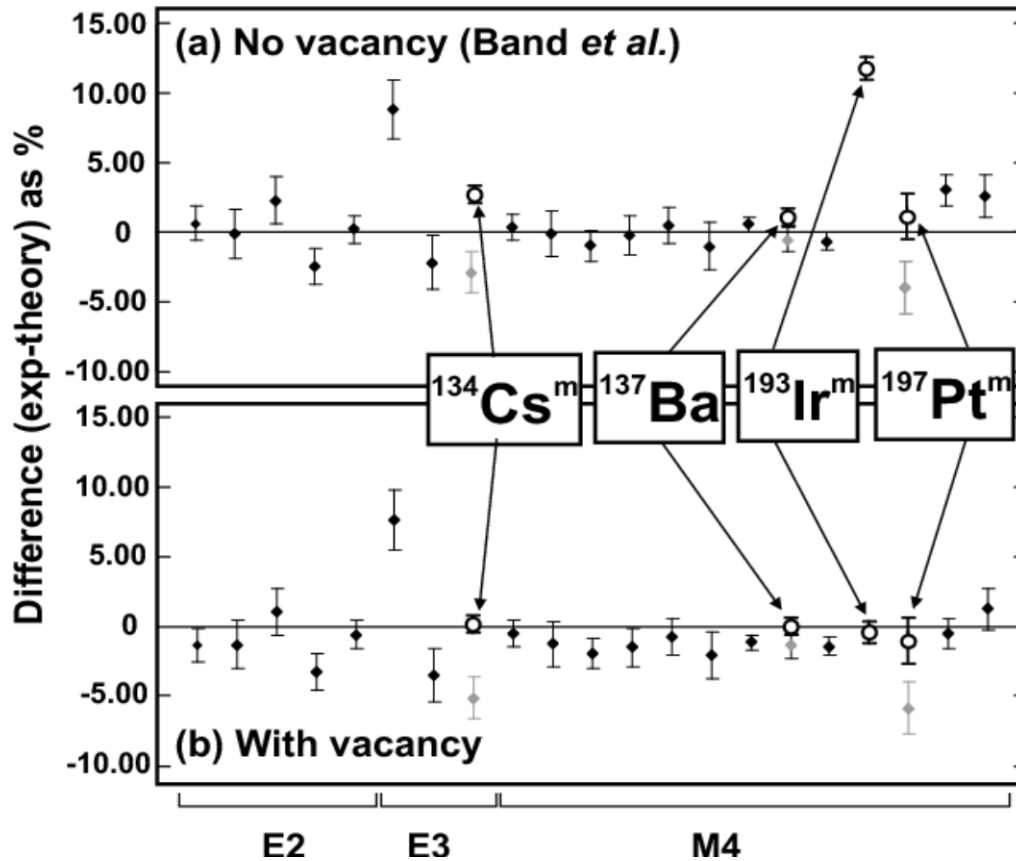
FIG. 1. Percentage differences between the measured and calculated ICCs for two Dirac-Fock calculations: one (top) is without the atomic vacancy and the other is with it included in the "frozen orbital" approximation. The points shown as solid diamonds in both plots correspond to the twenty cases that have better that 2% precision [1]; as indicated at the bottom, five are for E2 tranditions, three for E3, and the remainder are for M4 transitions. The points shown as open circles correspond to our recently measured α_K values. The grey points with error bars at the same horizontal positions are the previous α_K results, which our measurements replace.

[1] S. Raman *et al.*, Phys. Rev. C **66**, 044312 (2002).

[2] I.M. Band, M.B. Trzhaskovskaya, C.W. Nestor, Jr., P. Tikkanen, and S. Raman, At. Data Nucl. Data Tables **81,** 1 (2002).

[3] N. Nica, J.C. Hardy, V.E. Iacob, S. Raman, C.W. Nestor Jr., and M.B. Trzhaskovskaya, Phys. Rev. **C70**, 054305 (2004); N. Nica, J.C. Hardy, V.E. Iacob, J.R. Montague, and M.B. Trzhaskovskaya Phys. Rev. C **71**, 054320 (2005).

[4] N. Nica, J.C. Hardy, V.E. Iacob, W.E. Rockwell, and M.B. Trzhaskovskaya, Phys. Rev. C **75**, 024308 (2007); N. Nica, J.C. Hardy, V.E. Iacob, C. Balonek, and M.B. Trzhaskovskaya, Phys. Rev. C **77**, 034306 (2008).

[5] N. Nica, J.C. Hardy, V.E. Iacob, J. Goodwin, C. Balonek, M. Hernberg and J. Nolan, Phys. Rev. C **80**, 064314 (2009).

The [97]Ru half-life: high-precision measurement shows no temperature dependence

J. R. Goodwin, V. V. Golovko,[1] V. E. Iacob, and J. C. Hardy
[1]*Department of Physics, Queen's University, Stirling Hall, Kingston, ON, Canada*

This experiment was undertaken to investigate whether the half life of the electron-capture decay of [97]Ru located in a metallic environment shows any temperature dependence, as has been claimed for the electron-capture decay of [7]Be in a recent publication [1]. The results of our measurement on [97]Ru have now been published [2].

Previous publications claiming to observe temperature dependence of β^-, β^+ and electron-capture-decay half-lives [1, 3, 4] have used the so-called "Debye effect" to explain the phenomenon. The authors claim that the conduction electrons, present in a metal, comprise a sort of plasma, which they refer to as a Debye plasma. They argue that this plasma changes the phase space available for the decay and thus increases (for β^- or electron-capture decay) or decreases (for β^+-decay) the nuclide's half life. The change in phase space would be enhanced, they argue, if the source is cooled to very low temperatures. Although the half-life changes, which were reported at low temperature (~12K), were less than their proposed theory indicated, they were in the same direction.

We set out by repeating one of the reported experiments: the measurement of the half-life of [198]Au in gold at room temperature and at 19K [5]. Spillane *et al*. [3] had claimed a 3.6(10)% effect, but we found no effect and set an upper limit of 0.04%, two orders of magnitude lower than their claims. Having shown no effect to exist for the β^--decay of [198]Au, we next turned to a case of electron-capture: the decay of [97]Ru.

The details of this experiment were described in last year's Progress Report [6] and in our published paper [2]. From our analysis of the decay of the 216-keV delayed γ ray in [97]Tc, the daughter of [97]Ru, we obtained a half-life (statistical uncertainty only) of 2.8382(13) d for the cold-temperature measurement, and of 2.8370(13) d for the room-temperature measurement. The difference between these two results is 0.0012(18) d, which gives an upper limit of 0.0030 d, or 0.1%, on any temperature-dependent difference in the [97]Ru half-life at the 68% confidence level.

Since their delayed γ rays were present in the spectra as well, we have also obtained data at both temperatures for two other isotopes, [103]Ru and [105]Rh, which both decay by β^- emission. We were able to show that neither of these isotopes undergoes a change in half-life, as would be predicted by the "Debye theory":

- For [103]Ru, our measurements yield a half-life of 39.210 ± 0.016 d at room temperature and 39.219 ± 0.025 d at 19K. These results are also the same within 0.1%.

- For [105]Rh, our measurements obtain a half-life of 35.357 ± 0.036 h at room temperature, and a half-life of 35.319 ± 0.023 h at 19K. These results are the same within 0.2%

Obviously we cannot comment on the validity of the [7]Be measurement, which claimed to have observed a temperature effect [1], but we can certainly refute any suggestion that the half-lives of electron-capture decays in general exhibit significant temperature dependence when the source is placed in a metal host. Wang *et al*. [1] used their model to calculate that the half-life of [7]Be in a metal should

change by 1.1% between T = 293 and 12K, a result that agrees reasonably well with their measured values. Using the same model, we calculate that the half-life change for the [97]Ru decay should be 11.2% between T = 293 and 12K and 8.4% between T = 293 and 19K, the temperature we obtained. Our measured upper limit on any half-life change over this temperature range is nearly two orders of magnitude less than this model prediction. We have previously demonstrated that the "Debye model" has no validity for β^- decay [2] and have confirmed that conclusion in this work; we can now state with equal confidence that it also does not apply to electron-capture decay.

[1] B. Wang *et al*., Eur. Phys. J. A **28**, 375 (2006).

[2] J.R. Goodwin, V.V. Golovko, V.E. Iacob and J.C. Hardy, Phys. Rev. C **80**, 045501 (2009).

[3] B. Limata *et al*., Eur. Phys. J. A **28**, 251 (2006).

[4] T. Spillane *et al.*, Eur. Phys. J. A **31**, 203 (2007).

[5] J.R. Goodwin, V.V. Golovko, V.E. Iacob and J.C. Hardy, Eur. Phys J. A **34**, 271 (2008).

[6] J.R. Goodwin, V.V. Golovko, V.E. Iacob, and J.C. Hardy, *Progress in Research,* Cyclotron Institute, Texas A&M University (2008-2009), p. I-37.

Measurement of the half-life of ^{198}Au in an insulator

J. R. Goodwin, V. E. Iacob, N. Nica, A. Dibidad, and J. C. Hardy

This experiment was undertaken to investigate whether the half life of the β⁻ decay of ^{198}Au changes depending on whether the nucleus is located in a metallic or insulating environment. The "Debye plasma model," which was originally invoked to explain observed cross-section anomalies in the $d(d,p)t$ reaction, was later applied to radioactive decays by Limata *et al.* [1]. According to this model, the conduction electrons, present in a metal, comprise a sort of plasma, which is referred to as a Debye plasma. It is argued that this plasma changes the phase space available for the decay and thus increases (for β⁻ or electron-capture decay) or decreases (for β⁺-decay) the nuclide's half life. If this model were correct, this change in phase space would occur only in metals, not in an insulator, and would be enhanced if the metal were to be cooled to very low temperatures.

In their subsequent study of the β⁻ decay of ^{198}Au, Spillane *et al.* [2] claimed to observe both these effects, albeit to a lesser extent than the theory predicted. The theory predicts that at room temperature the ^{198}Au half-life in a metal would be 8% longer than in an insulator, while at 12K it would be 32% longer. The corresponding numbers reported by Spillane *et al.* were 0.4(7)% and 4.0(7)%. We repeated their measurement in a metal at two different temperatures and have already reported [3] that any temperature dependence is less than 0.04%, two orders of magnitude below the value claimed by Spillane *et al.* However, we have not yet addressed the possibility that there might be a difference between sources located in metal and insulators. We do so in the study reported here.

We focused again on ^{198}Au, which we chose because of its suitability for a precise measurement (monoisotopic, single β-delayed γ peak, *etc.*). This time though we chose to irradiate gold in the form of Au_2O_3 (gold(III) oxide), which is an insulator. With a single measurement at room temperature we could then compare our result with the value we previously obtained at room temperature for ^{198}Au in a conductor (gold metal) [3].

We used a gold(III) oxide sample obtained from the Alfa Aesar Corporation. This was in the form of a powder, with a purity of 99.99% (metals basis). The sample (0.170 g on an Al disc) was activated in a flux of ~10^{10} neutrons/cm^2·s for 10 s irradiation time, at the Texas A&M Triga reactor. The irradiated Au_2O_3 sample was then placed upon the cold head of a CryoTorr 7 cryopump, precisely as had been done previously for our ^{198}Au measurement [3], and for our ^{97}Ru [4] experiment. A 70% HPGe detector was placed directly facing the sample, and just outside the plate covering the cryopump. A cavity had been bored in the cover-plate such that only 3.5 mm of stainless steel remained between the sample and the face of the detector. The detector and cryopump were placed such that the distance between them remained constant throughout the measurement.

Six-hour γ-ray spectra, from the 411-keV delayed γ-ray in ^{198}Hg, were acquired and saved consecutively, for a period of 27 days. All these spectra were collected for an identical, pre-set live time. Throughout the experiment, we synchronized the time, prior to each day's collection, using the signal broadcast from radio station WWVB. We also kept the system's dead time below about 3% for all the spectra. Since the TRUMP^{TM} card used in our data collection corrects for dead time losses, our results

were basically independent of dead time losses. However, as before, we applied to all spectra a further experimentally-determined correction of $5.5 \pm 2.5 \times 10^{-4}$ per 1% increase in dead time to account for residual, rate-dependent effects.

We obtained a total of 107 spectra and extracted the peak area from each for the 412-keV β-delayed γ ray in ^{198}Hg, the daughter of ^{198}Au, using the same methods we used before [3, 4]. The resulting decay curve then yielded a half-life of 2.6948(9) d, a value that can be compared to the result we obtained for ^{198}Au in a metal at room temperature, 2.6949(9) d. The difference between the two measurements is 0.0001(12) d, which gives an upper limit of 0.0013 d or 0.05% at the 68% confidence level. We therefore conclude that the observed half-life is independent of the host material as well as being independent of its temperature.

[1] B. Limata *et al*., Eur. Phys. J. A **28**, 251 (2006).
[2] T. Spillane *et al.*, Eur. Phys. J. A **31**, 203 (2007).
[3] J.R. Goodwin, V.V. Golovko, V.E. Iacob and J.C. Hardy, Eur. Phys J. A **34**, 271 (2008).
[4] J.R. Goodwin, V.V. Golovko, V.E. Iacob and J.C. Hardy, Phys. Rev. **C 80**, 045501 (2009); and *Progress in Research*, Cyclotron Institute, Texas A&M University (2009-2010), p. I-16.

Test of claims that radioactive half-lives depend on the earth-to-sun distance

J. R. Goodwin, V. V. Golovko, V. E. Iacob, and J. C. Hardy

Several recent publications by J.H. Jenkins and E. Fischbach [1-4] have claimed evidence that radioactive half-lives vary as a function of the earth-to-sun distance at the time of measurement. When the first of these claims appeared as an arXiv preprint, we had already made three sequential measurements of the half life of the β-decay of ^{198}Au for another purpose [5, 6], so we decided to make four more measurements of that half-life at times chosen so that the dates of all seven measurements would span the complete range of earth-sun distances.

The main claims by Jenkins and Fischbach [2] are based on their interpretation of published data taken by others, one set of measurements done at Brookhaven National Laboratory [7] and another at the Physikalisch Technische Bundesanstalt in Germany [8]. The BNL measurements compared the decay rate of ^{32}Si ($t_{1/2}$ = 172 yr) to that of ^{36}Cl ($t_{1/2}$ = 300,000 yr) on a regular basis over four years; they used an end-window gas-flow proportional counter to detect decay β particles. The PTB measurements, which were made for calibration purposes, periodically obtained the decay rate of ^{226}Ra ($t_{1/2}$ = 1600 yr) over 11 years using a high-pressure $4\pi\gamma$ ionization chamber. The data from both groups show a weak but statistically significant oscillatory behavior of decay rate with a one-year period. Both groups acknowledged the oscillations in their data, with BNL noting that it corresponded with seasonal variations in temperature and humidity, which could have affected the relative absorption of the β particles from ^{32}Si and ^{36}Cl, while PTB attributed it to background radioactivity such as radon and daughter products, which are known to show seasonal concentration changes.

In their reanalysis of the data, Jenkins and Fischbach superimposed a plot of the earth-sun distance over the sequence of half-life values measured by each group. A copy of their plot [2] for the BNL ^{32}Si data appears in Fig. 1. The solid (cyclic) line is a plot of $1/R^2$, where R is the earth-sun distance in a.u. units; each individual data point represents the average of 4 runs, each lasting 10 hr. They conclude [2] that there is a strong correlation between the data and the earth-sun distance, and they speculate that this could arise from a terrestrial modulation in the fine-structure constant caused by a scalar field from the sun, or because the terrestrial radioactive nuclei are interacting in some way with the neutrino flux from the sun. They even present an argument for how the latter might cause the "phase shift" between the $1/R^2$ curve and the BNL (and PTB) data.

Since both the BNL and PTB measurements were of total un-discriminated decay rates for long-lived radioactivities, any observed cyclic variations cannot definitively be attributed to variations in the half-lives involved. A variety of other factors, such as the seasonal effects already mentioned, could plausibly be involved, and their elimination requires elaborate argumentation [4] – and is certainly open to debate [9].

We seek to avoid these ambiguities by measuring the half-life of the much shorter-lived ^{198}Au ($t_{1/2}$ = 2.695 d), which we uniquely identify by observing the decay of its prominent 411-keV β-delayed γ ray (in ^{198}Hg) in a HPGe detector. We also follow the decay for 10 half lives and determine the half-life from a fit to the decay curve over three decades. Contaminant activities are completely eliminated by

this process, as are the atmospheric effects previously indicated as possible sources of seasonal variations.
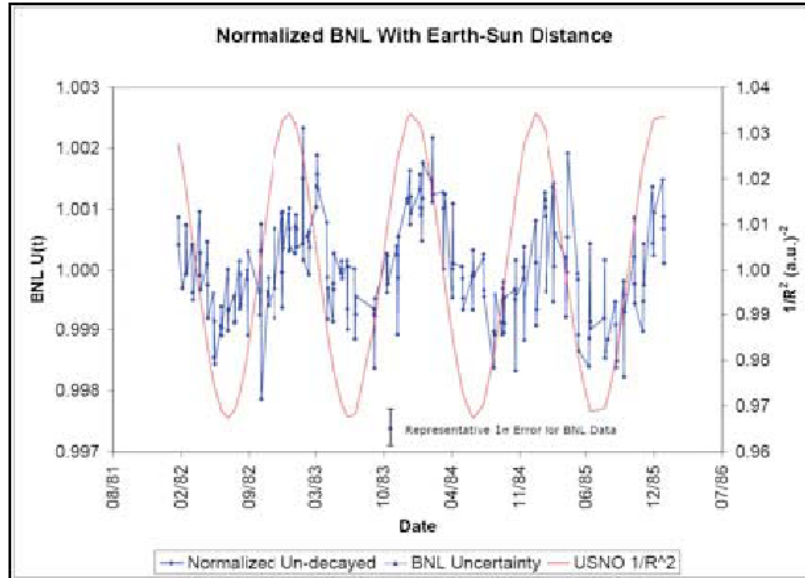
FIG. 1. Plot of $U(t)$ for the raw BNL ^{32}Si/^{36}Cl ratio (points) together with $1/R^2$, where R is the earth-sun distance. The values of $U(t)$ are obtained by multiplying each data point by $\exp(+\lambda t)$, where $\lambda = \ln(2)/t_{1/2}$ with $t_{1/2} = 172$ yr for ^{32}Si. The left axis gives the scale for the normalized $U(t)$, and the right axis denotes the values of $1/R^2$ in $1/(a.u.)^2$.

We used the procedures we have described previously [5]. For each measurement, a circular disc of 99.99+ % pure gold, 10 mm in diameter and 0.1 mm thick, was activated by being placed in a flux of ~10^{10} neutrons/cm^2·s for 10 s, at the Texas A&M Triga reactor. It was then placed in a fixed geometry with respect to a 70% HPGe detector, and not moved for the one-month duration of the measurement. Over 100 consecutive γ-ray spectra were acquired for a pre-set live time and saved in computer memory. We extracted the number of counts in the 411-keV γ-ray peak in each spectrum using the least-square peak-fitting program GF3 (in the RADware series) [10], and corrected the results for small residual, rate-dependent effects, which we had determined from an independent measurement [5,6]. We then fitted the decay curve obtained from this analysis using the method of maximum-likelihood with a single-exponential in a code based on ROOT [11].

The seventh measurement is only just completed and our analysis of some of the earlier measurements is still not finalized. However, the plot shown in Fig. 2 compares our preliminary results with BNL data and the 1/R^2 oscillations (both taken from Fig. 1). So far, we see no indication of any dependence of the half-life of ^{198}Au on the earth-sun distance.
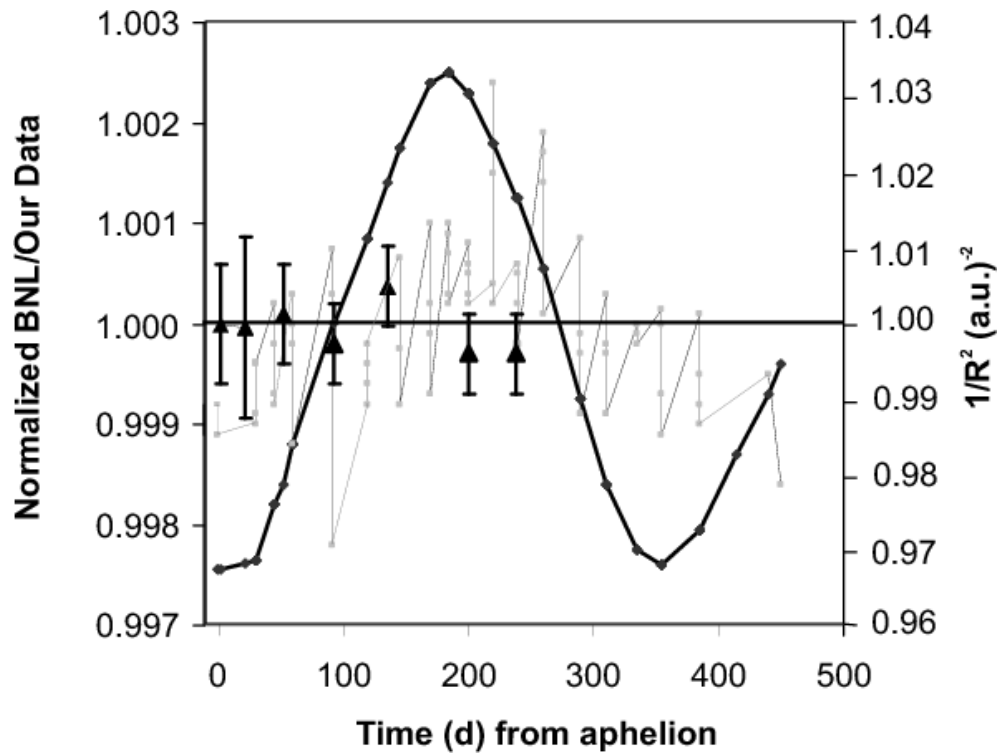
FIG. 2. Plot of a portion of the material shown in Fig. 1, starting at approximately 07/82 and ending at 09/83, about 450 days later. Superimposed on the BNL data (grey) and $1/R^2$ curve are our preliminary results for seven half-life measurements of ^{198}Au (solid triangles with error bars) placed at their appropriate time of measurement relative to the aphelion.

[1] J.H. Jenkins and E. Fischbach, Astropart. Phys. **31**, 407 (2009).

[2] J.H. Jenkins, E. Fischbach, J.B. Buncher, J.T. Gruenwald, D.E. Krause, and J.J. Mattes, Astropart. Phys. **32**, 42 (2010).

[3] E. Fischbach, J.B. Buncher, J.T. Gruenwald, J.H. Jenkins, D.E. Krause, J.J. Mattes, and J.R. Newport, Space Sci. Rev. **145**, 285 (2009).

[4] J.H. Jenkins, D.W. Mundy, and E Fischbach, arXiv:0912.5385v1.

[5] J. R. Goodwin, V.V. Golovko, V.E. Iacob, and J.C. Hardy, Eur. Phys. J. A **34**, 271 (2007).

[6] J.R. Goodwin, V.E. Iacob, N. Nica, A. Dibidad, and J.C. Hardy, *Progress in Research*, Cyclotron Institute, Texas A&M University (2009-2010) p. I-18.

[7] D. Alburger, G. Harbottle, and E.F. Norton, Earth and Planet. Sci. Lett. **78**, 168 (1986).

[8] H. Siegert, H. Schrader, and U. Schötzig, Appl. Radiat. Isot. **49**, 1397 (1998).

[9] H. Schrader, Appl. Radiat. And Isot., in press.

[10] D. Radford, http://radware.phy.ornl.gov/main.html (private communication).

[11] R. Brun and F. Rademakers, Nucl. Instrum. Methods Phys. Res. **A389**, 81 (1997).

Activity measurement of a ^{57}Co source for NIST

J. C. Hardy and V. E. Iacob

In October 2009, Ryan Fitzgerald of the Radioactivity Group at NIST asked us to determine the activity of a ^{57}Co source with our well-calibrated HPGe detector. He had determined the activity of the source based on β-γ anticoincidence measurements but his new calibration was "significantly different" from NIST's old calibration from 1978. He was seeking another activity determination based on an independent technique. Since the absolute efficiency of our γ-ray detector is known to ±0.2%, we were in a position to measure the activity by observing the decay rate of γ rays emitted from ^{57}Fe, the daughter of ^{57}Co, and we agreed to do so.

The source supplied by NIST, which reached Texas A&M on 4 November 2009, was described as being prepared as follows: "2 drops of cobalt chloride solution (in 1 mol/L HCl) and 1 drop of dilute Ludox solution were deposited on the sticky side of a piece of polyester tape, approximately 0.006 cm thick, that had been mounted on a 0.05-cm-thick aluminum annulus with 3.8-cm inside diameter and 5.4-cm outside diameter. The source was dried in a desiccator overnight. The dried solids in the source consisted of 2.3 μg of $CoCl_2$ and 0.3 μg of SiO_2. The dried source was then sandwiched with a second piece of tape." We were also supplied with a radiographic analysis of the source, which showed it to be deposited in a spot with 5.5 mm diameter (full width at half maximum activity). If we assume uniform distribution of the solid material, there is no significant self-attenuation in this small amount of source material, so in our analysis of the data we only include the effect of the polyester tape.
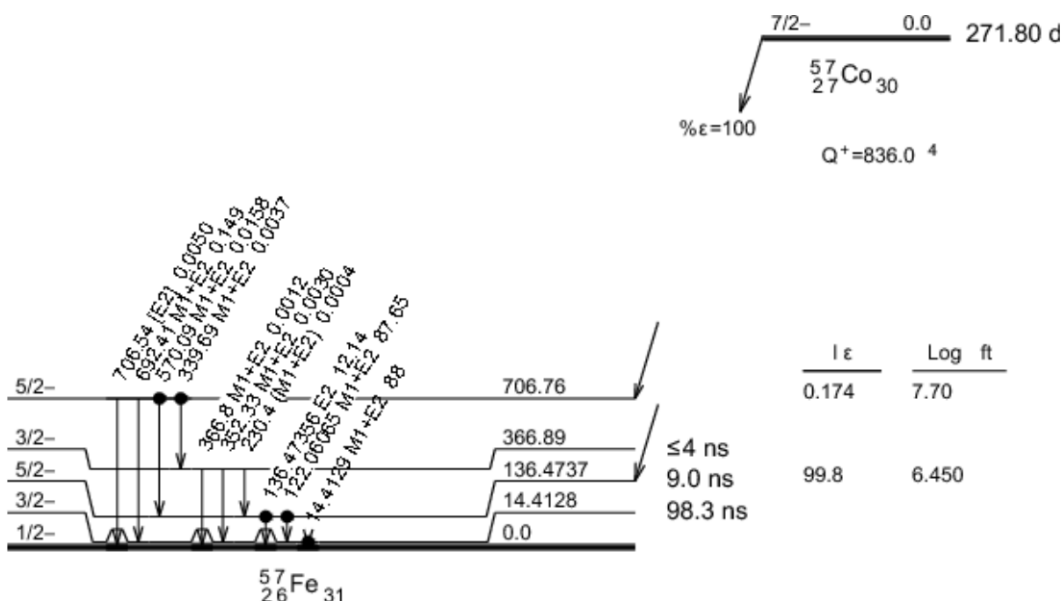
FIG. 1. Beta-decay scheme for ^{57}Co.

The decay scheme of ^{57}Co is shown in Fig. 1. The γ-ray spectrum from the decay is dominated by three γ rays: with 14.41, 122.06 and 136.47 keV. Our measurement focused on the latter two. Since

we only measure the decay rate of these γ rays, we need to know the emission probability per decay, P_γ, for each in order to determine the activity of ^{57}Co itself. We take these values and the half-life of ^{57}Co from Ref. [1]: they are listed in Table 1. Note that all three of the main transitions in ^{57}Fe convert to some extent, with the 14.41-keV transition having by far the largest conversion coefficient ($\alpha = 8.56$). All three are also populated by electron capture from ^{57}Co. Both processes lead to the production of x rays, so it is important in data analysis to take account of both γ-γ and γ-x-ray coincident summing.

Table 1. Properties required in the analysis (from [1]).

E_γ	P_γ per decay
122.06	0.8551(6)
136.47	0.1071(15)
$T_{1/2}$	271.80(5) d

Our measurements were conducted between 14 – 21 December 2009. All measurements were made with the source-to-detector-face distance of 151 mm, our standard setting at which the original calibration was made. After an initial background measurement, two spectra were obtained sequentially from the ^{57}Co source without the source being moved between measurements. Following that, the source was removed and another background spectrum was taken, after which the ^{57}Co source was replaced in position and a third spectrum recorded. Finally another background was obtained.

Following the ^{57}Co measurements, we measured several spectra with our precisely calibrated ^{60}Co source, originally provided to us by PTB with a certified precision on its activity of 0.06% [2]. This is the source upon which our absolute efficiency calibration is based [3] and we periodically use this source to check that our detector has not changed its properties. The result we obtained from the ^{60}Co source on this occasion yielded an activity that was within 0.11(22) % of the PTB-certified activity. Evidently our detector continues to maintain its calibration.

It can be seen from Fig. 2 that the ^{57}Co spectrum in the energy region between 110 and 150 keV in fact contains six peaks, none of which are in the background spectrum. In addition to the two principal peaks at 122 and 136 keV, there are the corresponding Ge-x-ray-escape peaks at 112 and 126 keV, each being ~0.1 % of the intensity of its associated photopeak, and there are the γ + K x-ray coincident-sum peaks at 128 and 142 keV, the former being ~0.3 % of the 122-keV peak and the latter being ~0.2% of the 136-keV peak. The γ + γ coincident sum of the 122- and 14-keV γ rays of course lies under the 136-keV peak.

We analyzed each of the three ^{57}Co spectra in two different ways: a) we summed all six peaks between 110 and 145 keV and treated the result as a measure of the total activity from the combined 122- and 136-keV γ rays, which have a combined P_γ per decay of 0.9622(16) (see table 1); and b) we analyzed the 122-keV peak and its associated escape and sum peaks independently. The first method requires no

coincident summing correction, while the second requires that the γ + γ coincident sum be calculated and applied. Both methods and all three spectra gave statistically consistent results.
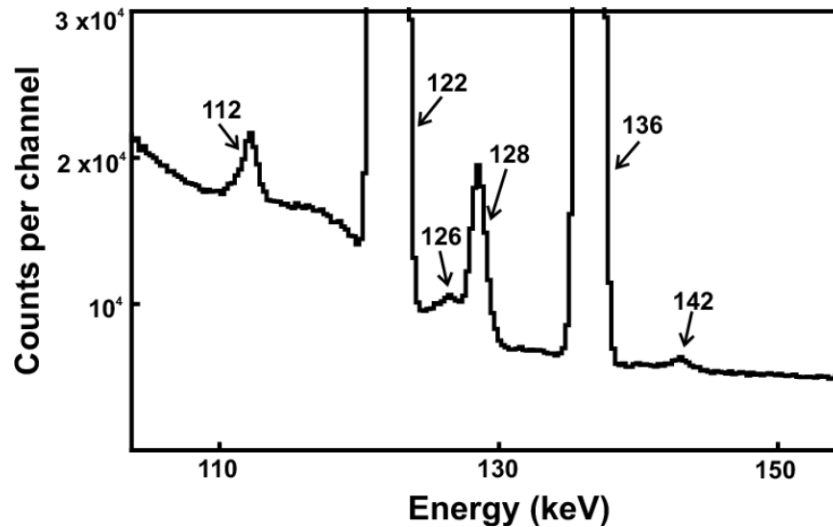
FIG. 2. Portion of the energy spectrum of γ rays from the decay of ^{57}Co in which the vertical scale has been chosen to show the weak peaks clearly. Note that the background sloping up to the left arises from γ rays Compton scattered by the aluminum annulus surrounding the source.

We were asked to provide our activity result extrapolated back to the reference time of 1200 EST 16 October 2009. Our final result for this reference time is 54.60(17) kBq. The uncertainty quoted on the result corresponds to ±0.31% and is made up of contributing factors that are listed in the uncertainty budget given in Table 2.

Table 2. Uncertainty budget for activity measurement for ^{57}Co source **.**

Source	Uncertainty (%)
Counting statistics	0.15
Detector efficiency	0.20
P_γ	0.18
$T_{1/2}$	0.003
Total	0.31

[1] *Update of X Ray and Gamma Ray Decay Data Standards for Detector Calibration and Other Applications, Volume 2,* IAEA, 2007.

[2] E. Schoenfeld, H. Janssen, R. Klein, J.C. Hardy, V. Iacob, M. Sanchez-Vega, H.C. Griffin, and M.A. Ludington, Applied Radiation and Isotopes, **56** (2002) 215.

[3] R.G. Helmer, J.C. Hardy, V.E. Iacob, M. Sanchez-Vega, R.G. Neilson and J. Nelson, Nucl. Instrum. Methods Phys. Res. **A511**, 360 (2003).

United States nuclear data program evaluated nuclear structure data file (ENSDF) at Texas A&M

N. Nica,[1] J. C. Hardy, and B. Singh[2]
[1]*under contract with Brookhaven National Laboratory*
[2]*McMaster University, Hamilton, Ontario, Canada*

This was the fifth year that the Cyclotron Institute at Texas A&M University has been an important participant in the nationwide United States Nuclear Data Program (USNDP). This is a national-interest activity financed by DOE, through which the relevant nuclear-science results in virtually all world publications are retrieved and put together in a large Evaluated Nuclear Structure Data File (ENSDF) database according to so-called *general policies* [1], a set of rules which make possible a standard approach through which the data are uniformly evaluated. The output is published in Nuclear Data Sheets, an Elsevier publication, and also it is disseminated via on-line databases, which can be retrieved at http://www.nndc.bnl.gov. The data are used by both the scientific and applications communities in the US and worldwide.

During these years we have covered essentially all the regions of the periodic table. The superheavy A=252 mass chain and the very data-rich mid-mass chains, A=147 and A=140, were published in past years. Last year we published or had accepted for publication the evaluations of four lighter mass chains: A=97 [2], A=84 [3], A=77 [4] and A=34 [5]. Since nuclear data evaluation depends critically on the experience of the evaluator, with an evaluator typically completing only a couple of mass chains per year, coverage of such a wide range of A chains in such a short time is a considerable accomplishment. This once more testifies to Texas A&M's qualifications to be a national evaluation center.

The studies actually performed in 2009-2010 were as follows: The individual nucleus, ^{84}Y, was evaluated in the framework of an international collaboration [3], which covered the entire $A = 84$ mass chain. The next two mass chains, $A = 77$ and 34, were done entirely by us. The former chain is a rather long one containing 12 nuclei (Ni, Cu, Zn, Ga, Ge, As, Se, Br, Kr, Rb, Sr, Y) with, in total, about 400 references, of which about 20% were more recent than the chain's last full evaluation in 1997. Now, it has about 13,000 ens lines [6], which ranks it among the more data-rich chains, as can be seen from Fig. 1.

The second chain, A=34, is an interesting and complex one. It consists of 11 nuclei (Ne, Na, Mg, Al, Si, P, S, Cl, Ar, K, and Ca) and about 300 references in total, which might make it appear to be a simple case. However, before our evaluation, this mass chain was handled for many years by P. Endt, who periodically published surveys that covered all nuclei in the range A=21-44. The last of these surveys appeared in Nuclear Physics **A633**, 1 (1998) and no more will appear since the author has retired. Unfortunately the format used by Endt was very different from that prescribed for ENSDF so we had to build our new evaluation from scratch, which required an exceptional effort. Furthermore, for the first time in an ENSDF evaluation, we included unbound resonant states in response to a growing interest in

such states by the astrophysics community. In total, there are now 12,000 ens lines of data for the whole A=34 (compared with Fig. 1).
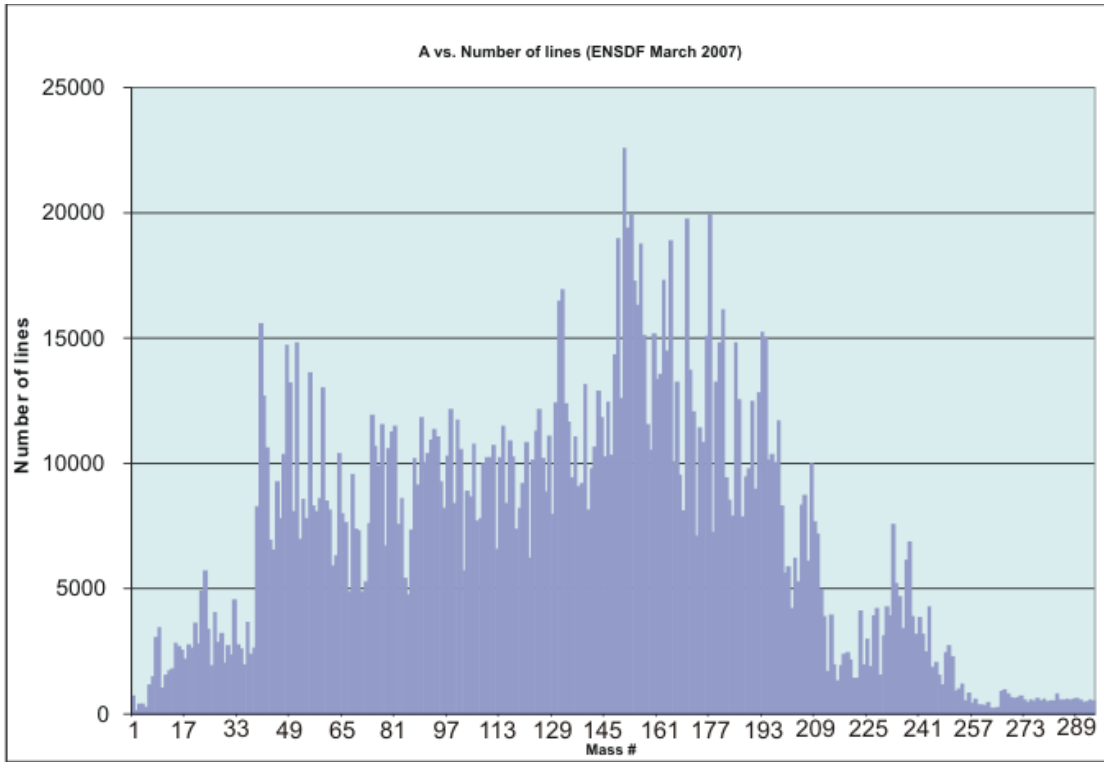
FIG. 1. The number of .ens lines for each mass chain in ENSDF on March 2007.

[1] Nucl. Data Sheets, **111**, p. v-vii, (2010).

[2] N. Nica, Nuclear Data Sheets **111**, 525 (2010).

[3] D. Abriola, M. Bostan, S. Erturk, M. Fadil, M. Galan, S. Juutinen, T. Kibedi, F. Kondev, A. Luca, A. Negret, N. Nica, B. Pfeiffer, B. Singh, A. Sonzogni, J. Timar, J. Tuli, T. Venkova, and K. Zuber, Nucl. Data Sheets **110**, 2815 (2009).

[4] B. Singh and N. Nica, Nucl. Data Sheets (accepted).

[5] N. Nica and B. Singh, Nucl. Data Sheets (accepted).

[6] The files in the ENSDF database are written in a special data format called ens format, and the total number of lines for an A chain is a measure of the amount of data collected for each mass chain.

Improved the half-life of the β+ emitter 31Cl

V. E. Iacob, L. Trache, J. C. Hardy, A. Banu, M. McCleskey, B. Roeder, E. Simmons,
G. Tabacaru, R. E. Tribble, T. Davinson,[1] G. Lotay,[1] P. J. Woods,[1]
A. Saastamoinen,[2] A. Jokinen,[2] and J. Aysto[2]
[1]University of Edinburgh, Edinburgh, United Kingdom
[2]University of Jyvaskyla, Jyvaskyla, Finland

We report here a significant improvement in the accuracy of the measured half-life of the proton-rich nucleus 31Cl, which is important for understanding explosive H-burning in novae. Previous measurements of this half-life [1] were based on the He-jet method and reported the result $t_{1/2} = 150 \pm 25$ ms. Our new value is $t_{1/2} = 189.7 \pm 1.8$ ms.

We produced a 31Cl radioactive beam via the $p(^{32}S,2n)^{31}Cl$ reaction in inverse kinematics: We used a 40-A MeV 32S beam and a cryogenic H_2 target kept at liquid nitrogen temperature and at 2 atm pressure. A >90%-pure 31Cl beam at 34.4-A MeV and with an intensity of up to 3000 pps was separated in the Momentum Achromat Recoil Separator (MARS) [2]. The radioactive beam was extracted in air, and then passed through a thin plastic scintillator, a series of Al degraders, and eventually implanted in the 76-μm-thick mylar tape of our fast tape-transport system (see Ref. [3]). The thickness of the Al degraders was experimentally tuned to optimize the implantation of the 31Cl beam. The measurement was performed in cycles. We collected a sample of 31Cl nuclei for 0.3 s; then the beam was turned off and the collected activity was moved in 60 ms to the center of a 4π proportional gas counter, where the decays were subsequently multiscaled for 10 s. Such collect-move-detect cycles were repeated until the desired
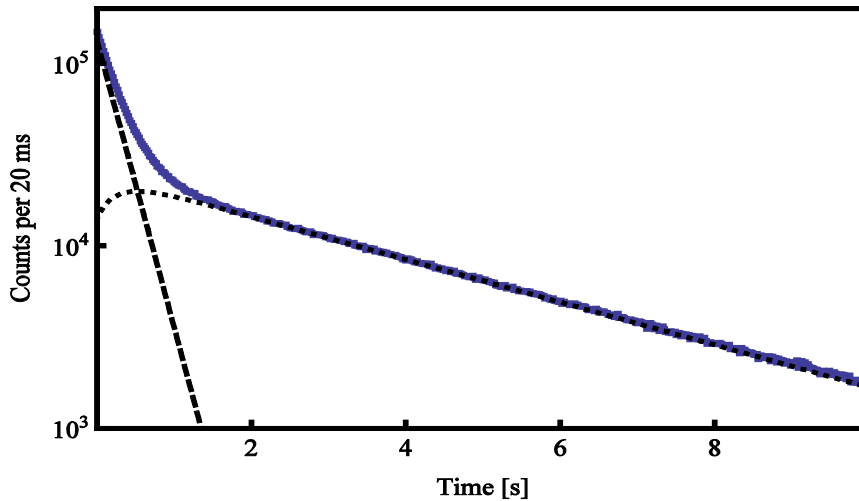
FIG. 1. Measured time-decay spectrum (solid line) for the total of all data obtained from the β+ decay of 31Cl and its daughter 31S. The dotted/dashed lines represent the derived 31Cl/31S contributions.

statistics had been achieved. We collected a total of 6×10^6 β^+ events from the combined decays of ^{31}Cl and ^{31}S. The total decay spectrum is presented in Fig. 1.

While the experimental setup was similar to the one used in Ref. [4], three differences should be noted:

(1) The short half-life of ^{31}Cl required us to reduce the time taken for the tape to move a sample into the detector. Using a close geometry, we were able to reduce our standard move-time of ~180 ms [4] to ~60 ms.

(2) The relatively short cycle time prompted us to use a loop arrangement for the mylar tape rather than the pair of reservoir/take-up tape units that unwind/wind-up the tape in our standard measurements [4]. The loop length was ~40 times longer that the distance moved in a single cycle, thus ensuring that an implanted sample could not possibly reenter the detector in less than ~7 min, ample time for it to have decayed to background level.

(3) The parent nucleus ^{31}Cl decays either by β^+ or β^+p, creating respectively ^{31}S or ^{30}P. Since their half lives are 2.6 s and 2.5 min, respectively, the ^{30}P contribution was indistinguishable from the background.

The electronic scheme used to process the data was identical to the one used in the ^{34}Ar experiment [4]. To allow us to test for possible systematic effects, the experiment was split into 16 separate runs, differing from one another in settings of various electronic parameters: detector bias,
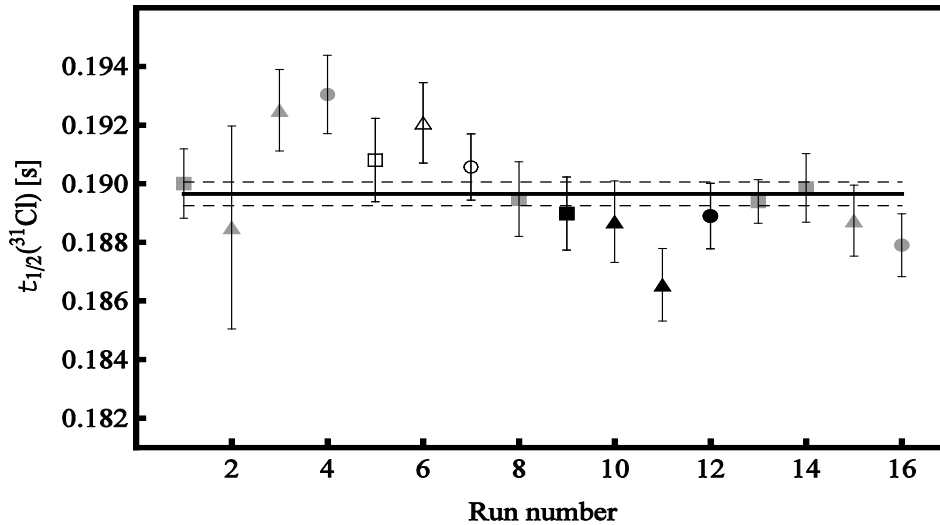
FIG. 2. Test for possible systematic bias in the ^{31}Cl half-life measurement resulting from different settings of the discriminator threshold or detector voltage. Open/grey/black symbols represent the three discriminator settings, 150 mV/200 mV/250 mV; the three detector biases, 2550 V, 2650 V, and 2750 V are represented by the symbol shapes Δ, $\square$, and O, respectively. The average value for the half-life is 189.65±0.40 ms (statistical uncertainty only) with $\chi^2/ndf = 26.2/15$. The average value appears as the solid line, with dashed lines as uncertainty limits.

discriminator threshold and dominant dead-time. As seen in Fig. 2, the half-life results show no systematic dependence on detector bias or discriminator threshold. Although not illustrated, the results were also found to be independent of the imposed circuit dead time.

In contrast with our ^{26}Si measurement [3], for ^{31}Cl decay the contributions of the two decaying nuclei to the total decay spectrum are easily disentangled. This allowed for an unlinked fit of the decay, which is described as the sum of two exponentials plus background:

$$\Lambda_{tot} = C_1 e^{-\lambda_1 t} + C_2 e^{-\lambda_2 t} + B,$$

where four parameters were determined in the least-squares fit: $C_{1,2}$, λ_1 and B. The daughter's decay constant λ_2 was held at the known value of its half life, 2.572±0.013 s [5]. The result of our fit for the ^{31}Cl half-life is $t_{1/2} = 189.65 \pm 0.40$ ms, with statistical uncertainty only. If we now include systematic uncertainties our final result is $t_{1/2} = 189.7 \pm 1.8$ ms. The complete error budget is detailed in Table I.

TABLE I. Error budget for the ^{31}Cl half life.

Contribution	Value [ms]
Statistics	0.40
$t_{1/2}(^{31}\text{S})$	0.71
Impurity ^{30}S	0.16
Impurity ^{28}P	1.61
Total	*1.81*

While the unlinked fit just described was the best option in this case since it did not limit the precision of the result, the linked parent-daughter procedure described in [2,3] can also be applied although it is essential to take account of the ^{31}Cl decay branches that go by β-delayed proton emission, thus bypassing the ^{31}S daughter. In effect, this means that the linked fit can be used to extract the magnitude of the total proton branching ratio, for which we obtain 8±1%.

[1] J. Äysto *et al.*, Phys. Lett. B **110**, 437 (1982).

[2] R.E. Tribble, A. Azhari, C.A. Gagliardi, J.C. Hardy, A. Mukhamedzhanov, X. Tang, L. Trache and S.J. Yennello, Nucl. Phys. **A701,** 278 (2002).

[3] V.E. Iacob, J.C. Hardy, A. Banu, L. Chen, V.V. Golovko, J. Goodwin, V. Horvat, N. Nica, H.I. Park, L. Trache and R.E. Tribble, *Progress in Research*, Cyclotron Institute, Texas A&M University (2009-2010), p. I-5.

[4] V.E. Iacob, J.C. Hardy, J.F. Brinkley, C.A. Gagliardi, V.E. Mayes, N. Nica, M. Sanchez-Vega, G. Tabacaru, L. Trache and R.E. Tribble, Phys. Rev. C **74,** 055502 (2006).

[5] http://www.nndc.bnl.gov/

Neutron-transfer and elastic scattering with ^{26}Mg

M. McCleskey, A. A. Alharbi, A. Banu, V. Z. Goldberg, B. T. Roeder, E. N. Simmons,
A. Spiridon, L. Trache, and R. E. Tribble

The one neutron transfer and elastic scattering of ^{26}Mg was studied using a 12 MeV/nucleon beam and the MDM spectrometer. The motivation is two fold. First, we use the transfer ^{13}C(^{26}Mg,^{27}Mg)^{12}C to obtain the ANC of ^{27}Mg and from it that of ^{27}P through mirror symmetry, which will allow the direct component of the radiative proton capture on ^{26}Si at stellar energies to be estimated. The second is to add to the systematics of elastic scattering data with *sd*-shell projectiles in this energy region.

^{26}Al, through its β-decay to the 2+ excited state ^{26}Mg and the subsequent decay into the ground state (0+) via a 1.809 MeV γ-ray, is an important observable for many astrophysical events, and many efforts have been put forth to map the Galaxy by means of this γ-ray [1]. It is therefore of great interest to understand the nucleosynthesis of ^{26}Al within the various astrophysical environments in which it is produced, including supernovae, novae, Wolf-Rayet stars and red giants. The nucleosynthesis of ^{26}Al is complicated by the presence of a low-lying (228.3 keV) 0+ isomeric state. This isomeric state is very strongly inhibited from decaying by γ-ray emission to the ground state (5+) of ^{26}Al due to the large spin difference. Its lifetime is much shorter (6.345 sec) and it β-decays directly to the ground state of ^{26}Mg through a super-allowed 0+ to 0+ transition, thus avoiding the observable 1.809 MeV γ-ray of interest. However, at high temperatures (T_9= 0.4 [2]) equilibrium is reached between ^{26gs}Al and ^{26m}Al which is relevant to some high temperature astrophysical events such as novae. The rate of the ^{26}Si(p,γ)^{27}P reaction is important because it depletes ^{26}Si that would otherwise be available to β$^+$ decay into the isomeric state of ^{26}Al.

Because of its short lifetime it is not possible to make a target of ^{26}Si that could then be bombarded by protons. Even if such a target could be made, the experiment could not be reasonably done in a terrestrial laboratory at astrophysical energies due to the Coulomb repulsion and the very small cross sections that result. The reaction in inverse kinematics would also be difficult due to the proton target, the radioactive ^{26}Si beam and the problem with the Coulomb repulsion. These difficulties indicate an indirect approach to the experimental problem. The ^{26}Si(p,γ)^{27}P reaction has been suggested [3] as a candidate to be studied by means of the relevant mirror nucleus, ^{27}Mg. The astrophysical reaction rate for the ^{26}Si(p,γ)^{27}P reaction can be determined from the ANC of ^{27}P which in turn can be determined by first finding the ANC of the mirror nucleus ^{27}Mg and then using charge symmetry considerations to extract that of ^{27}P (see [4]).

To find the ANC for ^{27}Mg, a ^{26}Mg beam was used on a thin (100 μg/cm^2) ^{13}C target and both elastic scattering and ^{13}C(^{26}Mg,^{27}Mg)^{12}C single neutron transfer were measured. The 12 MeV/nucleon ^{26}Mg beam was accelerated by the K500 superconducting cyclotron at Texas A&M University, and was delivered through the Beam Analysis System (BAS) and onto the ^{13}C target. Reaction products were separated using the Multipole-Dipole-Multipole (MDM) spectrometer and were observed by means of the Oxford detector. The Oxford detector consists of an ionization chamber filled with isobutene, with

two anode plates to measure energy loss in the gas, four position-sensitive avalanche counters (ACs) to measure the position and angle in the detector, and a plastic scintillator in which the reaction products stop and their residual energy is measured by means of two phototubes.
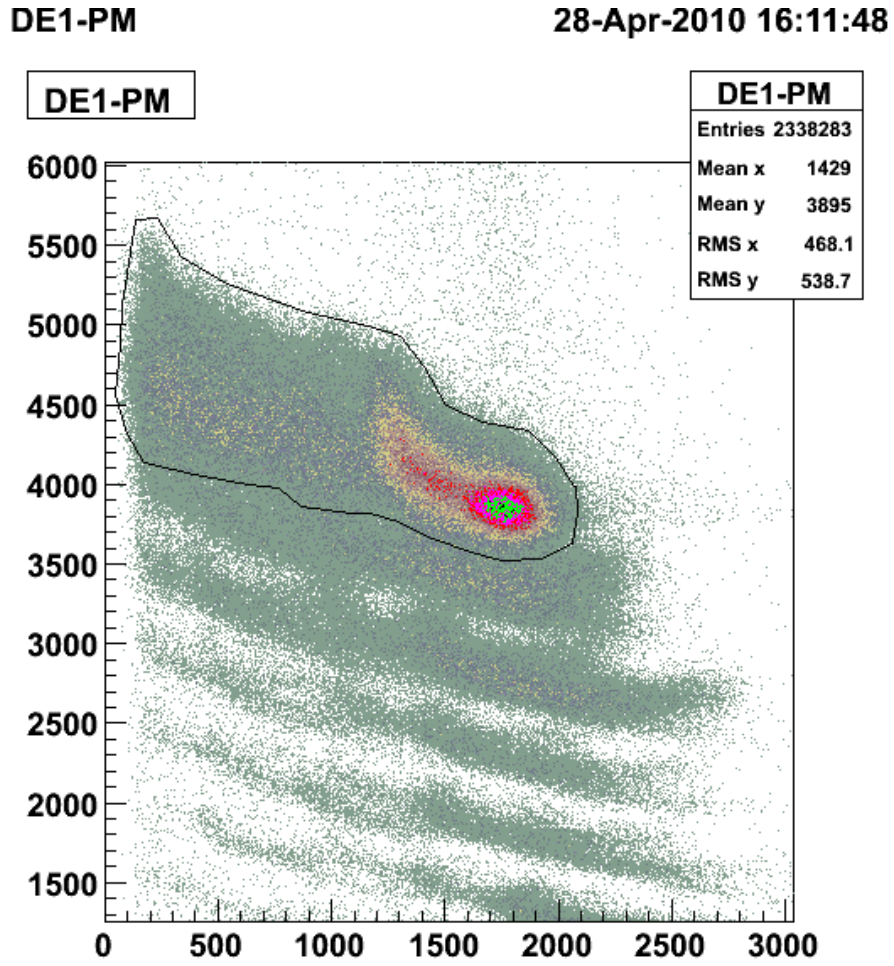
FIG. 1. ΔE-E_{res} measured with the MDM spectrometer centered at 6 deg.

As we go to increasingly higher masses, isotope identification with the detector becomes more difficult. In an attempt to reduce noise, this experiment was performed using a new electronics setup with all signal processing and recording electronics in the cave, utilizing CAEN 16ch shaper-amplifier modules and Mesytec VME ADCs. Particle identification was made in two steps. First, as Z separation is still good, Mg was selected using a polygon condition applied to a ΔE-E_{res} histogram [Fig. 1]. Next the isotopes of Mg (^{26}Mg and ^{27}Mg for the elastics and transfer respectively) were found to be well separated in a plot of their position in the focal plane vs. their residual energy [Fig. 2]. The focal plane position of the individual isotopes was then plotted as a function of the reconstructed target angle from which the angular distributions were obtained. Angular distributions for the ground state and first excited state for

^{26}Mg were measured from 2 to 14° in the laboratory frame, while distributions for the single neutron transfer to the ground state and first excited states of ^{27}Mg were measured from 2° to 11° lab.
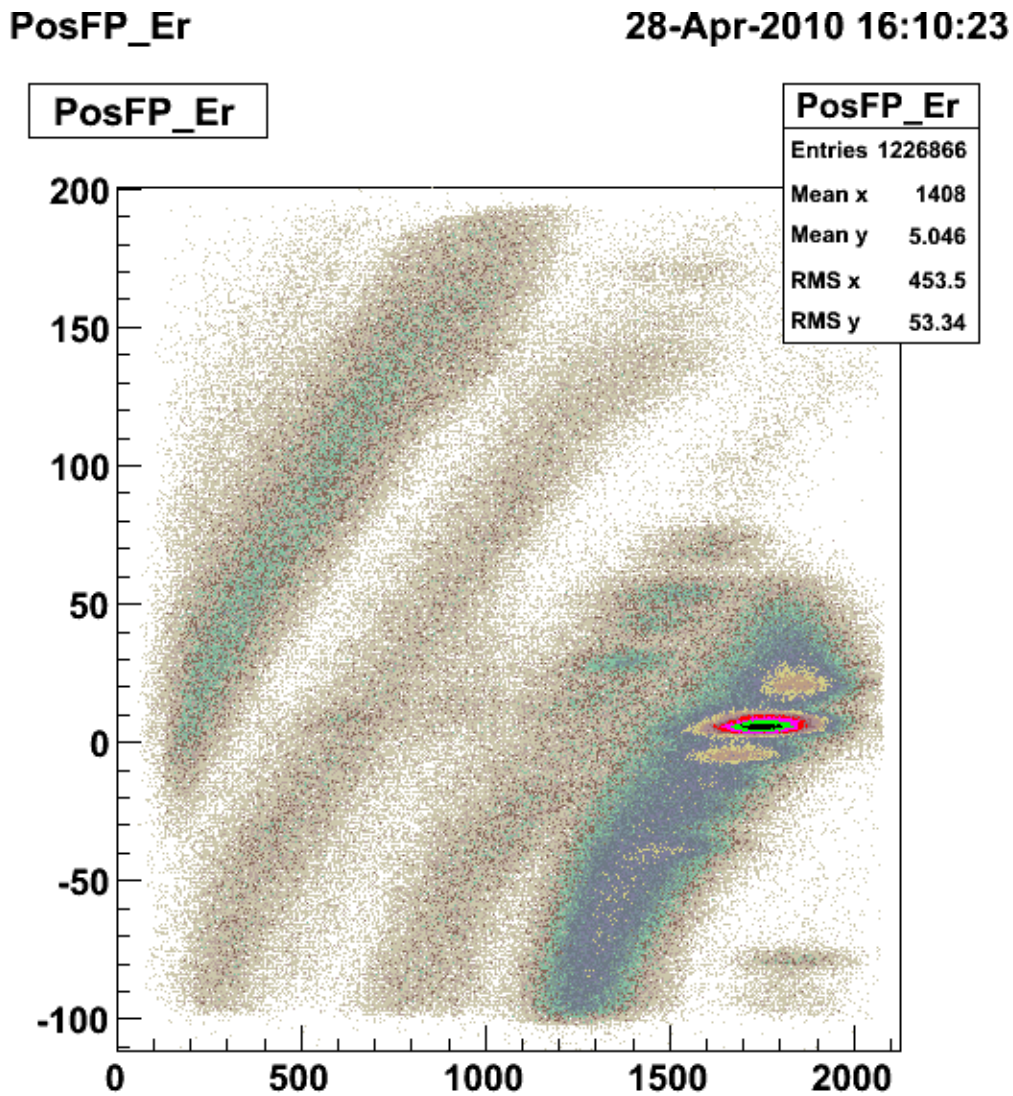
FIG. 2. Separation of Mg isotopes in a focal plane position vs. E_{res} histogram.

Work is currently underway to fit the elastic angular distribution starting from optical model potentials obtained by the double folding procedure of Ref. [5]. The optical model parameters found for the elastic scattering will be applied to the entrance and exit channels in DWBA calculations of the one neutron transfer. Preliminary angular distributions are shown in Fig. 3.
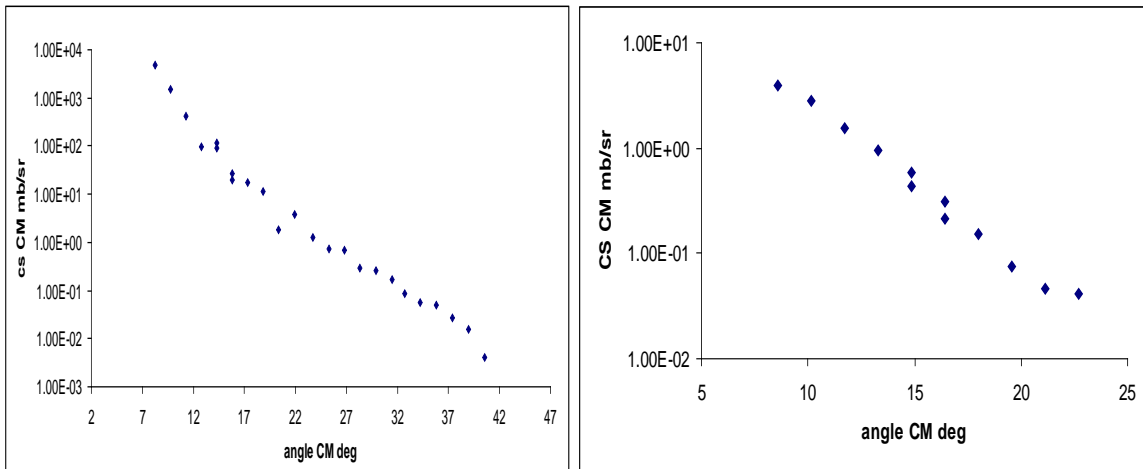
FIG. 3. On the left is the measured angular distribution for the elastic scattering of ^{26}Mg on ^{13}C. On the right is the angular distribution for the transfer reaction ^{13}C(^{26}Mg, ^{27}Mg) ^{12}C.

[1] N. Prantzos and R. Diehl, Phys. Rep. **267**, 1 (1996).

[2] A. Coc, M.-G. Porquet, and F. Nowacki, Phys. Rev. C **61**, 015801 (1999).

[3] R.E. Tribble, private communication.

[4] N.K. Timofeyuk, *Deducing Stellar Reaction Rates from Mirror Nuclear Decays*, Nuclear Physics News, Vol. **19**, No. 2

[5] F. Carstoiu *et al.*, Phys. Rev. C **70**, 054610 (2004).

First observation of ^{14}F

V. Z. Goldberg, B. T. Roeder, G. G. Chubarian, A. A. Alharbi, A. Banu, M. McCleskey,
E. Simmons. G. Tabacaru, L. Trache, R. E. Tribble, G. V. Rogachev,[1]
E. Johnson,[1] M. L. Avila,[1] J. P. Mitchell,[1] and C. Fu[2]

[1]*Department of Physics, Florida State University, Tallahassee, Florida 32306,*

[2]*Indiana University, Bloomington, Indiana 47408*

In an experiment conducted at the Cyclotron Institute at Texas A&M University in March-April 2009, the resonant elastic scattering of ^{13}O+p was studied with the Thick Target Inverse Kinematics (TTIK) method [1] to observe states in ^{14}F. ^{14}F is expected to be unbound to proton decay (as are ^{15,16}F). A rare beam of ^{13}O with intensity of 5 x 10^3 pps was produced for the experiment in the ^{1}H(^{14}N,^{13}O)2n reaction and was separated using MARS. Further details about the production of the ^{13}O beam and the experimental setup can be found in [2,3] as well as in the TAMU annual report for 2009.

Fig. 1 presents the excitation functions for the ^{13}O+p elastic scattering obtained in the measurement as compared with R-Matrix calculations. The top panel displays the data for ^{13}O+p where a
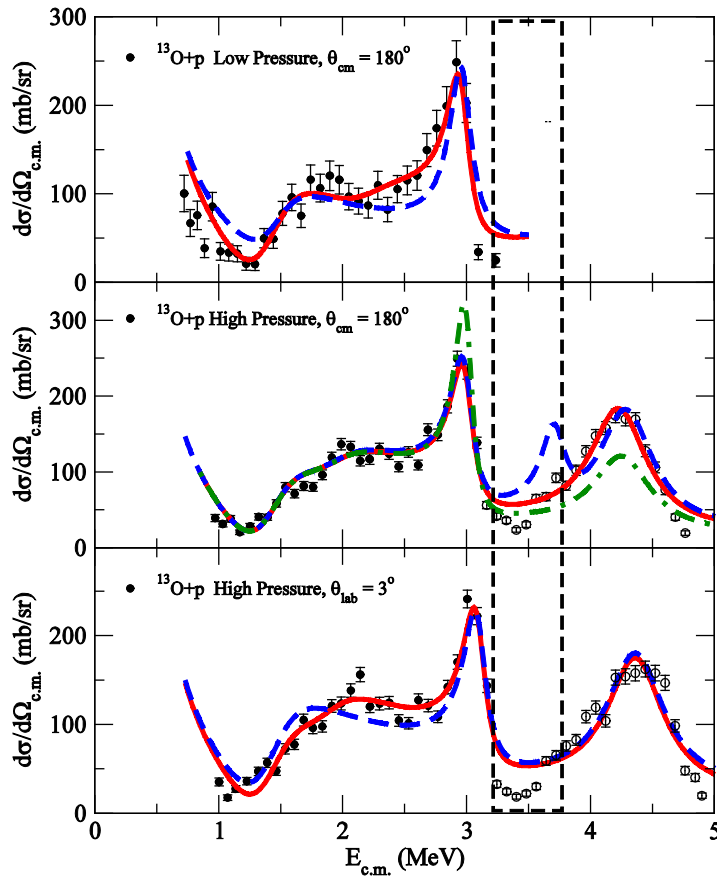
FIG. 1. Excitation functions for the ^{13}O+p elastic scattering compared with R-Matrix calculations. See text for further explanation.

lower CH$_4$ pressure (930 mbar) was used for the gas in the scattering chamber at θ_{cm} = 180° (θ_{lab} = 0°). These measurements allowed for better observation of the low energy part of the excitation function that was found to be related to the position of the ^{14}F ground state. The best fit to the data in the region between 0.7 MeV < E$_{cm}$ < 2.5 MeV was observed when the ground state of ^{14}F was assumed to have J^π = 2$^-$. The assumption of a 2$^-$ ground state agrees with the ab-initio [4] and shell model predictions [5], as well as the data from the mirror nucleus ^{14}B [6] (see figure 2). By contrast, a 1$^-$ ground state would be too weak to provide for the deep minimum in the excitation function at E$_{cm}$ ≈1.2 MeV as shown by the dashed line in Fig. 1.

Data from the ^{13}O+p measurements at higher CH$_4$ pressure (1040 mbar) are presented at θ_{cm} = 180° (θ_{lab} = 0°) in the middle panel of figure 1 and at θ_{lab} = 3° in the bottom panel of Fig. 1. At higher gas pressures, it was possible to obtain data for the ^{13}O+p excitation function up to E$_{cm}$≈ 5 MeV. The best overall fit to the data was obtained with the level scheme and resonance widths listed in Table I (as shown by the solid line in each plot). However, other values for the spins of these states were considered. First, as shown in the bottom panel, a 1$^-$ excited state at 2.1±1.7 MeV was added. This level, while not immediately obvious in an inspection by eye, is suggested by the *ab-initio* [4] and shell model calculations [5], and data from ^{14}B. The inclusion of this level improves the fit to the data by≈40% in χ^2 versus the exclusion of this level in the calculation. Including a state with higher spin (l >0) would produce a peak in this region that is too narrow to fit the data. Next, the peaks at E$_{cm}$ = 3 MeV and 4.3 MeV were considered (middle panel, figure 1). These peaks were fit by *d*-wave resonances (l=2) with large reduced widths and with spins 3$^-$ and 4$^-$ respectively. As shown by the dot-dashed line, exchanging the 3$^-$ and 4$^-$ spins in the R-matrix calculation results in a cross section that is too high for 3 MeV resonance and a cross section that is too low for the 4.3 MeV peak.

TABLE 1. Levels in ^{14}F.

E* (MeV)	J^π	Γ (keV)	Γ/Γ_{sp}
1.56±0.04	2$^-$	910±100	0.85
2.1±0.17	1$^-$	~ 1000	0.6
3.05±0.60	3$^-$	210±40	0.55
4.35±0.10	4$^-$	550±100	0.5

It should be noted that the region of the excitation function shown between 3.12 MeV < E$_{cm}$ < 3.6 MeV (as illustrated by the dashed box in Fig. 1) is distorted due to a thin dead layer in the back of the front Si detectors and to signals in the back (veto) Si detectors that were below the electronics threshold. As a result of this distortion, a resonance in this region would not be observed in our measurements. The shell model calculations and comparison with ^{14}B both predict a second 2$^-$ state in ^{14}F between the 3$^-$ and the 4$^-$. A calculation with this state included is shown in the dashed-line of the middle panel of Fig. 1. While the current data suggests that this resonance is not there, the calculation shows that its presence does not distort the other states in the excitation function. A future measurement with thicker Si detectors could better determine the parameters for this region of the excitation function.

The level scheme for ^{14}F as compared with the *ab-initio* [4] and shell model calculations [5], as well as the ^{14}B level scheme [6] is shown in Fig. 2. The experiment showed that ^{14}F was unstable to proton decay by 1.56 MeV. The measured level scheme and the separation of the states are in reasonable agreement with the *ab-initio* calculations and ^{14}B. However, the *ab-initio* calculations [4] and other previous predictions for ^{14}F [7,8] expected it to be unstable to proton decay by ~3 MeV. While new calculations are needed to specify the necessary corrections to the theoretical calculations, part of the disagreement between the predictions and the present work should be related with the Thomas-Ehrman
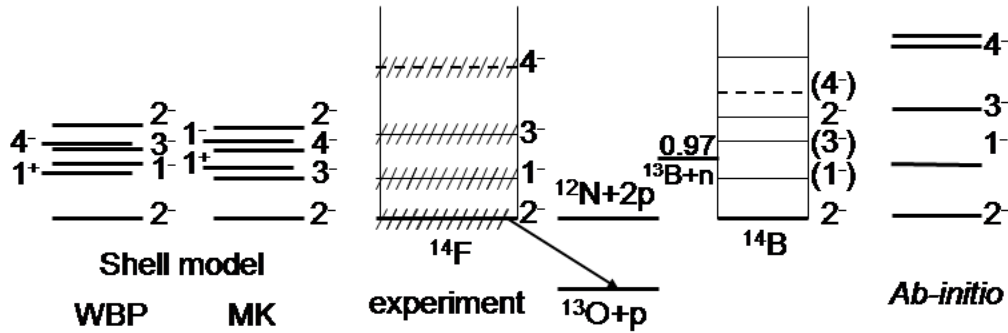
FIG. 2. Level scheme for ^{14}F compared with ab-initio calculations [1], shell model calculations [5], and the ^{14}B level scheme.

shift [9,10] and the single-particle structure of the states measured in ^{14}F (as determined in the R-Matrix calculations). A detailed discussion of this difference can be found in the upcoming paper [2]. It also should be noted that the shell model calculations produce a much more compressed level scheme than the measured data and the *ab-initio* calculations. This could indicate that the residual interactions should be modified to provide for a better description of nuclei beyond the proton dripline.

In summary, data for the previously unknown ^{14}F nucleus were measured with the ^{13}O+p reaction using the TTIK. The ground state and low-lying excited states were observed, and their spins and parities were determined by comparison with R-Matrix calculations. It is worthwhile to note that these measurements were made with a ^{13}O beam of relatively weak intensity (5 x 10^3 p/s) and initial energy of 31 MeV/u degraded to 11 MeV/u. Such an experimental approach should be useful in future measurements where a very rare beam with a short lifetime is needed at low energy.

[1] K.P. Artemov *et al.*, Sov. J. Nucl. Phys. **52**, 408 (1990).
[2] V.Z. Goldberg *et al.*, Phys. Lett. B (submitted).
[3] V.Z. Goldberg *et al.*, Phys. Rev. C **69**, 031302(R) (2004).
[4] P. Maris, A.M. Shirokov, and J.P. Vary, Phys. Rev. C **81**, 021301(R) (2010).
[5] A. Volya, Phys. Rev. C **79**, 044308 (2009).

[6] G.C. Ball *et al.*, Phys. Rev. Lett. **31**, 395 (1973).

[7] F. Ajzenberg-Selove, Nucl. Phys. **A564**, 1 (1993).

[8] M.S. Antony, J. Britz and A. Pape, At. Data Nucl. Data Tables **34**, 279 (1986).

[9] R.G. Thomas, Phys. Rev. **81**, 148 (1951).

[10] J.B. Ehrman, Phys. Rev. **81**, 412 (1951).

"Complete spectroscopy" of ^{31}S for nuclear astrophysics

L. Trache, V. E. Iacob, A. Banu, R. E. Tribble, P. J. Woods,[1] G. Lotay,[1] A. Saastamoinen,[2] D. Bucurescu,[3] N. V. Zamfir,[3] N. Marginean,[3] R. Marginean,[3] A. Negret,[3] D. Ghita,[3] and D. Filipescu[3]

[1]*Univ of Edinburgh, Edinburgh, United Kingdom,*
[2]*University of Jyvaskyla, Jyvaskyla, Finland*
[3]*IFIN-HH Bucharest, Romania*

Classical novae are relatively common events in our Galaxy, and a few per year are actually detected and studied. Space-based gamma-ray telescopes look for discrete gamma-ray lines that may give information about the nuclear processes occurring in these explosive H-burning events. There is considerable progress in the understanding of their dynamics, but there are many problems to solve before we can assess their contribution to the chemical evolution of the Galaxy. Novae are anticipated to become the first type of explosive cosmic events where all nuclear data for nucleosynthesis can be based on experimental data [1]. However, we are still far from reaching that goal. The groups at Texas A&M University, the University of Edinburgh and University of Jyvaskyla are engaged, separately or in collaboration, to the study of reactions occurring in novae. Among the key reactions for which the reaction rates are only known with large uncertainties is the radiative proton capture ^{30}P(p,γ)^{31}S. The reaction rate is dominated by capture through low-energy proton resonances, which correspond to excited states in ^{31}S nuclei. Considerable efforts are made to find these resonances and to determine their parameters (position and resonance strength) by direct or indirect methods, with no conclusive results so far. This leads to an uncertainty of a factor of about 100 in the astrophysical reaction rate [2].

In continuation of our efforts to identify and study the decay of these low spin excited states in ^{31}S, states that are also populated through the β-decay of ^{31}Cl [3] and which may be astrophysically relevant, we proposed the study of states in ^{31}S at excitation energies up to about 7 MeV using gamma-ray spectroscopy methods and the beam from the tandem accelerator of IFIN-HH Bucharest. We were particularly interested in locating and determining the decay paths of the low spin, positive parity states $(1/2^{+}, 3/2^{+}, …)$ in the excitation energy window E=6.1-7.0 MeV. We proposed to use a so called "complete spectroscopy" measurement, detecting γ-rays from the reaction ^{28}Si(α,nγ)^{31}S. This would include a γ-γ coincidence measurement at about the highest energy (24 MeV) using the Ge array of IFIN-HH and an excitation function at projectile energies E_{α}=15-25 MeV. The experiment was approved early in the spring of 2009 and was successfully conducted in summer.

Among the latest efforts is a series of measurements of β-γ and β-delayed proton decay of ^{31}Cl [3] made by the authors of the proposal from Texas A&M University, the University of Edinburgh and the University of Jyvaskyla. Beta-decay of ^{31}Cl populates states in ^{31}S and those above the proton binding energy Sp=6.133 MeV represent the resonances sought above. However, the rich (preliminary) level scheme was established from β-γ decay without gamma-gamma coincidences. The measurements proposed would complement the ones already made; support the decay scheme and the spin/parity assignments. They will assure a precise determination of the energy of the resonances sought and,

hopefully, their spins and parities. The new data will complement also information we have from other studies, including transfer reactions and HI induced gamma-ray studies.

In the early 80's the group of P. von Brentano in Cologne has shown that (α,n) reactions at relatively low bombarding energy from their tandem accelerator can be used to populate non-selectively low-to-medium spin states in nuclei and that standard gamma-ray spectroscopy techniques can be used to determine their decay scheme and spin/parity. The technique was dubbed "complete spectroscopy" for its non-selective population of states and was used later in several places, including at the Bucharest tandem [4].

In this experiment we have measured so far γ-γ and n-γ coincidences at E_α=24 MeV on a Si target. The natural Si target was prepared for us by the people at Micron Semiconductor Ltd, UK, from a Si wafer etched down to 20 μm and backed by layers of W (0.9 mm) and Ti (0.1 mm) to stop the recoiling residual nuclei. The un-reacted beam was stopped further downstream in a Faraday cup. We have used the Ge detector array of DFN Bucharest in its maximal configuration (of 2009) (see Fig. 1): seven HPGe detectors and one neutron detector and the associated acquisition system. The neutron detection was useful for channel identification.
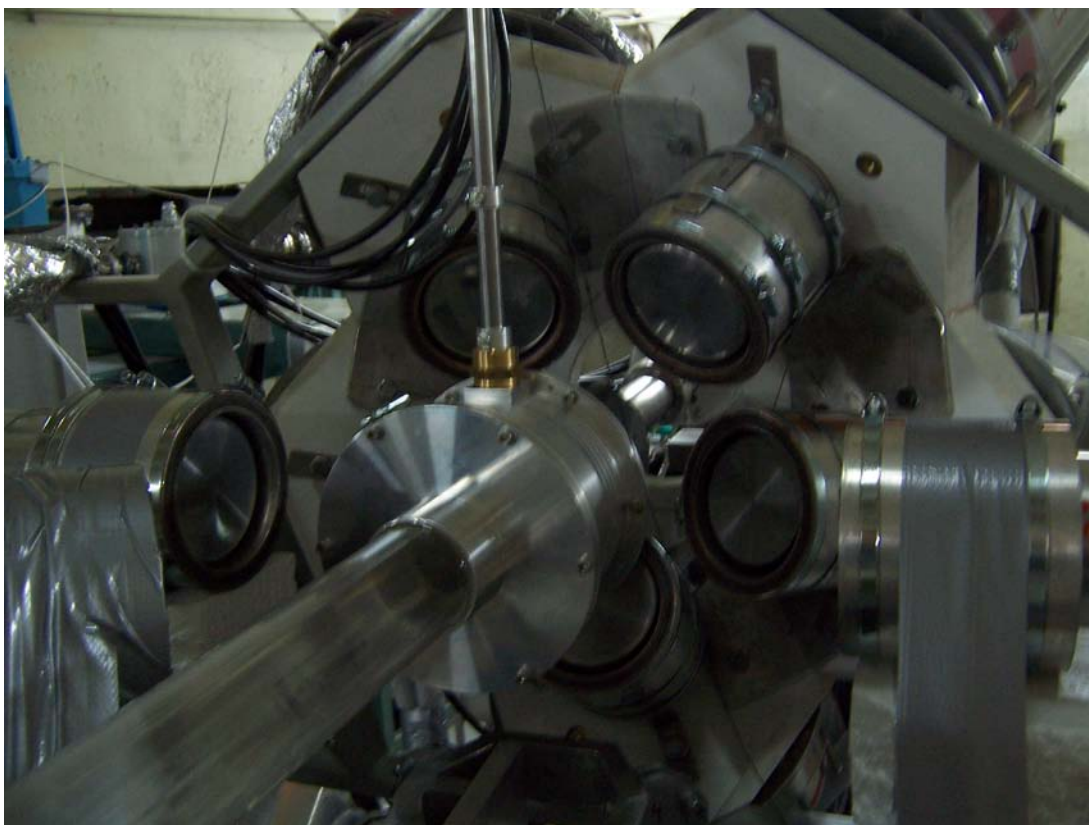
FIG. 1. The Ge detector array of DFN Bucharest. The quartz tube (front, left) was used to stop the beam away from the target position. The cylinder at right is the NE213 neutron detector.

The results were only partially analyzed in and show that the strongest channel was ^{28}Si(α,p) populating states in the mirror nucleus ^{31}P. These are going to be also useful, as we will be able to get more information about those states and use mirror symmetry to find information about the structure of corresponding states in ^{31}S. A large number of lines have Doppler affected shapes that will allow us to determine their lifetimes in the fs range (see Fig. 2).

Beam intensities of around 1 pnA alpha particles of excellent stability from the newly refurbished FN tandem in Bucharest were used in one week of beam time.
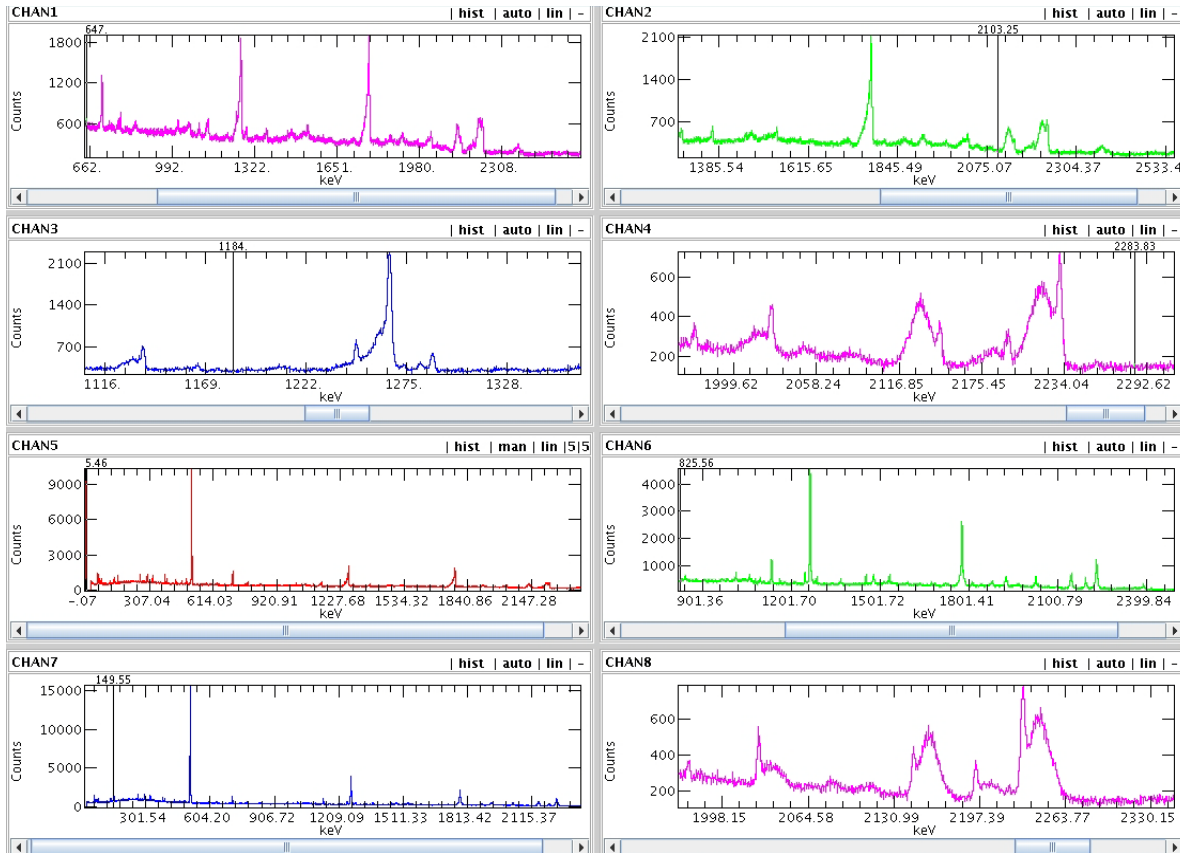
FIG. 2. Spectra from the online analysis. Lines affected by Doppler broadening are clearly visible in a number of detectors (panels 4 and 8), forward or backward oriented.

[1] C. Iliadis *et al.*, Ap. J. **142s**, 150 (2002); J. Jose, M. Hernandez, and C. Iliadis, Nucl. Phys. **A777**, 550 (2006).

[2] A. Coc, in *Origin of Matter and Evolution of Galaxies (OMEGA07)*, AIP Conference Proceedings **1016**, 119 (2008).

[3] L. Trache, A. Banu, J.C. Hardy, V.E. Iacob, M. McCleskey, E. Simmons, G. Tabacaru, R.E. Tribble, J. Aysto, A. Jokinen, A. Saastamoinen, M.A. Bentley, D. Jenkins, T. Davinson, P.J. Woods, N.L. Achouri, and B. Roeder, in P*roc. 10th Symposium Nuclei in Cosmos,* Mackinac Isl, MI, USA, 27 July – 1 Aug. 2008, and http://pos.sissa.it//archive/conferences/053/163/NIC%20X_163.pdf

[4] L. Trache *et al.*, Phys. Rev. C **40**, 1006 (1989).

Use of neutron transfer reactions to indirectly determine neutron capture cross sections on neutron-rich nuclei

M. McCleskey, A. M. Mukhamedzhanov, V. Goldberg, R. E. Tribble, E. Simmons, A. Spiridon,
A. Banu, B. Roeder, L. Trache, X. Chen,[*] and Y. -W. Lui

Cross sections for the capture of low-energy neutrons on unstable neutron-rich nuclei are important for nuclear science and their reliable knowledge is increasingly requested by nuclear astrophysics to test quantitatively the nucleosynthesis in the r-process, by nuclear engineering for the design of new reactors using novel fuel cycles, and by national security. It is difficult, and in many cases impossible, to make direct measurements for all the reactions for which good cross sections are needed. We must build systematics, make structure and reaction models, and use indirect approaches. One such approach proposed was to combine several neutron transfer reactions at different laboratory energies to extract information that can be used to determine reliably neutron capture cross sections at low energies [1].

The radiative neutron capture reaction $^{14}C(n,\gamma)^{15}C$ is being used as a test case for such an indirect determination. Our approach intends to combine information from the peripheral reaction of 12 MeV/nucleon ^{14}C on a thin ^{13}C target and the non-peripheral reaction of 60 MeV deuterons on a thin ^{14}C target, both populating the same states in neutron-rich nucleus ^{15}C. From the $^{13}C(^{14}C,^{15}C)^{12}C$ experiment we will determine the asymptotic normalization coefficient (ANC) and we will use the non-peripheral (d,p) reaction on ^{14}C to obtain the spectroscopic factor (SF) which will then be used to calculate the direct radiative capture to the ground state of ^{15}C, at astrophysical energies.

Unlike proton capture at astrophysical energies, neutron capture is not an entirely peripheral process. As such, there will be a contribution from the interior of the nucleus when computing the transition matrix element:

$$\sigma_{(n,\gamma)} = SF \left| \langle \Phi_{B=(An)} | O_{elm} | \Phi_A \chi_n^{(+)} \rangle \right|^2$$

$$= SF \left| M_< + M_> \right|^2 = \left| (SF)^{1/2} M_< + C_{nlj} \left(M_> / b_{nlj} \right) \right|^2 \qquad (1)$$

The overlap integral $<\Phi_B/\Phi_A>$ in the exterior region behaves as $b_{nlj}h_l(ikr)$ where h_l is a Hankel function and the normalization factor b_{nlj} is the single particle ANC. Therefore,

$$M_> \approx b_{nlj} \langle h_l(i\kappa r) | O_{elm} | \chi_n^{(+)} \rangle$$

and for the correct evaluation of the second term in Eq. (1), the knowledge of the ANC (Cnlj) extracted from peripheral reactions is sufficient, but for the evaluation of the first one an unambiguous determination of the SF and of the overlap integral in the interior of the nucleus are also needed. For a

---

peripheral reaction like (p, γ), the ANC would be all that is needed, however we will also have to consider the contribution from the interior for a (n,γ) reaction. Information to assess it can be extracted from a combination of neutron transfer reactions.

Both $^{13}C(^{14}C,^{15}C)^{12}C$ at 12 MeV/nucleon and $^{14}C(d,p)^{15}C$ at 30 MeV/nucleon have been measured at Texas A&M. The beams were accelerated by the K500 super-conducting cyclotron and reaction products were measured using the MDM high-resolution spectrometer.

THE ^{14}C+^{13}C EXPERIMENT

Initially performed in September of 2007, this experiment was done using a thin (100 μg/cm2) ^{13}C target and a ^{14}C beam at 12 MeV/nucleon. Elastic scattering and single neutron transfer $^{13}C(^{14}C,^{15}C)^{12}C$ were measured simultaneously. A significant angular shift was present, however, and this made it impossible to have a meaningful fit to optical model calculation for the elastic scattering at forward angles where the cross section is rapidly changing as a function of the scattering angle. To resolve this and to also improve the angular distribution for the transfer reaction, the experiment was repeated in May of 2009, and the preliminary results of this new experiment are presented here.
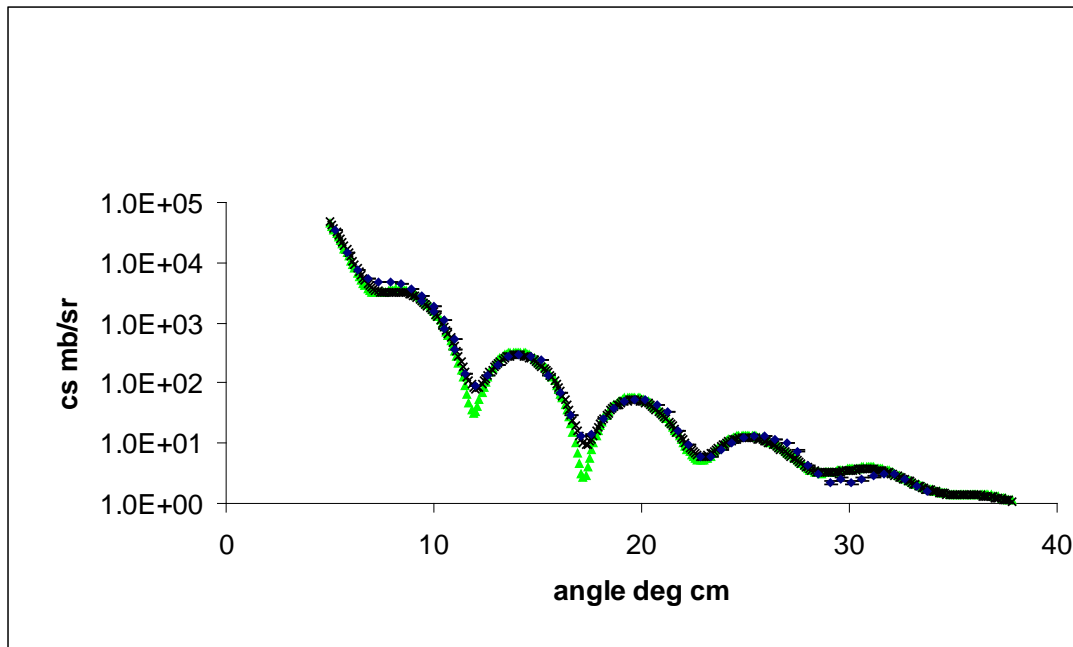
FIG. 1. Elastic scattering angular distribution of 12MeV/nucleon ^{14}C on ^{13}C. The diamonds are the measured elastic scattering with statistical error bars shown; the triangles are the calculation made using an optical model potential and a double folding procedure; the X's are the same calculation but smoothed using a Gaussian smearing function.

The elastic scattering cross section is compared in Fig. 1 with that calculated with an optical model potential (OMP) obtained from a semi-microscopic double folding procedure using the JLM effective interaction. The OMP parameters (renormalizations and ranges) N_V=0.45, N_w=0.90, t_V=1.2 fm and t_w=1.75 fm were those from the general procedure established earlier from the study of elastic

scattering of loosely bound p-shell nuclei [2,3]. The overall agreement is good; in particular, the position of the minima and maxima, the oscillation period and the trend of the absorption are reproduced, therefore no further optimization was attempted at this stage. Then, the surface region of this potential was fitted with a Woods-Saxon potential, which was used to perform a DWBA calculation of the neutron transfer $1p_{1/2} \rightarrow 2s_{1/2}$ using the PTOLEMY code. The normalization of the DWBA calculated cross section to the experimental measurement (Fig. 2) gives the spectroscopic factor which combined with the calculated single particle ANC and the previously measured ANC for ^{13}C [3] will give us the ANC for ^{15}C.

$$\frac{d\sigma}{d\Omega}_{exp} = SF(^{13}C,1p_{1/2}) \cdot SF(^{15}C,2s_{1/2}) \frac{d\sigma}{d\Omega}_{DWBA}$$

$$C^2 = SF \cdot b^2$$

We found $C^2(2s_{1/2}) = 2.08$ +/-? fm^{-1} (this value is still preliminary). The $J^{\pi}=5/2+$ first excited state at E*= 740 keV was also populated, and we could determine the ANC for both states. Analysis of this experiment is ongoing.
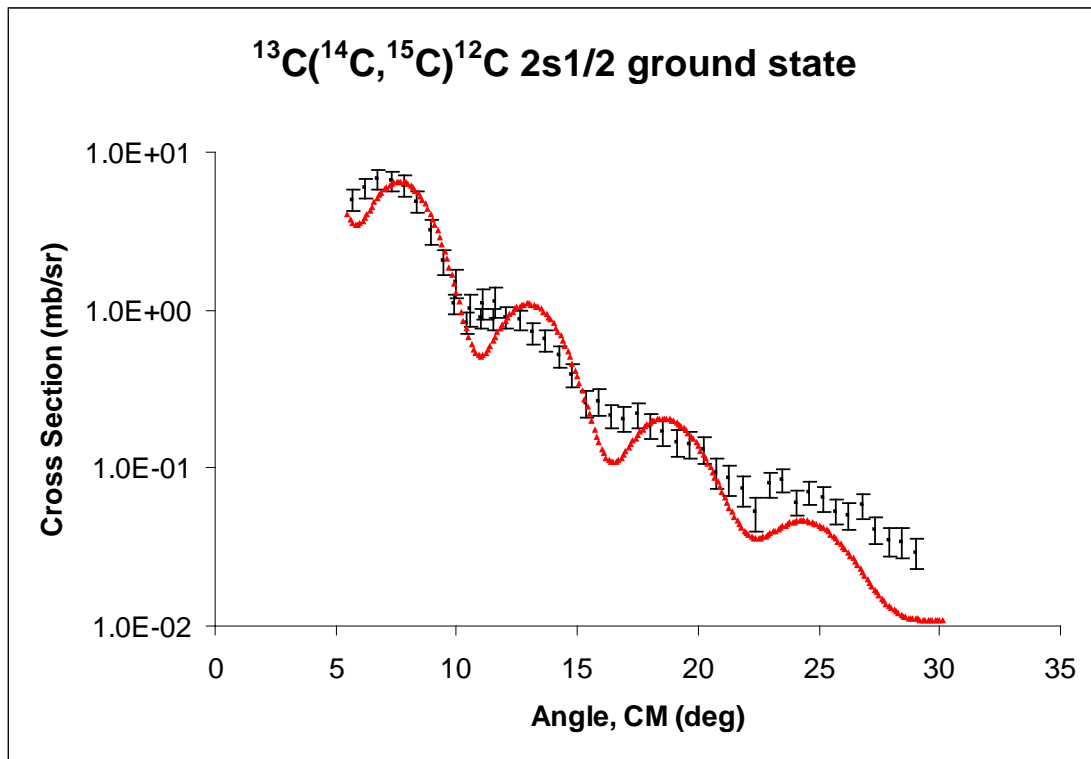
FIG. 2. Neutron transfer of 12MeV/nucleon 14C from 13C forming 15C in the ½+ (2s1/2) ground state. The squares are the experimental results, the triangles are the DWBA calculation using PTOLEMY.

The same states in ^{15}C were also populated using a 60 MeV deuteron beam on a ^{14}C target in February of 2008. The lowest two states were clearly identified and a measurement to obtain the angular

distribution is planned for the middle of 2010. At an incident deuteron energy of 60 MeV this reaction has a non-trivial interior contribution. Using the ANC for ^{15}C obtained from the HI neutron transfer experiment to fix the exterior component of the reaction, this will allow us to determine the SF for ^{15}C unambiguously by means of fitting the interior part.

[1] A.M. Mukhamedzhanov and F.M. Nunes, Phys. Rev. C **72**, 017602 (2005).

[2] L. Trache *et al.*, Phys. Rev. C **61**, 024612 (2000).

[3] F. Carstoiu *et al.*, Phys. Rev. C **70**, 054610 (2004).

[4]T. Al-Abdullah, PhD thesis, Texas A&M University, Cyclotron Institute, 2007.

The structure of ^{23}Al and ^{24}Si nuclei from proton breakup at intermediate energies

A. Banu, L. Trache, B. Roeder, E. Simmons, R. E. Tribble, F. Carstoiu,[1] F. Negoita,[1] F. Rotaru,[1]
N. Orr,[2] L. Achouri,[2] B. Laurent,[2] M. Chartier,[3] B. Fernandez-Dominguez,[3] S. Paschalis,[3]
B. Pietras,[3] P. Roussel-Chomaz,[4] L. Gaudefroy,[4] R. Lemmon,[5] M. Labische,[5] W. Catford,[6]
N. Patterson,[6] J. Thomas,[6] M. Freer,[7] M. HoroI,[8] and A. Bonaccorso[9]

[1]*IFIN-HH, Bucharest, Romania,* [2]*LPC, Caen, France,* [3]*University of Liverpool, Liverpool, UK,* [4]*GANIL, Caen, France,* [5]*CCLRC Daresbury Laboratory, Daresbury, UK,* [6]*University of Surrey, Surrey, UK,* [7]*University of Birmingham, Birmingham, UK,* [8]*Central Michigan University, Mount Pleasant, USA,* [9]*University of Pisa, Pisa, Italy*

This report is a follow-up of Ref. [1] in which we described the use of one proton-removal reactions of loosely bound nuclei at intermediate energies as an indirect method in nuclear astrophysics. We presented the E491 experiment carried out at GANIL that investigated reactions produced by a cocktail beam around ^{23}Al at 50 MeV/nucleon. Here we emphasize the results of the study of ^{23}Al and ^{24}Si nuclei from proton breakup in that experiment. These breakup reactions provide information on H-burning reaction rates for ^{22}Mg(p,γ)^{23}Al and ^{23}Al(p,γ)^{24}Si, important in novae and X-ray bursts, respectively [1]. To obtain those reaction rates from the data, we applied the ANC method [2, 3].

In the experiment E491 at GANIL, a primary ^{32}S beam at 95 MeV/u impinged on a C target and SISSI was used to separate 14 secondary beams at 1.95 Tm rigidity. They impinged on another C target at the entrance of the spectrometer SPEG that was tuned to measure the momentum of the cores after one-proton removal. EXOGAM detectors were positioned around the target. All these are illustrated in Fig. 1.
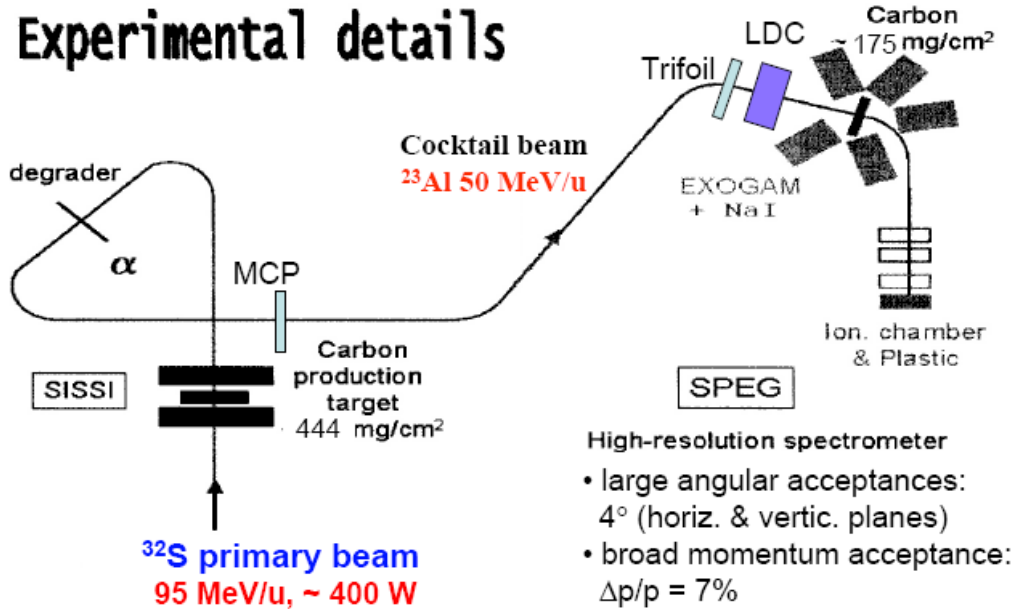
FIG. 1. Experimental setup for the E491 run at GANIL. See text for details.

Momentum distributions of the core breakup fragments, inclusive and in coincidence with gamma-rays, were measured. From them, we have determined configuration mixing in the structure of the ground states of the projectile nuclei.

In the following, we present results for the structure of ^{24}Si and ^{23}Al nuclei. Fig. 2 shows the gamma lines detected by EXOGAM in coincidence with the fragments resulting from the breakup of ^{23}Al. An add-back procedure was implemented and used here to increase the gamma-ray detection efficiency, and the spectrum is corrected for Doppler shift. The lines observed correspond to transitions in ^{22}Mg implying that the ^{22}Mg breakup core is left in various excited states after the removal of the least bound proton. That provides us with information about the configuration mixing that characterizes the ground state of ^{23}Al. We observe clearly three gamma lines: 1247.0 keV ($2_1^+ \rightarrow 0_{gs}^+$), 2061.1 keV ($4_1^+ \rightarrow 2_1^+$), and 1984.8 keV (($3^+,4^+,5^+$)$\rightarrow 4_1^+$), attesting for a large and complex configuration mixing.
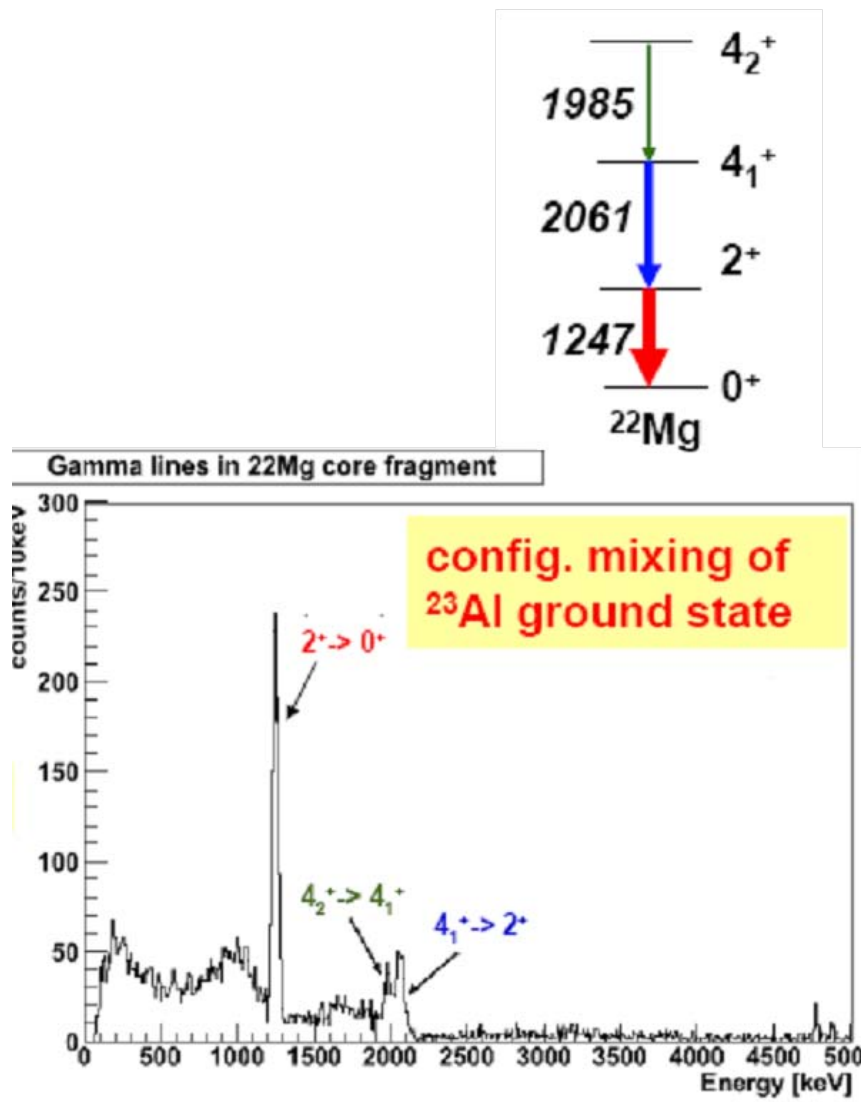
FIG. 2. Measured gamma lines (Doppler corrected) de-populating excited states in ^{22}Mg breakup fragments: 1246.98 keV, 1984.8 keV, and 2061.09 keV giving us information about the configuration mixing characterizing the ground state of ^{23}Al.

We did not observe gamma rays de-populating excited states from ^{23}Al as breakup core of ^{24}Si projectile implying that the ground state of ^{24}Si is built upon a configuration in which ^{23}Al core is left in its ground state after the one-proton removal process. Also, ^{23}Al has no bound excited states.

In Fig. 3 we present inclusive center-of-mass differential cross-sections for ^{23}Al and ^{24}Si proton breakup reaction as measured in this experiment, and compare them with theoretical calculations carried out with an extended version of the Glauber model [4].
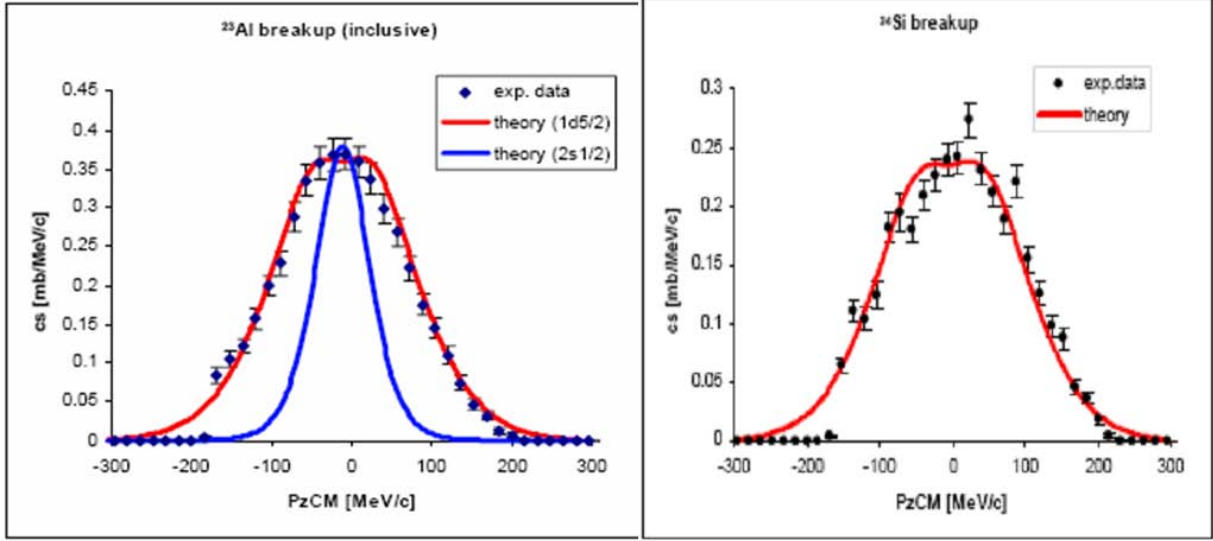
FIG. 3. Experimental inclusive differential cross-sections obtained for ^{23}Al (left) and ^{24}Si (right) one-proton breakup compared with theoretical calculations of Glauber-type model involving JLM effecting nucleon-nucleon interactions. See text for details.

In the case of ^{23}Al proton breakup, the measured momentum distributions for the ^{22}Mg core fragment agree in shape with the calculations that assume a $1d_{5/2}$ orbital (red line in Fig. 3) and do not agree with the calculations assume a $2s_{1/2}$ orbital (blue line in Figure 3). This confirms the ground state spin and parity for ^{23}Al to be $J^{\pi} = 5/2^{+}$, not $1/2^{+}$, a distinction very important for the rate of the astrophysical reaction ^{22}Mg$(p,\gamma)^{23}$Al, implying that direct proton capture on the ^{22}Mg in the ground state of ^{23}Al can not support the depletion of ^{22}Na in novae environments [5]. This was the original motivation of the experiment. Based on the mixing found in our measurement we can determine the ^{23}Al ground state wave function with the following configuration:

$$\left| ^{23}Al(5/2^{+})\right\rangle_{gs} = A_{1}\left\| core(0^{+}_{gs})\right\rangle \otimes \left| p(1d_{5/2})\right\rangle\right]_{5/2^{+}} + A_{2}\left\| core(2^{+}_{1})\right\rangle \otimes \left| p(1d_{5/2})\right\rangle\right]_{5/2^{+}} +$$
$$A_{3}\left\| core(4^{+}_{1})\right\rangle \otimes \left| p(1d_{5/2})\right\rangle\right]_{5/2^{+}} + A_{4}\left\| core(4^{+}_{2})\right\rangle \otimes \left| p(1d_{5/2})\right\rangle\right]_{5/2^{+}}$$

Here *core* refers to ^{22}Mg and *p* rfers to the removed proton, the two-body system that can characterize the ground state of the loosely bound ^{23}Al nucleus in the breakup process. The A_{i} (i=1-4) coefficients squared have the physics interpretation of spectroscopic factors that determine the orbital configuration

mixing in ^{23}Al ground state wave function. It is this expression of the ^{23}Al ground state wave function that translates into the breakdown of the inclusive differential cross-section into four components of exclusive differential cross-sections.

The component of differential cross-section for ^{23}Al breakup of astrophysical interest can be determined by subtracting the three exclusive experimental differential cross-sections (each obtained in coincidence with the corresponding γ-ray line of the three γ-ray lines detected) from the inclusive experimental differential cross-section.

By comparison between experimental differential breakup cross-sections and the corresponding theoretical calculations, we extract the squared asymptotic normalization coefficients for the two-body systems – core plus valence proton – under investigation here.

Hence, in the case of ^{23}Al one-proton removal, we obtained a squared ANC with a value of $C^2(1d_{5/2})=4.4*10^3$ fm^{-1}. The corresponding spectroscopic factor was determined to be 0.5 for the configuration with ^{22}Mg core in ground state and the valence proton occupying the $1d_{5/2}$ orbital (and assuming a proton binding potential with $r_0 = 1.20$ fm and $a = 0.65$fm). The value obtained in this experiment for the ANC is in excellent agreement with the value of $(4.63 \pm 0.77)*10^3$ fm^{-1} extracted from neutron transfer on the mirror nucleus ^{23}Ne [6]. In the of ^{24}Si one-proton removal, we obtained a squared ANC with a value of $C^2(1d_{5/2})=62.4 \pm 7.1$ fm^{-1} for a similar proton binding potential, and a corresponding spectroscopic factor of 2.7.

Based on the values of ANCs extracted from our data of ^{24}Si and ^{23}Al proton breakup reactions, we determine the astrophysical S-factors and from there calculate the reaction rates for direct radiative captures ^{22}Mg(p,γ)^{23}Al and ^{23}Al(p,γ)^{24}Si in the stellar temperature and density environments such as novae and X-ray burst. Details about these evaluations can be found soon here [7].

[1] A. Banu *et al.*, *Progress in Research*, Cyclotron Institute, Texas A&M University (2008-2009), p. I-13

[2] L. Trache *et al.*, Phys. Rev. Lett. **87**, 271102 (2001); L. Trache, F. Carstoiu, C.A. Gagliardi, R.E. Tribble, Phys. Rev. C **69**, 032802(R) (2004).

[3] H.M. Xu, C.A. Gagliardi, R.E. Tribble, A.M. Mukhamedzhanov, and N.K. Timofeyuk, Phys. Rev. Lett. **73**, 2027 (1994); A.M. Mukhamedzhanov *et al.*, Phys. Rev. C **56**, 1302 (1997); C.A. Gagliardi *et al.*, Phys. Rev. C **59**, 1149 (1999).

[4] F. Carstoiu, E. Sauvan, N.A. Orr, and A. Bonaccorso, Phys. Rev. C **70**, 054602 (2004).

[5] L. Trache *et al.*, Eur. Phys. J. A **27**, 237 (2006); V.E. Iacob *et al.*, Phys. Rev. C **74**, 045810 (2006).

[6] T. Al-Abdullah *et al.*, Phys. Rev. C **81**, 035802 (2010).

[7] A. Banu *et al.*, to be published.

Measurement of the β-delayed proton emission of ^{20}Mg and the breakout from the hot CNO cycles

J. P. Wallace,[1] G. Lotay,[1] P. J. Woods,[1] A. A. Alharbi, A. Banu, H. M. David,[1] T. Davinson,[1] M. McCleskey, B. Roeder, E. Simmons, A. Spiridon, L. Trache and R. E. Tribble

[1]*School of Physics and Astronomy, University of Edinburgh, Edinburgh, United Kingdom*

In explosive astrophysical environments, such as X-ray bursters and supernovae, sufficiently high temperatures and densities are reached that it is possible to breakout from the hot CNO cycle into the rp process. The main breakout sequence is thought to be ^{15}O(α,γ)^{19}Ne(p,γ)^{20}Na. Both reactions are important and have been investigated through many different experiments, using radioactive beams and indirect methods. It is the second reaction, ^{19}Ne(p,γ)^{20}Na, that will be discussed here.

It has been shown that this reaction rate is dominated by a single resonance at 450 keV above the proton threshold, corresponding to an excitation energy of 2.643 MeV. Over two decades of work has gone into finding the properties of this state through many different experiments. There have been direct measurements of the ^{19}Ne(p,γ)^{20}Na reaction, resulting in an upper limit being put on the resonance strength [1], as well as studies of the charge exchange reactions ^{20}Ne(^{3}He,t)^{20}Na and ^{20}Ne(p,n)^{20}Na, mirror nuclei analysis and a measurement of the β-p emission of ^{20}Mg [2]. However, despite all these experiments there is still a question mark concerning the spin-parity of the key resonant state. The uncertainty comes down to whether the state has a J^π=1$^+$ or 3$^+$ assignment. It is widely believed to be a 1$^+$ assignment, however the non-observation of the β-p branch from the decay of ^{20}Mg is strong evidence against this [2].

In [2] an experiment was performed where a total of 4.5*10^6 ^{20}Mg ions were selected by the LISE3 spectrometer at GANIL and implanted into a 300 micron position sensitive silicon detector, surrounded by β and Ge detectors. Many strong proton emissions were observed down to a resonance energy of 806 keV, however, below this, intense low energy beta's caused a high background decreasing the sensitivity at low energies. An estimate on the upper limit of the branching ratio was deduced to be 0.1%, corresponding to a lower limit on the log*ft* value of 6.24 [2]. However, these results don't rule out a 1$^+$ assignment as the analog mirror state, 3.173 MeV, in ^{20}F has not been observed to be fed by the β emission of ^{20}O, with a logft limit of 5.08 being set. It has been suggested that this 1$^+$ state in ^{20}O is an intruder state with only a weak *(sd)^4* admixture. There are also at least 3 cases where β emission is allowed with a logft value over 6, namely ^{17}N, ^{17}Ne, ^{18}N, associated with small *sd*-shell components [2].

As was previously mentioned the main source of background in the most recent study of the β-p emission from ^{20}Mg was the intense low energy beta's. Due to the method now available at TAMU [3] using thin segmented double sided silicon strip detectors (DSSSD) at the focal plane of MARS, it was possible to repeat this experiment with a 45 micron DSSSD. By using a thinner detector the low energy beta's were eliminated down to energies of about 200 keV. This can clearly be seen in Fig. 1 which shows a lack of the low energy beta background. The background at low energy is now predominately from escaping protons which was not visible in [2]. The K500 cyclotron was used to produce a primary beam of ^{20}Ne which impinged on a cryogenic ^{3}He target, producing a secondary beam of ^{20}Mg which was

separated from the contaminants also produced through the use of MARS. The [20]Mg ions were implanted into the 45 micron DSSSD, which was sandwiched between two thicker silicon detectors, a 140 micron detector in front and a 1000 micron silicon detector behind. As the half life of [20]Mg is 94 ms the beam was pulsed, with 200 ms of beam of 200 ms of acquisition, therefore reducing background further. Fig. 1 shows a preliminary spectrum of a subset of the data collected, showing the strong proton and alpha decay peaks from the decay of [20]Na. What is remarkable is that the measurement was done with a very low [20]Mg production rate of about 20 pps. This shows that the method itself is very sensitive and selective. Analysis is currently underway.
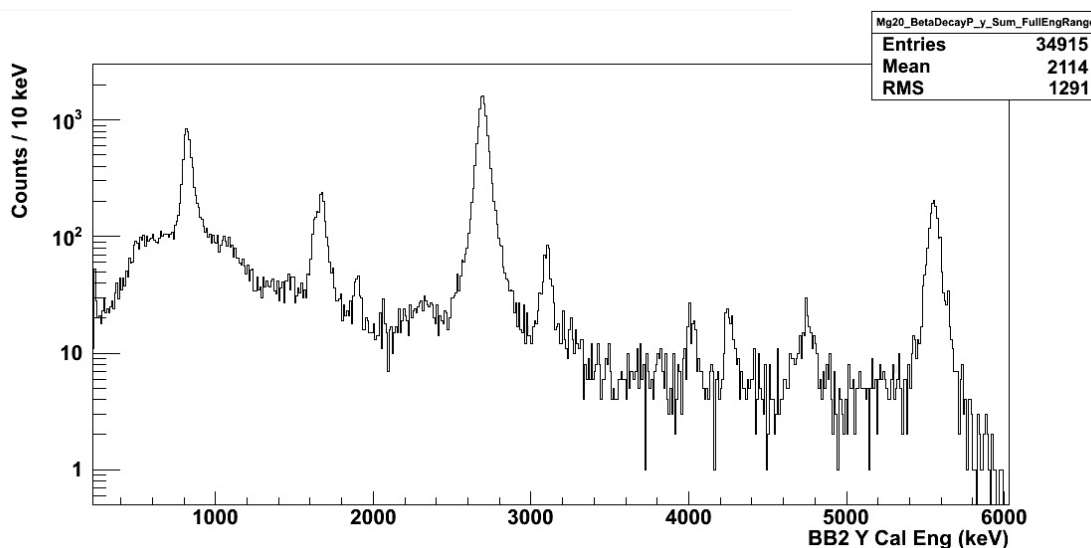
FIG. 1. Spectrum of a subset of the data, showing the strong beta delayed proton and alpha decay peaks from [20]Na.

[1] R.D. Page *et al.*, Phys. Rev. Lett. **23**, 3066 (1994).
[2] A. Piechaczek *et al.*, Nucl. Phys. **A584**, 509 (1995).
[3] L. Trache *et al.*, Proceedings of Nuclei in the Cosmos (2008).

The REU experiment: production and separation of new rare beams ^{20}Na and ^{20}Mg with MARS

L. Trache, B. T. Roeder, A. A. Alharbi, M. McCleskey, E. Simmons, A. Spiridon,
G. Subedi,[1] and REU students
[1]*Colby College, Waterville, Maine, 04901*

This year, our research group has included, for the first time, a dedicated experiment at the cyclotron in which all the REU students were directly involved. In past years, only a few students were participating in experiments with their respective groups depending on the beam time schedule of the accelerator. The experiment was designed to give the students some "hands-on" experience with the setup and calibration of experimental equipment, as well as first-hand experience in the running of an actual experiment at the cyclotron. This also allowed the students to appreciate some of the difficulties involved in scientific research.

In the days prior to the experiment, a series of lectures were presented by the host group, including the post-docs and graduate students, to explain the operation of MARS and the physics relevant to the experiment. The principles of radioactive beam production and their application to nuclear astrophysics were presented. In addition, presentations about the specific experiment our group conducted to explain the setup, electronics and pre-run calibration techniques were given such that the
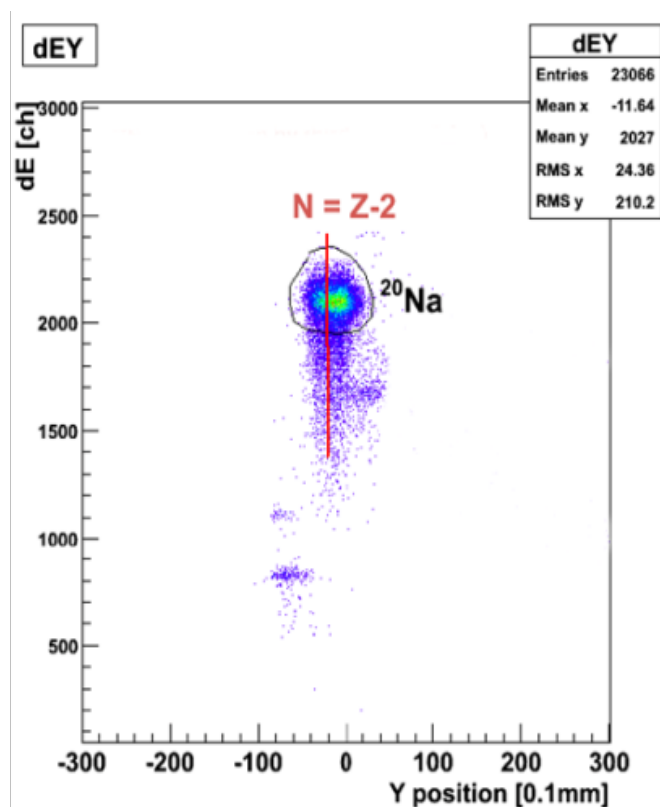
FIG. 1. Results obtained from the ^{20}Na beam production test.

students could follow what was happening in detail. As part of the preparation for the experiment, the students participated in the energy and efficiency calibration of the germanium (Ge) detector used in part 2 of the experiment.

The experiment was conducted in three parts. Part 1 consisted of the production and separation of the rare beam ^{20}Na. ^{20}Na was produced with a ^{20}Ne beam at 25 MeV/u impinging on a H_2 cryogenic gas target at a pressure of 2 atm. The resulting ^{20}Na beam was then separated with the MARS spectrometer [1]. To do this, the REU students had to apply the principles of magnetic separation and velocity filters they learned in the lectures to separate and optimize the ^{20}Na beam. The 12 students were separated into three groups that were led by members of the host group. The groups were in competition to produce the rare beam with the highest rate of ^{20}Na while minimizing the impurities in the beam. The best results were a production rate for ^{20}Na of 1900 events/nC with 11% impurities. In preparation for Part 2 of the experiment, the momentum slits of MARS were closed to ± 0.3 cm. This reduced the final production rate to 950 events/nC with 7.9% impurities. The resulting ΔE vs. Y-position spectrum for the ^{20}Na beam is shown in Fig. 1.

Part 2 of the experiment was to measure the complex (but known) β-, βα-, and βγ- decay of ^{20}Na. To do this, the ^{20}Na beam was implanted in the middle of a very thin (65 micron) Si detector using a simple energy degrading technique. Then, the decay of the ^{20}Na was observed using particle (Si for the positrons and alphas) and gamma detectors (Ge). The students participated by working in the experimental shifts and helping to identify the peaks in the α-particle and γ-ray spectra. A spectrum showing the β-delayed α decay spectrum measured in the experiment is shown in Fig. 2. The measured energies of the α-particles are in agreement with previously published work [2].
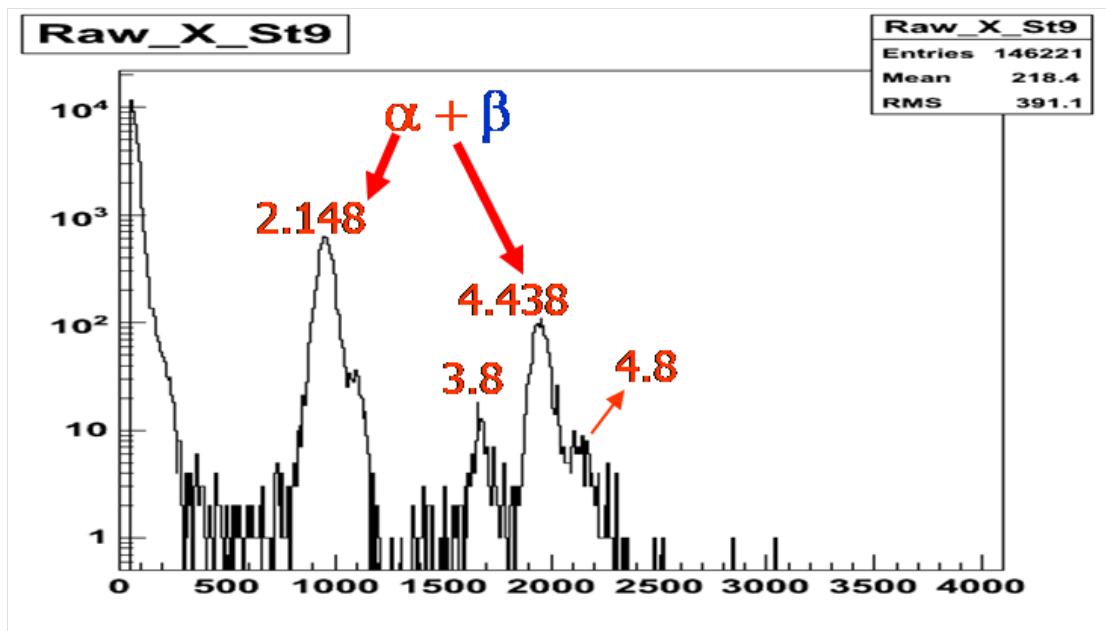
FIG. 2. β-delayed α decay spectrum measured in one strip of the thin Si detector for the ^{20}Na experiment. Energies labeled are in MeV.

Finally, part 3 of the experiment was to test the production of a rare beam of ^{20}Mg in preparation for a future experiment to measure its β-delayed proton decay. This part of the experiment did not involve the REU students, with the exception of the REU student (G. Subedi) that was working in our group. Our REU student's project was to predict the best way to produce ^{20}Mg with theoretical calculations, and to analyze the data from the production test run. The ^{20}Mg was produced with the same ^{20}Ne beam at 25 MeV/u that was used in the ^{20}Na part of the experiment, but the cryogenic gas target was filled instead with 1.5 atm of ^{3}He gas. It was found that the production rate for ^{20}Mg was much lower than the production of ^{20}Na and that there was a large, unavoidable contamination from ^{10}C. A production rate of 21 events/μC was measured for ^{20}Mg, while the ^{10}C contamination was approximately 10 times more intense. However, this method was preferred over other methods of ^{20}Mg production because the ^{20}Ne beam could be easily obtained at high intensity from the cyclotron, and the ^{10}C contamination turned out to not be a problem for the future measurement. The final ΔE vs. Y-position spectrum for the ^{20}Mg beam illustrating the contents of the beam with the MARS slits open is shown in Fig. 3.
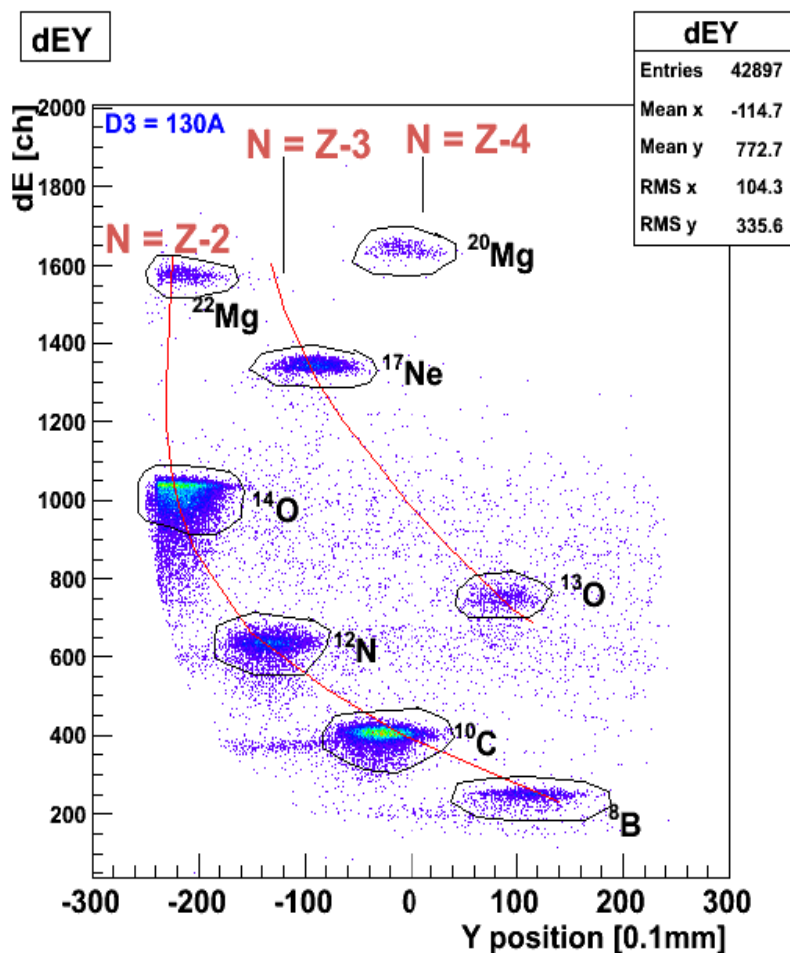
FIG. 3. Results of the ^{20}Mg beam production test run.

The results of the ^{20}Na production and decay measurements, as well as the ^{20}Mg production measurements, were presented by our group's REU student (G. Subedi) in a poster at the CEU conference at the Joint APS DNP/JSPS meeting in Hawaii in October 2009. Overall, the REU students enjoyed the experience of participating in a real experiment. Also, this experiment was beneficial to the host group as the post-docs and graduate students learned not only details about the setup and preparations for the experiment, but also how to explain what they were doing to the REU students. Because of these mutual benefits for both the host group and the REU students, future runs for the REU students are going to be planned.

[1] R.E. Tribble, R.H. Burch, and C.A. Gagliardi, Nucl. Instrum. Methods Phys. Res. **A285**, 441 (1989).
[2] E.T.H. Clifford *et al.*, Nucl. Phys. **A493**, 293 (1989).

Giant resonaces in ^{48}Ca

Y. –W. Lui, D. H. Youngblood, X. Chen,[*] and Y. Tokimoto[#]

The location of the giant monopole resonance (GMR) is important because it can be directly related to the compressibility of nuclear matter K_{NM} [1]. Systematic studies of GMR in various nuclei lead to the value of nuclear compressibility at 231±5 [2]. This property of the GMR and the variation of the compressibility with neutron number can also be used to extract the symmetry energy K_{sym} in the equation of state. In the early analysis, Leptodermous expansion similar to mass formula was used to parameterize compressibility of the nucleus into volume, surface, symmetry and Coulomb terms. However, Shlomo and Youngblood [3] show that this type of analysis cannot provide a unique solution even including all available data in the world. On the other hand, microscopic calculation with specific interactions can provide information on the location of GMR and the compressibility of nuclear matter as well as the symmetry energy. In recent years, the study of the isotope dependence and the extraction of symmetry energy are mostly concentrated in heavy nuclei, especially in Sn isotopes [4-6] with the neutron excess ratio (N-Z)/A value changes from 0.107 in ^{112}Sn to 0.194 in ^{124}Sn. This gives a relative large deviation in the isotope dependence. However, in the calcium isotope, the (N-Z)/A value is 0 in ^{40}Ca and is 0.167 in ^{48}Ca. Although the neutron access value in ^{48}Ca is not as large as in ^{124}sn, the difference is larger, thus it might provide larger difference in the location of GMR and more precise determination of the symmetry energy. Therefore, we have studied the giant resonances in ^{48}Ca.

A beam of 240 MeV α particles from the Texas A&M K500 superconducting cyclotron was used to bombard a self-supporting ^{48}Ca foil in the center of the target chamber of the Multipole-dipole-multipole spectrometer. The details of the setup and the experimental technique have been
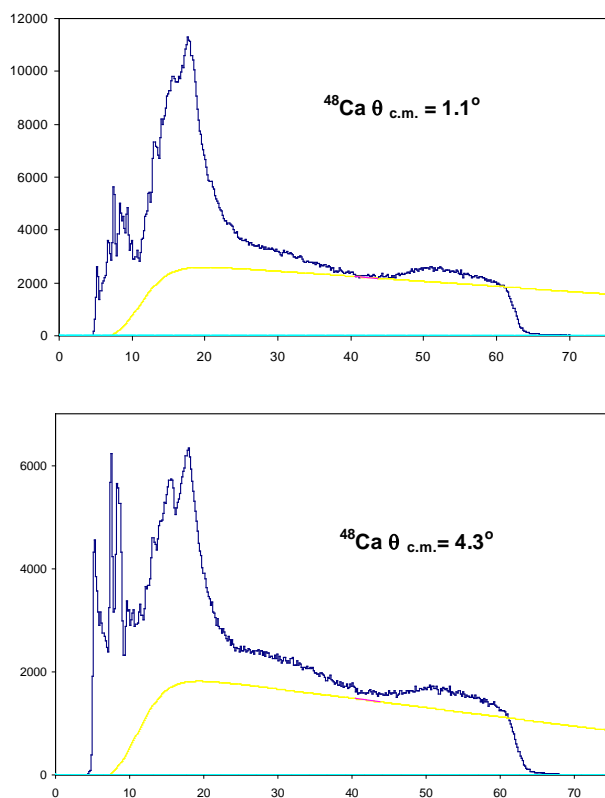
FIG. 1. Inelastic alpha spectra obtained at two angles for ^{48}Ca. The grey lines show the continuum chosen for the analysis.

described in Ref. [7]. Sample spectra obtained for ^{48}Ca at $\theta_{avg.}$ =1.1° and 4.3° are shown in Fig. 1.

Multipole decomposition analysis was performed to extract the strength of each multipole component of the giant resonances. Single folding density-dependent DWBA calculations were carried out. The transition density, sum rules, and DWBA calculations were discussed thoroughly in Ref. [7,8]. Preliminary result of the strength distributions of GMR and giant quadrupole (GQR) resonance strength are shown in Fig. 2.

Detailed analysis is in progress.
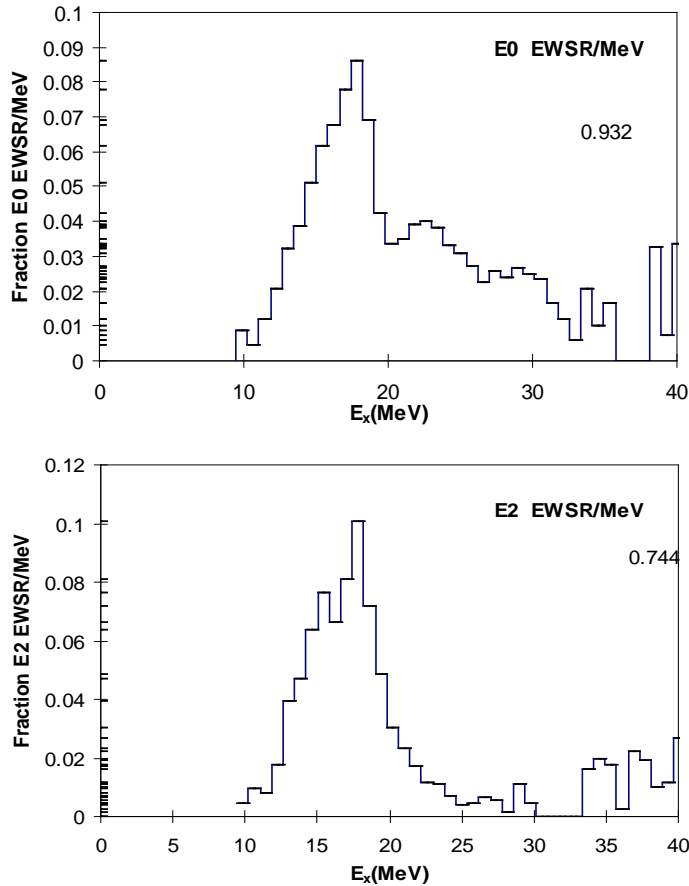
FIG. 2. Strength distributions of GMR and GQR obtained for ^{48}Ca.

[1] J.P. Blaizot, Phys. Rep. **64**, 171 (1980).

[2] D.H. Youngblood, H.L. Clark, and Y.-W. Lui, Phys. Rev. Lett. **82**, 691 (1999).

[3] S. Shlomo and D.H. Youngblood, Phys. Rev. C **47**, 529 (1993).

[4] Y.-W. Lui *et al.*, Phys. Rev. C **69**. 034611 (2004).

[5] Y.-W. Lui *et al.*, Phys. Rev. C **70**. 014307 (2004).

[6] T. Li *et al.*, Phys. Rev. C **81**, 034309 (2010).

[7] D.H. Youngblood, Y.-W. Lui, and H.L. Clark, Phys. Rev. C **65**, 034302 (2002).

[8] G.R. Satchler and Dao T. Hhoa, Phys. Rev. C **55**, 285 (1997).

Upgrade of the [37]K asymmetry measurement experiment

D. Ashery,[1] S. Behling, J. Behr,[2] I. Cohen,[1] A. Gorelov,[2] G. Gwinner,[3] K. P. Jackson,[2] T. Kong,[4]
M. Mehlman, D. Melconian, M. R. Pearson,[2] and P. Shidling

[1]*Tel Aviv University, Tel Aviv, Israel*
[2]*TRIUMF, Vancouver, Canada*
[3]*University of Manitoba, Saskatchewan, Manitoba, Canada*
[4]*University of British Columbia, Vancouver, British Columbia, Canada*

Our upgrade of the TRINAT apparatus has moved from the design stage to the construction stage. The main chamber, which is a complicated ultra-high vacuum vessel which will house the "detection trap", is shown in Fig. 1. Constraints in designing this chamber were numerous: it must allow six counter-propagating laser beams for the magneto-optical trap; another two ports allow for the counter-propagating, evenly balanced optical-pumping beams; two ports will house beta telescope detectors, each consisting of a 40x40 mm^2, 300μm-thick Micron BB1 design double-sided silicon strip detector (DSSSD) and a BC408 plastic scintillator with an Electron Tubes 5" 9823KB PMT with transistorized base; one port will be used to mount the Z-stack MCP recoil detector with delay-line anode readout; and one port will either house a larger beta telescope (a 64x64 mm^2, 300μm-thick Micron BB7 design with a scintillator) or a shake-off electron chevron MCP detector with hexagonal readout.
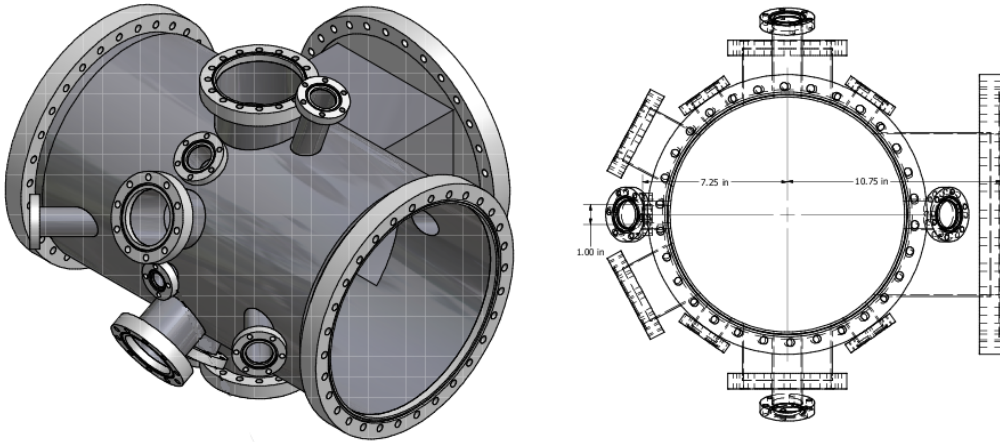
FIG. 1. AutoCAD drawing of the new chamber for the [37]K experiment. The new chamber, which has 17 ports to accommodate all the laser beams and detectors, is presently being constructed at TRIUMF.

We are in the process of designing special mounts in concert with Micron for the strip detectors, and are now turning our attention towards the final specifications of the re-entrant flange housing the beta telescopes. These will have very thin (30μm-thick) Si wafers coated to serve as mirrors for the optical-pumping light, and a 500μm-thick Be window to separate the ultra-high vacuum of the trapping region from air. The beta detection systems will be built and tested at the Cyclotron Institute before

being installed in the TRINAT system at TRIUMF this fall. Our collaborators at TRIUMF are mainly responsible for development of the novel AC-MOT, and progress is being made toward developing an off-line system with which to test the new coils and coil drivers required by this novel trap.

We expect to take beam and perform a measurement of A_β when ^{37}K next becomes available at TRIUMF either this fall or early next year after the shutdown.

The UCN-A experiment: measuring the β asymmetry using ultra-cold neutrons

D. Melconian and the UCNA collaboration[*]

A neutron is considered to be "ultra-cold" when it's kinetic energy is on the order of a few hundred nano-eV, the Fermi potential of typical materials. In this case, the neutron will undergo total internal reflection at any angle, and so can be stored in closed vessels with lifetimes approaching the beta decay lifetime ($\tau\sim900s$). Such neutrons are called Ultra-Cold Neutrons (UCN) and offer new opportunities for precision measurements of the neutron and its decay properties. The UCNA collaboration has developed an experimental program around the UCN source at Los Alamos National Laboratory's LANSCE facility, recently publishing the first measurement of the β asymmetry parameter, A_0, from UCN decay [1]. The statistics-limited result is consistent with – although with ≈4× the uncertainty – than the value currently accepted by the Particle Data Group. In 2008 we collected enough data that the statistical uncertainty will be reduced over a factor of five to 0.8% and we have reduced a number of our dominant systematic uncertainties. We are on the verge of completing our determination of corrections and systematic uncertainties, and will be unblinding the analysis in a collaboration meeting to be held at Texas A&M in May 2010. Preliminary results indicate a total systematic uncertainty of 0.9% (see Table I), dominated by our knowledge of the energy calibration of the beta detectors. Thus we

TABLE I. Error budget for the data collected by the UCNA experiment from 2008–2009.

Source of systematic uncertainty	$\Delta A/A$ [%]
Rate−dependent gain shift	0.08
Gain fluctuations	0.20
Deadtime	0.01
Linearity of scintillator	0.47
UCN background	0.02
Muon veto efficiency	0.30
Live−time uncertainty	0.24
Fiducial cut	0.24
UCN Polarization	0.52
Uniformity of magnetic field	0.20
Radiative corrections (theoretical)	0.05
Total	0.88

expect to publish a 1.2% measurement of A_0 by the summer of 2010 as we start another run at Los Alamos to collect more data and further improve our uncertainty budget.

[1] R.W. Pattie Jr. *et al.*, Phys. Rev. Letts. **102**, 012301 (2009).

Expanding the weak interaction program – a general purpose ion trapping station

S. Behling, M. Mehlman, D. Melconian, and P. Shidling

A new program on studying the weak interaction via precision β-decay measurements has begun at the Cyclotron Institute. With the upgrade of the facilities here, there are many exciting new opportunities for studying the properties of nuclei off the valley of stability. Penning traps offer a powerful tool to study these exotic nuclei due to their ability to purify and confine any species of ions in small volumes for long periods with a high degree of control. Ions in this type of trap are confined in 2D via the application of a strong magnetic field, and an electrostatic field is applied so as to trap the atoms in the third dimension. The versatility of these traps is evident by the number that are in use or planned for precision studies at every major rare isotope beam (RIB) facility. To capitalize on the increased RIB capability of the upgraded Cyclotron Institute, we are building a dedicated beam line system to guide low-energy ions from the heavy-ion gas catcher ending to a cylindrical Penning trap β-decay station. The ions in this trap will be purified (potentially with a mass-resolving power of up to 800,000), cooled and bunched. Decay studies of the the trapped ions may be performed *in situ* (e.g. β-ν correlation studies), or the low-emittance beam from the trap may be used for nuclear spectroscopy, lifetime and branching ratio measurements.

The initial goal of the program utilizing this decay station is to measure the *ft* values of $T=2$ superallowed β-delayed proton emitters. The T=2 nuclei are especially interesting because a recent comparison of isospin-mixing corrections by I. Towner [1] indicate a systematic dependence with isospin with the type of model used (either a Woods-Saxon plus Coulomb potential or a self-consistent Hartree-Fock calculation). To test the calculations and add new cases from which V_{ud} may be extracted requires measurements of the *ft* value to the sub-percent precision. For the β-delayed proton emitters, this corresponds to measuring the proton and γ branching ratios from the 0^+ state as well as the lifetime, all to the sub-percent level. A proof-of-principle measurement on ^{32}Ar has been demonstrated [2], and we plan to refine this measurement with the clean Penning trap system. Once the technique is refined and the *ft* value of ^{32}Ar is improved to ≲ 0.5%, the program will continue measuring a number of other $T=2$ nuclei as well as branching out into measuring β-ν correlations in these nuclei via the Doppler-broadened proton energy spectrum.

With a DOE-sponsored capital grant, we have recently ordered the 7 Tesla, 16 cm actively shielded bore magnet from Magnex Scientific for the planned Penning trap which is expected to arrive by the end of this year or early 2011. At present, design of the beam lines and decay station using the ion-optics simulation package SIMION8.0 is in progress.

[1] Ian Towner, private communication.
[2] M. Bhattacharya *et al.*, Phys. Rev. C **77**, 065503 (2008).

The Francium trapping facility at TRIUMF

S. Aubin,[1] J. Behr,[2] V. V. Flambaum,[3] E. Gomez,[4] G. Gwinner,[5] K. P. Jackson,[2] D. Melconian,
L. A. Orozco,[6] M. R. Pearson,[2] and G. D. Sprouse[7]

[1]*The College of William & Mary, Williamsburg, Virginia*
[2]*TRIUMF, Vancouver, Canada*
[3]*Univeristy of New South Wales, Sydney, Australia*
[4]*Universidad Autónoma de San Luis Potosí, San Luis Potosí, Mexico*
[5]*University of Manitoba, Saskatchewan, Manitoba, Canada*
[6]*University of Maryland, College Park, Maryland*
[7]*Stony Brook State University of New York, Stony Brook, New York*

The heaviest alkali element, Francium ($Z = 87$), has received much attention in recent years [1]. It possesses a unique combination of structural simplicity due to its single valence *s*-electron and a great sensitivity to effects such as atomic parity non-conservation (APNC) and possible electric dipole moments due to its high nuclear charge. The attractiveness of Fr for APNC experiments has been discussed since the early 1990s in the context of searches for physics beyond the Standard Model [2]. APNC, first observed in the late 1970s, arises from the parity-violating exchange of *Z*-bosons between electrons and the quarks in the nucleus, leading to a mixing of atomic levels of opposite parity [3]. As a result, otherwise forbidden electric dipole transitions can be excited between states of the same parity. The culmination so far has been a measurement by the Boulder group in ^{133}Cs [4]. APNC scales with the nuclear charge roughly as Z^3, favouring experiments in heavy atoms, but a successful extraction of the weak interaction physics from the measured atomic quantity also requires a detailed understanding of the atomic wave functions. This has limited the interpretation of Tl, Pb, and Bi data. The atomic theory of Fr, on the other hand, can be understood at a level similar to that of Cs ($Z = 55$), yet the APNC effect is almost 20 times larger. Among the existing and upcoming experiments, APNC is very competitive concerning searches for leptoquarks, compositeness, and extra gauge bosons [5].

The Francium program at TRIUMF was formed to take advantage of the actinide target being developed which will produce copious quantities of Fr. Experiments are planned on hyperfine anomalies, microwave measurements of the nuclear anapole moment, and optical atomic parity violation, all of which require a reliable atom trap setup. The system is being based on our experience with Fr at Stony Brook, with (offline) testing of the magneto-optical trap (MOT) apparatus, shown in Fig. 1, completed at the University of Maryland. The second ("science") chamber will consist of a second MOT for re-capturing the transferred atoms and an optical dipole trap, preferably blue-detuned to minimize the perturbation on the atoms. The electromagnetic environment will be controlled at the level necessary for precision atomic PNC measurements.

We are currently finalizing the environmentally controlled clean room and expect to install it on the floor of the ISAC facility in the fall of 2010. The lasers are scheduled to be installed in the first half of 2011 and, depending on the availability/capability of TRIUMF to produce Fr beams, we hope to attempt trapping Francium in mid-2011.
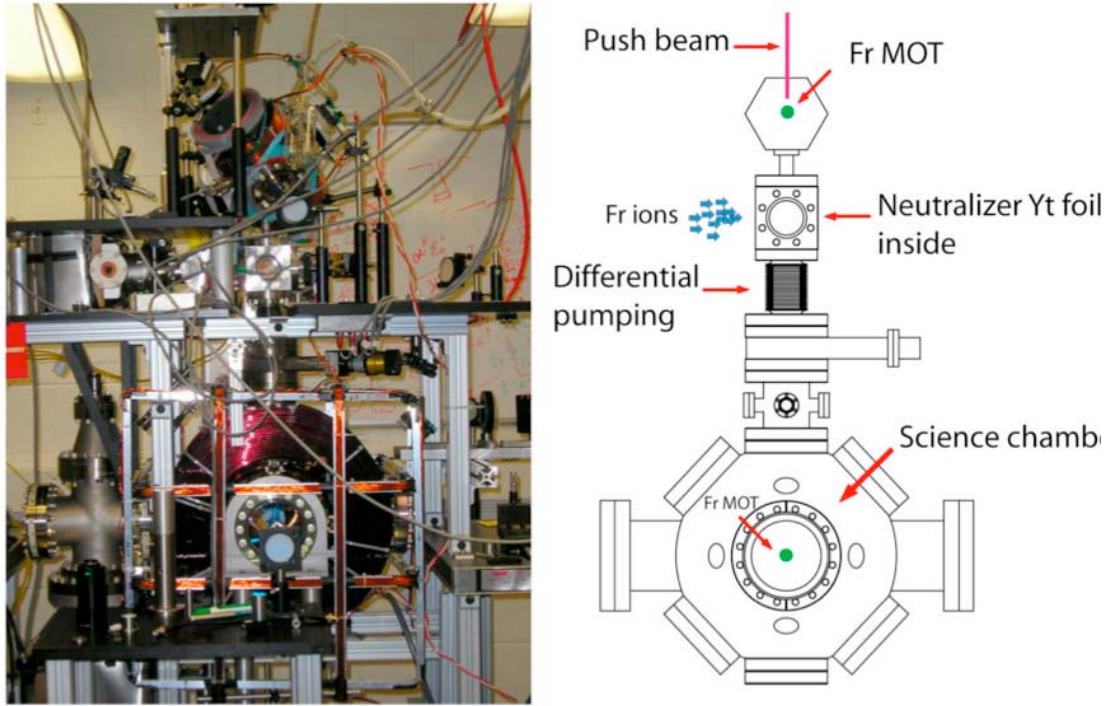
FIG. 1. Picture and schematic diagram of the MOT system at TRIUMF to be used for Fr studies.

[1] E. Gomez *et al.*, Rep. Prog. Phys. **69**, 79 (2006).

[2] W.J. Marciano and J.L. Rosner, Phys. Rev. Lett. **65**, 2963 (1990).

[3] M.A. Bouchiat and C. Bouchiat, J. Phys (Paris) **35**, 899 (1974).

[4] C.S. Wood *et al.*, Science **275**, 1759 (1997).

[5] J. Erler, A. Kurylov, and M.J. Ramsey-Musolf, Phys. Rev. D **68**, 016006 (2003).

Spin Physics with STAR at RHIC

P. Djawotho, J. L. Drachenberg, C. A. Gagliardi, L. Huo, R. E. Tribble,
and the STAR Collaboration

When the past year began, RHIC Run 9 was underway. The primary STAR goal for Run 9 was to collect a high-statistics sample of jet and di-jet data in longitudinally polarized *pp* collisions in order to constrain the gluon polarization in the proton. Our group played a significant role in the STAR Run 9 data taking. One of us (Gagliardi) served as chair of the STAR Trigger Board, which is responsible for ensuring that STAR records the data necessary to achieve the goals that the Collaboration set in the STAR Beam Use Request. Another group member (Djawotho) was responsible for monitoring the performance of the Barrel and Endcap Electromagnetic Calorimeters (BEMC/EEMC) and the corresponding parts of the Level-0 trigger, using code that was described in last year's progress report. Since the run ended, we have focused our efforts on optimization of the STAR jet analysis procedures in anticipation of the analysis of the Run 9 data, and on analysis of transversely polarized *pp* data that were recorded by the Forward Meson Spectrometer (FMS) and Forward Time Projection Chamber (FTPC) during Run 8.

Jets in STAR are reconstructed using a mid-point cone algorithm with a radius of 0.7 in pseudorapidity (η) and azimuthal angle (φ) space. The jet finding algorithm starts with a list of seeds, which can be charged tracks measured with the Time Projection Chamber (TPC) or neutral calorimeter towers from the BEMC/EEMC. All tracks and towers in the vicinity of a seed and within the cone radius are built into four-momenta and added to the seed in a covariant fashion. The Lorentz vectors for tracks assume the mass of the charged pion (a reasonable approximation that avoids inefficiencies associated with high-p_T particle identification), and tower Lorentz vectors are assumed to be massless photons. This scheme poses a potential problem. When electrons or hadrons are tracked through the TPC, then deposit a significant fraction of their energies in the calorimeter, that energy can be double-counted in the jets.

Traditionally, STAR Spin analyses have corrected for this double counting by applying a so-called "MIP subtraction", where the energy equivalent of a minimum-ionizing particle is subtracted from the energy of each calorimeter tower reached by a charged track. During the past year, we developed an alternative technique to correct the jet energy. We subtract a fixed fraction of the total momentum of a charged track from the hit tower. If the requested subtraction would result in a tower with negative energy, the tower is simply removed from the jet, and no further correction is applied. The algorithm was tuned through detailed comparisons of the true vs. reconstructed jet energies in high-statistics PYTHIA+GEANT simulations. We find little difference between 50% and 100% subtraction procedures. Both perform much better than the MIP subtraction. Fig. 1 shows the RMS of the difference between the true and reconstructed jet energies for the MIP scheme and for 50% and 100% subtractions. The 100% subtraction procedure leads to a significant improvement in the jet p_T resolution compared to the MIP subtraction. The 100% subtraction procedure also provides the smallest average difference between the true and reconstructed jet transverse momenta. This scheme has now been adopted by the Collaboration for the analysis of the 2009 jet data.
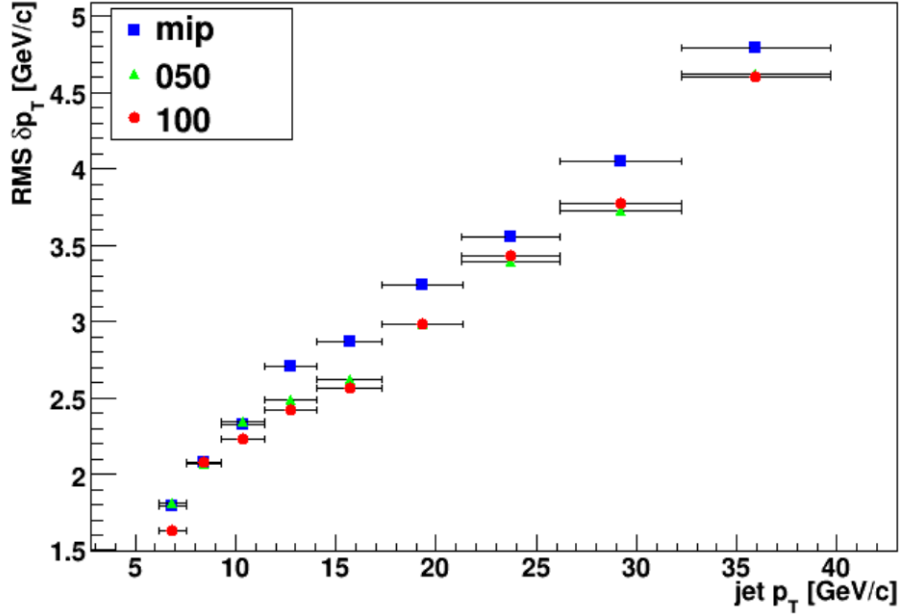
FIG. 1. RMS difference between true and reconstructed jet transverse momenta as a function of the reconstructed jet p_T, measured with 200 GeV pp PYTHIA events that have been processed through a detailed GEANT simulation of the STAR detector.

The PYTHIA+GEANT event sample that was used to evaluate the trigger and reconstruction bias in the 2006 pp jet analysis included nearly 5M events generated over a period of 3 months. The dataset was further subdivided into partonic p_T bins, *i.e.* bins of the transverse momentum of the outgoing partons in the partonic center-of-mass frame. This allowed for extra sampling of the underrepresented population of high-p_T jets with low production cross sections. However, at low p_T, a different problem arises. While the jet production cross sections there are rather large, only a tiny fraction of the jets fire the STAR online trigger. For example, at a partonic p_T of 2-3 GeV/c, only about 0.18% of the events actually satisfy any trigger of interest to the Spin Physics Working Group. The traditional method of generating Monte Carlo would produce the entire sample, then subsequent analyses would apply the trigger simulator. This process can be very costly, both in CPU usage and disk storage required.

This past year, we developed a trigger filter that makes possible substantial savings in CPU time and disk footprint. The idea is to filter out those events that would have failed the hardware trigger at a much earlier stage of the simulation. The PYTHIA events are generated and records saved regardless of trigger condition. They can then be used later for normalization and bias estimation. The events are then run through the GEANT simulation of the STAR detector, but not the TPC slow simulator. At this point, calorimeter ADCs are available and used by the trigger simulator to mimic the STAR trigger system. If the event fails the trigger, further processing is aborted. Otherwise, the full event is reconstructed, including simulation of the TPC response. This procedure reduces the required CPU time for aborted events by a factor of ~20. The current plan is to apply the trigger filter to all Monte Carlo samples below

partonic p_T of 15 GeV/c. This will reduce the number of fully simulated events by 60% and shorten the production time significantly, while allowing a much larger total luminosity to be simulated.

For many years, STAR has assumed a 5% uncertainty on the ability of our simulations to estimate the tracking efficiency of the TPC. This represents the largest single contribution to the current uncertainty on the reconstructed jet energy scale at high p_T. The 5% uncertainty was derived from studies of identified-particle tracking in central Au+Au collisions that were performed many years ago. Jet analyses in 200 GeV *pp* collisions represent a far more benign environment, so it is likely that the standard STAR simulations reproduce the tracking efficiency more accurately than has been assumed. We have developed a technique to take the track kinematics from a jet in one event, embed a track with the same relative kinematics into a jet in a different event, and then see if the track is successfully reconstructed or not. Preliminary results indicate that the PYTHIA+GEANT simulations that have provided the basis for all Run 6 jet analyses reproduce the true Run 6 tracking efficiency to within at least 2%.

Members of our group are working toward the goal of reconstructing jets at forward rapidity using the Run 8 transverse spin data from the FMS together with the west FTPC. One of the primary difficulties in this analysis is dealing with detector inefficiencies. During the 2008 RHIC run, the FMS employed a high-tower trigger, where the detector information was read out once a particular FMS tower reached a certain ADC threshold. Due to insufficient detector shielding, magnet ramps caused the trigger thresholds to be effectively much higher than anticipated. This resulted in "holes" in the FMS triggers, with a handful of towers dominating the trigger. By itself, this would not be a major issue. However, the FTPC also had hardware issues during the Run 8 *pp* collision period, which render complete sectors dead. To work around these issues, we have developed a mixed-event technique to determine the effective acceptance distribution. When this is divided out of the raw correlation distribution, a clear correlation distribution is obtained, with a near-side peak centered around $\Delta\varphi=0$, and an away-side peak centered around $\Delta\varphi=\pi$. The next step will be to clean up the background, which remains quite large at the moment.

Our group continues to carry a number of administrative tasks for the STAR Collaboration. This past year, Dr. Djawotho was named the Embedding Coordinator for the Spin Physics Working Group. Dr. Gagliardi is serving on the Trigger Board for Run 10. Mr. Drachenberg and Drs. Djawotho, Gagliardi, and Tribble have all served on god-parent committees, and Drs. Gagliardi and Tribble have chaired three of them. Finally, late this past year activities began to prepare a new Decadal Plan for the STAR Experiment. The STAR Spokesperson has appointed Dr. Gagliardi to chair this effort.

TWIST: measuring the space-time structure of muon decay

C. A. Gagliardi, R. E. Tribble, and the TWIST Collaboration

This past year, TWIST completed the blind analysis of final data sets, which were recorded in 2006 and 2007. The results were revealed when the "black box" was opened on Jan. 29, 2010. We found $\rho = 0.74991 \pm 0.00009$(stat.) ± 0.00028(syst.), $\delta = 0.75072 \pm 0.00016$(stat.) ± 0.00029(syst.), and $P_\mu\xi = 1.00084 \pm 0.00035$(stat.) $+0.00165$ -0.00063(syst.). The ρ and δ results have a large, positive correlation (+0.69). The δ and $P_\mu\xi$ results have a significant, negative correlation (-0.43) when $P_\mu\xi$ is below the central value. All other parameter correlations are relatively small.

These results can be combined to find $P_\mu\xi\delta/\rho = 1.00192$ $+0.00167$ -0.00066. This was a surprise. $P_\mu\xi\delta/\rho$ represents the asymmetry at the endpoint, and thus must≤be Since the unblinding, the collaboration has focused on trying to identify a possible source for this 2.9σ discrepancy. In nearly all cases, the new cross-checks have validated the original blind analysis results, but one issue has been identified. It appears that the energy calibration procedure did not compensate fully for differences in the mean muon stopping location between the data and Monte Carlo. It also appears that the 2006 data that were recorded with a Ag target are substantially more sensitive to this issue than the data that were recorded using an Al target. At present, it is not yet clear whether this issue is the cause of the $P_\mu\xi\delta/\rho$ discrepancy or not.

Prior to the unblinding, our group was responsible for the evaluation of the correlations among the various muon decay parameters. This task is complicated by the fact that both statistical and systematic effects contribute. We were also responsible for updating the final ρ and δ results from the 2004 data [1] to account for some small biases that had existed in the previous analysis and were revealed during the analysis of the 2006 and 2007 data. Since the unblinding, we have played a significant role in the cross-checking effort. Once the cross-checks are completed, we will perform a final global analysis of all muon decay parameter measurements in order to obtain the most precise, model-independent limits on the space-time structure of muon decay.

[1] R.P. MacDonald *et al*. (TWIST Collaboration), Phys. Rev. D **78**, 032010 (2008).

Toward understanding relativistic heavy-ion collisions with the STAR detector using photon-jet correlations

A. Hamed, S. Mioduszewski, and the STAR Collaboration

The γ-jet analysis was suggested as a means to study energy loss in a dense medium [1] because the photon trigger energy is known (since it escapes the medium with negligible interaction). The photon does not interact via the strong force, so it essentially escapes the medium unmodified; while the jet produced from the parton scattered into the opposite direction of the photon exhibits the effects of the dense medium. The analysis is performed through a correlation measurement, where the hadrons correlated to a direct photon trigger are studied in p+p collisions (no medium) and central Au+Au collisions (dense medium).

We have finalized this analysis from the Run-7 Au+Au and Run-8 p+p data and documented the results in a paper [2] for the STAR Collaboration. We submitted the manuscript of these results for publication in December of 2009, and recently resubmitted it with modifications to address comments by the referees. Two of the main plots from the paper are shown in Figs. 1 and 2. Figure 1 shows the yields
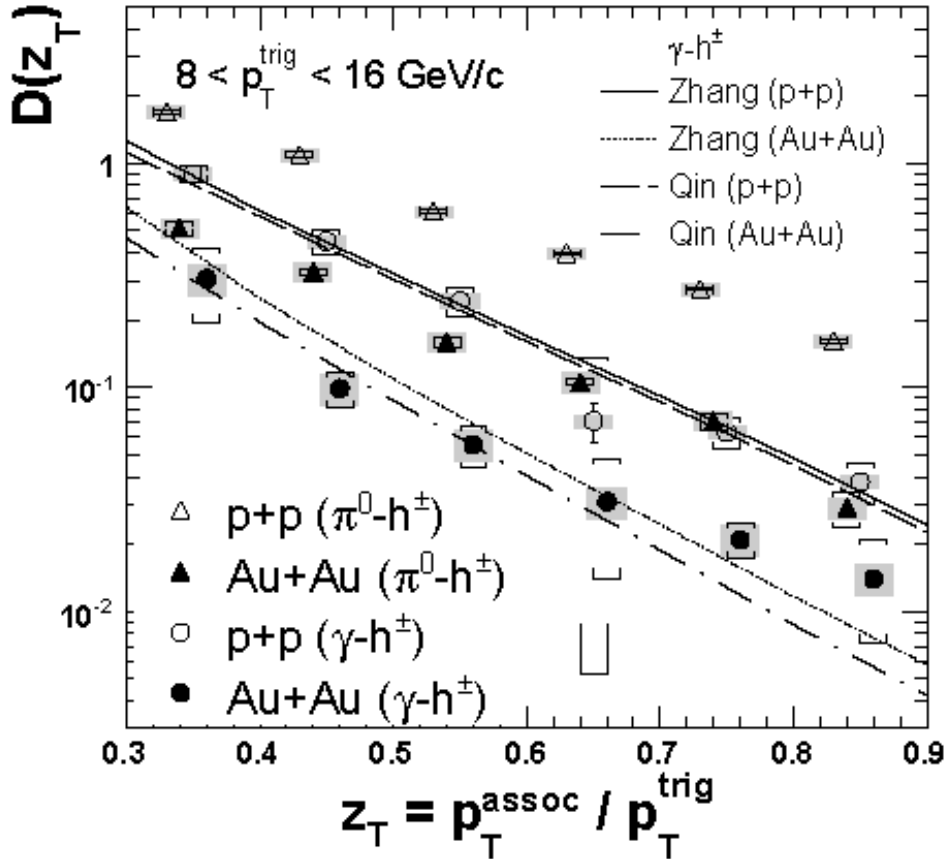
FIG. 1. Associated yields of hadrons correlated with a high-p_T direct γ (circles) or π^0 (triangles) trigger, as a function of z_T (=p_T^{assoc}/p_T^{trig}) for 0-10% central Au+Au collisions and p+p collisions.

associated with hadron (π^0) triggers compared to the yields associated with direct photon triggers for both p+p collisions and central Au+Au collisions, as a function of $z_T = p_T^{assoc}/p_T^{trig}$. Also shown are comparisons to theoretical calculations [3, 4]. The difference in yields for π^0 vs. direct-γ triggers is expected, even in p+p collisions, because hadrons originate from a fragmentation process and thus from a higher energy parton than the energy of the direct photon (which does not originate from fragmentation). The effect of the medium is seen by taking the ratio of yields in central Au+Au collisions to those in p+p collisions (Fig. 2). The surprising result is that the effect of the medium on hadron (π^0)-triggered yields is very similar to the effect on direct photon-triggered yields. Since direct photons are not expected to be
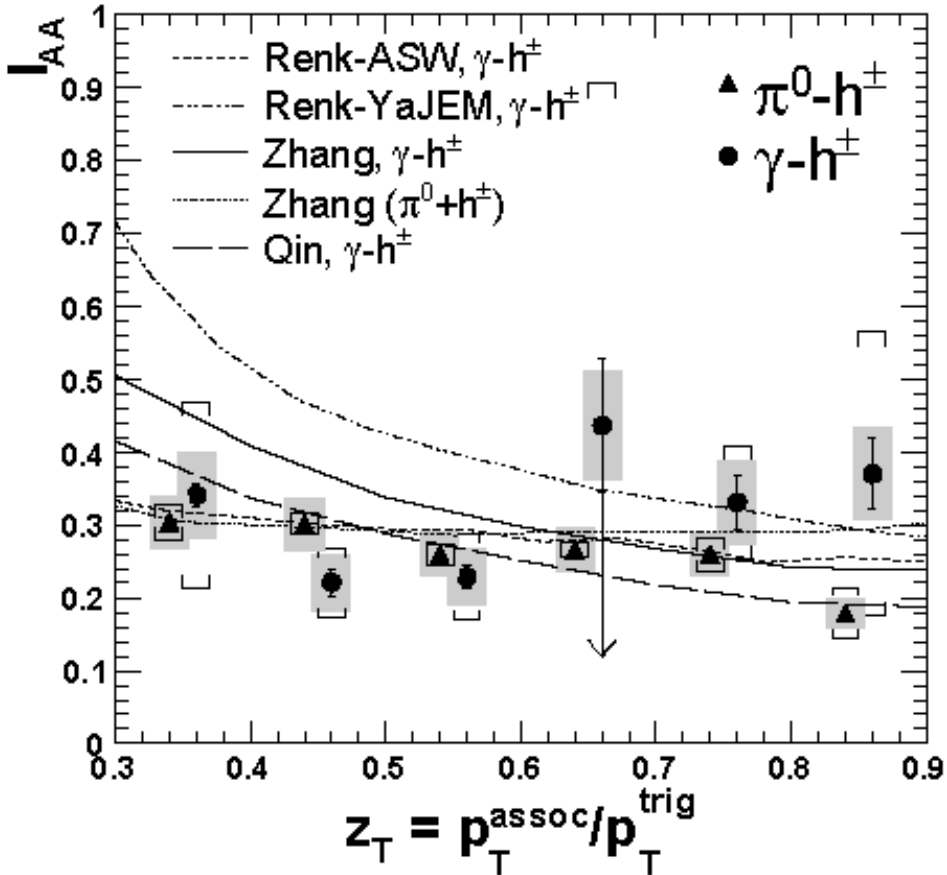
FIG. 2. Ratio of yields measured in central Au+Au to those measured in p+p collisions for direct photon triggers (circles) and π^0 triggers (triangles).

affected by the medium, direct photon triggers can originate from anywhere in the medium, while hadron triggers are biased to originate from the surface. This leads to a larger path length to traverse by the parton opposite to the hadron trigger than for the parton opposite to the direct photon trigger. Some of the model calculations [3-5] shown in Fig. 2 do predict this lack of dependence of the medium effect on the trigger species. In one calculation (Renk-ASW [5]), the explanation is that the fluctuations in energy loss dominate over any effect of geometry. Some of the models predict increased sensitivity to the

trigger species at lower z_T. With the increased statistics of the Run-10 Au+Au data (currently being written to tape), we will be able to extend the trigger p_T to higher values and thus lower the z_T. This will be one focus of future efforts on this topic.

[1] X.-N. Wang, Z. Huang, and I. Sarcevic, Phys. Rev. Lett. **77**, 231 (1996).
[2] B.I. Abelev *et al.* (STAR Collaboration), arXiv:0912.1871 [nucl-ex].
[3] H. Zhang *et al.*, Nucl. Phys. **A830**, 443c (2009).
[4] G.-Y. Qin *et al.*, Phys. Rev. C **80**, 054909 (2009).
[5] T. Renk, Phys. Rev. C **80**, 014901 (2009).

Upsilon measurements in the STAR experiment

M. Cervantes, R. Clarke, P. Djawotho, C. A. Gagliardi, A. Hamed, S. Mioduszewski,
and the STAR Collaboration

The main focus of the heavy flavor program at RHIC is to investigate the properties of the quark-gluon plasma (QGP) by studying its effect on open heavy flavor and quarkonia production. Suppression of the J/ψ induced by Debye screening of the static quantum chromodynamics (QCD) potential between charm-anti-charm pairs was original hailed as an unambiguous signature of QGP formation [1]. However, this simple picture is complicated by competing effects that either reduce the yield, such as co-mover absorption [2-3], or enhance it, such as in recombination models [4-6]. Recently, a growing interest in studying the Upsilon meson (Y) and its excited states has been kindled as it is expected that color screening will be the dominant effect contributing to any observed suppression of bottomonium production in heavy-ion collisions. A full spectroscopy of quarkonia states is now clearly recognized as one of the key measurements needed to understand the matter produced in high-energy heavy-ion collisions [7]. In particular, it has been recognized that data on the particle spectra of bottomonia can provide valuable information to constrain QGP models [8]. Due to the low production cross section of bottom-anti-bottom at RHIC (1.9 μb [9]), recombination effects in A+A collisions are negligible [10]. At the same time, the interaction cross section of bottomonium with the abundantly produced hadrons in these collisions is small [11], so suppression due to absorption by hadronic co-movers is expected by these models to be relatively unimportant. However, it will still be important to study production in d+Au collisions since available measurements by E772 [12] of cold nuclear matter effects on production at lower energy show some suppression. Nevertheless, the amount of suppression seen for the family is measured to be smaller than for charmonia. Therefore, bottomonium is expected to be a cleaner probe of high-temperature color screening effects. In addition to its important role in establishing deconfinement, a measurement of the Upsilon 1S, 2S, and 3S states in p+p and heavy-ion collisions can help to set limits on the medium temperature. The quarkonium measurements help in reaching these key goals because (*i*) an observation of suppression of Y production in heavy-ion relative to p+p collisions would strongly imply Debye screening and therefore deconfinement [10, 13], and (*ii*) the sequential suppression pattern of the excited states is sensitive to the temperature reached in the medium [7]. In this regard, lattice QCD studies have seen a burst of activity in recent years. Studies of quarkonia spectral functions and potential models based on lattice QCD indicate that while the Upsilon(3S) melts even before the deconfinement transition and the Upsilon(2S) is likely to melt at RHIC ($\sqrt{s}$=200 GeV), the Upsilon(1S) is expected to survive [7, 14, 15] beyond the parton-hadron phase transition. Recent results [13, 16] indicate further that almost all quarkonia states (J/ψ, ψ', χ_c, χ_b, Upsilon(2S)) melt below 1.357 T_c and the only one to survive to higher temperature is Upsilon(1S), which melts at 2T_c, where T_c≈175 MeV is the critical temperature for the phase transition. Therefore, a systematic study of all quarkonia states in p+p, d+Au, and Au+Au collisions will provide a clearer understanding of the properties of the QGP. Suppression of the Upsilon(2S) and Upsilon(3S) should be measurable at RHIC energies with increased integrated luminosity. In the near future, the larger luminosities proposed by the RHIC II program [17] will allow

for a statistically significant measurement of all 3 states. In the context of this objective, one of the first steps is to establish a baseline cross section measurement of the bottomonia states in p+p collisions. There are no previous measurements of Upsilon production in p+p at the top RHIC energy for heavy ions (an upper limit was estimated in the 2004 data with only half of the calorimeter [18]). The luminosities available at RHIC in the 2006 run provided the first opportunity to measure bottomonium at the previously unexplored center-of-mass energy of √s=200 GeV. A dedicated trigger algorithm exploiting the capabilities of the STAR electromagnetic calorimeter is essential for this measurement, and its development in STAR allows the Upsilon family to be studied in the e⁺e⁻ decay channel.

I. Upsilon cross section in p+p collisions at √s=200 GeV

The Cyclotron Institute was involved as primary author on a paper submitted by the STAR Collaboration to the journal publication Physical Review D which reports the Upsilon(1S+2S+3S) cross section at mid-rapidity, obtained with the STAR detector in p+p collisions at √s=200 GeV via the e⁺e⁻ decay channel. This measurement uses an integrated luminosity of 7.9 pb⁻¹ collected during RHIC Run VI (2006). The STAR data is compared to perturbative QCD calculations done at next-to-leading order (NLO) in the Color Evaporation Model (CEM) [17] and in the Color Singlet Model (CSM) [19].
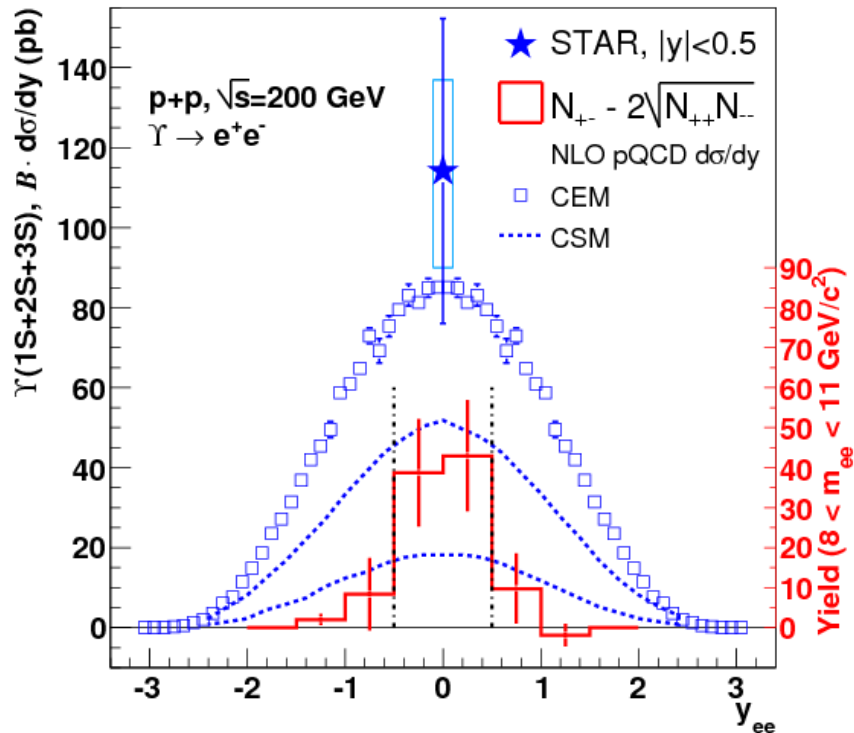
FIG. 1. The STAR measurement of the midrapidity Y(1S+2S+3S) cross section times branching ratio into electrons, compared to model calculations (COM and CSM).

We found the cross section to be 114 ± 38 (stat.)$^{+23}_{-24}$ (syst.) pb. Perturbative QCD calculations at NLO in the CEM are in agreement with our measurement, while calculations in the CSM underestimate it. Our result is consistent with the trend seen in the world data as a function of the center-of-mass energy of the collision and extends the availability of Upsilon data to RHIC energies. The di-electron continuum in the invariant mass range near the Upsilon is also studied to obtain a combined cross section of Drell-Yan plus b-bbar $\rightarrow e^+e^-$.
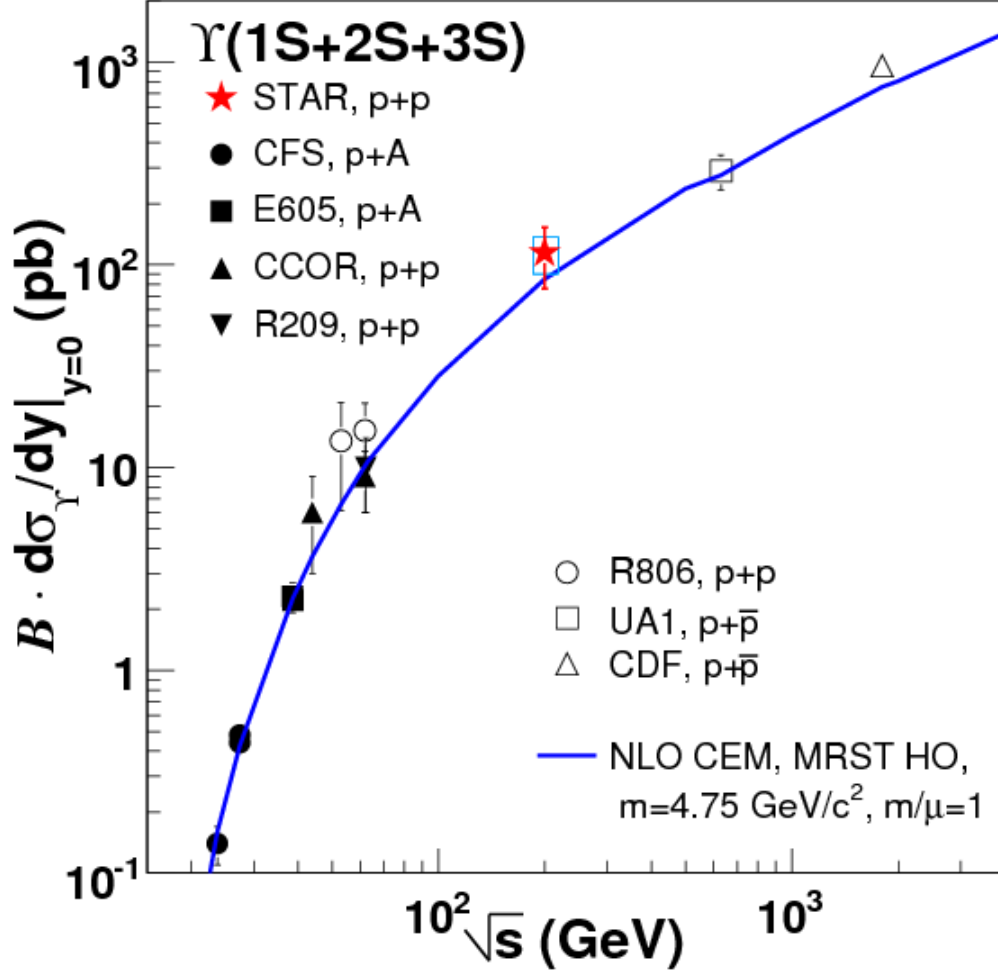
FIG. 2. Evolution of the Y(1S+2S+3S) cross section with center-of-mass energy for the world data and an NLO CEM calculation.

II. Upsilon + Hadron correlations in d+Au and p+p collisions at √s=200 GeV

In order to further study the systematics of prompt production of heavy quarkonium, e.g. via the Color Singlet Model (CSM) vs. the Color Octet Model (COM), we have explored additional experimental observables. Hadronic activity directly around the Upsilon has been proposed [20] as an

experimental observable to measure the radiation emitted off the colored heavy quark pair during production. Since the COM results in the radiation of a gluon off the produced quarkonium state, additional hadronic activity correlated with the Upsilon is expected for production through the color-octet channel vs. through a color singlet. Thus, possible insight into the prompt production mechanism of heavy quarkonium can be obtained from a correlation measurement. The high signal to background S/B ratio found in Upsilon reconstruction, even in d+Au collisions [21], enables us to perform an analysis of Upsilon + Hadron correlations. We performed the Upsilon + Hadron correlation analysis on the Run-8 d+Au and Run-9 p+p data, both at $\sqrt{(s_{NN})} = 200$ GeV.

Fig. 3 shows the reconstructed mass from e+e- pairs (black) and like-sign pairs (red) in p+p data. There is very little background observed even without background subtraction. The next steps in this analysis include the embedding Upsilon particles into real events in order to evaluate the efficiency corrections and the line shapes of the Upsilon(1S), Upsilon(2S) and Upsilon(2S) states.
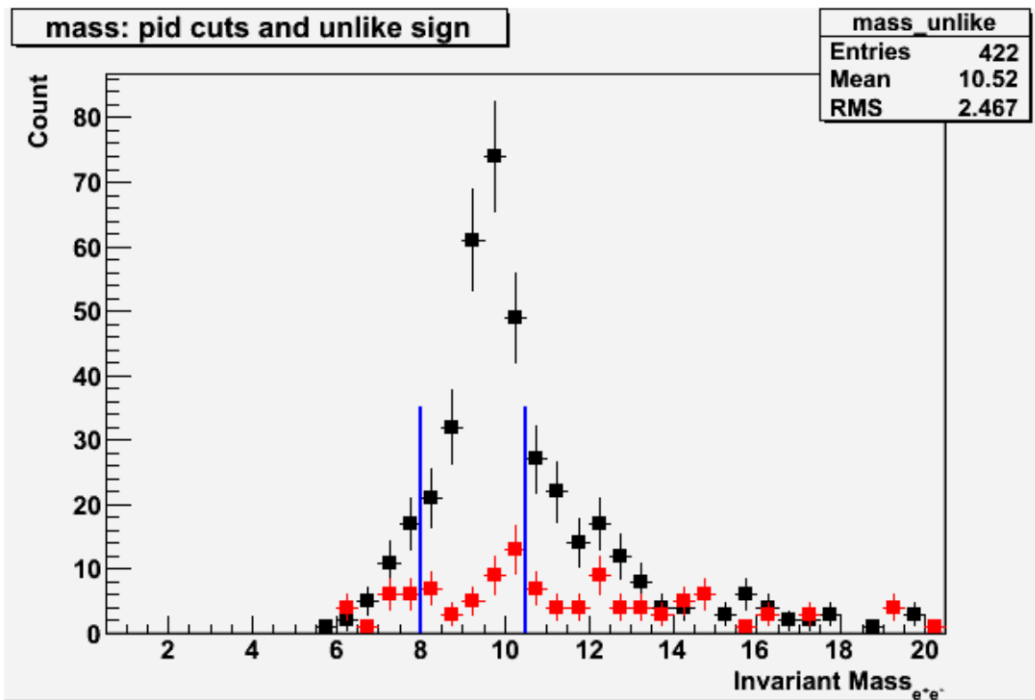
FIG. 3. Invariant mass distribution of e+e- pairs (black) and like-sign pairs (red) calculated in p+p events.

Fig. 3 also denotes the optimization for purity of the Upsilon's signal to background ratio (blue vertical lines) before the Upsilon + Hadron correlation is made. Fig. 4 shows the $\Delta\Phi$ - correlation measurement in p+p data (black), which is then corrected for background contributions (red). The results are compared to Monte Carlo (PYTHIA) [22] simulations (blue). Interpretation of the $\Delta\Phi$ – correlation shape is still in progress.
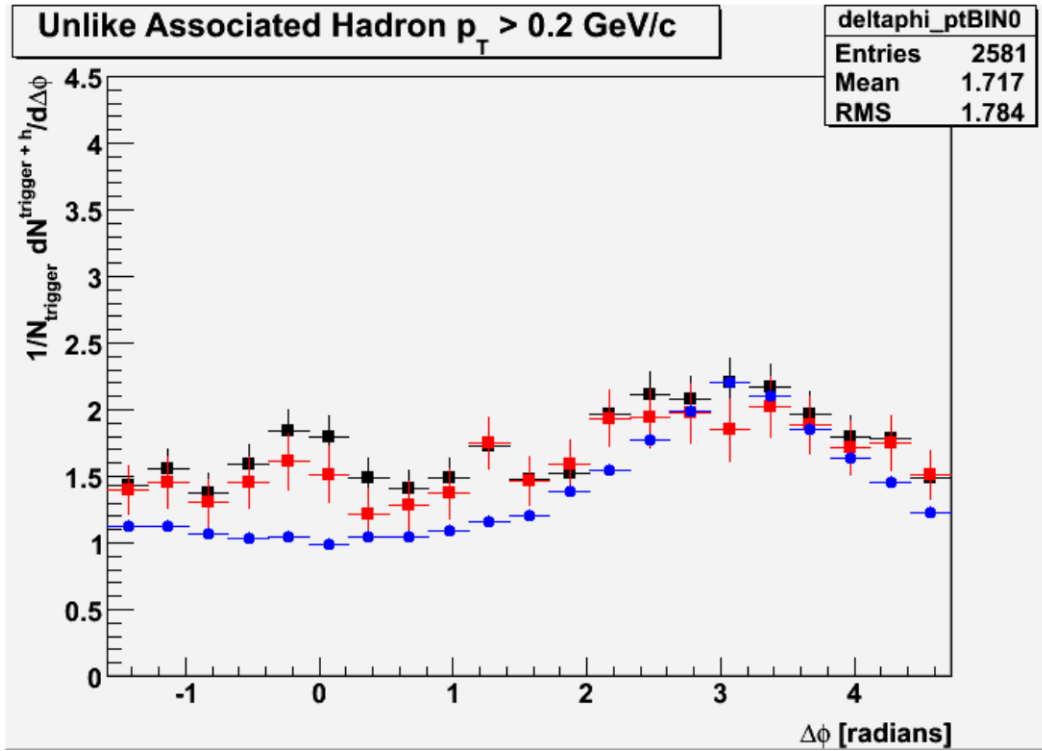
FIG. 4. $\Delta\phi$ - correlation: raw (black), corrected for background (red), and compared to Monte Carlo (blue) in p+p events.

[1] T. Matsui and H. Satz, Phys. Lett. B **178**, 416 (1986).

[2] S. Gavin, M. Gyulassy, and A. Jackson, Phys. Lett. B **207**, 257 (1988).

[3] J.-P. Blaizot and J.-Y. Ollitrault, Phys. Rev. D **39**, 232 (1989).

[4] L. Grandchamp *et al.*, Phys. Rev. Lett. **92**, 212301 (2004).

[5] R.L. Thews *et al.*, Eur. Phys. J. C **43**, 97 (2005).

[6] A. Andronic *et al.*, nucl-th/0611023.

[7] S. Digal, P. Petreczky, and H. Satz, Phys. Rev. D **64**, 56 094015 (2001); [arXiv:hep-ph/0106017].

[8] J.F. Gunion and R. Vogt, Nucl. Phys. **B492**, 301 (1997); [arXiv:hep-ph/9610420].

[9] M. Cacciari, P. Nason and R. Vogt, Phys. Rev. Lett. **95**, 60 122001 (2005); [arXiv:hep-ph/0502203].

[10] L. Grandchamp *et al.*, Phys. Rev. C **73**, 064906 (2006).

[11] Z.w. Lin and C. M. Ko, Phys. Lett. B **503**, 104 (2001); [arXiv:nucl-th/0007027].

[12] D.M. Alde *et al.*, Phys. Rev. Lett. **66**, 2285 (1991).

[13] A. Mocsy and P. Petreczky, Phys. Rev. Lett. **99**, 211602 65 (2007); [arXiv:0706.2183 [hep-ph]].

[14] S. Digal, P. Petreczky and H. Satz, Phys. Lett. B **514**, 57 (2001); [arXiv:hep-ph/0105234].

[15] C.-Y. Wong, Phys. Rev. C **72**, 034906 (2005).

[16] A. Mocsy and P. Petreczky, Phys. Rev. D **77**, 014501 (2008); [arXiv:0705.2559 [hep-ph]].

[17] A.D. Frawley, T. Ullrich and R. Vogt, Phys. Rep. **462**, 72 125 (2008).

[18] T. Kollegger, Ph.D. thesis, Johann Wolfgang Goethe-Universitat Frankfurt am Main, 2005.

[19] S.J. Brodsky and J. P. Lansberg, arXiv:0908.0754 [hep-ph].

[20] A.C. Kraan, arXiv:0807.3123.

[21] H. Liu (STAR Collaboration), arXiv:0907.4538.

[22] T. Sjöstrand, S. Mrenna, and P. Skands, Comput. Phys. Commun. **178**, 852 (2008).

SECTION II

HEAVY ION REACTIONS

The isospin dependence of the nuclear equation of state near the critical point

M. Huang, A. Bonasera, Z. Chen, R. Wada, K. Hagel, J. B. Natowitz, P. K. Sahu, L. Qin, T. Keutgen, S. Kowalski, T. Materna, J. Wang, M. Barbui, C. Bottosso, and M. R. D. Rodrigues

Recently, part of our reactions work has concentrated on probing the quantum nature of the liquid-gas phase transition using isotopic yield distributions [1] which may be discussed in terms of a modified Fisher model [2, 3]:

$$Y = y_0 A^{-\tau} e^{-\beta \Delta \mu A},\qquad(1)$$

where y_0 is a normalization constant, $\tau = 2.3$ is a critical exponent [2], β is the inverse temperature and $\Delta\mu = F((N-Z)/A)$ is the free energy per particle.

Projectiles of 40 A MeV ^{64}Zn, ^{70}Zn and ^{64}Ni beams were used to irradiate ^{58}Ni, ^{64}Ni, ^{112}Sn, ^{124}Sn, ^{197}Au, and ^{232}Th targets. Intermediate mass fragments (IMFs) were detected by a detector telescope placed at 20 degrees relative to the beam direction. For each atomic number 6-8 isotopes of very high quality were identified using the $\Delta E - E$ technique. Multiplicities of IMFs were evaluated from moving source fits. The yields of p, d, t, h and α particles, which were identified by the pulse shape discrimination method, were also evaluated by a moving source fit. After correction for accidental contributions, the multiplicities of ^{6}He and ^{8}He were calculated using the source fit parameters obtained for Li isotopes.

According to the Fisher equation given above, we can compare all systems on the same basis by normalizing the yields and factoring out the power law term. For this purpose we have chosen to normalize the yield data for each system to the ^{12}C yield (I = 0) in that system, i.e. we define a ratio:

$$R = \frac{YA^{\tau}}{Y\left(^{12}C\right)12^{\tau}},\qquad(2)$$

Our data organized by the order parameter m = (N-Z) /A, (the difference in neutron and proton concentration of the fragment). suggest that we are near the critical point for a liquid gas phase
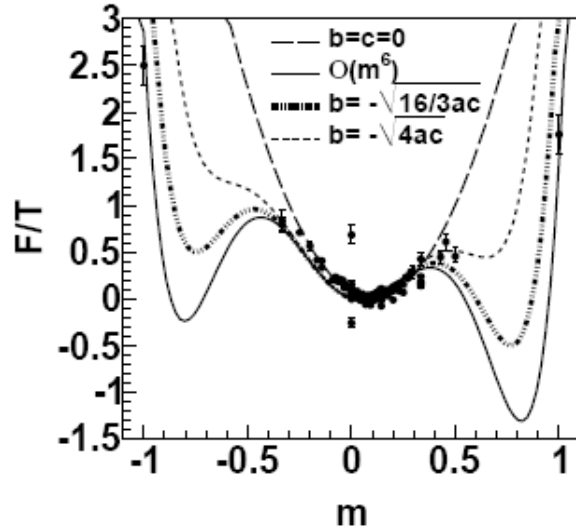
FIG. 1. Free energy versus m for the case ^{64}Ni+^{232}Th. The full line is a free fit based on Landau O(m^6) free energy. The dashed-dotted-dotted-dotted line is obtained imposing in the fit $b = -\sqrt{16/3ac}$ and it is located on a line of first order phase transitions. The short dashed line corresponds to $b = -\sqrt{4ac}$, i.e. superheating. The O(m^2) case, F/T = a(m − m$_s$)^2,i.e. b = c = 0, ms = 0.1, is given by the long dashed line.

transition (volume and surface terms equal to zero, Coulomb energy contribution not so important compared to the symmetry energy) Fig. 1 shows the quantity F/T= −ln(R)/A versus m = (N-Z)/A. As expected the normalized yield ratios depend strongly on m.

Pursuing the question of phase transitions, in the Laudau approach [1, 4] the ratio of the free energy (per particle) to the temperature is written in terms of an expansion:

$$\frac{F}{T} = \frac{1}{2}am^2 + \frac{1}{4}bm^4 + \frac{1}{6}cm^6 - m\frac{H}{T} \qquad (3)$$

where m is the order parameter, H is its conjugate variable and a−c are fitting parameters.

The use of the Landau approach is for guidance only. A free fit using Eq. (3) is displayed in Fig.1 (full line). The dashed-dotted-dotted-dotted line is obtained imposing in the fit $b = -\sqrt{16/3ac}$ and it is located on a line of first order phase transitions. The short dashed line corresponds to $b = -\sqrt{4ac}$, i.e. superheating. The O(m²) case, F/T = a(m − m$_s$)², i.e. b = c = 0, ms = 0.1, is given by the long dashed line. Similar to the phase transitions occurring in ^{4}He-^{3}He liquid mixtures, a nucleus, which can undergo a liquid-gas phase transition, should be influenced by the different neutron to proton concentrations. Thus the discontinuity observed in Fig.1 (m = 0) could be a signature for a tricritical point as in the ^{4}He-^{3}He case. We believe that our data, analyzed in terms of the the Landau O (m⁶) free energy, suggest such a feature but are not sufficient to clearly demonstrate this.

Once we know the free energy (at least in some cases) we can calculate the NEOS by means of the Fisher model [5]. Since we do not have at present experimental information on the density ρ, temperature T and pressure P of the system we can only estimate the 'reduced pressure' [6]:

$$\frac{P}{\rho T}(m) = \frac{M_0}{M_1}, \qquad (4)$$

where M$_i$ are moments of the mass distribution given by:

$$M_k = \sum_A A^k Y(A, m) = y_0 \sum A^k A^{-\tau} e^{-F/T(m)A}; k = 0,...n \ . \qquad (5)$$

Using the relations above we can calculate the NEOS for the situations illustrated in Fig. 1 but H/T=0 case. The results are displayed in Fig. 2 where the reduced pressure is plotted versus m for vaporization, superheating and first order phase transitions on the tri-critical line. Notice that there is not a large difference between the first two cases, while the last case displays two critical points (a third one is on the negative m axis).
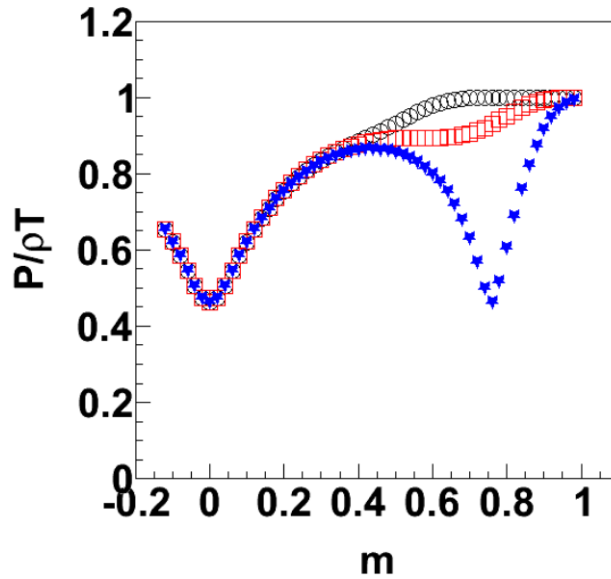
FIG. 2. Reduced pressure versus m of the fragments obtained from the a, b and c parameters fit to the Landau free energy, Eq.(3) for the $^{64}Ni+^{232}Th$. The curves correspond to vapor(open circles), superheating(open squares), first order (3 critical line-solid stars), see text.

[1] A. Bonasera *et al.*, Phys. Rev. Lett. **101**, 122702 (2008).

[2] A. Bonasera *et al.*, Rivista Nuovo Cimento, **23**, 1 (2000).

[3] R.W. Minich *et al.*, Phys. Lett. **118B**, 458 (1982).

[4] K. Huang, *Statistical Mechanics*, 2nd edition, Ch.16-17, (J. Wiley and Sons, New York, 1987).

[5] M.E. Fisher, Rep. Prog. Phys. **30**, 615 (1967).

[6] P. Finocchiaro *et al.*, Nucl. Phys. **A600**, 236 (1996); T. Kubo et al. Z. Phys. A **352**,145 (1995).

Variance of the isotope yield distribution and symmetry energy

Z. Chen, S. Kowalski, M. Huang, R. Wada, T. Keutgen, K. Hagel, J. Wang, L. Qin,
J. B. Natowitz, T. Materna, A. Bonasera, and P. K. Sahu

The ratio of symmetry energy coefficient relative to the temperature, a_{sym}/T , has been extracted as a function of Z from the variance of the observed isotope distributions from the experiments described in Ref.[1]. In order to explore the relation between the symmetry energy term in the free energy and the variance of the isotope distribution, Ono *et al.* introduced a generalized function K(N,Z) for the free energy in Ref. [2] as given below.

$$K(N,Z) = \sum_{i=1}^{n} w_i(N,Z)\left[-\ln Y_i(N,Z) + \alpha_i(Z)N + \gamma_i(Z)\right] \qquad (1)$$

Here i represents each reaction. The summation is taken over i for the reaction systems of different N/Z in order to get isotope multiplicity distributions over a wide range from proton rich to neutron rich isotopes. The average weights, $w_i(N,Z)$, are determined by minimizing the statistical errors in K(N,Z) for a given (N,Z). The isoscaling parameter, $\alpha_i(Z)$, is the isoscaling parameter value obtained by the method described in Ref. [1]. The K(N,Z) distribution from the experiment is shown in Fig. 1.
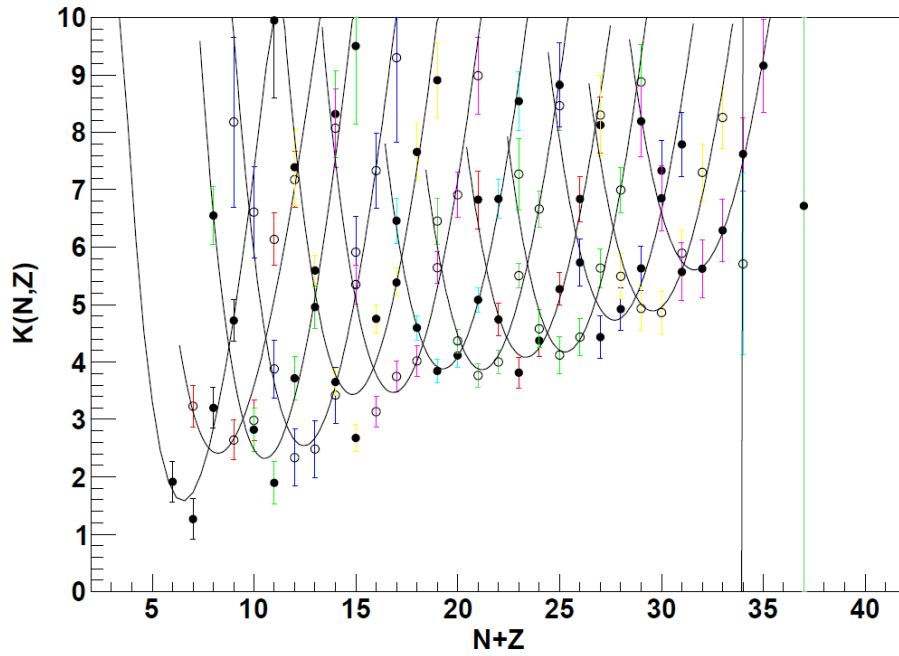
FIG. 1. K(N,Z) distribution from five reaction systems, ^{64}Ni+^{58}Ni, ^{64}Ni,^{112}Sn, ^{197}Au, ^{232}Th.

The isotope distributions for a given Z exhibit a smooth quadratic distribution and they can be fit by a function:

$$K(N,Z) = \xi(Z)N + \eta(Z) + \varsigma(Z)\frac{(N-A)^2}{A} \tag{2}$$

where $\xi(Z)$, $\eta(Z)$, $\zeta(Z)$ are the fitting parameters. The functional form, $\zeta(Z)$ is related to the symmetry energy coefficient as:

$$\varsigma(Z) = a_{sym}/T \tag{3}$$

In order to explore the experimental observation, the dynamical simulations have been made, using an Antisymmetrized Molecular Dynamics (AMD) model [3,4] with a statistical decay code, Gemini [5] , as an afterburner. All calculations shown in this report have been performed in a newly installed computer cluster in the Cyclotron Institute [6]. Using the same analysis as for the experimental data, the ratio a_{sym}/T has been obtained from the calculations.

The experimental values of a_{sym}/T obtained by the isoscaling technique is shown by solid circles in Fig. 2 [1], the values of $\zeta(Z)$ extracted using the technique described in this report are shown by solid squares. A comparisons between the experimentally extracted ratios of symmetry energy coefficient to temperature with those from the AMD model (open circles) is also presented in Fig. 2.
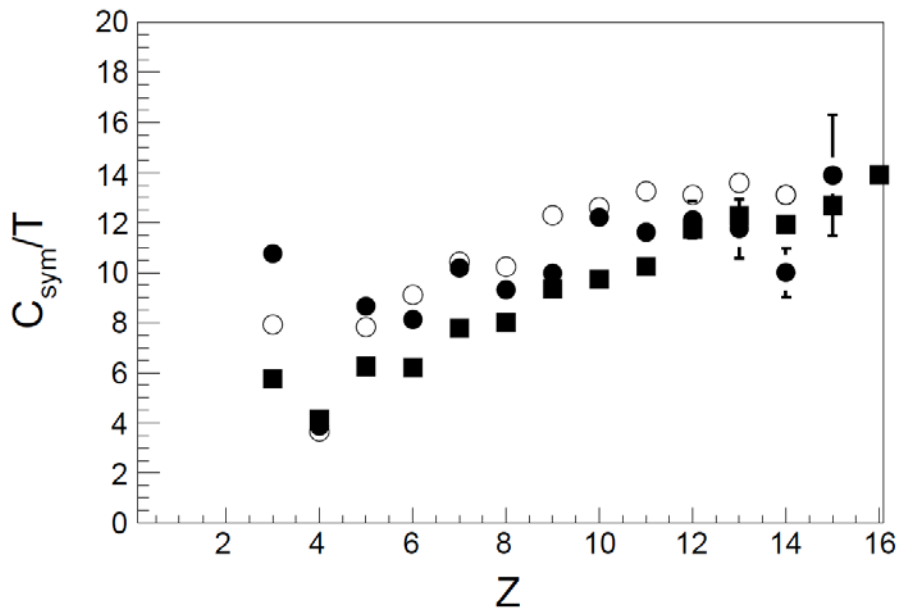
FIG. 2. Experimental and theoretical a_{sym}/T values as the function of Z. The values obtained by isoscaling technique is presented by solid circles. Squares are results of technique described in this report, open circles show values from AMD-Gemini calculations.

The results from the two experimental techniques are in reasonable agreement. The values and trends observed for the final fragments are well reproduced by the AMD plus Gemini model simulations.

[1] Z. Chen *et al.*, arXiv:1002.0319

[2] A. Ono *et. al.*, Phys. Rev. C **70**, 041604 (2004).

[3] A. Ono, Phys. Rev. C **59**, 853 (1999).

[4] A. Ono and H. Horiuchi**,** Phys. Rev. C **53**, 2958 (1996).

[5] R.J. Charity, Nucl. Phys. **A483,** 371 (1968).

[6] R. Wada *et al.*, *Progress in Research*, Cyclotron Institute, Texas A&M University (2008-2009), p. V-45.

A novel approach to Isoscaling: the role of the order parameter
m=(N-Z)/A

M. Huang, Z. Chen, S. Kowalski , R. Wada, T. Keutgen, K. Hagel, J. Wang, L. Qin, J. B. Natowitz,
T. Materna, P. K.Sahu, M. Barbui, C. Bottosso, M. R. D.Rodrigues, and A. Bonasera

The ratio of the isotope yields, R_{21}, between two similar reaction systems with different N=Z ratios can be expressed by the following isoscaling relation[1,2]:

$$R_{21}(N,Z) = C \exp(\alpha N + \beta Z) \tag{1}$$

where $\alpha=(\mu^1_n-\mu^2_n)/T$, $\beta=(\mu^1_p-\mu^2_p)/T$ are isoscaling parameters, representing the differences of the neutron (or proton) chemical potentials between systems 1 and 2, divided by the temperature. C is a constant.

Pursuing the question of phase transitions, in the Laudau approach [3,4] the ratio of the free energy (per particle) to the temperature is written in terms of an expansion:

$$\frac{F}{T} = \frac{1}{2}am^2 + \frac{1}{4}bm^4 + \frac{1}{6}cm^6 - m\frac{H}{T} \tag{2}$$

where m is the order parameter, H is its conjugate variable and a−c are fitting parameters. In our case m = (N-Z)/A.

Because of the symmetries of the free energy when we take the ratio between two different systems, presumably at the same temperature T and density ρ, we can obtain the difference between the free energies by taking the ratio dividing each experimental yield by the ^{12}C yield following in Ref. [5, 6] between two systems as in Eq. (1) as:

$$\frac{-\ln(R_{21}(m))}{A} = \Delta H / Tm + \text{constant} , \tag{3}$$

where $\Delta H/T = H_1/T - H_2/T$. Comparing the latter equation with Eq.(1) we obtain: $\Delta H/TmA = \alpha N + \beta Z$ i.e. $\alpha = -\beta = \Delta H/T$.

For an experiment, the projectiles ^{64}Zn, ^{70}Zn and ^{64}Ni, were used to irradiate targets of ^{58}Ni, ^{64}Ni, ^{112}Sn, ^{124}Sn, ^{197}Au and ^{232}Th at 40A MeV. Isotopes were detected inclusively at θ = 20° using quad-Si detector telescope. Isotopes are clearly identified up to Z<= 18. The measured energy spectrum of each isotope was integrated using a moving source fit to evaluate the multiplicity.

The scaling of Eq. (3) is satisfied for this set of data as seen in Fig. 1. Compared to 'traditional' isoscaling where a fit is performed for each detected charge Z (or each N) we see that all the data collapse into one curve.
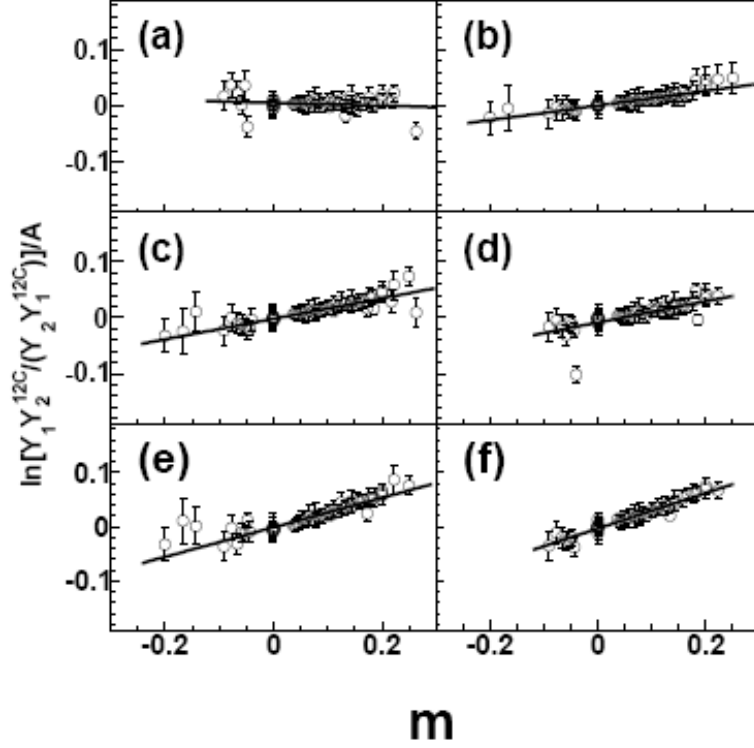
FIG. 1. Experimental ratios vs m for isotopes with $3 \leq Z \leq 13$ for (a) $\frac{^{64}Ni\,^{232}Th}{^{70}Zn\,^{197}Au}$, (b) $\frac{^{64}Ni\,^{112}Sn}{^{64}Ni\,^{58}Ni}$, (c) $\frac{^{64}Ni\,^{124}Sn}{^{64}Ni\,^{64}Ni}$, (d) $\frac{^{64}Ni\,^{197}Au}{^{64}Ni\,^{112}Sn}$, (e) $\frac{^{64}Ni\,^{124}Sn}{^{70}Zn\,^{58}Ni}$ and (f) $\frac{^{64}Ni\,^{124}Sn}{^{70}Zn\,^{112}Sn}$, respectively at 40MeV/A. The lines are the results of a linear fit according to Eq. (3).

We can further elucidate the role of the external field H/T writing the Landau expansion and 'shifting' the order parameter by m_s which is the position of the minimum of the free energy. Such a position depends on the neutron to proton concentration of the source [4]. Thus

$$\frac{F}{T} = \frac{1}{2}a(m - m_s)^2 + \frac{1}{4}b(m - m_s)^4 + \frac{1}{6}c(m - m_s)^6. \tag{4}$$

The Landau approach should be equivalent to it under certain conditions. In our experimental case that b and c are of comparable magnitude to parameter a, we can easily obtain:

$$\frac{\Delta H}{T}mA = \alpha\Delta m_s(N - Z) - \frac{1}{2}a(m_{s1}^2 - m_{s2}^2)A = \alpha N + \beta Z, \tag{5}$$

$$\alpha + \beta = -a(m_{s1}^2 - m_{s2}^2), \tag{6}$$

Eq. (6) shows that the two approaches are equivalent and that m is an order parameter if $\alpha + \beta = 0$ i.e. neglecting $O(m_s^2)$ terms in the external field. In Fig. 2 we plot $\alpha + \beta$ vs. $m_{s1}^2 - m_{s2}^2$, unfortunately the error bars are rather large but we can see a systematic deviation from zero as expected from Eq. (6) for large differences in concentration. This indicates that, at the level of sensitivity so far achieved with data of this type the presence of higher order terms in m is difficult to quantify. Thus, within the error bars, m could be considered an order parameter when relatively neutron (or proton) rich sources are considered. In particular, phase transitions in finite systems could be studied using the same language of macroscopic systems i.e., 'turning on and off' an external field [4].
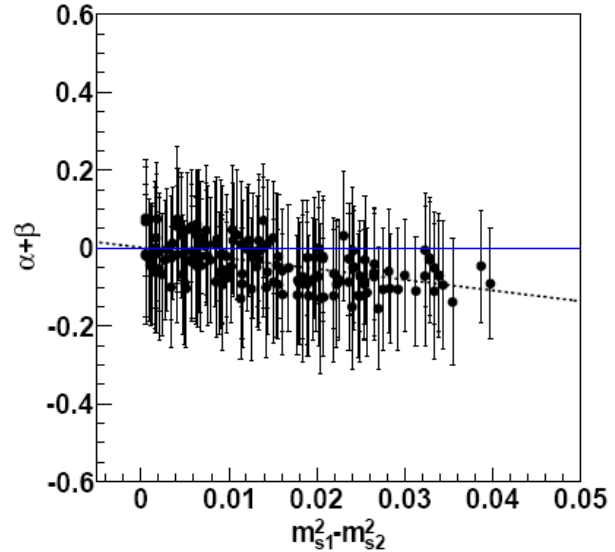
FIG. 2. $\alpha(Z) + \beta(N)$ vs the difference (solid circles) in concentration for the two reaction systems for the case of Z=N=7. The dotted line is the result of a linear fit.

[1] H.S. Xu, *et al.*, Phys. Rev. Lett. **85**, 716 (2000).

[2] M.B. Tsang *et al.*, Phys. Rev. Lett. **86**, 5023 (2001).

[3] K. Huang, *Statistical Mechanics*, 2nd edition, Ch.16-17, (J. Wiley and Sons, New York, 1987).

[4] A. Bonasera *et al.*, Phys. Rev. Lett. **101**, 122702 (2008).

[5] M.E. Fisher, Rep. Prog. Phys. **30**, 615 (1967).

[6] R.W. Minich *et al.*, Phys. Lett. B **118**, 458 (1982).

Isobaric yield ratios and the symmetry energy in Fermi energy heavy ion reactions

M. Huang, Z. Chen, S. Kowalski , Y. G. Ma, R. Wada, T. Keutgen, K. Hagel, J. Wang,
L. Qin, J. B. Natowitz, T. Materna, P. K. Sahu, M. Barbui, C. Bottosso,
M. R. D.Rodrigues, and A. Bonasera

According to the Modified Fisher model[1,2], the fragment yield of A nucleons with I = N-Z, Y(A,I) is given by,

$$Y(A,I) = CA^{-\tau} \exp\{[(W(A,I) + \mu_n N + \mu_p Z)/T] + N\ln(N/A) + Z\ln(Z/A)\}. \tag{1}$$

C is a constant. The $A^{-\tau}$ term originates from the entropy of the fragment and the last two terms are from the entropy contributions for the mixing of two substances in the Fisher Droplet Model [3]. μ_n is the neutron chemical potential and μ_p is the proton chemical potential. W(A,I) is the free energy of the cluster at temperature T. In the model W(A,I) is given by the following generalized Weiszacker-Beth semi-classical mass formula at a given temperature T and density ρ,

$$W(A,I) = a_v(\rho,T)A - a_s(\rho,T)A^{2/3} - a_c(\rho,T)Z(Z-1)/A^{1/3} - a_{sym}(\rho,T)I^2/A - \delta(N,Z). \tag{2}$$

The indexes, v, s, c and sym represent volume, surface, Coulomb, and symmetry energy, respectively. I=N-Z.

The isotope yield ratio between isobars differing by 2 units in I, R(I,I+2,A) can be deduced from Eq. (1) and Eq. (2),

$$\begin{aligned} R(I+2,I,A) = \exp\{&[(\mu_n - \mu_p) + 2a_c(Z-1)/A^{1/3} - 4a_{sym}(I+1)/A \\ &- \delta(N+1,Z-1) - \delta(N,Z)]/T + \Delta(I+2,I,A)\}. \end{aligned} \tag{3}$$

Hereafter, in order to simplify the description, the density and temperature dependence of the coefficients in Eq.(2) is omitted as $a_i = a_i(\rho,T)$ (i=v,s,c,sym,p).

^{64}Zn, ^{70}Zn and ^{64}Ni projectiles were incident on targets of ^{58}Ni, ^{64}Ni, ^{112}Sn, ^{124}Sn, ^{197}Au and ^{232}Th at 40A MeV. Isotopes were measured inclusively at $\theta = 20^o$ using quad-Si detector telescope. Isotopes are clearly identified up to Z<= 18. The measured energy spectrum of each isotope was integrated using a moving source fit to evaluate the multiplicity.

Initially we focus on the isobars with I= -1 and 1. For these isobars the symmetry term in Eq. (3) drops out and, since these isobars are even-odd nuclei, the pairing term also drops out. Taking the logarithm of the resultant equation, one can get

$$\ln R(1,-1,A) = [(\mu_n - \mu_p) + 2a_c(Z-1)/A^{1/3}]/T. \tag{4}$$

In Fig.1 the experimental values of ln[R(1,-1,A)] plotted for ^{64}Zn+^{112}Sn reactions as a function of A. Fitting these values using $(\mu_n - \mu_p)/T$ and a_c/T as fitting parameters, Eq.(3) leads to $(\mu_n - \mu_p)/T = 0.71$ and $a_c/T = 0.35$.
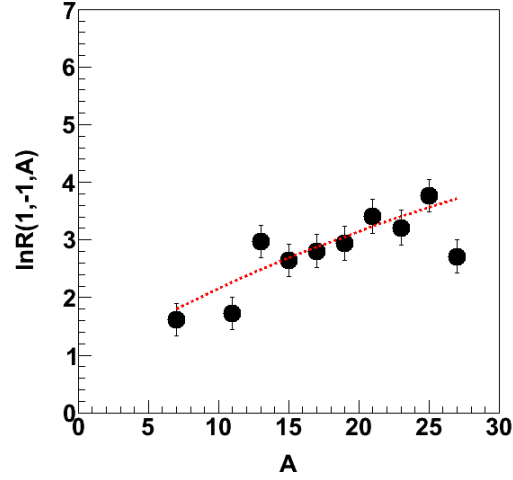
FIG. 1. The experimental values (solid circles) of ln[R(1,-1,A)] for ^{64}Zn+^{112}Sn reactions is plotted as a function of A for the isobars of I=-1. The dotted line shows the result of fitting with Eq.(4) .

We next compare isobars with I=1 and 3, the symmetry energy coefficient term in Eq.(3) is given as a function of A by

$$a_{sym}/T = -A/8\{\ln[R(3,1,A)] - [(\mu_n - \mu_p) + 2a_c(Z-1)/A^{1/3}]/T - \Delta(3,1,A)\} \tag{5}$$
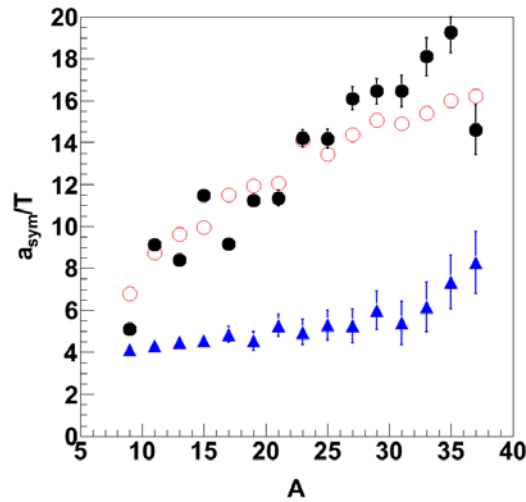
FIG. 2. Extracted values of the symmetry energy coefficient from ^{64}Zn + ^{112}Sn reactions (solid circles) and results of calculations for the secondary fragments (circles). Triangles show results obtained for primary fragments.

In Fig.2 results for ^{64}Zn+^{112}Sn reactions (solid circles) of a_{sym}/T calculated from Eq. (5), using the values $(\mu_n - \mu_p)/T$ and a_c/T determined in Eq. (4), are plotted as a function of A. The extracted values from the experiments are in good agreement with those calculated for the secondary fragments. In general the values increase from ~5 to ~16 as cAincreases from 9 to 37. These values are generally much larger than those extracted for the primary fragments (triangles) observed in the AMD calculations. Over the same mass interval the primary fragment values range from 4 to 5. The comparisons between the experimentally extracted results and those of the calculations indicate that the experimental determination of symmetry energy coefficients, a_{sym}/T, are significantly affected by these secondary decay processes of the primary fragments.

[1] R.W. Minich *et al.*, Phys. Lett. B **118**, 458 (1982).
[2] A.S. Hirsch, A. Bujac, J.E. Finn, L.J. Gutay, R.W. Minich, N.T. Porile, R.P. Scharenberg, B.C. Stringfellow, F. Turkot, Nucl. Phys. **A418**, 267c (1984).
[3] M.E. Fisher, Rep. Prog. Phys. **30**, 615 (1967).

Isoscaling and the symmetry energy in the central heavy ion collisions at intermediate energy

Z. Chen, S. Kowalski, M. Huang, R. Wada, T. Keutgen, K. Hagel, A. Bonasera,
J. B. Natowitz, T. Materna, L. Qin, P. K. Sahu, and J. Wang

In heavy reactions at intermediate energies the isoscaling relation , which is give below,

$$R_{21}(N,Z) = \frac{Y_2(N,Z)}{Y_1(N,Z)} = C\exp(\alpha N + \beta Z) \qquad (1)$$

has been generally observed [1,2]. Here $Y_i(N,Z)$ are the fragment yield for systems i=1,2 with different neutron and proton composition. α, β are isoscaling parameters. As discussed in refs. [3-5], the isoscaling parameters and the symmetry energy coefficient are closely related. For a multifragmentation regime, as pointed out in Ref. [6], this relation is given by:

$$\alpha(Z) = 4a_{sym}\Delta\left(Z/\overline{A}\right)^2 / T \qquad (2)$$

where a_{sym} is the symmetry energy coefficient, T is the temperature of the source and $\Delta(Z\overline{A})^2 = \Delta(Z/\overline{A})_1^2 - \Delta(Z/\overline{A})_2^2$ represents the difference in that quantity of $(Z/\overline{A})$ for the two systems and $\overline{A}$ is the average mass number of isotopes for a given Z.

Experiments were performed, using ^{64}Zn, ^{70}Zn and ^{64}Ni beams at 40 AMeV incident on ^{58}Ni, ^{64}Ni, ^{112}Sn, ^{124}Sn, ^{197}Au and ^{232}Th targets. Details of the analysis are given in Ref. [7]. Isoscaling parameters, $\alpha(Z)$ and $\beta(N)$, have been evaluated for all possible combinations between two reactions. The extracted isoscaling parameters are plotted as a function of $\Delta(\overline{\frac{Z}{A}})^2$ in Fig. 1 for Z=6 and Z=12. The
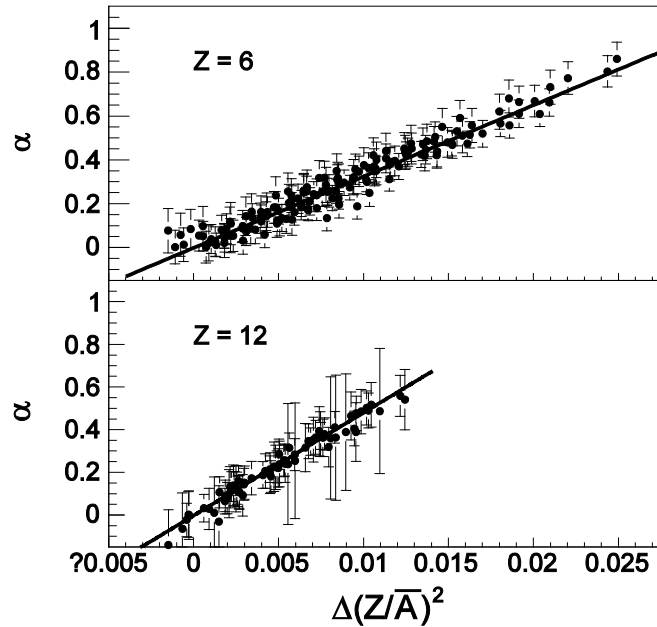
FIG. 1. $\alpha(Z)$ values as a function of $\Delta(Z/\overline{A})^2$ for Z=6 (upper) and Z=12 (lower).

correlations have been fit by a linear function for each Z and the slope values, which correspond to the value $4\,a_{sym}/T$ in Eq. (2), have been extracted.

In Fig. 2, the extracted values of a_{sym}/T are plotted as a function of Z and shown by solid dots. In order to elucidate the experimentally extracted ratio, a_{sym}/T, dynamical model simulations have been made, using an Antisymmetrized Molecular Dynamics (AMD) model [8-10] and a statistical decay code, Gemini [11]. The systems examined are ^{64}Ni + ^{64}Ni, ^{64}Ni + ^{124}Sn, ^{64}Zn + ^{58}Ni, and ^{64}Zn + ^{112}Sn at 40 AMeV. All calculations have been performed in a newly installed computer cluster in the Cyclotron Institute [12]. The calculated values of a_{sym}/T are shown by open circles in Fig.2. The calculated values are typically one to two units higher than the experimental values (dots) but the trends are essentially the same. This is also consistent with the values extracted from $\zeta(Z)$ by an independent analysis described in Ref.[7].
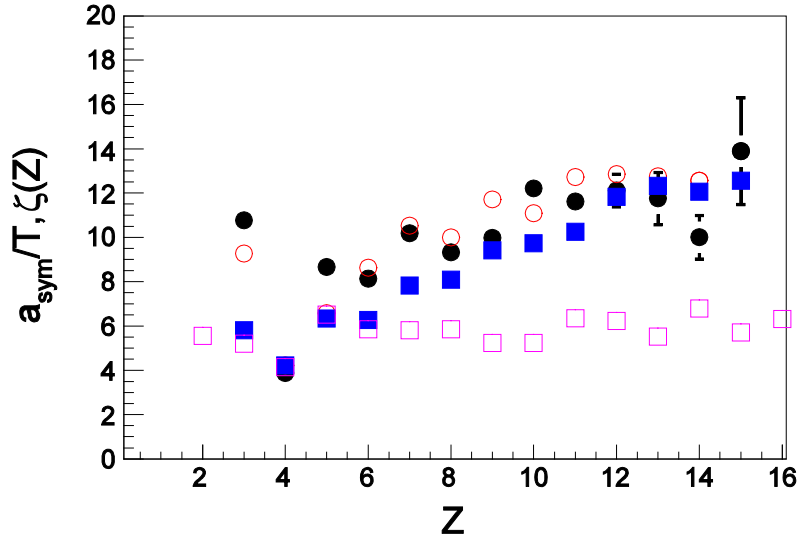
FIG. 2. Experimental a_{sym}/T values extracted from Eq. (2) are shown by dots as a function of Z. Open circles show calculated values, extracted in the same way, from the fragments yields in AMD-Gemini calculations, and open squares indicated results from the primary fragments of the AMD simulation with. The experimental results from ζ (Z) in ref.[7] are shown by the solid squares.

On the other hand the a_{sym}/T values extracted from the primary fragments of AMD show a rather flat distribution, as shown by the open squares in the figure, suggesting that the experimentally observed strong Z dependence of a_{sym}/T originates from the secondary decay process of the excited fragments after their formation.

[1] H.S. Xu *et al.*, Phys. Rev. Lett. **85**, 716 (2000).
[2] M.B. Tsang *et al.*, Phys. Rev. Lett. **86**, 5023 (2001).
[3] A.S. Botvina, O.V. Lozhkin, and W. Trautmann, Phys. Rev. C **65**, 044610 (2002).
[4] L.G. Moretto, C.O. Dorso, J.B. Elliott, and L. Phair, Phys. Rev. C **77**, 037603 (2008).

[5] A. Ono *et al.*, Phys. Rev. C **70**, 041604(R) (2004).

[6] A. Ono *et al.*, Phys. Rev. C **68**, 051601(R) (2003).

[7] Z. Chen *et al*., arXiv:1002.0319, 2010.

[8] A. Ono and H. Horiuchi, Phys. Rev. C **53**, 2958 (1996).

[9] A. Ono, Phys. Rev. C **59**, 853(1999).

[10] S. Hudan, R.T. de Souza, and A. Ono, Phys. Rev. C **73**, 054602 (2006).

[11] R.J. Charity *et al.*, Nucl. Phys. **A483**, 371(1988).

[12] R. Wada *et al., Progress in Research*, Cyclotron Institute, Texas A&M University (2008-2009), p. V-45.

The search for super heavy elements using alternative mechanisms

M. Barbui, K. Hagel, J. B. Natowitz, R. Wada,T. Materna, Z. Chen, L. Qin, P. K.Sahu, G. Souliotis, G. Chubaryan, F. D. Bechetti,[1] T. W. O'Donnell,[1] H. Griffin,[1] S. Moretto,[1] D. Fabris,[2] M. Lunardon,[2] M. Morando,[2] G. Nebbia,[2] S. Pesente,[2] V. Rizzi,[2] G. Viesti,[2] V. Bocci,[3] A. Andrighetto,[4] M. Cinausero,[4] G. Prete,[4] Z. Majka,[5] A. Wieloch,[5] and S. Kowalski[6]

[1]*Department of Physics, University of Michigan, Ann Arbor, Michigan*
[2]*Dipartamento di Fisica dell'Universita di Padova and INFN Sezione di Padova, Italy*
[3]*Dipartimento di Fisica dell'Universita di Brescia and INFN, Italy*
[4]*INFN Laboratori Nazionali di Legnaro, Italy*
[5]*Smoluchowski Institute of Physics, Jagiellonian University, Krakow, Poland*
[6]*Institute of Physics, Silesia University, Katowice, Poland*

We reported a scheme of filtering events [1] in our search for Super Heavy Elements (SHEs) [2] to minimize the probability of identifying accidental events as super heavy element candidates. That analysis employed the profile of energy loss through successive segments of the ionization chamber (IC). We have continued the analysis of this data in an effort to assign an estimate of the charge and mass of the filtered SHEs. To accomplish this, we refined the filtering of the events to compare the IC energy loss profile of heavy elements to the predictions of an extrapolation based on the stopping power parameterization discussed in Ref. [3] which would lead to an estimate of the charge.

The comparison of the previously filtered heavy element candidates to the predictions of the extrapolated energy loss profile led us to the conclusion that the previously filtered events could not be real. We therefore used the extrapolated energy loss profile prediction as a filter in itself. This has the advantage that any SHE candidate that passes the filter will be consistent with the energy loss prediction of the particular assigned charge.

The complete unfiltered charge distribution of detected products that pass the hardware pileup filter is shown in Fig. 1. We note that there is a concentration of products in the region of the projectile. Above the target charge, we observe a small number of events. Even though the hardware pileup rejection has been applied, many of these events might result from pileup events that our hardware rejection missed. We therefore use all of the redundant measurements described in [1] to examine whether any of these higher charge events might be real.

The first check we make is to compare the measurement of the total energy obtained with the peak sensing ADC with that of the Flash ADC. That comparison is shown in Fig 2. The small scatter points represent the total event sample. The large solid points indicate the events that survived the filtering on charge as described above. The pileup rejection condition was not applied to these events. We note that only a few of the filtered events lie on or within a few percent of the diagonal line. The other events lie above the line. We speculate that these events result from accidental pileup in which the peak sensing ADC is integrating an event from a previous beam burst that occurred while the data acquisition was busy and then adding to it the triggered event that occurred a short moment later. We reject the events that do not line within a few percent of the diagonal line.
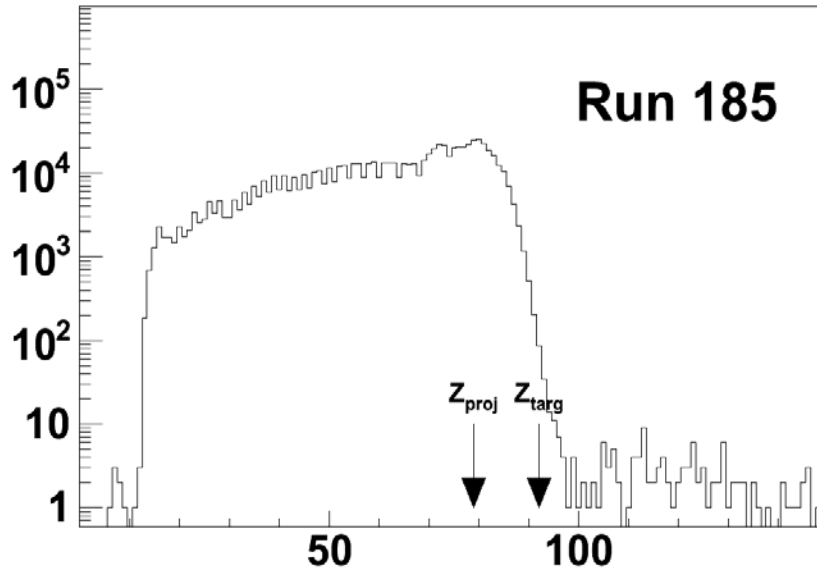
FIG. 1. Z distribution of all products that pass the hardware pileup rejection from a typical run.

We then further filter the accepted high charge events using the hardware pileup rejection.
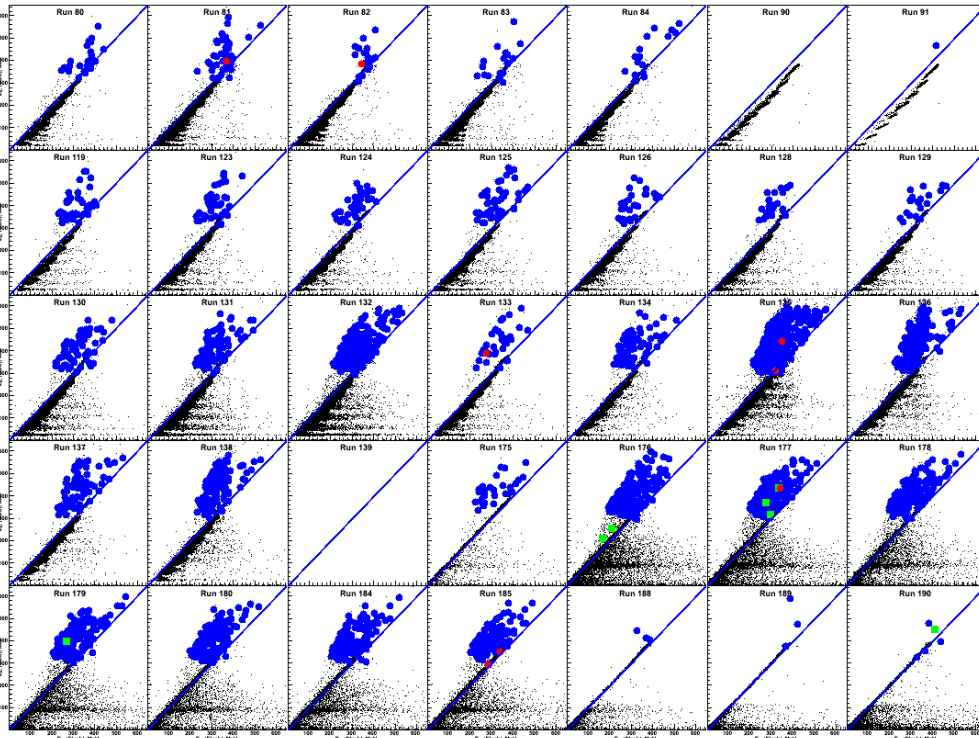
FIG. 2. Comparison of E measured from peak sensing ADC (y axis) with E measured from Flash ADC (x axis). A consistent measurement lies on the diagonal line.

Those points are shown in red in Fig. 2. That brings the total number of candidates to 5. We note that of those five, only 4 ie within 10% of the diagonal line, ie are a consistent measurement between the peak sensing ADC and the Flash ADC. One of the events fails one of the redundant time of flight tests and is therefore rejected as well.

The fit of the extrapolated stopping powers to the remaining events is shown in Fig. 3. We note that the
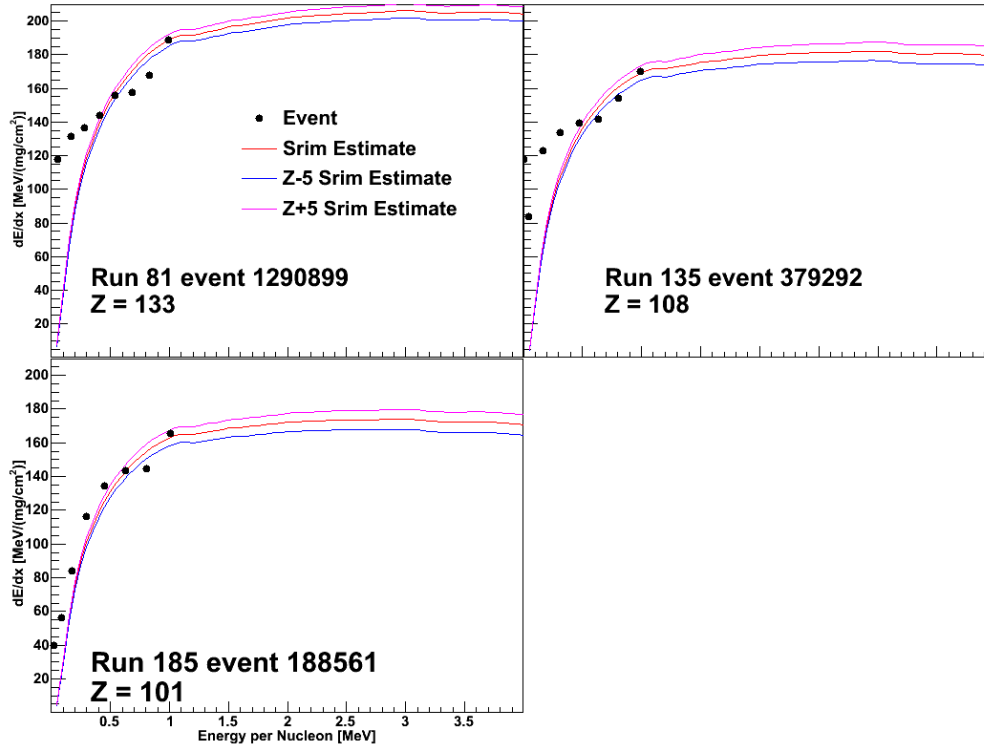
FIG. 3. Fits of the data to extrapolated SRIM. The calculated charge is shown.

data in the top two panels show a completely different characteristic as compared to the prediction of the extrapolated version of SRIM. We therefore reject those two events.

We are left with one event that has a charge near 100 that passes all of the tests. We have calculated based on an extension of what we reported previously [1] that we have a sensitivity of about 11nb per event.

That we have one event that passes all of the stringent tests gives us hope that we can use this technique in the search for super heavy elements. It is necessary, however, to build in several enhancements. We are planning an experiment to extend this study in which we hope to increase our sensitivity by a factor of 10-50. In addition, we plan to pulse the beam to eliminate the possibility of the spurious events in the peak sensing ADC. The plans also call for segmenting the IC in order to directly detect more of the events where more than one enter the IC at the same time.

[1] J.B. Natowitz *et al*, *Progress in Research*, Cyclotron Institute, Texas A&M University (2008-2009) p. II-1.

[2] P. Sahu *et al*, *Progress in Research*, Cyclotron Institute, Texas A&M University (2006-2007) p. II-1.

[3] M. Barbui *et al.*, Nucl. Instrum. Methods Phys. Res. **B** (in press), doi:10.1016/j.nimb.2010.04.018.

A new stopping power parameterization for 0.5-15 MeV/nucleon heavy and superheavy ions in solids and gases

M. Barbui, K. Hagel, J. B. Natowitz, R. Wada, D. Fabris,[1] M. Lunardon,[1] S. Moretto,[1] G. Nebbia,[1] S. Pesente,[1] and G. Viesti[1]

[1]*Dipartimento di Fisica Università degli Studi di Padova and INFN Sezione di Padova, Via Marzolo 8, I-35131 Padova, Italy*

Electronic stopping powers of heavy ions in several media are deduced from the corresponding proton data by using new effective charge parameterizations. Separate sets of parameters were deduced for solid and gaseous materials using the available data for heavy ions in the energy range from 0.5 to 15 MeV/nucleon. Using these results, predictions are made for stopping powers of heavy and superheavy elements with $Z=100$ to 130 in the energy range of 0.5 to 15 MeV/nucleon.

In a given stopping medium, the stopping power (S_I) of an ion is related to that of a reference ion (S_{Ref}) with the same velocity by the scaling law

$$\frac{S_I}{(\gamma_I Z_I)^2} = \frac{S_{\text{Ref}}}{Z_{\text{Ref}}^2}$$

(1)

where $\gamma_I Z_I$ is the effective charge of the ion with atomic number Z_I. In this equation, the reference ion having atomic number Z_{Ref} is assumed to be fully stripped.

The effective charge fraction γ can be defined empirically by

$$\gamma^2 = \frac{S_I(v, Z_I, \text{target})/Z_I^2}{S_{\text{Ref}}(v, Z_{\text{Ref}}, \text{target})/Z_{\text{Ref}}^2}$$

(2)

where v is the ion velocity and "target" labels the stopping material.

We use protons as reference ions since they can be fully stripped at lower energies than ^{4}He. The proton stopping powers are obtained using the SRIM-2008 code [1], a widely employed stopping power tool. Using these reference stopping powers, the effective charge values, γ were extracted using relationship (2) and the experimental stopping powers for Ar, Kr, Au, Pb and U ions in solid and gaseous materials.

The empirical γ values were then reproduced using the relationships:

$$\gamma = 1 - P_0 \exp(-P_1 E_A^{p_2}/Z^{p_3})$$
$$P_0 = p_0 + p_1 \ln(Z)$$
$$P_1 = p_4 + p_5 \ln(Z)$$

(3)

where p_0, p_1, p_2, p_3, p_4 and p_5 are fitting parameters, Z is the atomic number of the ion and E_A is the specific energy in MeV/nucleon.

The available experimental stopping powers for Ar, Kr, Au and U ions in isobutane [2] (258 experimental points in the energy range from 0.1 to 15 MeV/nucleon) were used to determine the parameters for gaseous media, whereas data relative to the same projectiles but in aluminum, silver, gold and mylar were used for solid media [2,3].

To assess the quality of our work, Fig. 1 shows how results of our parameterization compare with the SRIM-2008 and Hubert predictions [4] and with the experimental stopping powers of Ar and U in Aluminum. It is clear that, while for Ar ions the quality of all the calculations is comparable, for U ions our parameterization gives the best reproduction of the experimental data.
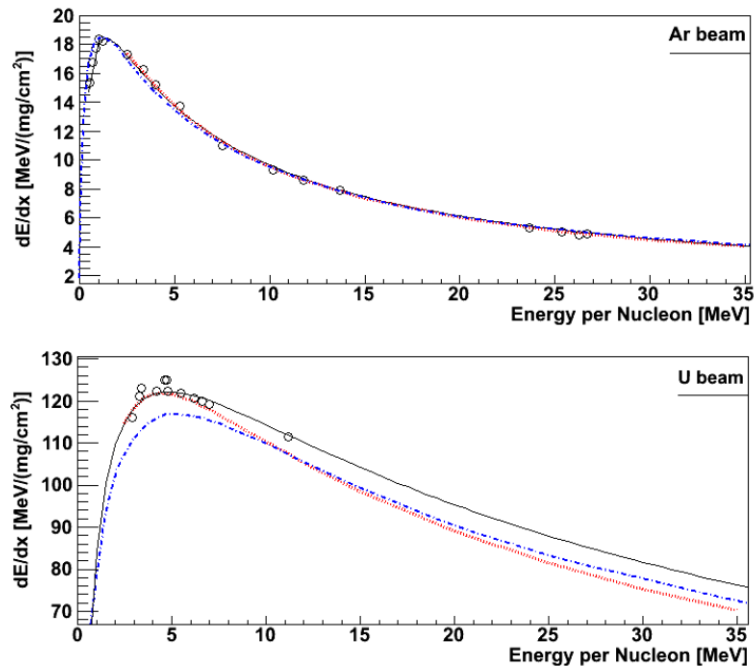
FIG. 1. Comparison of experimental stopping powers for Ar and U in aluminum (open circles) with the values calculated using our parameterization of the effective charge data (black solid line), using SRIM-2008 (blue dot-dashed line), using the Hubert tables (red dotted line)

Our parameterization is valid for projectiles with atomic number from Z=18 to Z=92 in the energy range from 0.5 to 15 MeV/nucleon, for the tested stopping materials. On average, in the energy range from 1.5 to 15 MeV/nucleon, the predicted stopping powers agree with the experimental data to within 5% whereas the agreement is to within 10% for lower energies.

Given the good reproduction of the stopping powers of high Z projectiles we believe that we can extrapolate the results to ions with atomic number larger than 100. Therefore the parameterization was

used to predict stopping power values for superheavy elements with Z>100 in Al, mylar and isobutane. The results are shown in Fig. 2.
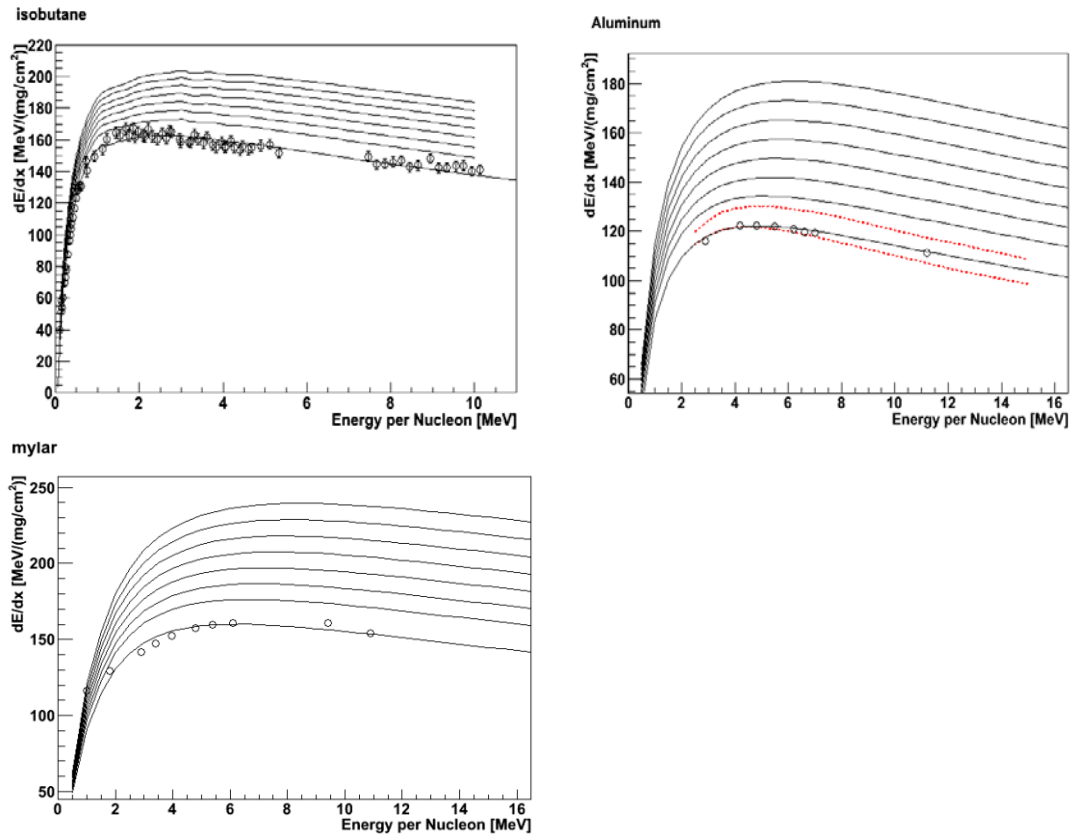
FIG. 2. The calculated stopping powers of heavy ions with atomic number Z=92, 100, 105, 110, 115, 120, 125, 130 in isobutane, aluminum and mylar are shown as a function of the specific energy (solid lines). For comparison, the measured stopping powers of U (Z=92) ions are also shown (open circles). The dashed lines in the Al target figure represent the prediction of the Hubert tabulations for Z=92 and Z=100.

[1] http://www.srim.org

[2] M. Barbui *et al.*, Nucl. Instrum Methods Phys. Res. **B268** ,20 (2010).

[3] A collection of experimental data is available at the H. Paul web page (http://www.exphys.uni-linz.ac.at/stopping/).

[4] F. Hubert *et al.*, At. Data Nucl. Data Tables **46**, 1 (1990).

Progress in BRAHMS

K. Hagel, R. Wada, J. B. Natowitz and the BRAHMS Collaboration

The last data from the BRAHMS experiment at RHIC were taken in 2006. Most, if not all, of the data analysis of the various data sets has been completed. There are a number of papers in preparation, notably a summary of the 200 and 62 GeV p + p data, a long paper showing results on the 200 and 62 GeV Cu + Cu data, a summary paper on 200 GeV Au + Au that, among other topics, extends the analysis of the stopping[1] to include the centrality dependence.

We have completed the analysis of the 200 GeV p + p data of run V at the Cyclotron Institute and are in the process of preparing the summary of the 200 and 62 GeV data. Among the analysis that we performed in the past year builds on the net proton rapidty distributions previously shown[2]. In that work we demonstrated longitudinal scaling from 17 GeV to 200 GeV.

We have extended that work to extract net baryon distributions. This is done by correcting the net protons for other baryons that are not observed in our experiment:

$$\frac{dN_{B-\bar{B}}}{dy} = \frac{dN_{p-\bar{p},meas}}{dy} \frac{n_p + n_n + n_\Lambda}{n_p + c_1 n_\Lambda}$$

where n_i is the true net number of each particle species and c_1 is the number of protons from weak decays for each lambda which was determined from Hijing calculations[1]. This expression can be rewritten in terms of ratios of the various particles to protons and then the important parameters are the net proton to net lambda and net proton to net neutron ratios. We employed Pythia[3] calculations to estimate these ratios as a function of rapidity. We checked the results of nl/n_p at mid rapidty with measured data[4] and found the results to agree within error.

The solid points in the bottom two panels of Fig. 1 show the net baryon distribution extracted in this way for the 62 GeV and 200 GeV data, respectively. The solid points in the top panel show the net baryon distribution extracted from net proton distributions at 17 GeV[5]. This study details a complete measurement over the entire rapidity range at 17 GeV.

We wish to study stopping in 200 and 62 GeV p + p collisions. Without a measurement over the entire rapidity distribution, results must be corrected for the unobserved yield. We have, in fact, performed such corrections in several studies of Au + Au at 200 GeV[1] and 62 GeV[6]. The largest rapidity measured in the p + p data, both at 62 and 200 GeV, is well below the beam rapidity. Although we could, in principle, perform estimates of the corrections for the unobserved yield, we examine whether the longitudinal scaling observed in the net proton distributions [2] can provide information on the stopping at 200 and 62 GeV.

The study at 17 GeV also quoted the results in terms of dN/dx_F. The open squares in the top panel of Fig. 1 show the dN/dx_F transformed to dN/dy. As expected they overlap in the region of rapidity where dN/dx_F is quoted. If there is longitudinal scaling in the net baryon distributions, the dN/dx_F should be constant. We therefore transform the dN/dx_F to dN/dy for each of the systems at 200 and 62 GeV. These data transformed from 17 GeV are shown as open squares in the bottom two panels of Fig. 1. We
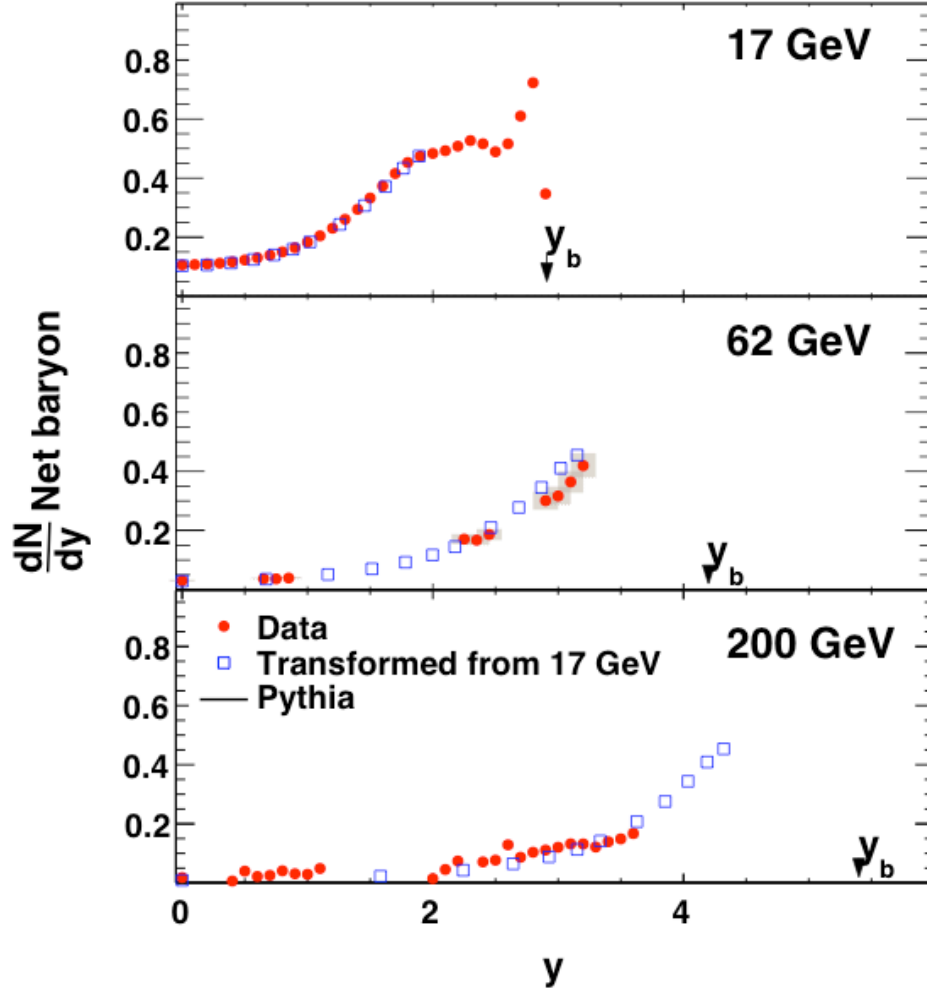
FIG. 1. Net baryon distributions for 17 GeV (top panel), 62 GeV (middle panel) and 200 GeV (bottom panel).

note nearly complete overlap in the regions of common rapidity. We interpret this to mean that we do, indeed, observe longitudinal scaling in the net baryon rapidity density from 17 GeV to 200 GeV implying that the mechanism of baryon transport does not change over this large range of $\sqrt{s_{nn}}$.

We have also extracted 4π multiplicities for the products measured in our experiments. This was done by integrating the rapidity densities that we measured [7] from mid-rapidity to the beam rapidity. To accomplish the integration, we fit the data to a Gaussian and then integrated the Gaussian from y=0 to y=y_p. Fig. 2 shows the 4π multiplicities that we extracted along with data from earlier measurements. Also shown in the figure are data from earlier measurements at lower energies [8,9]. We note that the BRAHMS data at 62.4 and 200 GeV extends the earlier systematics. The dashed curves show fits to our data as well as the earlier data. These fits are extrapolated to LHC energies and provide a prediction of particle multiplicities that can be expected at those energies.

The results of the 200 and 62.4 GeV p + p data are summarized in a detailed paper that is in final preparation by the BRAHMS collaboration.
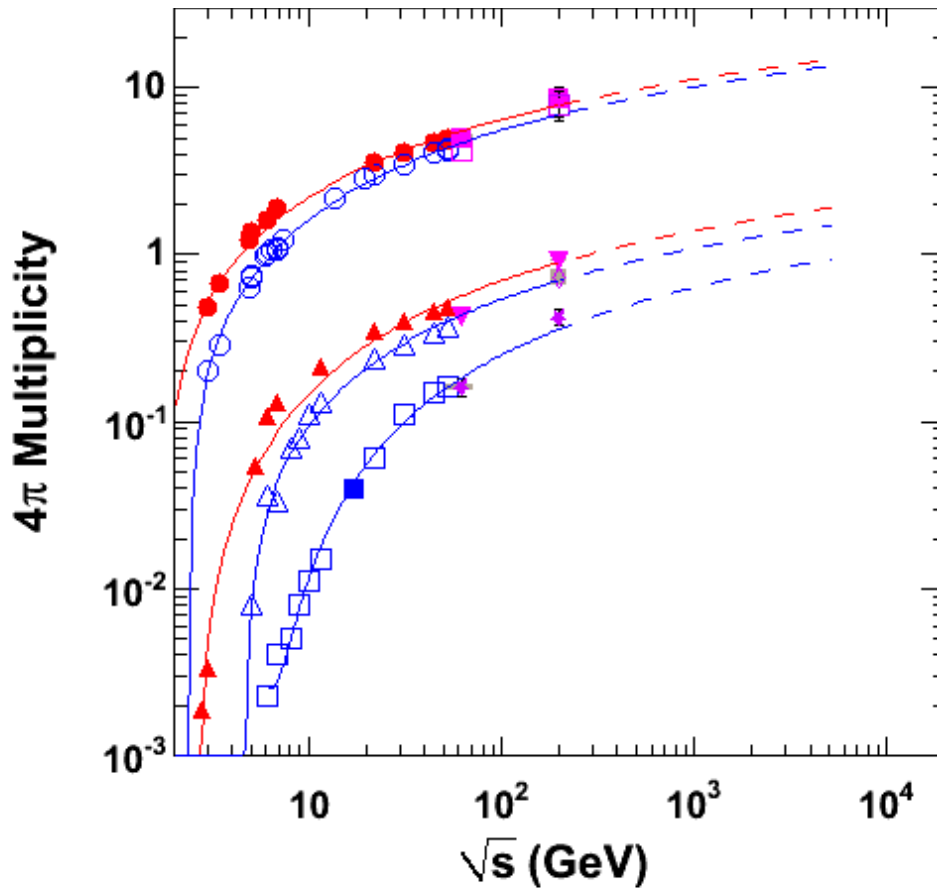
FIG. 2. 4π multiplicities as a function of $\sqrt{s_{nn}}$. The points at 62.4 and 200 GeV represent our data while the points at lower energies are from [8] and [9]. Solid symbols represent positive particles and open symbols represent negative particles. Circles represent pions, triangles represent kaons and squares represent anti-protons.

[1] I. G. Bearden *et al.*, the BRAHMS Collaboration, Phys. Rev. Lett. **93** (2004) 102301**.**

[2] K Hagel *et al.*, *Progress in Research*, cyclotron Institute, texas A&M University (2008- 2009) p.II-22.

[3] T. Sjostrand *et al.*, JHEP **05** (2006) 26.

[4] B. I. Abelev *et al.* (the STAR Collaboration), Phys. Rev. C **75**, 064901 (2007).

[5] T. Anticic *et al.*, Eur. Phys. J **65**, 9 (2010).

[6] I. Arsene *et al.*, Phys. Lett. B **677**, 267 (2009).

[7] BRAHMS collaboration, in preparation.

[8] M. Aguilar-Benitez *et al.*, Z. Phys. C **50**, 405 (1991).

[9] C. Alt *et al.* (NA49), Eur. Phys. J. C **45**, 343 (2006).

Measurement of the ^{40}Ar + ^{165}Ho excitation function

C. M. Folden III, M. C. Alfonso, A. A. Alharbi, E. Berdugo, P. J. Cammarata, K. R. Lawrence,
D. A. Mayorov, A. C. Raphelt, and B. Roeder

A new program to study the heaviest elements has begun at the Texas A&M University Cyclotron Institute (CI). Experiments to produce these elements require high-intensity beams, efficient separation techniques, and long irradiation times for study. As part of a DOE-sponsored upgrade program, the idle K150 88-Inch Cyclotron is being recommissioned to provide intense, stable beams for experiments in fundamental interactions, rare isotope production, etc. [1]. This upgrade is underway and during the interim the K500 superconducting cyclotron is being used to develop the capabilities at the CI for heavy element experiments.

As a proof-of-principle experiment, the ^{165}Ho(^{40}Ar, xn)$^{205-x}$At excitation function has been measured. This reaction was previously studied by Andreev *et* al. [2] and was chosen for several reasons. The compound nucleus velocity ($0.0204c$) is comparable to that in the ^{208}Pb(^{50}Ti, n)^{257}Rf reaction ($0.0195c$), a future benchmark for our program. The ^{40}Ar + ^{165}Ho reaction has large evaporation residue (EVR) cross sections (up to 12 mb), and our results could be compared to the previously measured excitation function. The target is monoisotopic, making target preparation easier. The half-lives of the most important EVRs are not too long [$t_{1/2}$(^{199}At) = 7 s, $t_{1/2}$(^{200}At) = 43 s], and their alpha branches are large (greater than 50%) [3]. These properties made this reaction suitable for test purposes, and preliminary results are reported here.

A beam of ^{40}Ar^{5+} was delivered by the K500 cyclotron at energies of 200, 205, and 213 MeV with an intensity of typically 50-70 pnA. Stationary targets of 300-μg/cm^2 ^{165}Ho deposited on three thicknesses of ^{nat}Al (0.63, 1.08, and 1.71 μm) were mounted at the target position of the Momentum Achromat Recoil Separator (MARS) [4-5], with the Ho on the downstream side. Using the different target backings as degraders, a total of eight center-of-target energies were studied. A 50-μg/cm^2 ^{nat}C stripper foil was located downstream of the targets to provide charge equilibration. MARS was used to remove unwanted reaction products and unreacted beam. The achromatic section was set for $B\rho \approx 0.64$ T m, corresponding to At^{18+} EVRs. This magnetic rigidity is also less than that of the fully stripped primary beam (^{40}Ar^{18+}, $B\rho \approx 0.71$ T m), reducing the number of scattered beam particles that traversed the separator. The MARS velocity filter was set based on the calibration determined using degraded ^{241}Am alpha particles (described in a separate contribution to this annual report). A 50 mm x 50 mm, 16-strip, position-sensitive detector was used to observe implanting ions and subsequent decays.

The measured excitation function is shown in Fig. 1. The various reaction products were discriminated based on their differing alpha decay energies. The analysis of the overall separator transmission is ongoing, although the separation factor (defined as the number of events with energy greater than 30 MeV divided by the beam dose) was $>8 \times 10^{11}$. If the field strengths in the velocity filter are increased then the separation factor can also be increased, at the expense of transmission, and this will be quantified in a future experiment. These results indicate that it may be feasible to produce heavy elements at the CI.
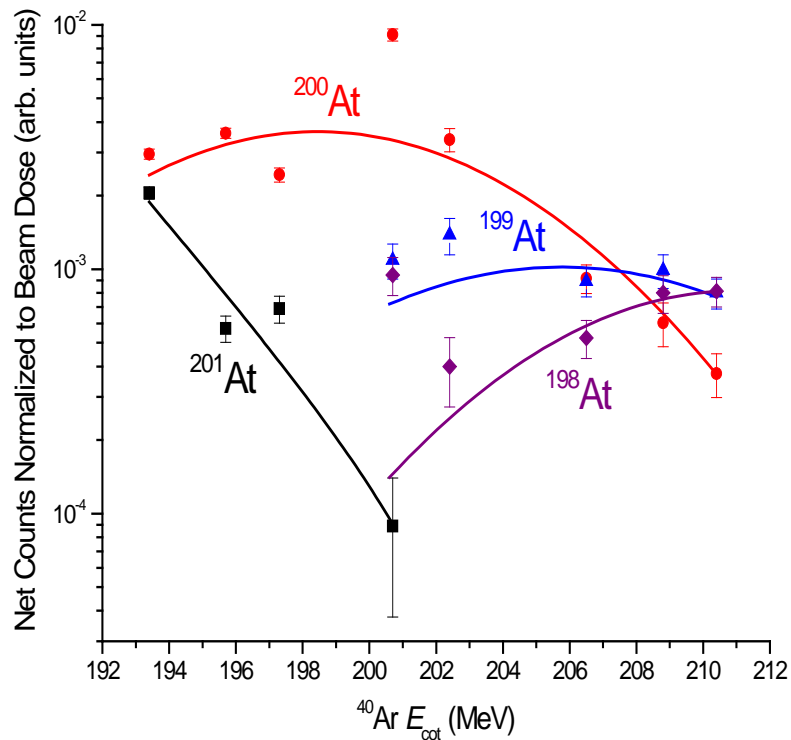
FIG. 1. Preliminary excitation function for the production of At isotopes in the ^{165}Ho(^{40}Ar, xn) reaction. Symbols are: squares, ^{201}At ($4n$); circles, ^{200}At ($5n$); triangles, ^{199}At ($6n$); and diamonds, ^{198}At ($7n$). E_{cot} represents the ^{40}Ar beam energy at the center of the ^{165}Ho targets.

[1] *A Proposed Facility Upgrade for the Texas A&M University Cyclotron Institute* (College Station, TX, 2001); available at http://cyclotron.tamu.edu/facility_upgrade.pdf.

[2] A.N. Andreev *et al.*, Sov. J. Nucl. Phys. **52**, 412 (1990).

[3] *National Nuclear Data Center* (2006); available at http://www.nndc.bnl.gov.

[4] R.E. Tribble, R.H. Burch, and C.A. Gagliardi, Nucl. Instrum. Methods Phys. Res. **A285**, 441 (1989).

[5] R.E. Tribble, C.A. Gagliardi, and W. Liu, Nucl. Instrum. Methods Phys. Res. **B56/57**, 956 (1991).

Characterization of the MARS velocity filter for low-velocity ions

M. C. Alfonso, A. A. Alharbi, E. Berdugo, P. J. Cammarata, R. Lawrence,
B. Roeder, and C. M. Folden III

Physical separation of evaporation residues produced in fusion reactions is necessary to remove the unwanted reaction products and beam particles from the heavy element of interest. A velocity filter uses crossed electric and magnetic fields to select ions of a specific velocity. The MARS velocity filter has been used in past experiments to select ions in the range of 8% to 30% of the speed of light, c. Fusion reactions produce heavy elements at much lower velocities, in the range of 1.5% to 2% of c. To calibrate the velocity filter in this range, offline experiments were preformed using an alpha source, ^{241}Am, to simulate the products of a beam experiment. The source was covered with 45-µg/cm^2 ^{nat}C cover foil to prevent contamination. Aluminum degraders of various thicknesses (0, 6.1, 12.3, and 18.4 µm) were used to decrease the velocity of the alpha particle to 5.33%, 4.92%, 4.20%, and 3.20% of c, respectively.

A silicon strip detector was placed at the focal plane of MARS to detect the alpha particles that passed through the separator. For the different velocities of alpha particles, the optimum electric and magnetic field ratio was determined for the MARS velocity filter. This was done by first turning off the velocity filter and tuning the rest of MARS for the maximum rate. Next the velocity filter was turned on, the electric field was set, and the rate was determined as a function of magnetic field; this was repeated for a total of five different electric field settings. This complete process was repeated for the four alpha particle velocities.

A representative distribution of the alpha particles that reached the end of MARS can be seen in Fig. 1. As expected, the acceptance decreased as the electric field increased (Table I). Overall, the data showed a slight positive deviation in the calibration

FIG. 1. Position spectrum of the alpha particles implanted on the detector.

when compared to the calibration used in past experiments. This means a larger magnetic field is needed to compensate. The results were confirmed in a beam experiment with the detection of ^{199}At (~1.9% of c); results of this experiment are discussed in a separate contribution to this annual report.

TABLE I. The acceptance as a function of electric field and alpha velocity. Velocities of alphas are shown in the parentheses.

Electric Field (arbitrary units)	No Degrader (5.33% of c)	6.1μm Degrader (4.92% of c)	12.3μm Degrader (4.20% of c)	18.4μm Degrader (3.20% of c)
13.3	12.51%	12.29%	7.46%	4.34%
18.3	10.56%	8.05%	4.88%	4.62%
23.3	6.99%	6.99%	4.63%	4.61%
33.3	6.00%	4.43%	3.99%	4.33%
43.3	4.36%	3.90%	3.87%	—

Measuring the temperature of hot nuclear fragments

S. Wuenschel, A. Bonasera, L. W. May, G. A. Souliotis, R. Tripathi, S. Galanopoulos , Z. Kohley,
K. Hagel, D. V. Shetty, K. Huseman, S. N.Soisson, B. C. Stein, and S. J. Yennello

A new thermometer based on fragment momentum fluctuations is presented. This thermometer exhibited residual contamination from the collective motion of the fragments along the beam axis. For this reason, the transverse direction has been explored. Additionally, a mass dependence was observed for this thermometer.

This mass dependence may be the result of the Fermi momentum of nucleons or the different properties of the fragments (binding energy, spin etc..) which might be more sensitive to different densities and temperatures of the exploding fragments. We expect some of these aspects to be smaller for protons (and/or neutrons); consequently, the proton transverse momentum fluctuations were used to investigate the temperature dependence of the source.
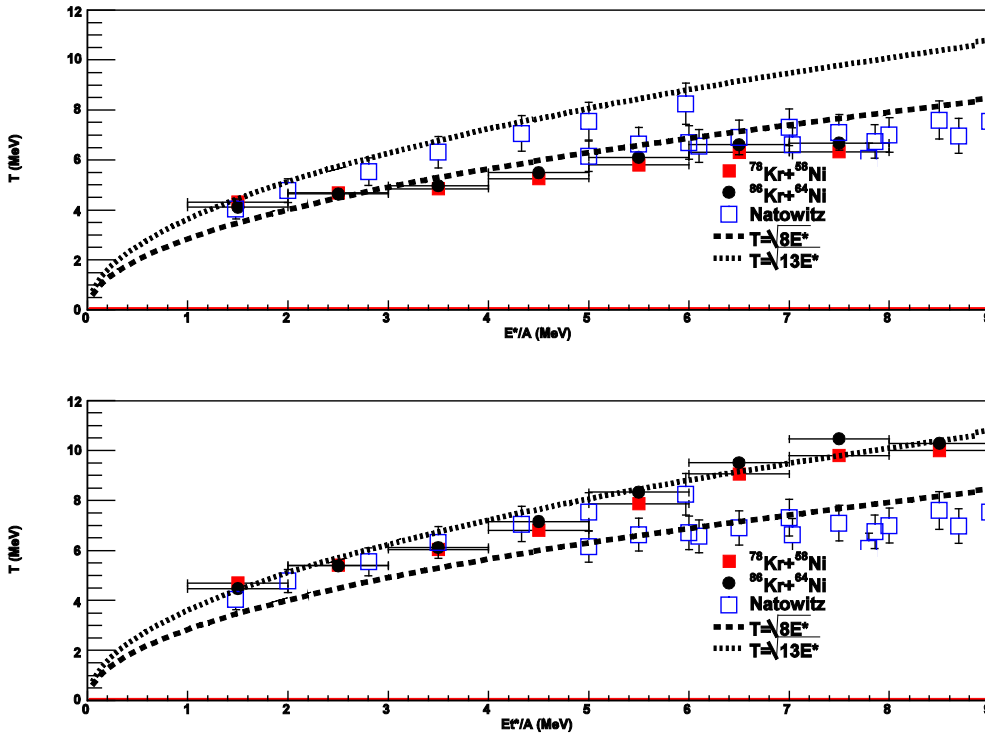
FIG. 1. Temperatures derived from proton momentum fluctuations as a function of E*/A of the source event. For reference the caloric curve for A=60-100 from the Natowitz compilation as well as two Fermi Gas ($T = (aE/A)^{1/2}$ with a = 8, 13) curves are plotted(Top panel). (Bottom panel) same as above but for the corresponding 'transverse' quantities.

[1] S.Wuenschel *et al.*, ArXiV(nucl-ex) 1004.0021v1, Nucl. Phys. **A** (submitted).

Transverse collective flow of isotopically identified light charged particles

Z. Kohley, L. W. May, S. Wuenschel, M. Di Toro, M. Colonna, M. Zielinska-Pfabe, K. Hagel, R. Tripathi, A. Bonasera, G. A. Souliotis, D. V. Shetty, S. Galanopoulos, M. Mehlman, W. B. Smith, S. N. Soisson, B. C. Stein, and S. J. Yennello

The transverse flow of light charged particles (LCPs) has been investigated for the 35 MeV/u ^{70}Zn+^{70}Zn, ^{64}Zn+^{64}Zn, and ^{64}Ni+^{64}Ni systems. The experimental data was obtained at the Texas A&M University Cyclotron Institute using the NIMROD-ISiS array [1]. An estimate of the impact parameter, for the experimental data, was completed using the minimum bias 2-D distributions of the raw neutron multiplicity plotted against the charged particle multiplicity for each system. The mid-peripheral collisions were used to investigate the effects of different isospin concentrations in both the colliding system and the LCPs.

The azimuthal correlations method [2] was used to reconstruct the reaction plane from the experimental data. The transverse flow is often quantified as the slope of the average in-plane momentum, <Px/A>, over mid-rapidity. In Fig. 1, the average in-plane momentum per nucleon is plotted as a function of the reduced rapidity, $Y_r=Y_{cm}/Y_{cm,proj}$, for the different isotopically identified LCPs. The solid line, shown in each panel, represent a linear fit over the region -0.35 ≤ Yr ≤ 0.35. The extracted slope of the linear fit represents the transverse flow of the LCPs and is referred to as the flow parameter.
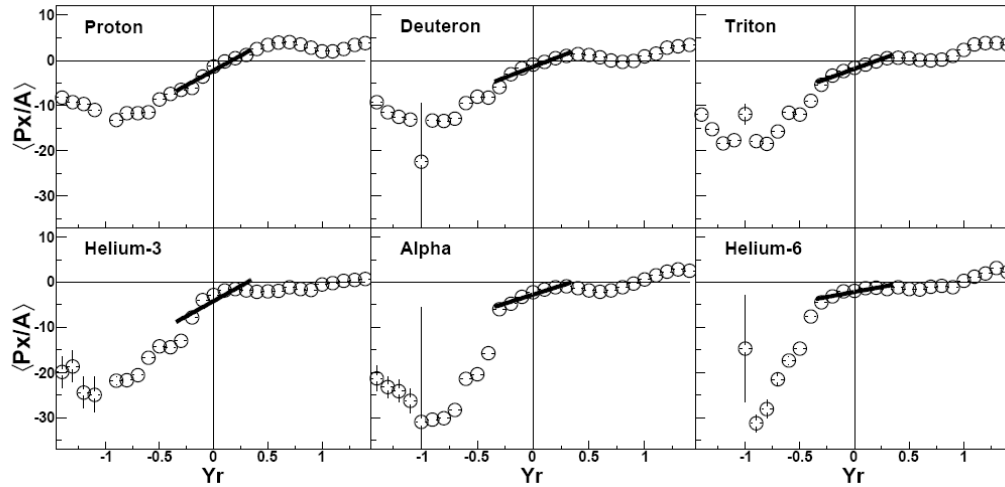
FIG. 1. Average in-plane momentum, <Px/A>, as a function of the reduced rapidity for protons, deuterons, tritons, ^{3}He, alpha and ^{6}He particles. The results shown are from the mid-peripheral collisions of the ^{64}Ni+^{64}Ni system. The solid black line represents a linear fit from -0.35 ≤ Yr ≤ 0.35.

The flow of the isotopically identified light charged particles is shown in Fig. 2 for the mid-peripheral collisions. An enhancement in the transverse flow for the ^{64}Ni (N/Z=1.28) system is observed

in comparison to the ^{64}Zn (N/Z=1.13) system demonstrating an (N/Z)$_{sys}$ dependence. This expands on the work of Pak *et al*. for inclusive Z=1-3 fragments from systems with the same mass (A$_{sys}$) and different (N/Z)$_{sys}$ [3]. Additionally, the results from the ^{70}Zn (N/Z=1.33) system show, for all isotopes except tritons and ^{3}He, a decreased flow in comparison to the A$_{sys}$=128 systems, which can be attributed to the mass dependence of the transverse flow [4].
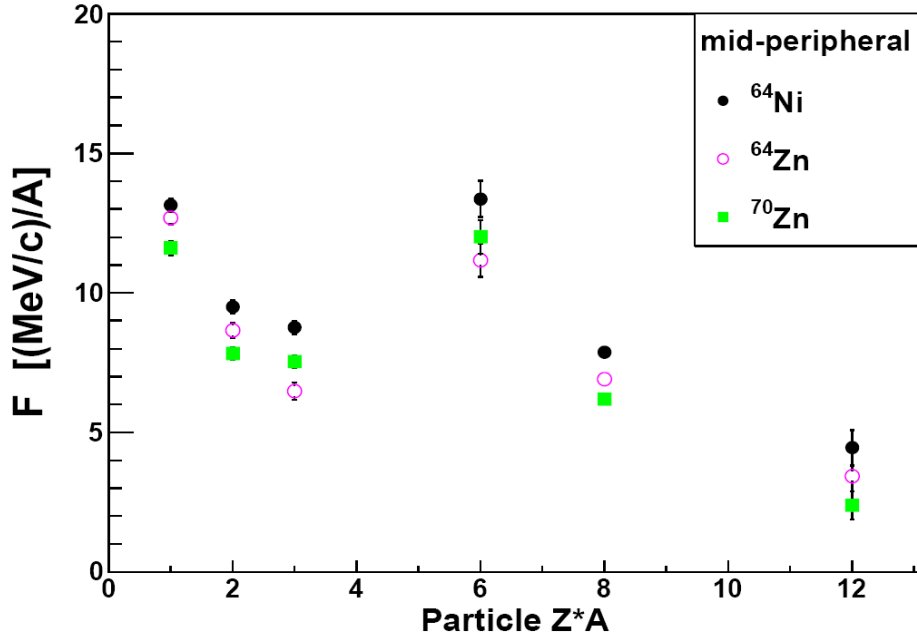
FIG. 2. The extracted flow parameters (F) for the protons, deuterons, tritons, ^{3}He, alpha and ^{6}He particles are shown as a function of the mass times charge (Z*A) of the particle. Results are presented from ^{64}Ni, ^{64}Zn, and ^{70}Zn systems for mid-peripheral collisions as shown by the legend.

Isotopic and isobaric trends can also be explored from the extracted flow parameters in Fig. 2. A distinctive isotopic trend is observed, in which the transverse flow per nucleon is decreasing with increasing neutron content. This would suggest a smaller flow for neutrons in comparison to protons or that the neutron-rich fragments are originating from a different source, such as a neutron-rich neck-like region. Examination of the transverse flow of the triton and ^{3}He fragments provides an isobaric comparison. The results, as shown in Fig. 2, demonstrate an enhancement in the ^{3}He flow in comparison to the triton flow. This, again, demonstrates a decreasing flow with increasing neutron content. Therefore, in comparing fragments with a constant charge (isotopes) or a constant mass (isobars) a consistent trend is observed showing a decreased flow for the more n-rich fragments.

The experimental results were compared to the Stochastic Mean-Field (SMF) model [5]. While the SMF model was unable to reproduce the magnitude of the experimental flow, the (N/Z)$_{sys}$ dependence for the inclusive Z=1 and fragment flow trends were in agreement with the experimental data. In

addition, the SMF reproduced the isotopic/isobaric trends, with respect to the experimental results, more closely using a mean-field potential that produces a stiff density dependence of the symmetry energy.

[1] S. Wuenschel *et al*. Nucl. Instrum. Methods Phys. Res. **A604,** 578 (2009).

[2] W.K. Wilson, R. Lacey, C.A. Ogilvie, and G.D. Westfall, Phys. Rev. C **45,** 738 (1992).

[3] R. Pak *et al.*, Phys. Rev. Lett. **78,** 1022 (1997).

[4] G.D. Westfall *et al.*, Phys. Rev. Lett. **71,** 1986 (1993).

[5] J. Rizzo, M. Colonna, M. Di Toro, and V. Greco, Nucl. Phys. **A732**, 202 (2004).

Investigation of transverse collective flow of intermediate mass fragments

Z. Kohley, L. W. May, S. Wuenschel, A. Bonasera, K. Hagel, R. Tripathi, R. Wada, G. A. Souliotis, D. V. Shetty, S. Galanopoulos, M. Mehlman, W. B. Smith, S. N. Soisson, B. C. Stein, and S. J. Yennello

The transverse flow of intermediate mass fragments (IMFs) has been investigated for the 35 MeV/u $^{70}Zn+^{70}Zn$, $^{64}Zn+^{64}Zn$, and $^{64}Ni+^{64}Ni$ systems [1]. The experimental data was obtained at the Texas A&M University Cyclotron Institute using the NIMROD-ISiS array[2]. An estimate of the impact parameter, for the experimental data, was completed using the minimum bias 2-D distributions of the raw neutron multiplicity plotted against the charged particle multiplicity for each system. Five bins were created in order to examine the transverse flow in the most violent to the peripheral collisions.

The azimuthal correlations method [3] was used to reconstruct the reaction plane from the experimental data. In the NIMROD-ISiS array thresholds produced incomplete detection of IMFs at negative reduced rapidities ($Y_r=Y_{cm}/Y_{cm,proj}$). Therefore, the transverse flow was quantified by calculating the average in-plane transverse momentum from $0.0 \leq Y_r \leq 0.45$. Thus, the flow, or $<\overline{Px}>$, was extracted only from the positive rapidity fragments.

The transverse flow for Z=1-9 particles is shown in Fig. 1 for the five centrality bins, ranging from Bin 0 (most violent collisions) to Bin 4 (most peripheral collisions). A transition from the IMF transverse flow strongly depending on the mass of the system, in the most violent collisions, to a dependence on the charge of the system, for the peripheral reactions, is shown. This demonstrates the importance of both mass and charge dependent forces in the transverse flow.
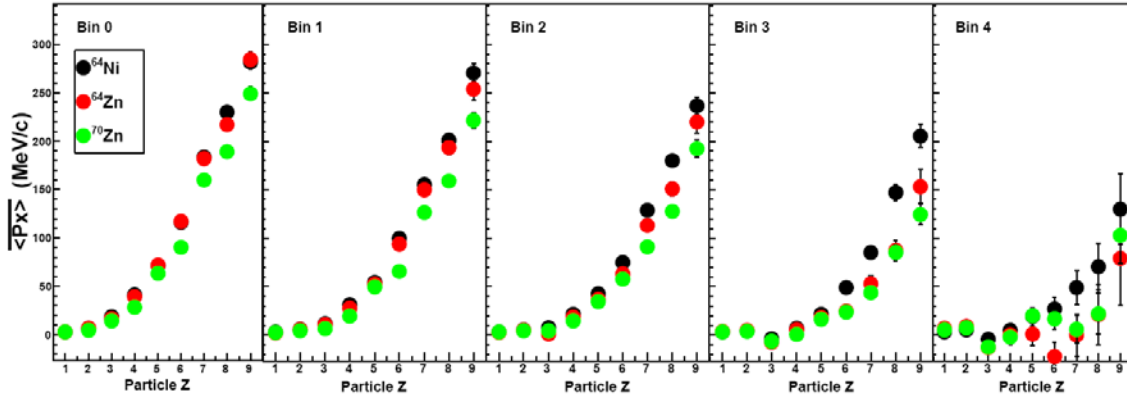
FIG. 1. Transverse flow, $<\overline{Px}>$, for Z=1-9 particles in five different centrality bins. Bin 0 represents the most violent collisions, while Bin 4 represents the most peripheral. The results are shown for the ^{64}Ni, ^{64}Zn, and ^{70}Zn systems as shown in the legend.

The antisymmetrized molecular dynamics model [4] was used to investigate the sensitivity of the IMF transverse flow to the density dependence of the symmetry energy. To compare the system mass to charge dependence of the IMF flow the ratio,

$$R_{Flow} = \frac{\overline{<Px>}_{64Zn} - \overline{<Px>}_{70Zn}}{\overline{<Px>}_{64Ni} - \overline{<Px>}_{70Zn}}$$

can be used to define the magnitude of the flow from the ^{64}Zn system in comparison to the ^{64}Ni and ^{70}Zn systems. Thus, when $R_{Flow}=1$ the IMF flow of the ^{64}Zn system equals that of the ^{64}Ni system (mass dependent flow) and when $R_{Flow}=0$ the ^{64}Zn and ^{70}Zn systems (charge dependent flow) have equivalent values of flow. The comparison of theoretical and experimental results are presented in Fig. 2 where the R_{Flow} was averaged over Z=4-9 fragments. The results demonstrate that the choice of interaction, Gogny or Gogny-AS, is important in being able to reproduce the experimental data. The best agreement between the experiment and theory was achieved with a stiff density dependence of the symmetry energy (Gogny-AS interaction).
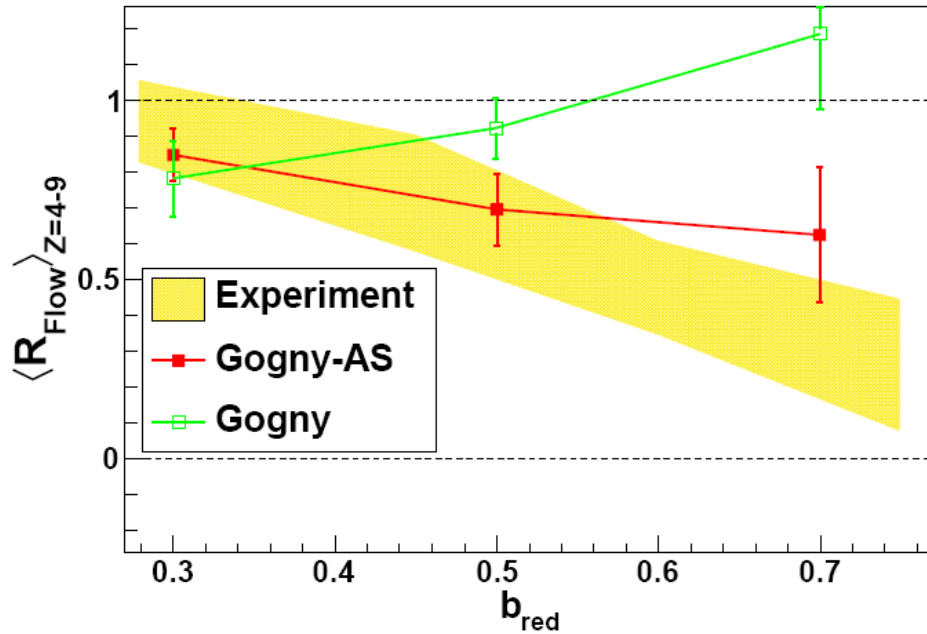
FIG. 2. Average R_{Flow} for Z=4-9 fragments is plotted as a function of the reduced impact parameter, bred, for the experimental data (yellow area) and AMD-Gemini simulation with both a stiff (red squares) and soft (green open squares) Esym(ρ).

[1] Z. Kohley *et al.* Phys. Rev. Lett. (Submitted).

[2] S. Wuenschel, *et al.* Nucl. Instrum. Methods Phys. Res. **A604,** 578 (2009).

[3] W.K. Wilson, R. Lacey, C.A. Ogilvie, and G.D. Westfall, Phys. Rev. C **45,** 738 (1992).

Correlations with projectile-like fragments and emission order of
light charged particles

Z. Kohley, L. W. May, S. Wuenschel, A. Bonasera, K. Hagel, R. Tripathi, G. A. Souliotis, D. V. Shetty,
S. Galanopoulos, M. Mehlman, W. B. Smith, S. N. Soisson, B. C. Stein, and S. J. Yennello

The 35 MeV/u ^{70}Zn+^{70}Zn, ^{64}Zn+^{64}Zn, and ^{64}Ni+^{64}Ni systems have been used to examine correlations of light charged particles (LCPs) and intermediate mass fragments (IMFs) with projectile-like fragments (PLFs). A new method was developed to examine the "flow" of the particles with respect to the PLF (PLF-flow). The PLF-flow was examined by plotting the average scaled PLF-plane momentum, $< \tilde{p}_x >$, of the fragments as a function of the scaled rapidity, $\tilde{Y}$, defined as

$$\tilde{p}_x = p_{x,frag} / p_{t,PLF} \qquad (1)$$

$$\tilde{Y} = Y_{cm,frag} / Y_{cm,PLF} \qquad (2)$$

with $p_{x,frag}$ representing the PLF-plane momentum of the fragment, $p_{t,PLF}$ representing the transverse momentum of the PLF, and $Y_{cm,frag}$ ($Y_{cm,PLF}$) equaling the center-of-mass rapidity of the fragment (PLF). This presents a method to examine the fragments in a PLF-invariant frame. The invariant PLF-scaled flow was used to examine the dynamics of the mid-rapidity proton, deuteron, triton, ^{3}He, alpha, ^{6}He, ^{8}He, Z=3, and Z=4 particles.

The slope of the $< \tilde{p}_x >$ over the mid-rapidity region can provide information about the movement of the fragments with respect to the PLF. For example, a positive slope would imply that on average the fragments are moving towards, or following, the PLF. In order to investigate the movement of the mid-rapidity fragments a linear fit was applied to the $< \tilde{p}_x >$ vs. $\tilde{Y}$ plot from -0.1$\leq$ $\tilde{Y}$ $\leq$0.45. The fit range focuses on the forward rapidity fragments since we are examining correlations with the PLF and also excludes any backward angle detector threshold effects. Fig. 1 presents $< \tilde{p}_x >$ plotted against $\tilde{Y}$ for protons, deuterons, and tritons in correlations with a Z=24 PLF. The linear fit is shown as the solid colored line for each isotope. The slope of the linear fit is then used to quantify the PLF-flow for the different particle types.

The slopes observed in Fig. 1 suggest that the mid-rapidity protons, deuterons, and tritons are moving in different directions with respect to the PLF. The positive slope exhibited by the protons would imply that they are, on average, moving toward or are more aligned with the PLF. In contrast, the tritons appear to move in the opposite directions, away from the PLF, implied by the negative slope or PLF-flow.

We propose that the different trajectories of the mid-rapidity fragments, shown in Fig. 1, are connected to their proximity to the PLF and TLF at their time of formation. Fig. 2 presents a simplified illustration of the possible effect of the PLF-TLF proximity to the mid-rapidity fragments. If the mid-rapidity fragment is emitted while in a close proximity to the PLF and TLF (left side of Fig. 2) then the Coulomb potential would likely force the fragment trajectory to be anti-aligned, or perpendicular, with
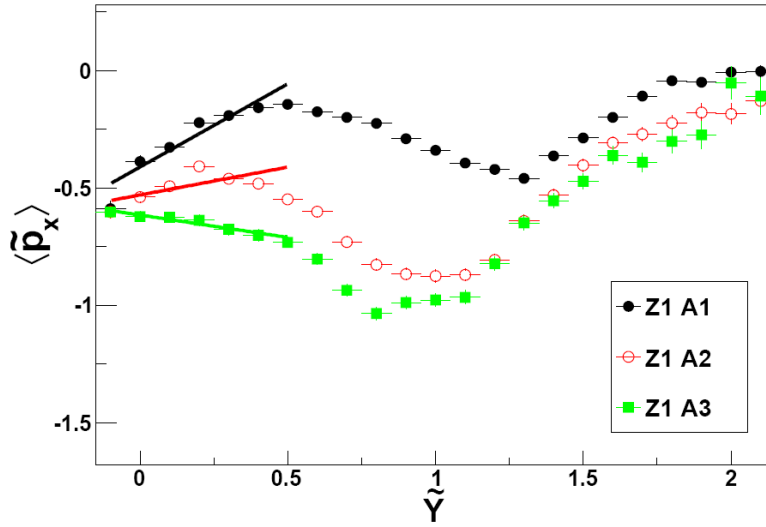
FIG. 1. The average scaled PLF-plane momentum, $< \tilde{p}_x >$, of protons, deuterons, and tritons is shown as a function of the scaled rapidity, $\tilde{Y}$. The solid lines represent linear fits over the range $-0.1 \leq \tilde{Y} \leq 0.45$.

the PLF-TLF axis. This would result in a negative slope of the $< \tilde{p}_x >$. If the formation of the fragment occurs at a later time, where the PLF-TLF proximity is decreased, then it is possible for a more aligned emission to occur (right side of Fig. 2). Particles following the trajectory of the PLF would produce a positive slope value or PLF-flow.
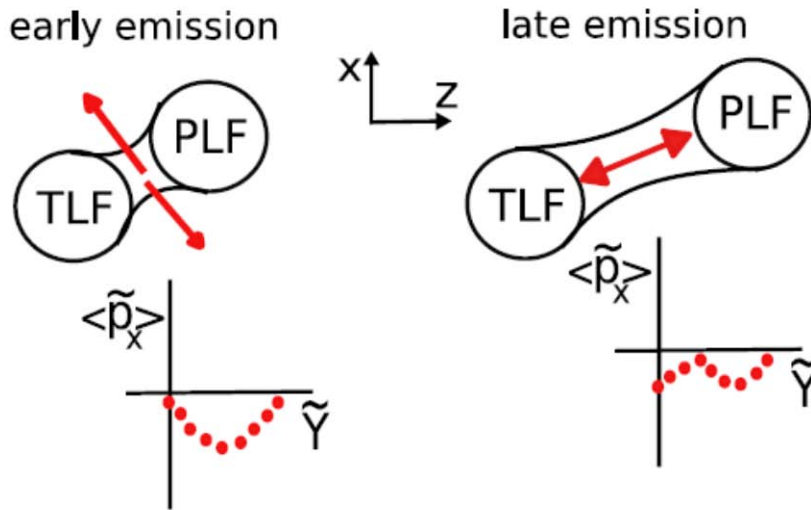
FIG. 2. Simple illustration demonstrating the proposed PLF-TLF proximity effect on the mid-rapidity fragments. The left side depicts the mechanism producing negative slopes due to an early emission of fragments. The right side shows a later emission of mid-rapidity fragments producing a positive slope.

The results suggest that on average tritons, ^{6}He, ^{8}He, and Z=3-4 fragments are emitted relatively early in the mid-rapidity region followed by deuterons and ^{3}He fragments. Protons and alpha, on average, are emitted last in comparison to the other fragments. These results are particularly interesting in the context of current research on the mid-rapidity, or neck, region which have observed increased IMF and n-rich fragment production in the neck region relative to the PLF region [1].

The validity of the method for determining the average order of emission was examined in the context of a Coulomb trajectory calculation and the classical molecular dynamics simulation [2]. The results demonstrated that the proximity of the PLF-TLF, or time of emission, has a direct connection to the observed PLF-Flow. The statistical multifragmentation model (SMM) [3] demonstrated that the observed average emission order is likely due to proximity of the second source which modifies the Coulomb energy of the system during the fragmentation. Lastly, the average emission order of the LCPs and IMFs was extracted from the antisymmetrized molecular dynamics (AMD) [4] and constrained molecular dynamics CoMD [5] simulations and showed good agreement with the experimentally determined mid-rapidity emission order.

[1] M. Di Toro, A. Olmi, and R. Roy, Eur. Phys. J. A **30,** 65 (2006).
[2] V. Latora, M. Belkacem, and A. Bonasera, Phys. Rev. Lett. **73,** 1765 (1994).
[3] J.P. Bondorf, A.S. Botvina, A.S. Iljinov, I.N. Mishustin, and K. Sneppen, Phys. Rep. **257,** 133 (1995).
[4] A. Ono and H. Horiuchi, Prog. Part. Nucl. Phys. **53,** 501 (2004).
[5] M. Papa, G. Giuliani, and A. Bonasera, J. Comput. Phys. **208**, 403 (2005).

The effects of source definition on the quality of Isoscaling

L. W. May, Jennifer Erchinger, Trisha Fagan, and S. J. Yennello

The effects of varying source definition used in Isoscaling analyses have been studied. Isoscaling is the observed trend seen by taking the yield ratio of a specific nuclei between two sources, differing in isospin concentration (I=(N-Z)/A), and plotting this yield ratio for many different fragments as a function of either the N or Z value of the fragment. The resulting scaling should follow the form given in Eq. (1) [1]:

$$R_{21}(N,Z) = \frac{Y_2(N,Z)}{Y_1(N,Z)} = C * \exp^{(N\alpha + Z\beta)} \tag{1}$$

The α parameter value extracted from this equation can be used in various other analyses including calculations of the symmetry energy coefficient and transport studies [1,2]. The experimental data used in this analysis comes from the reactions of $^{78,86}Kr$ beams on $^{58,64}Ni$ targets at 35 MeV/u collected using the NIMROD-ISiS array [3].

Previous isoscaling work was done by comparing the fragment yields between two different systems. In the work by Wuenschel *et. al.* [1], this was replaced by looking at the yield ratio between two quasi-projectile (QP) sources that differed in N/Z content. This was done by taking two QPs selected from specific bins in the QP N/Z distribution as seen in red on Fig. 1. This improved source definition led to an improved quality of isoscaling.
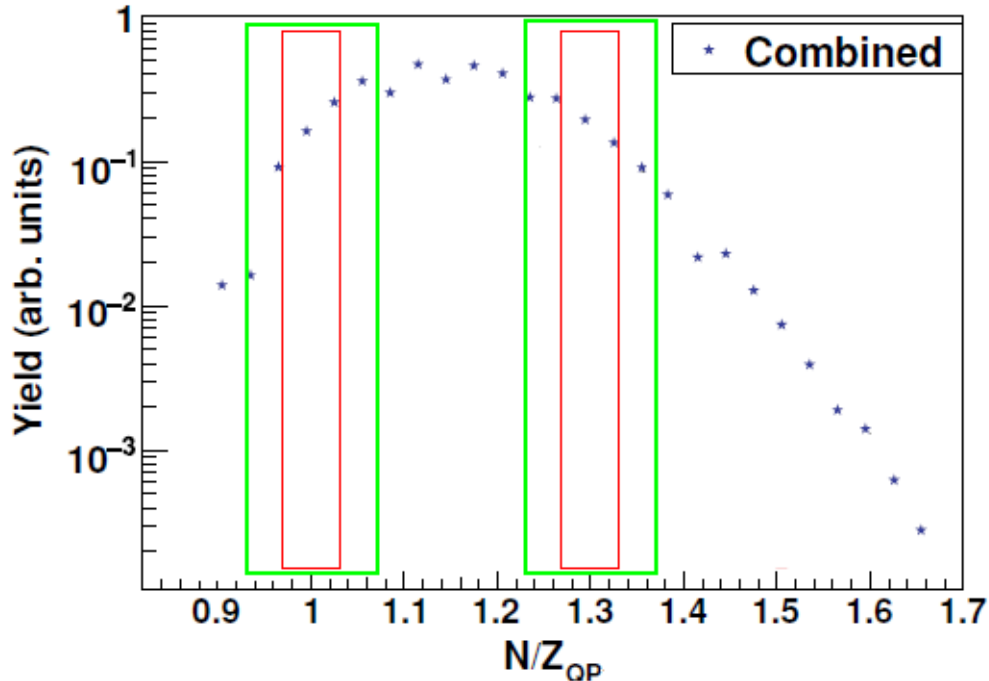
FIG. 1. N/Z distribution of quasi-projectiles. Red and green boxes correspond to bins of different width in N/Z for specifically selected sources for use in isoscaling.

This idea was expanded by varying the widths of the N/Z bins used to determine the QPs for the yield ratio. An example of the expanded N/Z bin can be seen in green in Fig. 1. By comparing the quality of the isoscaling as a function of bin width, it was hoped that some optimal binning value could be found that would generate the best isoscaling.

In order to quantify the improvement of quality, we took a simple relative error calculation on the isoscaling parameter α by dividing the error in the fit parameter by the parameter value and taking that as a percentage. The results can be seen in Fig. 2 where the relative error in a is plotted as a function of the width of the N/Z bins. We can see here that a clear trend is observed where some optimal region of bin width can be used to provide the best quality isoscaling.

Future work to be investigated includes determining the isoscaling quality as a function of Δ (where $\Delta=(Z/A)_1^2-(Z/A)_2^2$) as well as the effect that changing the position of the bins within the N/Z distribution has on the quality of the isoscaling.

α relative error as a function of Bin Width
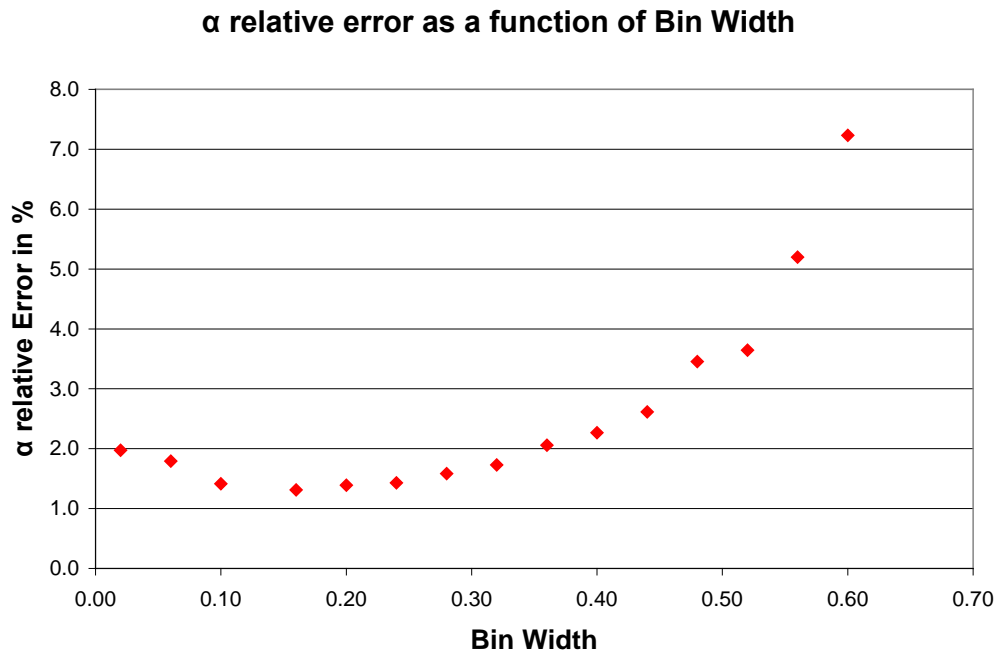
FIG. 2. Plot of the relative error in the isoscaling parameter α as a function of varying bin widths in the isoscaling analysis. A minimum region is observed between widths of 0.1 and 0.2 in N/Z suggesting that bin widths of these sizes should produce better quality isoscaling.

[1] S. Wuenschel, R. Dienhoffer, G.A. Souliotis, S. Galanopoulos, Z. Kohley, K. Hagel, D.V. Shetty, K. Huseman, L.W. May, S.N. Soisson, B.C. Stein, A.L. Caraley, and S.J. Yennello, Phys. Rev. C **79**, 1 (2009).
[2] M.B. Tsang, T.X. Liu, L. Shi, C.K. Gelbke, X.D. Liu, P. Danielewicz, W.G. Lynch, W.P. Tan, A. Wagner, H.S. Xu, W.A. Friedman, G. Verde, R.T. de Souza, V.E. Viola, R.J. Charity, L. Beaulieu, L.G. Sobotka, B. Davin, Y. Larochelle, T. Lefort, and R. Yanez, Phys. Rev. Lett. **92**, 1 (2004).

Measurements of production cross sections of neutron-rich nuclides from peripheral collisions of [86]Kr (15 MeV/nucleon) projectiles with [64]Ni,[58]Ni and [124]Sn, [112]Sn targets

G. A. Souliotis, M. Veselsky, S. Galanopoulos, M. Jandel, Z. Kohley, D. V. Shetty,

S. N. Soisson, B. C. Stein, S. Wuenschel and S. J. Yennello

Recent efforts have been devoted to the production and separation of RIBs in peripheral collisions below the Fermi energy. High intensity beams at this energy range are expected from the refurbished K150 cyclotron and can be exploited for the production of RIBs with the aid of a large-bore superconducting solenoid as a preseparator before a heavy-ion gas stopper [1]. Our recent measurements and simulations indicate that the application of the deep-inelastic transfer mechanism [2-4] appears to be a very effective way to obtain neutron-rich rare isotopes at the K150 energies.

Along these lines, aiming at obtaining systematics on production rates, we performed a series of measurements with a 15 MeV/nucleon [86]Kr beam stricking targets of [64]Ni,[58]Ni and [124]Sn, [112]Sn. The projectile fragments were collected and identified using the MARS recoil separator applying the techniques developed and documented in [2,3]. The Kr beam impinged on the primary target location of MARS with an inclination of 4°. After interaction with the target, the fragments traversed a PPAC at the intermediate image location (for position/Bρ measurement and START time information) and then they were focused at the end of the device passing through a second PPAC (for image size monitoring and STOP time information). Finally the fragments were collected in a 5x5 cm^2 ΔE-E Si detector telescope (60 and 1000 μm thickness). Following standard techniques of Bρ-ΔE-E-TOF (magnetic rigidity, energy-loss, residual energy and time-of-flight, respectively), the atomic number Z, the mass number A, the velocity and the ionic charge of the fragments were obtained on an event-by-event basis (see, e.g., [3]).

Data were obtained in a series of magnetic rigidity settings of the spectrometer to cover the energy and charge state distributions of the fragments. In order to obtain total cross sections from the measured yields at 4°, we used a model approach as described in our previous works [2-4]. First we performed calculations of the yields with the codes DIT [5] for the primary interaction stage and GEMINI [6] for the deexcitation stage of the reaction. We then performed filtering of the DIT/GEMINI results for the limited angular acceptance of the spectrometer and the Bρ range covered in the measurements. We used the ratio of the filtered to unfiltered simulations to correct the measured data (obtained in the limited angular acceptance of the spectrometer) and extract total production cross sections for each projectile-like fragment.

Fig. 1 shows the cross sections of projectile-like fragments of elements Z=35-30 from the reaction [86]Kr + [64]Ni as follows: black points E/A=15 MeV/nucleon (this work), red points E/A=25 MeV/nucleon [2,3]. The (green) dashed line is from the DIT/GEMINI calculation, and the (blue) dotted line shows the expectation of the EPAX parametrization [7]. The results indicate that along with proton-removal products, neutron-pickup products are produced in substantial yields, as expected from a deep-inelastic transfer mechanism at these energies [2-4]. Especially for the present 15 MeV/nucleon data, we observe enhanced cross sections of neutron pick-up products near the projectile. The standard DIT calculation seems to underestimate the most neutron-rich products. We are currently working on detailed
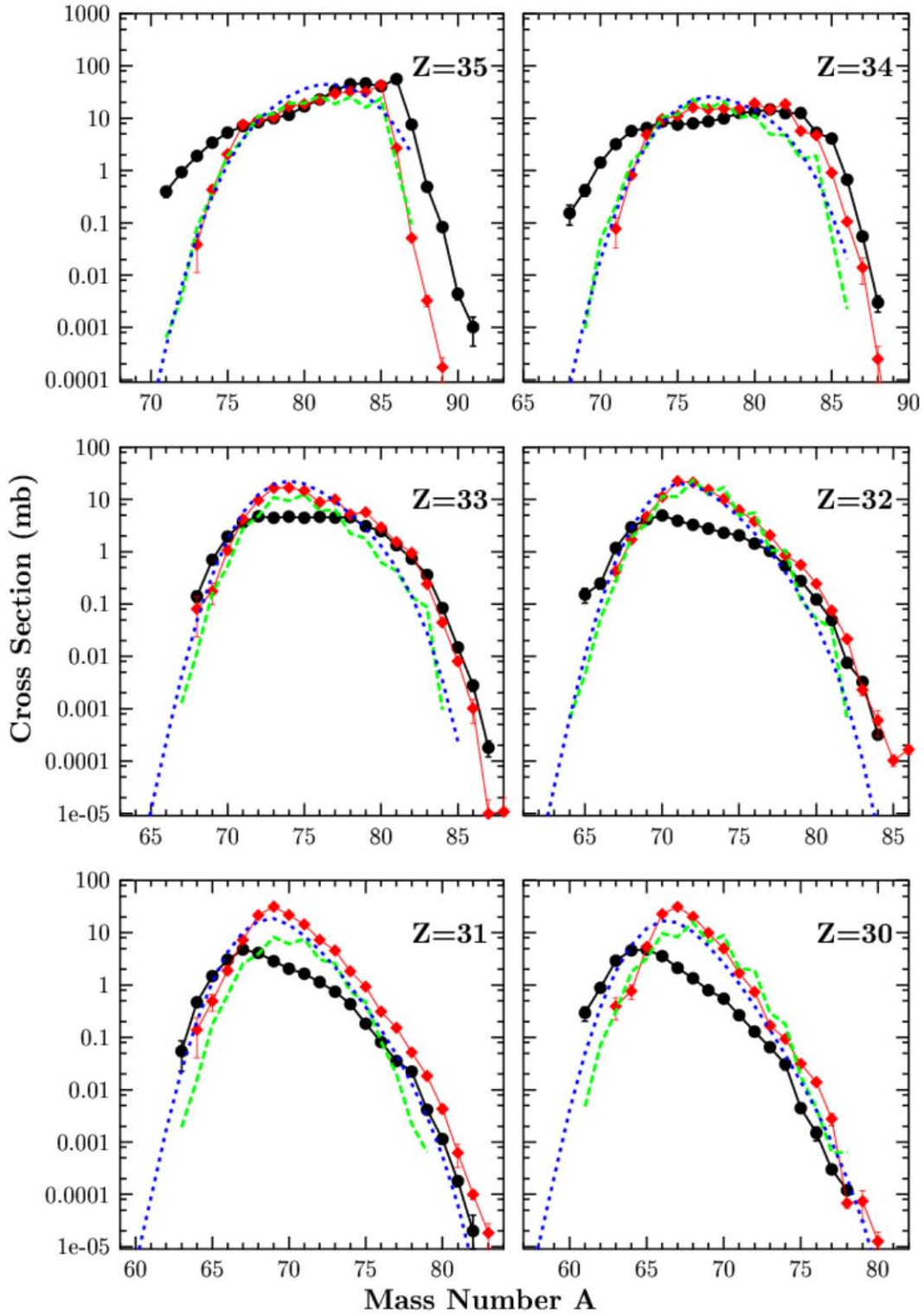
FIG. 1. Cross sections of projectile-like fragments of elements Z=35-30 from the reaction ^{86}Kr + ^{64}Ni as follows: black points E/A=15 MeV/nucleon (this work), red points E/A=25 MeV/nucleon [2,3]. The (green) dashed line is from the DIT/GEMINI calculation, and the (blue) dotted line shows the expectation of the EPAX parametrization [7].

simulations of the cross sections using the improved version of the DIT model approach [4], as well as, the CoMD code [8]. On the experimental front, we are in the process of completing the analysis of the data on projectile-like fragments from the ^{86}Kr (15 MeV/nucleon) with the ^{124}Sn, ^{112}Sn targets measured at 7°.

[1] *A Proposed Facility Upgrade for the Texas A&M University Cyclotron Institute* (College Station, TX, 2001); http://cyclotron.tamu.edu/facility_upgrade.pdf.

[2] G.A. Souliotis *et al.*, Phys. Rev. Lett. **91**, 022701 (2003).

[3] G.A. Souliotis *et al.*, Nucl. Instrum. Methods Phys. Res. **B204**, 166 (2003).

[4] M. Veselsky and G.A. Souliotis, Nucl.Phys. **A765**, 252 (2006).

[5] L. Tassan-Got, Nucl. Phys. **A524**, 121 (1991).

[6] R. Charity, Nucl. Phys. **A483**, 391 (1988).

[7] K. Suemmerer *et al.*, Phys. Rev. C **61**, 034607 (2000).

[8] M. Papa *et al.*, Phys. Rev. C **64**, 024612 (2001).

Probing densities of hot nuclei

R. Tripathi, S. Wuenschel, G. A. Souliotis, S. Galanopoulos, Z. Kohley, K. Hagel, D. V. Shetty, K. Huseman, L. W. May, S. N. Soisson, B. C. Stein, and S. J. Yennello

Nuclear density is an important quantity in the studies related to the nuclear equation of state. A systematic decrease in fragment kinetic energy with increasing excitation energy of the fragmenting source has been considered as a signature of expansion of the fragmenting source [1]. Fragment kinetic energy spectra were used to deduce the information about nuclear density in ^{3,4}He, ^{14}N+^{197}Au reactions using a statistical emission model [2]. In the present work, this method has been applied to the fragments produced in quasiprojectile fragmentation in ^{78,86}Kr+^{58,64}Ni reactions (E_{lab}= 35 MeV/A). The calculation of Coulomb energy has been modified to account for the variation in Coulomb repulsion felt by fragments in different fragmentation events. Various cuts were applied to the experimental data to reduce the non-equilibrium effects and select quasiprojectiles with Z value close to that of the projectile [3].

In order to investigate the excitation energy dependence of the nuclear density, kinetic energy spectra of fragments (Z=4-8), gated on different excitation energy of the fragmenting source, were fitted using the following equation for statistical emission [2],

$$P(x)dx \propto \left\{ (2x-p)\exp\left(-\frac{x}{T}\right)erfc\left(\frac{p-2x}{2\sqrt{pT}}\right) + 2\sqrt{\frac{pT}{\pi}}\exp\left(-\frac{p^2+4x^2}{4pT}\right) \right\}dx \quad (1)$$

where x is the kinetic energy of the fragment in the projectile frame of reference, corrected for the Coulomb energy contribution. T is the temperature of the source and p is an amplification parameter governing the width of the kinetic energy spectra [2]. In order to account for the variation in Coulomb repulsion felt by a fragment in different break up events, an average Coulomb repulsion was calculated by varying the charge of the residual nucleus. There are two extreme cases possible for the Coulomb push to the fragment. In one case, the fragment of interest may be present at the center of the fragmenting system and, therefore, no net Coulomb force is acting on it at the freeze out stage. In the other case, the fragment of interest may be present at the surface of the fragmenting system as shown in FIG. 1 and, therefore, feels
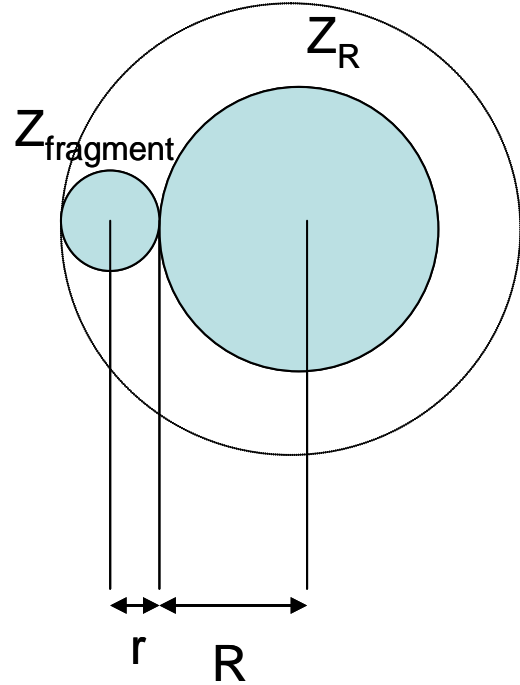
FIG. 1. Touching sphere configuration.

maximum Coulomb repulsion. For other configurations, the Coulomb energy will lie between the values corresponding the two extreme cases. The average Coulomb energy was calculated using the following equation

$$E_C = \frac{\sum_n E_C(R)}{n} \quad (2)$$

Where $E_C(R)$ is the Coulomb energy for a given configuration, and is given by the following equation

FIG. 2. r_0 values obtained by fitting the fragment kinetic energy spectra at different excitation energies for ^{78}Kr+^{58}Ni reaction.

$$E_C(R) = \frac{1.438 Z_{fragment} Z_R(R)}{r+R} = \frac{1.438 Z_{fragment}\left[R^3(Z/A)_{QP}\right]}{r_0^4(E^*)\left[\left\{Z_{fragment}(A/Z)_{QP}\right\}^{1/3} + R/r_0(E^*)\right]} \quad (3)$$

where Z_R varies from unity to (Z_{QP}-$Z_{fragment}$), The limits on $Z(R)$ were translated into the limits on R. Z_{QP} was taken as sum of the Z of the fragments obtained after event reconstruction. In the calculations, $(A/Z)_{QP}$ was assumed to be equal to that of the projectile. In the fitting of kinetic energy spectra with eq. 1, r_0 was a free parameter. The r_0 values obtained for ^{78}Kr+^{58}Ni reaction are shown in FIG. 2. Similar trends were observed for other reaction systems. In FIG. 3, the density profile obtained using the r_0 values for different reaction system is compared to that observed in ref. [1]. The density profile determined in the present work is normalized with respect to that in ref. [1] at excitation energy of 2.5 MeV. It can be seen from this figure that the density profile obtained in the present work is similar to that in ref. [1], showing a reduction in nuclear density with increasing excitation energy of the fragmenting source up to a saturation value of about $0.2\rho_0$, where ρ_0 is nuclear density in ground state.

FIG. 3. Density profiles obtained from the present work and from ref. [1].

[1] Viola *et al.*, Phys. Rev. Lett. **93**, 132701 (2004).

[2] L. G. Moretto, Nucl. Phys. **A247**, 211 (1975).

[3] S. Wuenschel, Ph. D. Thesis, Texas A&M University, 2009.

Highlighting critical phenomena using nuclear fragment yield ratios

R. Tripathi, A. Bonasera, S. Wuenschel, L. W. May, Z. Kohley, G. A. Souliotis, S. Galanopoulos,
K. Hagel, D. V. Shetty, K. Huseman, S. N. Soisson, B. C. Stein, and S. J. Yennello

Investigation of the nuclear phase transition is currently one of the important research objectives of heavy-ion collisions in the Fermi energy domain. Recently, Bonasera *et al.* [1,2] used fragment yield data from different reactions to investigate nuclear phase transition using the Landau free energy approach [3,4], which is applicable to the systems in the vicinity of the critical point. In this approach, the free energy per nucleon F of a fragment is related to an order parameter m, where $m = (N-Z)/A$, N, Z and A are the neutron, proton and mass numbers of the fragment respectively. The quantity m can be defined as an order parameter if $m = -\partial F/\partial H$, where H is its conjugate variable [3,4], which acts as an external field. Ignoring the higher order terms in the external field, dependence of fragment yield ratio on the isospin asymmetry of the source (m_s) and that of fragment (m) can be expressed by the following equation

$$\frac{1}{A}\ln\left(\frac{Y_2}{Y_1}\right) = a\left(m_{S2}m_2 - m_{S1}m_1\right) \tag{1}$$

Using Eq. (1), fragment yields can be used to test the applicability of Landau approach to nuclear phase transition. In the present work, the yield ratios of mirror nuclei pairs for $A=3$ (^{3}H, ^{3}He) and $A=7$ (^{7}Li, ^{7}Be) formed in the fragmentation of the quasiprojectiles in the reactions ^{78,86}Kr+^{58,64}Ni at beam energy of 35MeV/nucleon have been analyzed.

The experiments were performed at the Texas A&M University K500 superconducting cyclotron. The details of the experiment can be found in [5,6]. With the four reaction systems, the yield ratios of mirror nuclei were determined over a wide range of m_s from -0.03 to 0.21. The m_s values were calculated after correcting for free neutrons emitted by the quasiprojectile [5,6].

For yield ratios of mirror nuclei arising from a source with given m_s value, Eq. 1 reduces to '$0.5\ln(Y_2/Y_1)=am_s$'. Mirror nuclei yield ratios averaged over different reaction systems along with the fitted lines for $A=3$ and 7 are shown in Fig. 1. The slope values for $A=3$ and 7 were 6.90±0.17 and 6.87±0.31 respectively. The observed linearity in Fig. 1
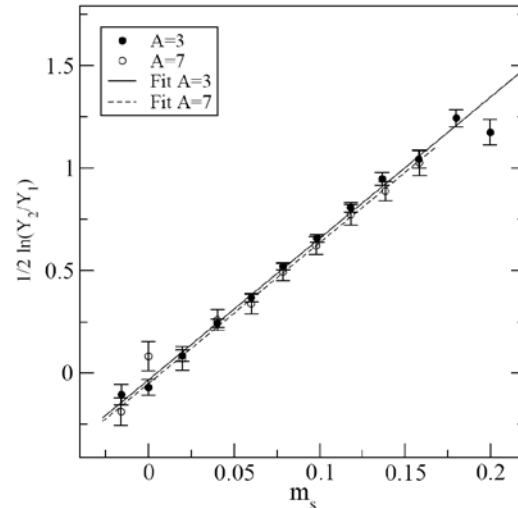
FIG. 1. Plot of '$0.5\ln\left(Y_2/Y_1\right)$', averaged over different reaction systems for $A=3$ and 7 as a function of m_s. Solid and dashed lines are linear fit to the data for $A=3$ and 7 respectively.

indicates that the condition $m=-\partial F/\partial H$ is fulfilled and m is an order parameter [3,4].

In the literature [1,2], a physical interpretation of the slope parameter 'a' can be obtained from the equivalence of the quantity F/T with the symmetry energy per nucleon normalized with respect to the temperature of the source. In order to investigate the evolution of nuclear symmetry energy with the excitation energy of the source, slope parameter a was deduced from the mirror nuclei yield ratio data gated with excitation energy. It can be seen from Fig. 2 that slope parameter a decreases with increasing excitation energy, indicating a decrease in nuclear symmetry energy. This observation is similar to that in conventional isoscaling studies.

The comparison of the Landau approach with the conventional isoscaling was further extended by taking the ratio of yields of the same fragments arising from two sources with different m_s values as done in isoscaling. For this case, Eq. 1 reduces to '$(1/A)\ln(Y_{ms2}/Y_{ms1})=am(m_{s2}-m_{s1})$'.

where Y_{ms2} and Y_{ms1} are, respectively, the yields of a given fragment with mass A from fragmenting sources with isospin asymmetry values m_{s1} and m_{s2}. A reasonably good linearity in Fig. 3, further suggests that m is an order parameter and H is its conjugate field. The slope of this plot gives the value of the parameter a as 6.82±0.10, close to that obtained from the mirror nuclei yield ratio data. Moreover, the slope values were also determined from the isoscaling plots for E^*/A=4.6, 5.2 and 5.8 MeV/nucleon. This excitation energy range was chosen due to the larger statistics of the data. The slope values obtained from the isoscaling plots at different excitation energies (open
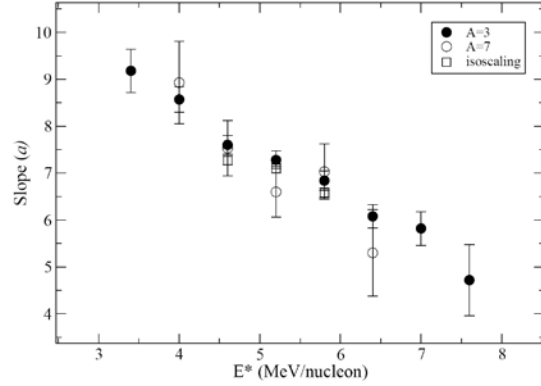
FIG. 2. Slope (a) values, obtained by fitting the plots of mirror nuclei yield ratios for A=3 (filled circle) and A=7 (open circle), as a function of excitation energy of the quasi projectile. Squares were obtained by fitting the isoscaling plots, similar to that in FIG. 3 with a gate on excitation energy.
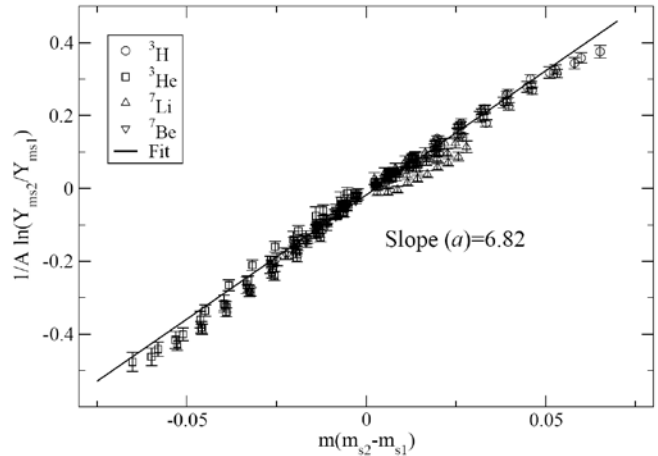
FIG. 3. Plot of '$1/A\ln(Y_{ms2}/Y_{ms1})$' as a function of $m(m_{s2}-m_{s1})$. Y_{ms1} and Y_{ms2} are, respectively, the yields of a fragment from sources with isospin asymmetry of m_{s1} and m_{s2}. m is the isospin asymmetry of the fragment.

squares in Fig. 2) were in reasonable agreement with those obtained from the analysis of the data of mirror nuclei yield ratios.

Thus, the mirror nuclei yield ratios and isoscaling gave consistent results within the framework of Landau free energy approach for critical phenomena. The successful application of Landau approach, justifies the isospin asymmetry (*m*) as an order parameter for nuclear phase transition.

[1] A. Bonasera *et al*., Phys. Rev. Lett. **101**, 122702 (2008).

[2] M. Huang *et al*., arXiv:nucl ex 1002.1738 and 1002.0311, submitted for publication.

[3] K. Huang, *Statistical Mechanics* (Wiley and Sons, New York, 1987), 2nd ed.

[4] L. D. Landau and E. M. Lifshitz, *Statistical Physics* (Pergamon, New York, 1989) 3rd ed..

[5] S. Wuenschel *et al*., Phys. Rev. C **79**, 061602 (2009).

[6] S. Wuenschel, Ph. D. Thesis, Texas A&M University, 2009 and S. Wuenschel *et al*., submitted for publication.

Isoscaling, SMM and the symmetry energy: connecting the dots

P. Marini, A. Botvina, A. Bonasera, Z. Kohley, L. W. May, R. Tripathi, S. Wuenschel,
and S. J. Yennello

Knowledge of the nuclear symmetry energy (E_{sym}) is essential for understanding not only the structure of radioactive nuclei [1], but also many important issues in astrophysics [2] and significant theoretical and experimental works [3-5] have been devoted to its study. While the value of symmetry energy has been well constrained at normal nuclear density and zero temperature, heavy ion collisions remain the most powerful way to study the nuclear matter behaviour in extreme conditions of temperature and density, that can otherwise be encountered only in astrophysical environments, like supernova explosions and neutrons stars. Several observables in heavy ion collisions are known to be affected by the symmetry energy (E_{sym}), but quantitative information is difficult to extract, due to secondary decay of excited primary fragments, which can distort signatures contained in primary fragment observables. Among those observables, isoscaling [6] applies for a variety of reaction mechanisms that are dominated by phase space, including evaporation, multifragmentation, and deep inelastic scattering under the condition of statistical emission. Isoscaling has been observed for the secondary fragments from ^{78,86}Kr+ ^{58,64}Ni at 35AMeV reactions, taken on the NIMROD-ISiS array. The details of the experiment can be found in Ref. [7]. A comparison to models is now needed to constrain E_{sym}. The Statistical Multifragmentation Model (SMM) [8] has been widely used for interpreting experimental data on multiple fragment production in different nuclear reactions and to extract information on the symmetry energy starting from secondary fragments.

In the present work we are analysing SMM, paying special attention to the effects of the secondary de-excitation on the value of observables which can be extracted from experimental data and their correlation with input symmetry energy value in the model. Among the observables we focus on is the isoscaling parameter α_1 to figure out how the symmetry energy values, which can be extracted from it for both hot and cold fragments, are related. Starting from SMM, the isotopic yield of each fragment (N,Z) emitted in the multifragmentation of the quasi-projectile has been determined for both the quasi-projectile sources (^{78}Kr and ^{86}Kr), in order to compute the isoscaling parameter α. For hot fragments (i.e. before the secondary de-excitation) the behaviour of α as a
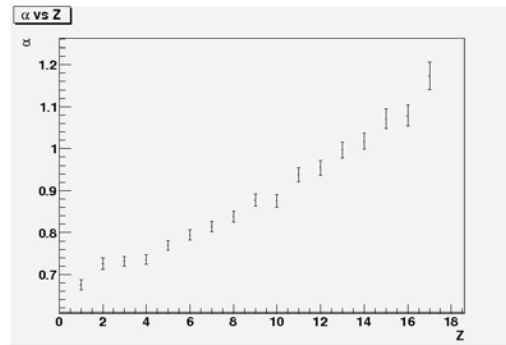
FIG. 1. Isoscaling parameter α from the fitting of the yield ratios of each Z for hot SMM fragments.

function of the fragment charge Z for a chosen source excitation energy (5 MeV/nucleon) and input symmetry energy coefficient (25 MeV) is shown in Fig. 1. The α parameter shows the same behaviour as function Z, even for other values of source excitation energy (3, 4 and 7 MeV/nucleon) and input symmetry energy values C_{sym} (4, 8 and 14 MeV). Attempts to physically interpret this trend have been done by varying the source size, to eventually figure out finite size effects, by isolating the Coulomb contribution ($C_{sym} = 0$) and by selecting a narrow hot fragment excitation energy window. A selection based on the source temperature seems to be the most promising, but work is still in progress.
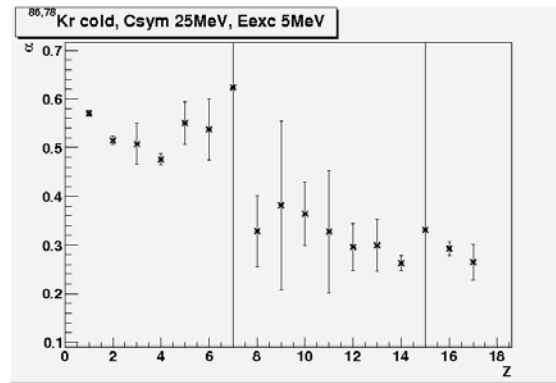
FIG. 2. Isoscaling parameter α from the fitting of the yield ratios of each Z for cold SMM fragments.

Experimentally only cold fragments can be detected and, unless we rely on models to reconstruct primary quantities, information has to be extracted from secondary fragments (i.e. after de-excitation). The behaviour of the α parameter as a function of the fragment charge is plotted in Fig. 2. The same trend has been observed varying the source excitation energy and the symmetry energy input parameter. The physical interpretation of gap in the α value between Z=7 and Z=8 is still under analysis.

The isoscaling parameter α can be linked theoretically [6,9-11] to nuclear symmetry energy by the relation:

$$\alpha = \frac{4C_{sym}}{T}\left[\left(\frac{Z}{A}\right)_1^2 - \left(\frac{Z}{A}\right)_2^2\right] \qquad (1)$$

where C_{sym} is the symmetry energy coefficient, T is the temperature and the Z/A values correspond to the neutron richness of the neutron-rich and neutron-poor sources, respectively. An analysis of α, such as the one performed on experimental data, will allow us to reconstruct the C_{sym} value ($C_{sym}out$) and to study its correlation with the input C_{sym} value ($C_{sym}in$). The correlations for both hot and cold fragments are plotted in Figs.3(a) and Figs.3(b), respectively. The $C_{sym}out$ values extracted from hot fragments are in good agreement with the input values $C_{sym}in$, suggesting that information on C_{sym} can be extracted from

primary fragments. The correlation is significantly damped for excitation energy above 3 AMeV by the secondary de-excitation, which distorts the signatures of the symmetry energy.
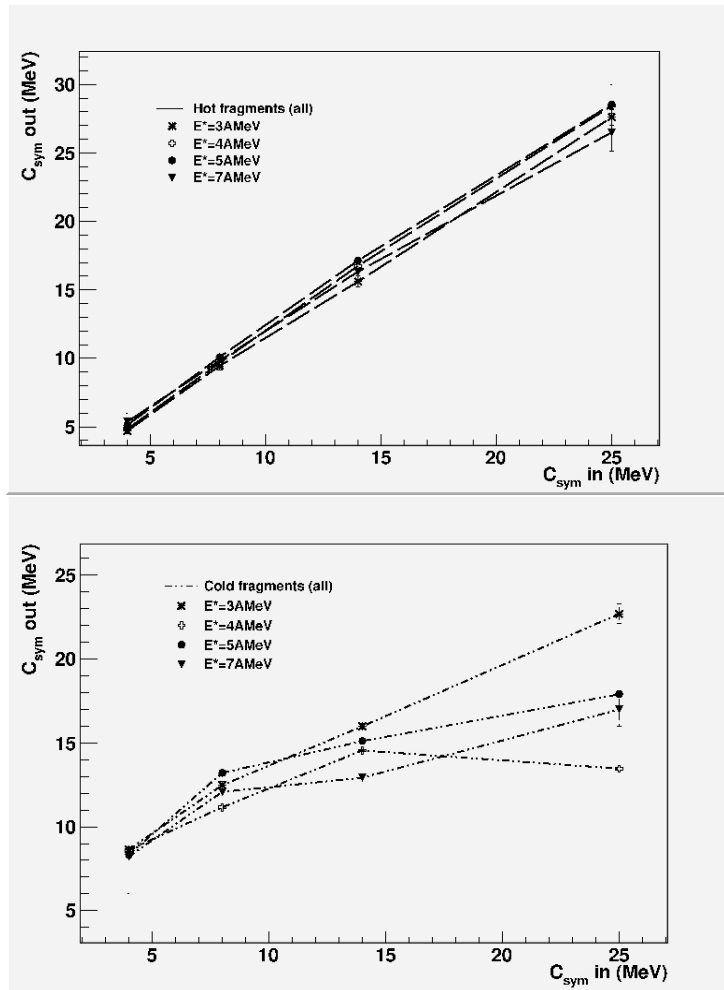
FIG. 3. Correlation between the SMM input symmetry energy coefficient value ($C_{sym}in$) and the symmetry energy coefficient value determined by the isoscaling parameter α obtained by the analysis of hot (upper part) and cold (lower part) fragments.

[1] B.A. Brown, Phys. Rev. Lett. **85**, 5296 (2000).

[2] J.M. Lattimer *et al.*, Astrophys. J. **550**, 426 (2001).

[3] D.V. Shetty *et al.*, Phys. Rev. C **76**, 024606 (2007).

[4] B.A. Li *et al.*, Phys. Rep. **464**, 113 (2008).

[5] V. Baran *et al.,* Phys. Rep. **410**, 335(2005) and refs. therein.

[6] M.B. Tsang *et al.,* Phys. Rev. Lett. **86**, 5023 (2001).

[7] S. Wuenschel *et al.*, Phys. Rev. C **79**, 061602 (2009).

[8] J.P. Bondorf *et al.*, Phys. Rep. **257**, 133 (1995).

SECTION III

NUCLEAR THEORY

Symmetry energy of dilute warm nuclear matter

J. B. Natowitz, G. Röpke,[1] S. Typel,[2,3] D. Blaschke,[4,5] A. Bonasera,[6] K. Hagel,
T. Klähn,[4,7] S. Kowalski, L. Qin, S. Shlomo, R. Wada, and H. H. Wolter[8]

[1]*Institut für Physik, Universität Rostock, Universitätsplatz 3, D-18055 Rostock, Germany*

[2]*Excellence Cluster Universe, Technische Universität München, Boltzmannstraße 2, Garching, Germany*

[3]*GSI Helmholtzzentrum für Schwerionenforschung GmbH, Theorie, Planckstraße 1, Darmstadt, Germany*

[4]*Instytut Fizyki Teoretycznej, Uniwersytet Wrocławski, pl. M. Borna 9, 50-204 Wrocław, Poland*

[5]*Bogoliubov Laboratory for Theoretical Physics, JINR Dubna, Joliot-Curie str. 6, 141980 Dubna, Russia*

[6]*Laboratori Nazionali del Sud-INFN, w. S. Sofia 64, 95123 Catania, Italy*

[7]*Theory Group, Physics Division, Building 203, Argonne National Laboratory, Argonne, Illinois*

[8]*Fakultät für Physik,Universität München, Am Coulombwall 1, D-85748 Garching, Germany*

The symmetry energy in the nuclear equation of state governs phenomena from the structure of exotic nuclei to astrophysical processes. The structure and the composition of neutron stars depend crucially on the density dependence of the symmetry energy [1]. As a general representation of the symmetry energy coefficient we use the definition

$$E_{sym}(n,T) = \frac{E(n,1,T) + E(n,-1,T)}{2} - E(n,0,T) \qquad (1)$$

where $E(n; \delta; T)$ is the energy per nucleon of nuclear matter of N neutrons and Z protons with density n, asymmetry $\delta = (N-Z)/A$, and temperature T.

Our empirical knowledge of the symmetry energy near the saturation density, n_0, is based primarily on the binding energies of nuclei. The Bethe-Weizsäcker mass formula leads to values of about $E_{sym}(n_0; 0) = 28$-34 MeV for the symmetry energy at zero temperature and saturation density $n_0 \approx 0.16$ fm^{-3}, if surface asymmetry effects are properly taken into account. In contrast to the value of $E_{sym}(n_0; 0)$, the variation of the symmetry energy with density and temperature is intensely debated. Many theoretical investigations have been performed to estimate the behavior of the symmetry energy as a function of n and T. Typically, quasiparticle approaches such as the Skyrme Hartree-Fock and relativistic mean field (RMF) models or Dirac-Brueckner Hartree-Fock (DBHF) calculations are used. In such calculations the symmetry energy tends to zero in the low-density limit for uniform matter. However, in accordance with the mass action law, cluster formation dominates the structure of low-density symmetric matter at low temperatures. Therefore, the symmetry energy in this low-temperature limit has to be equal to the binding energy per nucleon associated with the strong interaction of the most bound nuclear cluster. A single-nucleon quasiparticle approach cannot account for such structures. The correct low-density limit can be recovered only if the formation of clusters is properly taken into account.

TABLE I. Temperatures, densities, free and internal symmetry energies for different values of the surface velocity as derived from heavy-ion collisions (cols. 2-6), from the QS approach (cols. 7-8) and self consistently with clusters (cols. 9-12), see text.

V_{surf}	T	n	F_{sym}	S_{sym}^{NSE}	E_{sym}	F_{sym}^{QS}	E_{sym}^{QS}	T^{sc}	n^{sc}	F_{sym}^{sc}	E_{sym}^{sc}
(cm/ns)	(MeV)	(fm^{-3})	(MeV)	(k_B)	(MeV)	(MeV)	(MeV)	(MeV)	(fm^{-3})	(MeV)	(MeV)
0.75	3.31	0.00206	5.64	0.5513	7.465	6.607	8.011	3.26	0.00493	9.211	9.666
1.25	3.32	0.00165	6.07	0.5923	8.036	6.087	7.502	3.45	0.00511	9.295	9.647
1.75	3.61	0.00234	6.63	0.4137	8.124	6.877	7.896	3.54	0.00510	9.284	9.612
2.25	4.15	0.00378	7.81	0.1557	8.456	8.184	8.305	3.66	0.00495	9.193	9.524
2.75	4.71	0.00468	8.28	-0.0162	8.204	8.967	8.321	4.02	0.00510	9.274	9.386
3.25	5.27	0.00489	9.30	-0.1358	8.584	9.395	7.785	4.65	0.00574	9.683	9.227
3.75	6.24	0.00549	10.69	-0.2936	8.858	10.73	7.623	5.75	0.00684	10.49	8.978
4.25	7.54	0.00636	11.83	-0.4197	8.665	11.4	7.807	7.46	0.00866	11.98	8.964

In this work we employ a quantum statistical (QS) approach which includes cluster correlations in the medium. It interpolates between the exact low-density limit and the very successful RMF approaches near the saturation density. In this QS approach the cluster correlations are described in a generalized Beth- Uhlenbeck expansion. The advantage of this method is that the medium modifications of the clusters at finite density are taken into account. The method requires a sufficiently accurate model for the quasiparticle properties, for which we employ a RMF model with density dependent couplings which gives a good description both of nuclear matter around normal density and of ground state properties of nuclei across the nuclear chart. In order to extend the applicability of this RMF model to very low densities, it has been generalized in Ref. [2] to account also for cluster formation and dissolution.

Recently, the experimental determination of the symmetry energy at very low densities produced in heavy ion collisions of ^{64}Zn on ^{92}Mo and ^{197}Au at 35 MeV per nucleon has been reported [3]. Results of this study are given in the first four columns of Table I. The surface velocity V_{surf}, i.e. the velocity before the final Coulomb acceleration, was used as a measure of the time when the particles leave the source under different conditions of density and temperature. The yields of the light clusters $A \leq 4$ were determined as a function of V_{surf}. Temperatures were determined with the Albergo method [4] using a H-He thermometer based on the double yield ratio of deuterons, tritons, ^{3}He and ^{4}He, and are given in Table I as the average for the two reactions. The free neutron yield is obtained from the free proton yield and the yield ratio of ^{3}H to ^{3}He. To determine the asymmetry parameter of the sources the total proton and neutron yields including those bound in clusters are used. The proton chemical potential is derived from the yield ratio of ^{3}H to ^{4}He. The corresponding free proton and free neutron densities are calculated, and the total nucleon density is obtained by accounting also for the bound nucleons according to their respective yields [3]. The total nucleon densities are of the order of 1/100th to 1/20th of saturation density, as seen in Table. I.

An isoscaling analysis [5] has been employed (as a function of V_{surf}) to determine the free symmetry energy F_{sym} via the expression $\alpha = 4F_{sym} \Delta(Z/A)^2/T$. Here α is the isoscaling coefficient

determined from yield ratios of $Z = 1$ ejectiles of the two reactions and $\Delta(Z/A)^2$ is the difference of the squared asymmetries of the sources in the two reactions. With $\Delta(Z/A)^2$ and the temperature determined as above, the free symmetry energy is extracted. From the free symmetry energy derived in this way from the measured yields, the internal symmetry energy can be calculated if the symmetry entropy is known. The values of the symmetry entropy S_{sym}^{NSE} for given parameters of temperature and density within the nuclear statistical equilibrium (NSE) model are shown in Table I, column 5. They are calculated with the equivalent expression of Eq. (1) as the difference between the entropies of pure proton or neutron and symmetric nuclear matter. The results obtained in this way for the internal symmetry energy $E_{sym} = F_{sym} + T\, S_{sym}^{NSE}$ are shown in Table I, column 6. In Table I, we also give results of the QS model [2] for the free and internal symmetry energies (columns 7 and 8) at given T and n. There are large discrepancies between the measured values and the results of calculations in the mean-field approximation when cluster formation is neglected. On the other hand, the QS model results correspond nicely to the experimental data.

In Fig. 1 we present results for different approaches to extracting the internal symmetry energy and compare with the experimental values. In the left panel of the figure we show theoretical results for T at or close to zero. A widely used momentum-dependent parameterization of the symmetry energy (MDI) at temperature $T = 0$ MeV was given in Ref. [6] and is shown for different assumed values of the stiffness parameter x. For these parameterizations the symmetry energy vanishes in the low-density limit. We compare this to the QS result at $T = 1$ MeV. In this approach the symmetry energy is finite at low density. The $T = 1$ MeV curve will also approach zero at extremely low densities of the order of 10^{-5} fm^{-3} because the temperature is finite. The RMF, $T = 0$ curve is discussed below. Also note that the underlying RMF model for the quasiparticle description with $n_0 = 0.149$ fm^{-3}, $E_{sym}(n_0) = 32.73$ MeV gives a reasonable behavior at high density similar to the MDI, $x=0$ parameterization. We thus see that our approach successfully interpolates between the clustering phenomena at low density and a realistic description around normal density. In the right panel of Fig. 1 we compare to the experimental results, full circles (Tab. I, col. 6) in an expanded low-density region. Besides the MDI parameterization we show the QS results [2] for $T=1$, 4, and 8 MeV, which are in the range of the temperatures in the experiment. The QS results including cluster formation agree well with the experimental data points, as seen in detail in Fig. 1. We conclude that medium-dependent cluster formation has to be considered in theoretical models to obtain the low-density dependence of the symmetry energy that is observed in experiments.

The temperatures and densities of columns 2 and 3 in Table I will be modified if medium effects on the light clusters are taken into account [7]. We have carried out a self-consistent determination of the temperatures T^{sc} and densities n^{sc} taking into account the medium dependent quasiparticle energies as specified in Ref. [8] (columns 9 and 10 of Table I). Compared to the Albergo method results [3], the temperatures T^{sc} are about 10% lower. Significantly higher values are obtained for the inferred densities n^{sc} which are more sensitive to the inclusion of medium effects. We have also calculated the free and internal symmetry energies corresponding to these self-consistent values of T^{sc} and n^{sc} according to Ref. [2] (columns 11 and 12 of Table I). These results are also shown in the right panel of Fig. 1 as open
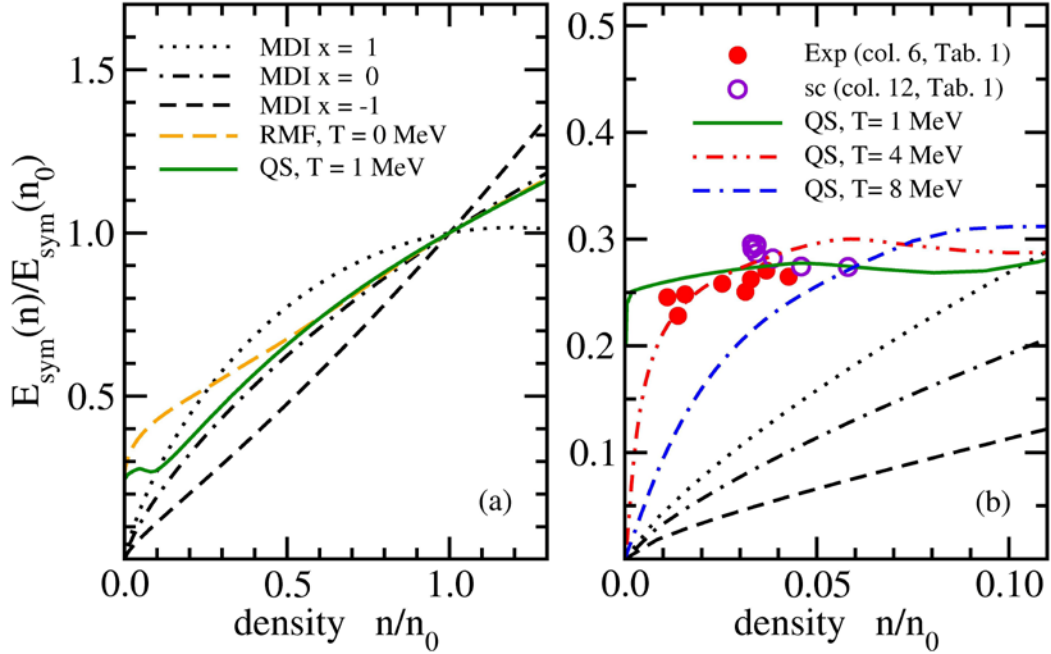
FIG. 1. Comparisons of the scaled internal symmetry energy $E_{sym}(n)/E_{sym}(n_0)$ as a function of the scaled total density n/n_0 for different approaches and the experiment. Left panel: The symmetry energies for the commonly used MDI parameterization for $T = 0$ and different asy-stiffnesses, controlled by the parameter x (dotted, dot-dashed and dashed lines); for the QS model including light clusters for temperature $T = 1$ MeV (solid line), and for the RMF model at $T = 0$ including heavy clusters (long-dashed line). Right panel: The internal scaled symmetry energy in an expanded low density region. Shown are again the MDI curves and the QS results for $T = 1$, 4, and 8 MeV compared to the experimental data with the NSE entropy (solid circles) and the results of the self-consistent calculation (open circles) from Table I.

circles. The resultant internal symmetry energies are 15 to 20% higher than the QS model values for T and n given in columns 2 and 3 in Table I.

We have restricted our present work to that region of the phase diagram where heavier clusters with $A > 4$ are not relevant. The simplest approach to model the formation of heavy clusters is to perform inhomogeneous mean-field calculations in the Thomas-Fermi approximation assuming spherical Wigner-Seitz cells. In Fig. 1 (left panel) preliminary results for the zero-temperature symmetry energy of such a calculation is shown by the long-dashed line using the same RMF parameterization as for the QS approach introduced above; for details see Ref. [9]. The symmetry energy in this model approaches a finite value at zero density in contrast to the behavior of the MDI parameterizations and conventional single-nucleon quasiparticle descriptions.

In conclusion, we have shown [10] that a quantum statistical model of nuclear matter, that includes the formation of clusters at densities below nuclear saturation, describes quite well the low-density symmetry energy which was extracted from the analysis of heavy-ion collisions. Within such a theoretical approach the composition and the thermodynamic quantities of nuclear matter can be modeled

in a large region of densities, temperatures and asymmetries that are required, e.g., in supernova simulations.

[1] J.M. Lattimer and M. Prakash, Phys. Rep. **442**, 109 (2007).

[2] S. Typel, G. Röpke, T. Klähn, D. Blaschke and H.H. Wolter, Phys. Rev. C **81**, 015803 (2010).

[3] S. Kowalski *et al.*, Phys. Rev. C **75**, 014601 (2007).

[4] S. Albergo, *et al.*, Nuovo Cimento A **89**, 1 (1985).

[5] M.B. Tsang *et al.*, Phys. Rev. Lett. **86**, 5023 (2001).

[6] L.W. Chen *et al.*, Phys. Rev. Lett. **94**, 032701 (2005); Phys. Rev. C **76**, 054316 (2007).

[7] S. Shlomo *et al.*, Phys. Rev. C **79**, 034604 (2009).

[8] G. Röpke, Phys. Rev. C **79**, 014002 (2009).

[9] S. Typel *et al.*, in preparation.

[10] J.B. Natowitz *et al.*, Phys. Rev. Lett. **104**, 202501 (2010).

The η/*s* ratio in finite nuclei

N. Auerbach[1] and S. Shlomo

[1]*School of Physics and Astronomy, Tel Aviv University Tel Aviv, 69978, Israel*

In certain supersymmetric gauge theories one finds [1] that the ratio of shear viscosity η to entropy density *s* is equal to:

$$\frac{\eta}{s} = \frac{\hbar}{4\pi k_B} \approx 6.05 \times 10^{-13} \, Ks \qquad (1)$$

Where k_B is the Boltzmann constant. It has been conjectured that this ratio is the lower limit for a large class of quantum field theories. The analysis of the ultrarelativistic heavy ion collisions data from RHIC leads to [2]

$$\frac{\eta}{s} \leq 5 \times \frac{\hbar}{4\pi k_B} \qquad (2)$$

It seems to indicate that the state of matter produced behaves like a liquid with the above ratio being close to the lower limit [2]. Thus the matter produced behaves as a perfect fluid. In this work [3] we first demonstrate that a consistent value for η is deduced from (i) analysis of the width of giant resonances within the hydrodynamic model, (ii) kinetic theory, and from (iii) the process of fission described using liquid drop models. We then provide a simple assessment of the entropy density.

Most of the giant resonances, at excitation energies in the range of 10-40 MeV have a finite life time and carry a width. Following the success of the hydrodynamical models an attempt was made to link the widths of these resonances to the viscosity of the proton-neutron fluids [4]. In Ref. [4] a set of coupled hydrodynamical equations of the Navier- Stokes type was used to describe the flow of two viscous fluids, of protons and neutrons. Solving these equations with appropriate boundary conditions and for various multipolarities one obtains eigenvalues containing a real and imaginary part. The real part represents the energy of the excitation and the imaginary part depends represents the lifetime of the excitation. The mass dependence A of the computed widths exhibits the experimental trends of the giant isoscalar resonances. As a result of such calculation one obtains a value for the shear viscosity is:

$$\eta \approx 1 \times 10^{-23} \text{ MeVfm}^{-3} \text{ sec} \qquad (3)$$

Recently, in Ref. [5], the authors described the dynamics of cold and hot nuclei within a generalized Fermi liquid drop model by employing a collision kinetic equation, which properly accounts for the dissipative propagation of sound waves in finite nuclei and nuclear matter. For a temperature $T<\varepsilon_F$ and excitation energy $\hbar\omega < \varepsilon_F$ of the sound wave, one finds for the collision viscosity

$$\eta = \frac{2}{5}\rho\varepsilon_F \frac{\tau_{coll}}{1+\left(\omega\tau_{coll}\right)^2}, \quad \tau_{coll} = \frac{\tau_0}{1+\left(\hbar\omega/2\pi T\right)^2}, \quad \tau_0 = \hbar\alpha/T^2 \qquad (4)$$

In Eq (4), τ_{coll} is the Landau ansatz for the collision relaxation time deducted from the collision integral. The value of α is sensitive to the in-medium-nucleon-nucleon scattering cross section. Taking the in-medium cross-section to be ½ of the free nucleon-nucleon cross section, one finds [5] that α=9.2 MeV. In Fig. 1a the value of η as a function of the temperature T, obtained using the values of ε_F = 40 MeV, ρ = 0.16 fm^{-3}, α = 9.2 MeV and $\hbar\omega$ = 20 MeV. Note that our results are relevant for temperature 0.5 MeV < T < 5 MeV, were giant resonances exist.

At low temperature, T $\ll$ ε_F, the relation between the thermal excitation energy E^* and T is given by

$$E^* = aT^2 \tag{5}$$

where a is the level density parameter. For an ideal Fermi gas, for A=200 and a thermal excitation energy $E^* \approx \hbar\omega$ = 20 MeV, one obtains $T \approx 1$ MeV which then, using Eqs. (4-6), gives:

$$\eta \approx 0.5 \times 10^{-23} \text{ MeV fm}^{-3} \text{ sec} \tag{6}$$

Another type of collective motion encountered in the dynamics of nuclei is the process of fission. A number of works appeared in the literature which dealt with the dynamics of fission in heavy nuclei using viscous liquid drop models. For example, in [6] the authors use a macroscopic approach and solve classical equations of motion for the fissioning nucleus. They apply this to spontaneous and induced fission. They find that the average value for the shear viscosity that reproduces best the data is:

$$\eta \approx (0.9 \pm 0.3) \times 10^{-23} \text{ MeV fm}^{-3} \text{ sec} \tag{7}$$

For low temperature, T < ε_F, the entropy density s of a nucleus is given in terms of the entropy S by the simple expression [5]:

$$s = \frac{\rho}{A} S, \qquad\qquad S = 2aT, \tag{8}$$

In Fig. 1c we show η/s as a function of temperature. The curve has the characteristic behavior found in other fluids [1], the minimum at $T = 3$ MeV, with the value of $\eta/s \approx 3 \times \hbar/4\pi k_B$.

We therefore have for a nucleus the value [3]:

$$\frac{\eta}{s} \approx (2 - 12) \times \frac{\hbar}{4\pi k_B} \tag{9}$$

Comparing our results for finite nuclei at low temperature to that of RHIC, Eq. (2), we see that the deduced ratio (especially the lower limit) is not drastically different from the RHIC result. More studies are required in order to understand this point.
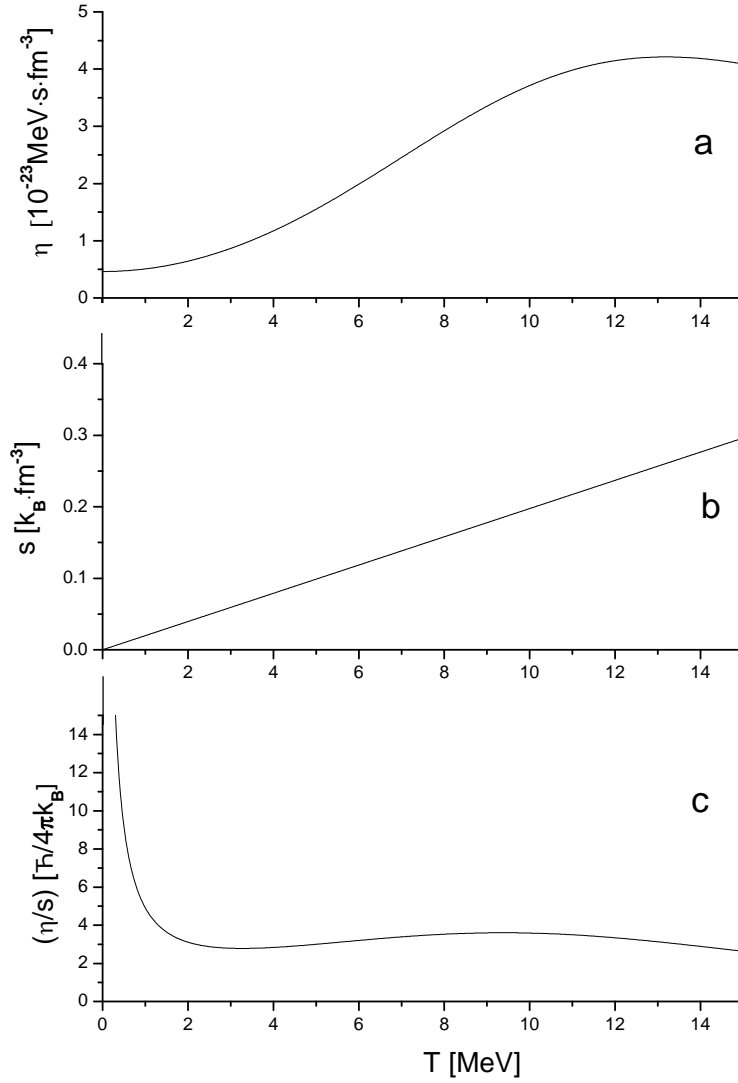
FIG. 1. The nuclear shear viscosity η (a), entropy density *s* (b) and their ratio, (η/*s*) (c), in units of $\hbar/4\pi k_B$, as functions of the temperature, T. The values of the parameters used in the calculations are; $\varepsilon_F = 40$ MeV, $\rho = 0.16$ fm^{-3}, $\alpha = 9.2$ MeV and $\hbar\omega = 20$ MeV.

[1] P. Kovtun, T.D. Son, and A.O. Starinets, Phys. Rev. Lett. **94**, 111601, (2005).

[2] See for example, T. Schafer and D. Teaney, arXiv: 0904.3107v2 [hep-ph].

[3] N. Auerbach and S. Shlomo, Phys. rev. Lett. **103**, 172501 (2009).

[4] N. Auerbach and A. Yeverechyahu, Annals Physics (N.Y.) **95**, 35 (1975).

[5] V.M. Kolomietz and S. Shlomo, Phys. Rep. **390**, 133 (2004).

[6] K.T. Davies, A.J. Sierk, and J.R. Nix, Phys. Rev. C **13**, 2385 (1976).

Effects of one and two-body relaxations on isoscalar compression modes

D. C. Fuls, V. M. Kolomietz,[1] S. V. Lukyanov,[1] and S. Shlomo
[1]*Institute for Nuclear Research, Kiev 03680, Ukraine*

We study [1] the sensitivities of the centroid energy *E0* of the isoscalar giant monopole resonance (ISGMR) and the centroid energy *E1* of the isoscalar giant dipole resonance (ISGDR) to the effect of relaxation. We use the semi-classical kinetic approach in *(r,p)* phase space, also called the fluid dynamic approach (FDA). A small variation of the distribution function $\delta f(r, p)$ can be evaluated using the linearized kinetic equation. To evaluate δf we will apply the linearized Landau-Vlasov equation, augmented by a source term $\delta St(f)$ for relaxation processes, in the form

$$\frac{\partial}{\partial t}\delta f + \mathbf{v}\cdot\nabla_{\mathbf{r}}\delta f - \nabla_{\mathbf{r}}\left(\delta U_{\text{self}} + U_{\text{ext}}\right)\cdot\nabla_{\mathbf{p}}f_{\text{eq}} = \delta St[f], \qquad (1)$$

where $v = p/m^*$ is the quasi-particle velocity and m^* is the effective mass of the nucleon. U_{self} and U_{ext} are the mean field and external field, respectively. The right-hand side of Eq. (1) represents the change of the distribution function due to relaxation. In this work we use the approximation

$$\delta St[f] = -\frac{\delta f}{\tau_{\text{eff}}}, \qquad \frac{1}{\tau_{\text{eff}}} = \frac{1}{\tau_2} + \frac{1}{\tau_1} + \frac{1}{\tau_{\uparrow}}. \qquad (2)$$

Here, the term $1/\tau_2$ is due to the two-body collisions on the distorted Fermi surface, $1/\tau_1$ determines the change in the distribution function resulting from one-body relaxation on the moving nuclear surface and $1/\tau_{\uparrow}$ takes into account the possibility of particle emission. We assume

$$\tau_2 = \frac{\hbar\beta}{\left(\hbar\omega_R/2\pi\right)^2}, \qquad \tau_1 = \frac{2R_0}{\bar{v}}\xi. \qquad (3)$$

In Eq. (3) ω_R is the real part of the eigenfrequency of the sound mode. The coefficient β depends on the *NN*-scattering cross sections. We will use the value of β=4.6 MeV which corresponds to the isotropic energy independent *NN*-cross sections $\sigma_{pp} = \sigma_{nn} = 25$ mb and $\sigma_{pn} = \sigma_{np} = 50$ mb. R_0 is a nuclear radius, $\bar{v} = 3v_F/4\,v$ and ζ is a free numerical factor which depends on the excitation mode. For heavy nuclei, the value of the emission width $\Gamma_{\uparrow} \approx 1/\tau_{\uparrow}$ is quite small and we neglect the contribution of the particle emission to the total relaxation time τ_{eff}. Evaluating the *p*-moments to the kinetic equation (1), one can reduce the kinetic equation to the equation for the particle density eigenvibrations, $\delta\rho_L$, depending on momenta q and frequencies ω. Imposing the boundary conditions for the consistent

solutions of both the continuity and the Euler equations, taken at the moving nuclear surface, one obtains a solution for $\delta\rho_L(q,\omega)$ by solving a dispersion relation for $\omega = E + i\Gamma$ and a secular equation for q.

In the figure below, we show the dependence of the energy ratio $E1/E0$ on the nuclear mass number A. Considering the dependence of the FDA ratio $(E1/E0)_{FDA}$ on the relaxation time τ_{eff}, we find a good agreement between experimental data and the results of the FDA model calculations (solid line 2) for the value of ζ fitted to the widths $\Gamma0$ and $\Gamma1$. In the figure, the ratio $(E1/E0)_{FDA}$ for the rare collision regime (solid line 1) was obtained for the limit $\tau_{eff} \to \infty$, and $(E1/E0)_{RPA}$ is obtained from quantum and fully self-consistent Hartree-Fock based Random Phase Approximation (HF-RPA) calculations. The ratio $(E1/E0)_{scaling}$ (dotted line) is obtained from the scaling model. Also shown is the liquid drop (LDM) limit of ≈ 1.43. The ratios $(E1/E0)_{RPA}$, $(E1/E0)_{scaling}$ and $(E1/E0)_{FDA}$ in a rare collision regime significantly exceed the liquid drop model (LDM) estimate $(E1/E0)_{LDM}$ and the experimental data $(E1/E0)_{exp}=1.6\pm0.1$ [2, 3].
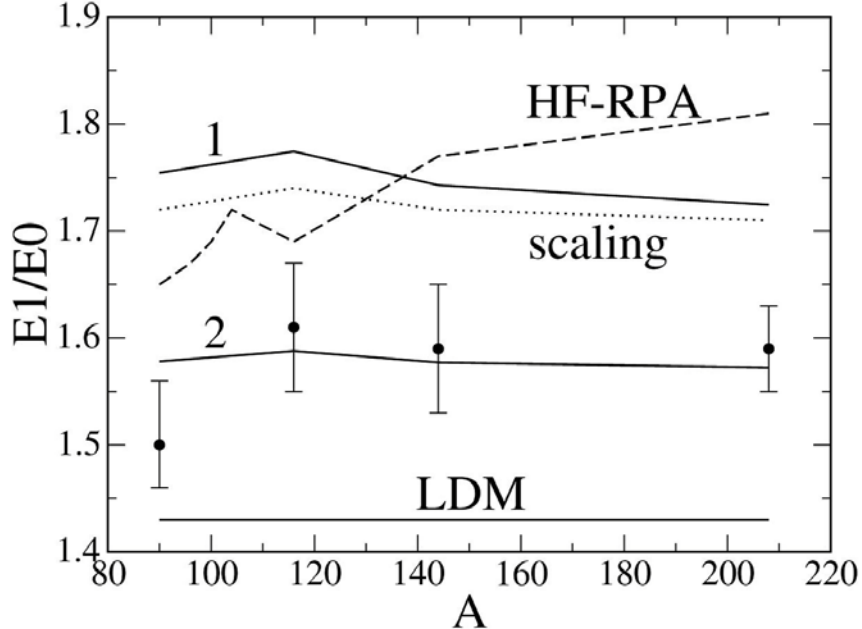
FIG. 1. Dependence of the energy ratio $E1/E0$ on the nuclear mass number A.

We have demonstrated that one can obtain an agreement with the experimental data on $E1/E0$ in the presence of relaxation processes. Besides the collisional width, the experimentally observable widths of the ISGMR and the ISGDR include the fragmentation width. Within our semi-classical kinetic theory, this mechanism of resonance spreading is considered an additional relaxation effect (one-body relaxation) due to the single particle scattering on the moving surface of the nucleus [3].

[1] D.C. Fuls, V.M. Kolomietz, S.V. Lukyanov, and S. Shlomo, EPL (accepted).
[2] D.H. Youngblood, H.L. Clark and Y.-W. Lui, Phys. Rev. C **69**, 034315 (2004).
[3] D.H. Youngblood, H.L. Clark and Y.-W. Lui, Phys. Rev. C **69**, 054312 (2004).

Bound, virtual and resonance S-matrix poles from the Schrödinger equation

A. M. Mukhamedzhanov , B. F. Irgaziev,[1] V. Z. Goldberg, Yu.V. Orlov,[2] and I. Qazi[1]

[1]*GIK Institute of Engineering Sciences and Technology,Topi, District Swabi, N.W.F.P.,Pakistan*

[2]*Skobeltsyn Institute of Nuclear Physics, Moscow State University, Russia*

A general method, which we call the potential S-matrix pole method, is developed for obtaining the S-matrix pole parameters for bound, virtual and resonant states based on numerical solutions of the Schrödinger equation. This method is well-known for bound states. In this work we generalize it for resonant and virtual states, although the corresponding solutions increase exponentially when $r \to \infty$. Concrete calculations are performed for the 1^+ ground state of ^{14}N, the resonance ^{15}F states $(1/2^+, 5/2^+)$, low-lying states of ^{11}Be and ^{11}N, and the subthreshold resonance in the proton-proton system. We also demonstrate that in the case of the broad resonances their energy and width can be found from the fitting of the experimental phase shifts using the analytical expression for the S-matrix. We compare the S-matrix pole and the R-matrix for broad resonances in the ^{14}O-p and in ^{26}Mg-n.

As example, in Table I we present the results of the calculations of the resonance states $\frac{1}{2}^{\pm}$ and $5/2^+$ in ^{11}N. In the 6-th and 7-th columns are shown the calculated energies and single-particle proton partial resonance widths.

TABLE I. Energies and widths calculated for low-lying levels of ^{11}N by S-matrix pole method. The Coulomb radius $r_C = 1.1$ fm ($r_{ls} = r_0$, $a_{ls} = a$).

J	r_0 (fm)	a (fm)	V_0 (MeV)	V_{ls} (MeV)	E_{sp} (MeV)	Γ_{sp} (MeV)
$1/2^+$	1.20	0.753	57.057	0	1.014	0.843
	1.22	0.713	57.057	0	1.039	0.881
	1.25	0.650	57.057	0	1.081	0.944
	1.27	0.607	57.057	0	1.112	0.993
	1.29	0.562	57.057	0	1.146	1.048
$1/2^-$	1.20	0.819	37.505	6.0	1.919	0.944
	1.22	0.760	37.505	6.0	1.991	0.963
	1.25	0.650	37.505	6.0	2.134	0.996
	1.27	0.545	37.505	6.0	2.284	1.024
	1.28	0.451	37.505	6.0	2.426	1.047
$5/2^+$	1.20	0.753	57.057	7.13	3.672	0.959
	1.22	0.713	57.057	6.222	3.719	0.927
	1.25	0.650	57.057	4.743	3.793	0.878
	1.27	0.607	57.057	3.671	3.845	0.847
	1.29	0.562	57.057	2.520	3.900	0.8167

Reaction rates for the ^{17}O(p,α)^{14}N reaction at astrophysical temperature via the Trojan Horse method

M. L. Sergi,[1] C. Spitaleri,[1] M. La Cognata,[1] A. Coc,[2] A. M. Mukhamedzhanov,
M. Gulino,[1] L. Lamia,[1] R. G. Pizzone,[1] S. Cherubini,[1] V. Crucilla,[1] S.M.R. Puglia,[1] G. G. Rapisarda,[1] S. Romano,[1] S. Tudisco,[1] and A. Tumino,[1] V. Burjan,[3] Z. Hons,[3] V. Kroha,[3] F. Hammache,[4] and N. de S´er´eville,[4] B. Irgaziev,[5] G. G. Kiss,[1,6] and E.Somorjai[6]

[1]*INFN-Laboratori Nazionali del Sud, Catania, Italy*
[2]*CSNSM,CNRS/IN2P3/UPS Bˆatiment 104 91405 Orsay Campus, France*
[3]*Nuclear Physics Institute of ASCR Rez near Prague, Czech Republic*
[4]*IPN, IN2P3-CNRS et Universit´e de Paris-Sud 91406 Orsay Cedex, France*
[5]*GIK Institute of Engineering Sciences and Technology Topi District Swabi NWFP,Pakistan*
[6]*ATOMKI, Debrecen,Hungary*

The ^{17}O(p,α)^{14}N reaction is of fundamental relevance in several astrophysical scenarios, such as novae and AGB nucleosynthesis and gamma-ray astronomy. We report on the indirect measurement of the low-energy region of the ^{17}O(p,α)^{14}N reaction bare nucleus cross section. In particular the two resonances at $E_R = 65$ keV and $E_R = 183$ keV, which dominate the reaction rate inside the Gamow window, have been observed and the strength of the 65 keV resonance has been deduced to evaluate the reaction rate. The estimate of the screening potential U was obtained and it was compared with the upper limit given by theoretical adiabatic approximation.

Astrophysical factors of the $^{18}O(p,\alpha)^{15}N$ through the Trojan Horse method in the vicinity of the interfering broad resonances

M. La Cognata,[1,2] C. Spitaleri, [1,2] and A. M. Mukhamedzhanov

[1]*INFN Laboratori Nazionali del Sud & DMFCI Universit`a di Catania, Catania, Italy*

[2]*Centro Siciliano di Fisica Nucleare e Struttura della Materia, Catania, Italy*

^{19}F is one of the few naturally occurring isotopes whose nucleosynthesis is still uncertain. SNe, AGB and WR stars are its most likely sources. In particular fluorine abundances observed in AGB stars can constrain AGB star models since they are sensitive to the environmental conditions in the intershell region and to the dynamics of the mixing phenomena taking place in such stars. The $^{18}O(p,\alpha)^{15}N$ reaction can affect fluorine yield from AGB stars since it produces ^{15}N nuclei which are later burnt to ^{19}F through the $^{15}N(\alpha,\gamma)^{19}F$ capture reaction during a thermal pulse. Large uncertainties characterize ^{19}F nucleosynthesis since experimental ^{19}F abundances are not reproduced by current AGB models. A possible solution of these experimental problems can come from nuclear physics studies. Indeed the measurement of nuclear cross sections at ultra-low energies is a very difficult task because of the presence of the Coulomb barrier exponentially suppressing the cross section. Therefore extrapolation is necessary when data at astrophysical energies are unavailable. Even when measurements are available inside the Gamow window, electron screening makes the bare-nucleus cross section inaccessible. Thus indirect techniques such as the Trojan Horse Method (THM) have been developed to extract low-energy cross sections with no need of extrapolation. Previously we have determined the astrophysical S factors contributed by low-energy resonances in ^{19}F at 19.5, 96.6 and 145.5 keV. However, at higher energies the reaction rates for the $^{18}O(p,\alpha)^{15}N$ are governed by broad ½$^+$ interfering resonances at 574 and 796 keV.

In this work we analyze the TH data at energies $E > 400$ keV using the generalized R matrix approach. Before, we reanalyzed the S factor for the $^{18}O(p,\alpha)^{15}N$ reaction obtained from direct measurements. In the analysis we used the two-channel, two-level R matrix and determined new resonance energies and partial widths. In particular, our determined α - particle partial width for the resonance at 574 is almost factor of two lower than previously obtained. Using these resonance and using the ratio of the amplitudes for the $^{18}O(d,n)^{19}F$ direct reaction populating 574 and 796 keV resonances as fitting parameter we are able to reproduce the TH data. The further analysis is still in progress.

Asymptotic normalization coefficient from the ^{14}C(d, p)^{15}C reaction

A. M. Mukhamedzhanov, V. Burjan,[1] M. Gulino,[2] Z. Hons,[1] V. Kroha,[1] J. Mrazek,[1] J. Novak,[1]
S. Piskor,[1] S. Romano,[2] M. L. Sergi,[2] C. Spitaleri,[2] L. Trache and R. E. Tribble

[1] *Nuclear Physics Institute, Czech Academy of Sciences, 250 68   Rez-Prague, Czech Republic*

[2] *Universita di Catania and INFN Laboratori Nazionali del Sud, Catania, Italy*

The measurement of the differential cross section of the ^{14}C(d,p)^{15}C reaction was carried out at the U-120M cyclotron isochronous cyclotron at the Nuclear Physics Institute of the Czech Academy of Sciences. The deuteron beam with the energy of 17.06 MeV was led into a target chamber with ^{14}C and mylar targets. At all angles we alternately measured spectra from both these targets. In this way we were able to determine exact contents of the ^{14}C isotope in ^{14}C targets. Reaction products were measured by four $\Delta E-$ E telescopes assembled from thin surface barrier silicon and thick Si(Li) detectors with thickness about 200 µm and 4 mm respectively. One telescope serving as a monitor of the target was fixed at the angle of 15°. All telescopes were mounted at 160 mm distance from the center of the irradiated target and were provided with 2 mm x 3 mm rectangular collimators.

The angular distributions of deuterons from the reaction ^{14}C(d,p)^{15}C corresponding to the two bound states in ^{15}C calculated with different combinations of the optical model parameters are shown in Fig. 1. The angular distribution of the transition to the ground state of ^{15}C is best described by the
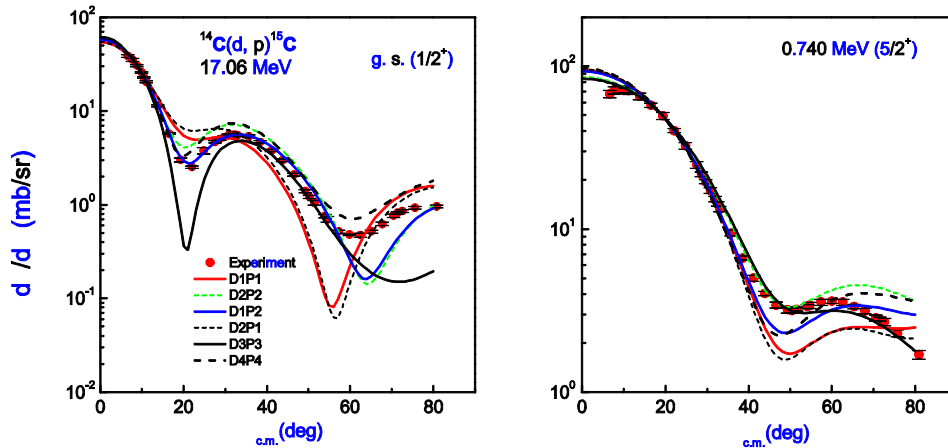
FIG. 1. Angular distributions from the ^{12}C(d,p)^{15}C reaction for the transitions leading to the ground and 0.740 MeV states in ^{15}C. DWBA calculations were made with optical model parameter sets given in Tables 1 (input chanel) and 2 (output channel): D1-P1, red solid curve; D1-P2, blue solid curve; D2-P1, red dotted curve and D2-P2, black dashed curve.   D1 (fit of Cole seed data [1]) and D2 (fit of seed data taken from [2])- optical potentials in the initial channel, P1 [3]   and P2 [2] - optical potentials in the final channel.

combination of optical model potentials D1-P2. For the transition to the 0.740 MeV state of ^{15}C the optical model parameters D2-P2 are the best. By normalization of the differential cross section calculated within the DWBA to the experimental one we determine the ANC. In Table I the deduced values of the ANCs are given. The spectroscopic factors are calculated from the relation $Slj = C_{lj}^2/b_{lj}^2$, where blj is the single-particle ANC determined for the bound state potential with parameters $r_o = 1.25$ fm and $a = 0.65$ fm.

TABLE I. Di(Pj) is the optical potential in the initial (final) state of the reaction ^{14}C(d,p)^{15}C, C is the neutron ANC in ^{15}C, S is the spectroscopic factor.

	Potential	C^2(fm^{-1})	S
gr. state (1/2+)	D1-P1	1.390	0.675
	D1-P2	1.551	0.754
	D2-P1	1.545	0.751
	D2-P2	1.818	0.884
	D3-P3	1.635	0.794
	D4-P4	1.888	0.917
	Mean value	1.638 ± 0.170	0.796

[1] W.S. Cole, T. Mo, H.R. Weller, and J.J. Ramirez, Nucl. Phys. **A213**, 107 (1973).

[2] C.M. Perey, F.G. Perey, At. Data and Nucl. Data Tables **17**, 1 (1976).

[3] T.H. Curtis, H.F. Lutz, D.W. Heikkinen, and W. Bartolini, Nucl. Phys. **A165**, 19 (1971).

Unitary correlation in nuclear reaction theory

A. M. Mukhamedzhanov and A. S. Kadyrov[1]

[1]*Curtin University of Technology, GPO Box U1987, Perth, WA 6845, Australia*

Since the dawn of nuclear physics *(d,p)* reactions have been the main tool to extract spectroscopic factors (SFs) (we call them phenomenological SFs), which were compared with predictions of the independent-particle shell model (ISPM). Later on electron-induced breakup reactions and nucleon knockout reactions became new tool to determine the SFs. Reduction of the phenomenological SFs deduced from the *(e,e'p)* reactions compared to the IPSM ones has been discussed in [1]. Recently a similar reduction has been observed for the SFs determined from the analysis of the single-nucleon knockout nuclear reactions [2].

Although the reason for this reduction is not yet known, there are different possible sources of this reduction: the single-particle approximation of the overlap function, antisymmetrization effects, ambiguity of the optical potentials, accuracy of the DWBA, contribution of the coupled channels, the effect of the short-range NN correlations. A very interesting observation has been pointed out in [3]. The reduction of the SFs can be explained if they are calculated as the square of the norm of the overlap functions found from the inhomogeneous equation, which contains the correlation-dependent effective nucleon-nucleon potential.

In the IPSM the model wave functions are given by the linear combination of the Slater determinant wave functions. However, such model wave functions don't take into account short-range NN correlations caused by the repulsive core in the NN potential. In [4] the Unitary Correlation Operator Method (UCOM) has been developed, which allows one to correct the IPSM by taking into account the short-range repulsive NN correlations by applying unitary correlation operators (UCOs) onto the trial functions. In this work we consider the impact of the short-range NN correlations on *(d,p)*, *(d,pn)* and *(e,e'p)* reactions. Using the surface integration we have proved that the exact reaction amplitude for the *(d,p)*, and *(d,pn)* and reactions is invariant under finite-range unitary correlations while the SFs are not. It makes impossible unambiguous determination of the SFs from*(d,p)*, and *(d,pn)* reactions if the exact approach is used.

[1] G.J. Kramer, H.P. Blokb, and L. Lapikás, Nucl. Phys. **A679**, 267 (2001).

[2] A. Gade *et al.*, Phys. Rev. C **77**, 044306 (2008).

[3] N.K. Timofeyuk, Phys. Rev. Lett. **103**, 242501 (2009).

[4] H. Feldmeier *et al.*, Nucl. Phys. **A632**, 61 (1998).

The evaluation of V_{ud} and its impact on the unitarity of the Cabbibo-Kobayashi-Maskawa quark-mixing matrix

I. S. Towner and J. C. Hardy

We have written an invited review article [1] on the determination of the Cabibbo-Kobayashi-Maskawa (CKM) matrix element V_{ud}. Data from $0^+ \rightarrow 0^+$ superallowed beta decay in nuclei, neutron decay, beta decay of odd-mass mirror nuclei and pion decay were considered. Theoretical radiative and isospin symmetry-breaking corrections were applied. The most precise result comes from the nuclear $0^+ \rightarrow 0^+$ decays, which yield a recommended value of $|V_{ud}| = 0.97425(22)$. We further summarized the data leading to the CKM matrix element V_{us}: K_{l3} and K_{l2} decays, hyperon decays and hadronic tau decay. Again radiative corrections and $SU(3)$-symmetry breaking corrections (from lattice QCD) were applied. We adopted values from K_{l3} decay of $|V_{us}| = 0.2246(12)$ and from K_{l2} decay of $|V_{us}/V_{ud}| = 0.2319(14)$. From the three data just cited, a least-squares fit determines two CKM matrix elements: $|V_{ud}| = 0.97425(22)$ and $|V_{us}| = 0.22521(94)$. Data leading to the third member of the top row of the CKM matrix, V_{ub}, were summarized as well but, being of order 10^{-3}, that matrix element contributes negligibly to the unitarity sum, $|V_{ud}|^2 + |V_{us}|^2 + |V_{ub}|^2$. We found this sum to be $0.99990(60)$, showing unitarity to be satisfied to a precision of 0.06%. We also discussed the constraints that this result places on several selected extensions to the standard model.

[1] I.S. Towner and J.C. Hardy, Rep. Prog. Phys. **73**, in press.

Efficacy of the isospin-symmetry-breaking correction in Fermi beta decay

I. S. Towner and J. C. Hardy

In the determination of the Cabibbo-Kobayashi-Maskawa (CKM) matrix element V_{ud} from superallowed Fermi beta decay, a crucial requirement is the application of nuclear-structure-dependent theoretical corrections. True, these corrections are small – of the order of 1% or less – but their evaluation is subject to some uncertainty. One of the most important of these corrections is the isospin-symmetry-breaking correction, δ_C, which is wholly nuclear-structure dependent. It is defined as

$$M_F^2 = M_0^2 \, (1 - \delta_C) \,, \tag{1}$$

where M_F is the Fermi matrix element and M_0 is its value in the isospin-symmetry limit. The most widely used calculations of δ_C are those of Towner and Hardy (TH) [1] but those calculations have recently been criticized by Miller and Schwenk (MS) [2], who claim that they are based on a formally incorrect interpretation of the isospin operator. Although MS claim that this "incorrect" usage must have led to incorrect results for δ_C, they do not produce any "exact" calculations with which to compare. Instead they proceed to make significant model-dependent assumptions of their own, from which they conclude – without numerical results – that the omissions from TH must be significant in magnitude. In our opinion, their model is considerably less sophisticated than ours and has not been independently corroborated by experimental data as ours has. Thus, if there is indeed any omission in the TH corrections, there is currently no valid estimate of the importance of that omission.

For now, the best that can be done to validate any set of calculated corrections is to test their efficacy in achieving agreement with the basic tenets of weak-interaction theory, particularly the conserved vector current (CVC) hypothesis, but also the unitarity of the CKM matrix. It is in tests such as these that the TH calculations perform astonishingly well, strongly suggesting that the putative omissions, if any, must have a negligible effect.

A variety of different models have been used in the past for the isospin-symmetry-breaking correction. They are:

- **Shell model – Saxon-Woods (SM-SW)**. This is the model of TH, in which proton and neutron radial functions are taken as eigenfunctions of a Saxon-Woods potential whose parameters are adjusted to match experimental separation energies.
- **Shell model – Hartree-Fock (SM-HF)**. This is similar to SM-SW except that the radial functions are taken to be eigenfunctions of a mean-field Skyrme-Hartree-Fock potential. First proposed by Ormand and Brown [3], their protocol was recently altered by Hardy and Towner [4] to ensure that the proton mean field had the asymptotically correct form.
- **Hartree-Fock -- Random Phase Approximation (HF-RPA).** A Skyrme-Hartree-Fock calculation is performed for the even-even A-body system (the decaying state when $T_Z = -1$,

the daughter state when $T_Z = 0$). The odd-odd nucleus is then treated as a particle-hole excitation built on the even-even Hartree-Fock state. The particle-hole spectrum is computed in the RPA with charge-dependent interactions. First calculations of this type were performed by Sagawa, van Giai and Suzuki [5]. Recently, they were extended by Liang, van Giai and Meng [6] who replaced Skyrme zero-range interactions by finite-range meson-exchange potentials. They performed relativistic Hartree-Fock (RHF-RPA) calculations and relativistic Hartree-only (RH-RPA) calculations with density-dependent meson-nucleon couplings and non-local interactions.

- **Isovector Monopole Resonance (IVMR).** A particle-hole picture was also envisaged by Auerbach [7] in which isospin-symmetry breaking in the parent and daughter states of beta decay is attributed to the difference in their couplings to the giant isovector monopole resonance. To obtain numerical estimates, Auerbach appealed to a number of "gross" models discussed in ref [8]. Each model enabled him to obtain a simple expression for δ_C as a function of the mass number A. As an example, his expression in the microscopic model is

$$\delta_C = 18.0 \text{ X } 10^{-7} A^{5/3}. \tag{2}$$

- **Damgaard Model.** First estimates of δ_C were provided by Damgaard [9], who expanded the proton radial function in terms of a complete set of neutron oscillator functions. The set comprises states of the same orbital angular momentum, ℓ, but differing in the number of radial nodes, n. Most of the mixing was with the state with one more radial node. Attributing this mixing to the Coulomb force, Damgaard derived

$$\delta_C = 0.2645 \, Z^2 \, A^{-2/3} (n + 1)(n + \ell + 3/2), \tag{3}$$

which exhibits a general behavior $\delta_C \, \alpha \, A^{4/3}$ with some shell structure superimposed through the choice of oscillator quantum numbers n and ℓ. In particular, a proton radial function with one radial node gets a factor of two enhancement in its δ_C value over that with no radial nodes, simply from the factor $(n+1)$ in Eq. (3). Such factors are absent in the formulae of Auerbach [7].

The computation of isospin-symmetry breaking in Fermi beta decay is patently model dependent. So on what grounds can one assert that one model is better than another? The usual way forward in such situations is to appeal to experiment, but in this case experiment does not directly measure the correction δ_C. However, experiment has led to precise values for the *ft* values of a large number of superallowed transitions – 13 in all – and, if we assume that both CKM unitarity and CVC are satisfied, we can convert those experimental ft values into experimental values for δ_C and compare the results with each calculation in turn. To be more specific, the application of our two assumptions is described as follows:

- *The conserved vector current (CVC) hypothesis is correct.* Under this hypothesis, the corrected Ft values in superallowed Fermi beta decay must be the same for all nuclei with the same isospin assignment. The relation between the corrected Ft value and the experimental ft value is

$$Ft = ft\,(1 + \delta_R)\,(1 - \delta_C)\,, \tag{4}$$

where δ_R is the nucleus-dependent part of the radiative correction and δ_C is the isospin-symmetry-breaking correction. To date, 13 nuclei ranging from ^{10}C to ^{74}Rb have superallowed transitions with ft values measured to an accuracy of $\pm0.4\%$ or better. Thus we can obtain an "experimental" value of δ_C from the relation

$$(1 - \delta_C) = [Ft]_{av}\,/\{ft(1+\delta_R)\} \tag{5}$$

using ft values from the most recent data survey [4] and the calculated radiative corrections ($\delta_R = \delta_R{}'\; + \delta_{NS}$) from ref. [1]. The value we use for $[Ft]_{av}$ follows from our second assumption.

- *The CKM matrix is unitary.* The sum of the squares of the top-row elements of the matrix is assumed to be exactly equal to one. The value of V_{us} obtained from the analysis of kaon-decay data, 0.22521(94) [10], and V_{ub} from the Particle Data Group, 0.00393(36) [11], are also assumed to be correct. Under these conditions the value of $|V_{ud}|^2$ is given by:

$$|V_{ud}|^2 = 1 - |V_{us}|^2 - |V_{ub}|^2 = 0.94927 \pm 0.00042\,. \tag{6}$$

Further, $|V_{ud}|^2$ is inversely proportional to $[Ft]_{av}$, the average corrected ft value. Consequently we can write

$$[Ft]_{av} = (2915.64 \pm 1.08)/\,|V_{ud}|^2 = 3071.47 \pm 1.78\ \text{s}\,, \tag{7}$$

the value we use in evaluating Eq. (5).

Thus, we have a set of "experimental" δ_C values, compared to which the various theoretical calculations can be assessed. In Fig. 1 we plot these "experimental" δ_C values as points with error bars, together with theoretical values from the different models available. The success of each model can be

judged by the quality of the fit. To quantify this we evaluate the χ^2 per degree of freedom using the equation

$$\frac{\chi^2}{\nu} = \sum_{i=1}^{N} w_i (\delta_C^{theo}(i) - \delta_C^{expt}(i))^2 / (N-1) \tag{8}$$

where N is the number of cases computed with a particular theory (*e.g.* the authors of HF-RPA only compute δ_C for 9 of the 13 cases). The weights, w_i, are taken to be $1/\sigma_i^2$, where σ_i is the standard
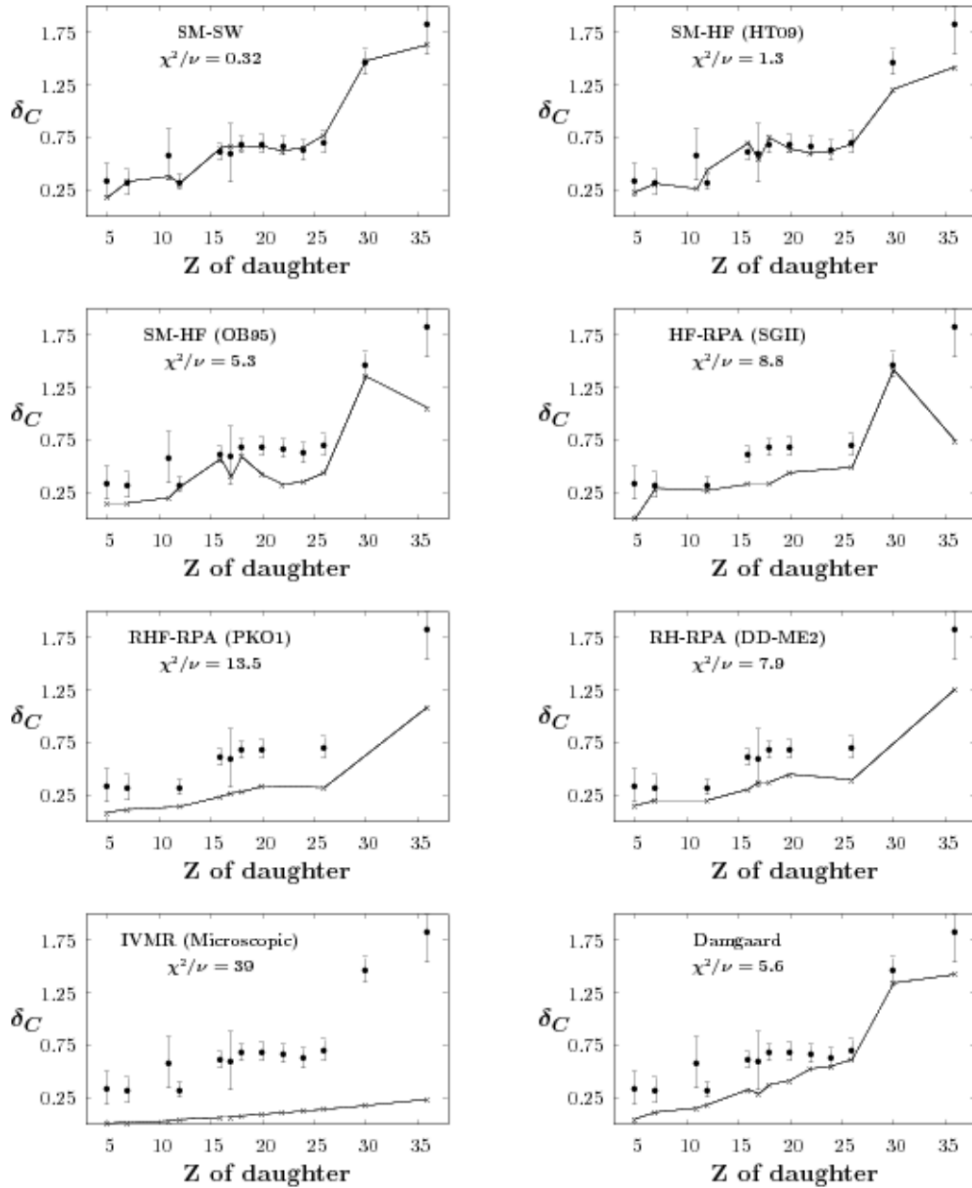
FIG. 1. Isospin-symmetry breaking correction, δ_C, in percent units as a function of the charge number, Z, for the daughter nucleus. "Experimental" values of δ_C (points with error bars) are those required of the theory if the experimental data is to satisfy the CVC hypothesis and the unitarity of the CKM matrix. The references for each calculation are as follows: SM-SW [1], SM-HF (HT09) [4], SM-HF (OB95) [3], HF-RPA (SGII) [5], RHF-RPA (PK01) [6], RH-RPA (DD-ME2) [6], IVMR (Microscopic) [7,8], Damgaard [9].

deviation assigned to the "experimental" δ_C value. It is clear from the figure that the best agreement comes from the shell model, with Saxon-Woods radial functions doing better than Hartree-Fock radial functions. The HF-RPA and IVMR particle-hole models are generally under-predicting the correction, particularly in the heavier nuclei.

Obviously, if superallowed beta decay is to continue to be used to test the unitarity of the CKM matrix, one has to accept the possibility that the "true" correction terms might lead to $\mathcal{F}t$ values that do not satisfy the unitarity condition. However, if they lead to $\mathcal{F}t$ values that change from transition to transition – thus violating CVC – one would not even be justified in extracting a value for V_{ud} at all, let alone using that value to test CKM unitarity. In judging the results of Fig. 1 in that context, we might consider that the most definitive test of the isospin-symmetry-breaking corrections is whether they fit the variations in the "experimental" values from one Z value to another as required by CVC, irrespective of a possible overall additive constant, which would be the effect of a violation of CKM unitarity. Using this criterion, the shell-model results remain the best, but the RHF-RPA (PK01) model ranks as a close second.

With no numerical calculations to check, the Miller and Schwenk claims [2] cannot be tested at all, but with respect to the many models that actually can be checked, the shell-model calculations of Towner and Hardy [1, 4] stand up very well.

[1] I.S. Towner and J.C. Hardy, Phys. Rev. C **77**, 025501 (2008).
[2] G.A. Miller and A. Schwenk, Phys. Rev. C **78**, 035501 (2008).
[3] W.E. Ormand and B.A. Brown, Phys. Rev. C **52**, 2455 (1995); W.E. Ormand and B.A. Brown, Phys. Rev. Lett. **62**, 866 (1989); W.E. Ormand and B.A. Brown, Nucl. Phys. **A440**, 274 (1985).
[4] J.C. Hardy and I.S. Towner, Phys. Rev. C **79**, 055502 (2009).
[5] H. Sagawa, N. Van Giai, and T. Suzuki, Phys. Rev. C **53**, 2163 (1996).
[6] H. Liang, N. Van Giai, and J. Meng, Phys. Rev. C **79**, 064316 (2009).
[7] N. Auerbach, Phys. Rev. C **79**, 035502 (2009).
[8] N. Auerbach, Phys. Rep. **98**, 273 (1983).
[9] J. Damgaard, Nucl. Phys. **A130**, 233 (1969).
[10] FlaviaNet Kaon working group, arXiv:0801.1817 [hep-ph] (2008), as updatedin 2009.
[11] C. Amsler *et al*. [Particle Data Group] Phys. Lett. B **667**, 1 (2008) and partial update for the 2010 edition.

Transition density and pressure in hot neutron stars

J. Xu, L. W. Chen,[1] C. M. Ko, and B. A. Li[2]

[1]*Department of Physics, Shanghai Jiao Tong University, Shanghai and Center of Theoretical Nuclear Physics, National Laboratory of Heavy Ion Accelerator, Lanzhou, China*

[2]*Department of physics and Astronomy, Texas A&M University-Commerce, Commerce, Texas*

Using the momentum-dependent MDI interaction we have studied the transition density and pressure at the boundary that separates the liquid core from the inner crust of neutron stars. Both the neutrino-trapped matter and the neutrino-free matter at finite temperatures [1], which are expected to exist during the early evolution of neutron stars, have been considered. In particular, we have investigated the effect of nuclear symmetry energy by varying the parameter x in the MDI interaction from 1 to -1, corresponding to the values $15<L<106$ MeV for the slope of the nuclear symmetry energy at normal density that have been constrained by both the isospin diffusion data [2-4] and other experimental observables [5]. We have found that both the transition density and pressure are larger in the neutrino-trapped matter than in the neutrino-free matter. Furthermore, both are found to roughly decrease with increasing temperature and L for both the neutrino-trapped and the neutrino-free matter as shown in the left window of Fig.1, except that the transition pressure shows a complicated relation to the temperature for the neutrino-trapped matter as shown in the right window of Fig. 1. Also, negative values of the pressure at the transition density have been obtained, which can be used to rule out a very stiff symmetry
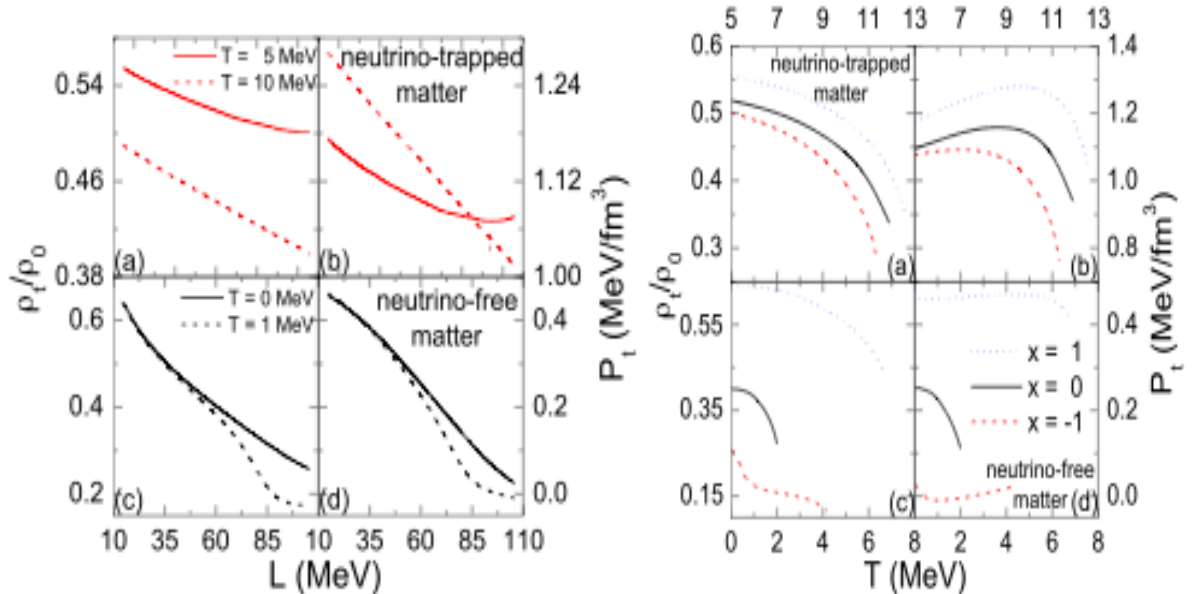
FIG. 1. Transition densities ρ_t ((a) and (c)) and pressure P_t ((b) and (d)) as functions of the slope parameter L of the nuclear symmetry energy at different temperatures (left window) and as functions of temperature for different nuclear symmetry energy parameter x (right window) in both the neutrino-trapped matter ((a) and (b)) and the neutrino-free matter ((c) and (d)).

energy at subsaturation densities. We have also studied the critical temperature above which the inner crust described by the so-called nuclear pasta phase cannot be formed in newly born neutron stars and found that it depends sensitively on the density dependence of the nuclear symmetry energy at subsaturation densities.

[1] J. Xu, L.W. Chen, C.M Ko, and B.A. Li, Phys. Rev. C (in press); arXiv:1003.3695 [nucl-th].

[2] M.B. Tsang *et al.*, Phys. Rev. Lett. **92**, 062701 (2004).

[3] L.W. Chen, C.M. Ko, and B.A. Li, Phys. Rev. Lett. **94**, 032701 (2005); Phys. Rev. C **72**, 064309 (2005).

[4] B.A. Li and L.W. Chen, Phys. Rev. C **72**, 064611 (2005).

[5] D.V. Shetty and S.J. Yennello, arXiv:1002.0313 [nucl-ex].

Isospin-dependent pion in-medium effects on charged pion ratio in heavy ion collisions

J. Xu, C. M. Ko, and Y. Oh[*]

We have studied [1] the dependence of the pion spectral function in asymmetric nuclear matter on the charge of the pion by using results from the chiral perturbation theory for the pion-nucleon s-wave interaction [2] and from the Δ-hole model for the pion-nucleon p-wave interaction [3,4]. Because of increasing π^- and decreasing π^+ in-medium masses due to the pion-nucleon s-wave interaction in neutron-rich matter, the strength of π^+ spectral function at low energies is somewhat larger than that of π^- spectral function, and the strength around the peak of the Δ resonance mass distribution decreases while that near the threshold increases with increasing charge of the Δ resonance. In a thermal model that assumes that nucleons, pions, and Δ resonances produced in heavy ion collisions are in thermal but not chemical equilibrium, with the latter needed to maintain the final pion to nucleon ratio, the π^-/π^+ ratio is slightly reduced in comparison with the case without pion in-medium effects. As shown in Fig. 1, this is the case for all values of nuclear symmetry energy parameter x=0, 0.5, and 1, corresponding to increasingly softer nuclear symmetry energy at high densities, and of the Migdal parameter g' that describes the repulsive Δ-hole interaction. Taking into consideration of the isospin-dependent pion in-medium effects in the transport model thus will have some, albeit not very significant, influence on the extraction of the nuclear symmetry energy from the measured π^-/π^+ ratio of about 3, which is also shown in Fig.1 with a large error bar, by the FOPI Collaboration [5]. Further theoretical work is needed to understand the relation between
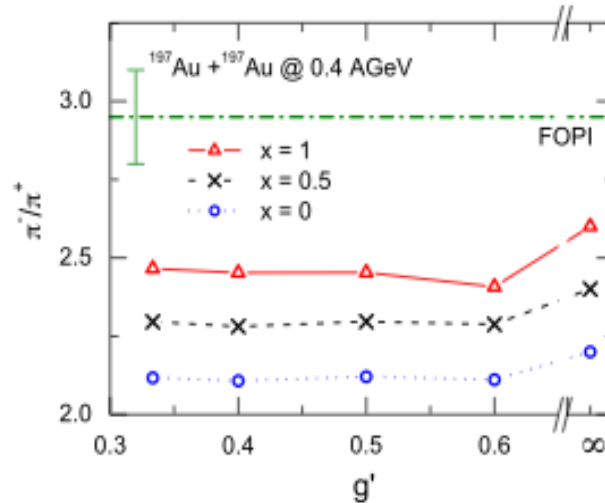
FIG. 1. The π^-/π^+ ratio in Au+Au collisions at the beam energy of 0.4 AGeV for different values of nuclear symmetry energy (x=0, 0.5, and 1) and the Migdal parameter g'=0.3, 0.4, 0.5, and 0.6. Results for g'=∞ correspond to the case without the pion medium effects.

[*] Present address: School of Physics and Energy Sciences, Kyungpook National University, Daegu, Korea

the π^-/π^+ ratio and the behavior of the nuclear symmetry energy at high densities in the transport model description of heavy ion collisions.

[1] J. Xu, C.M. Ko, and Y. Oh, Phys. Rev. C **81**, 024910 (2010).

[2] N. Kaiser and W. Weise, Phys. Lett. B **512**, 283 (2001).

[3] G.E. Brown and W. Weise, Phys. Rep. **22**, 279 (1975).

[4] C.M. Ko, L.H. Xia, and P.J. Siemens, Phys. Lett. B **231**, 16 (1989).

[5] W. Reisdorf *et al.* (FOPI collaboration), Nucl. Phys. **A781**, 459 (2007).

Isospin- and momentum-dependent effective interactions for the baryon octet and the properties of hybrid stars

J. Xu, L. W. Chen,[1] C. M. Ko, and B. A. Li[2]

[1]_Department of Physics, Shanghai Jiao Tong University, Shanghai and Center of Theoretical Nuclear Physics, National Laboratory of Heavy Ion Accelerator, Lanzhou, China_

[2]_Department of physics and Astronomy, Texas A&M University-Commerce, Commerce, Texas_

We have extended the momentum-dependent interaction (MDI) for the nucleon-nucleon effective interaction in nuclear medium [1] to include the nucleon-hyperon and hyperon-hyperon interactions by assuming that they have the same density and momentum dependence as that for the nucleon-nucleon interaction [2]. The parameters in this extended MDI interaction (MDI-Hyp) were determined by fitting the empirical hyperon single-particle potentials in symmetric nuclear matter at its saturation density. As an example for the application of the extended MDI interaction, we have investigated the properties of hybrid stars that include not only the hyperon degrees of freedom but also those of quarks by taking into account the phase transition between the hadron and quark phases. Our results indicate that the extended MDI interaction can give a reasonable description of the properties of hypernuclear matter. We have also found that the equation of state (EOS) of hypernuclear matter is much softer than that of pure nuclear matter and that it becomes even softer if the hadron-quark phase transition is included. The masses and
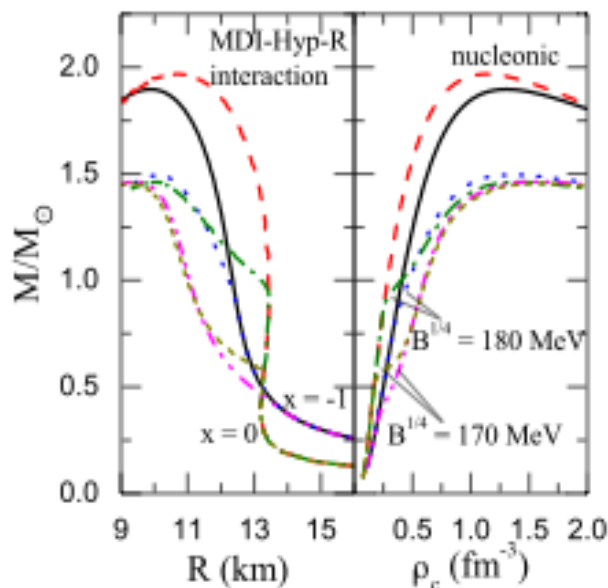
FIG. 1. The hybrid star mass as a function of radius (left panel) and central density (right panel) in the presence of the hadron-quark phase transition. Results from the MDI-Hyp-R interaction for the hadron phase with $x=0$ and $x=-1$ and the MIT bag model for the quark phase with $B^{1/4}$=180 MeV and 170 MeV are shown for comparison. Results from a pure nucleonic approach are also displayed.

radii of hybrid stars have also been studied with these EOSs, and they were found to remain reasonable after including hyperons and the hadron-quark phase transition as shown in Fig. 1 for a repulsive ΣN interaction (MDI-Hyp-R) and for both a soft (x=0) or a stiff (x=-1) nuclear symmetry energies as well as for different values for the bag constant B. We have further studied the effects of using attractive and repulsive ΣN interactions and different symmetry energies on the hybrid star properties. The results show that the appearance of the Σ hyperon in hybrid stars depends sensitively on the sign of the ΣN interaction with a repulsive ΣN interaction giving a higher critical density for the appearance of Σ hyperons. In addition, a stiffer symmetry energy usually leads to a larger fraction of hyperons in the hypernuclear matter. We have further found that both the low-density boundary of the hadron-quark phase transition and the EOS at high densities in hybrid stars are more sensitive to the bag constant than to the stiffness of the nuclear symmetry energy at high densities. This extended MDI interaction will also be very useful in transport models that simulate heavy-ion reactions in future radioactive beam facilities, particularly at the FAIR/GSI energies.

[1] C.B. Das, S. Das Gupta, C. Gale, and B.A. Li, Phys. Rev. C **67**, 034611 (2003).
[2] J. Xu, L.W. Chen, C.M. Ko, and B.A. Li, arXiv:1001.2239 [nucl-th].

Transport model study of deuteron production in relativistic heavy ion collisions

Y. Oh,[*] C. M. Ko, and Z.W. Lin[1]

[1]*Physics Department, East Carolina University, Greenville, North Carolina*

The hadronic transport model ART [1] has been extended to include the production and annihilation of deuterons via the reactions $BB \leftrightarrow dM$ involving baryons and mesons as well as their elastic scattering in the hadronic matter. With initial hadron distributions taken from a blast wave model with parameters such as the initial temperature as well as the transverse flow velocity and anisotropy fitted to reproduce the measured transverse momentum spectra and elliptic flows of protons, the transverse momentum spectrum and elliptic flow of deuterons produced in relativistic heavy ion collisions have been investigated [2]. As shown in Fig. 1, the resulting transverse momentum spectrum of deuterons from the transport model is comparable to, although somewhat softer than, the experimentally measured one.
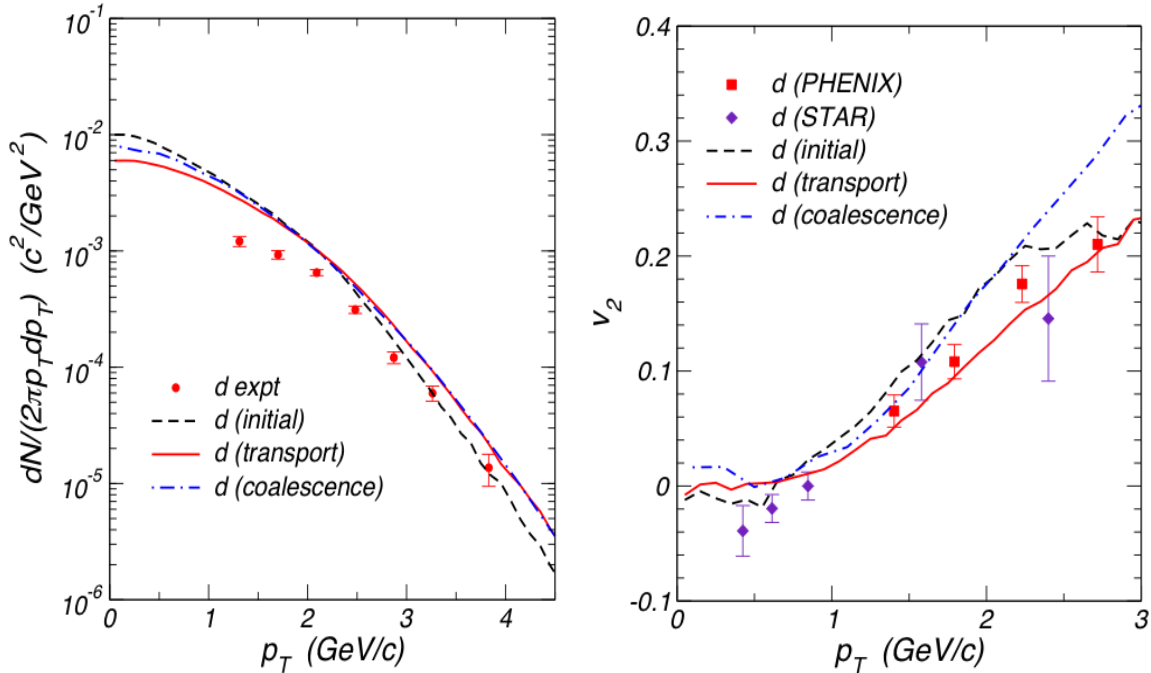
FIG. 1. Transverse momentum spectra (left window) and elliptic flow (right window) of protons and deuterons in minimum biased Au+Au collisions at $s_{NN}^{1/2} = 200$ GeV.

The deuteron elliptic flow from the transport model also agrees reasonably with that measured by the PHENIX Collaboration [3] but is found to be positive at small transverse momenta in contrary to the

---

[*] Present address: School of Physics and Energy Sciences, Kyungpook National University, Daegu 702-701, Korea.

negative values observed by the STAR Collaboration [4]. These results have been compared with those from the coalescence model [5] using the freeze-out proton and neutron distributions from the transport model, which are also shown in Fig. 1. While the two give very similar deuteron transverse momentum spectra, the elliptic flows obtained in the two models are different, particularly at high transverse momenta. In addition, the coalescence model is found to give almost exact nucleon number scaling of the elliptic flow, while the elliptic flow from the transport model shows a deviation from this scaling behavior, although it is closer to the measured data. Part of the difference between the results from the two models may be due to the neglect of rescattering of deuterons produced in the coalescence model. Although deuterons are produced from freeze-out nucleons in the coalescence model, they may undergo additional scattering in the hadronic matter, leading to a delayed emission time as results from the transport model have shown. In the transport model, a negative deuteron elliptic flow is possible if the final radial flow velocity is smaller than that reached in the present study. Whether this can still lead to a good description of the measured deuteron transverse momentum spectrum needs to be checked. Further investigations both in theory and experiment are thus required to understand the elliptic flow of deuterons at low transverse momenta and to shed more light on the mechanisms for the production of low transverse momentum hadrons in relativistic heavy ion collisions.

[1] B.A. Li and C.M. Ko, Phys. Rev. C **52**, 2037 (1995).
[2] H. Liu *et al.* (STAR Collaboration), J. Phys. G **34**, S1087 (2007).
[3] S. Afanasiev *et al.* (PHENIX Collaboration,), Phys. Rev. Lett. **98**, 162301 (2007).
[4] Y. Oh, Z.W. Lin, and C.M. Ko, Phys. Rev. C **80**, 064902 (2009).
[5] Y. Oh and C.M. Ko, Phys. Rev. C **76**, 054910 (2007).

Density slope of nuclear symmetry energy from a novel correlation analysis

L. W. Chen,[1] C. M. Ko, B. A. Li,[2] and J. Xu

1_Department of Physics, Shanghai Jiao Tong University, Shanghai and Center of Theoretical Nuclear Physics, National Laboratory of Heavy Ion Accelerator, Lanzhou, , China_

2_Department of physics and Astronomy, Texas A&M University-Commerce, Commerce, Texas_

Expressing explicitly the Skyrme interaction parameters in terms of the macroscopic properties of asymmetric nuclear matter, we have found in the Skyrme-Hartree-Fock approach that unambiguous correlations exist between observables of finite nuclei such as the neutron skin thickness Δr_{np} and nuclear matter properties such as the nuclear symmetry energy $E_{sym}(\rho_0)$ and its slope L at saturation density [1]. Combining constraints on $E_{sym}(\rho_0)$ and L from the application of this novel correlation analysis to existing data on the neutron skin thickness of Sn isotopes [2,3] with those from recent analyses of isospin diffusion and double neutron/proton ratio [4] in heavy ion collisions at intermediate energies leads to a value of $L=58\pm18$ MeV, approximately independent of $E_{sym}(\rho_0)$, as shown by the shaded region in the $E_{sym}(\rho_0)$-L plane shown in Fig. 1. Using this constrained value of L, we have evaluated the transition density ρ_t and pressure P_t at the boundary of the liquid core and inner crust in a neutron star following the dynamic method of Ref.[5]. The resulting values of $\rho_t=0.069\pm0.017$ fm^{-3}, shown in the left panel of Fig.1, and $P_t=0.322\pm0.2.2$ MeV/fm^3 agree with the empirical ones [6], This value of L has also allowed us to
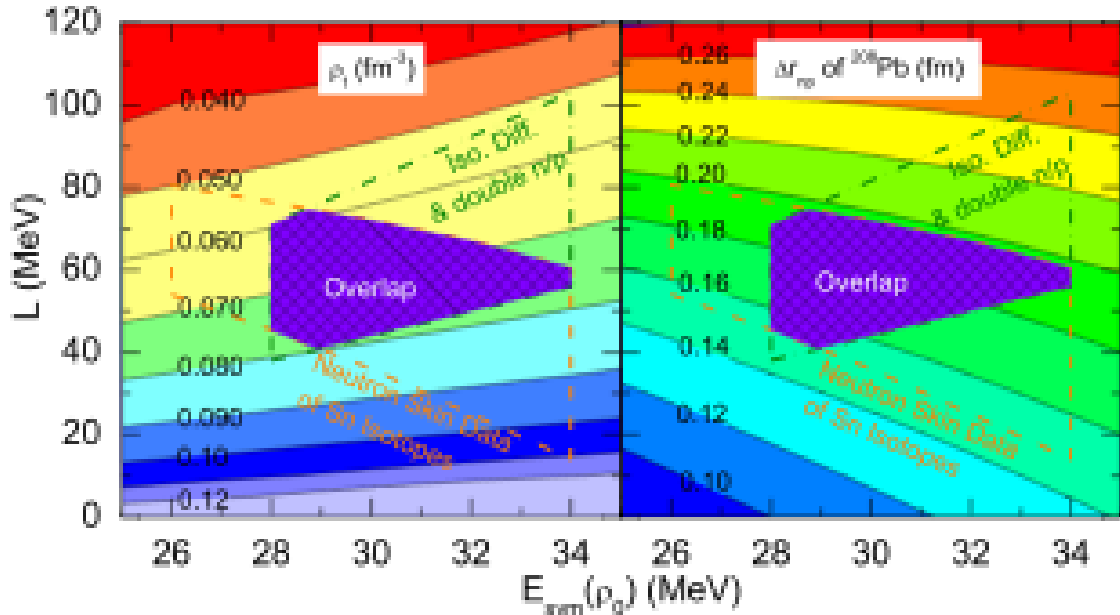
FIG. 1. Contour curves in the $E_{sym}(\rho_0)$-L plane for the core-crust transition density ρ_t (left panel) and the neuteron skin thickness Δr_{np} of ^{208}Pb (right panel) from Skyrme-Hartree-Fock calculation with MSL0. The shaded region represents the overlap of constraints obtained in the present work (dashed lines) and that from Ref.[4] (dash-dotted lines).

constrain the neutron skin thickness of ^{208}Pb to a narrow region of 0.175±0.02 fm as shown in the right panel of Fig. 1. and this is consistent with other constraints from various experiments [7] but with a much smaller uncertainty.

[1] L.W. Chen, C.M Ko, B.A. Li, and J. Xu, arXiv:1004.4672 [nucl-th].
[2] A. Klimkiewicz *et al.*, Phys. Rev. C **76**, 051603 (R) (2007).
[3] S. Terashima *et al.*, Phys. Rev. C **77**, 024317 (2008).
[4] M.B. Tsang *et al.*, Phys. Rev. Lett. **102**, 122701 (2009).
[5] J. Xu, L.W. Chen, B.A. Li and H.R. Ma, Phys. Rev. C **75**, 014607 (2007).
[6] J.M. Lattimer and M. Prakash, Science **304**, 536 (2004); Phys. Rep. **442**, 109 (2007).
[7] B.A. Li, L.W. Chen, and C.M. Ko, Phys. Rep. **464**, 113 (2008).

Charmonia in medium: from euclidean to minkowski time

X. Zhao and R. Rapp

Charmonia are valuable probes of hot and dense matter as created in heavy-ion collisions (HICs) because (i) they are bound states of charm quarks which are exclusively produced in primordial hard collisions; (ii) they have large binding energies so that their dissolution is expected only at rather high temperatures. Further studies [1] have shown that primordial production, followed by various phases of dissociation (direct component), should be complemented by the inverse processes in which open-charm states coalesce into charmonia (regeneration component). An important quantity controlling the strengths of these competing mechanisms is the charmonium binding energy, ε_B. E.g., for $J/\Psi+g\leftrightarrow c+\bar{c}$, a larger ε_B reduces the initial-state phase space for dissociation while increasing the final-state phase space for the reverse process of coalescence.

In this work [2] we calculate the production of charmonia in HICs with their binding energies extracted from a T-matrix approach [3] which utilizes input potentials from lattice QCD (lQCD). Specifically, we study limiting cases of strong- and weak-binding scenarios representing the use of the internal and free energy as the heavy-quark potential, respectively. The latter also determines the in-medium HQ mass, $m_c(T)=m_c^0+ V(r\rightarrow\infty;T)/2$, via its non-zero asymptotic value. With $\varepsilon_B(T)$ and $m_c(T)$
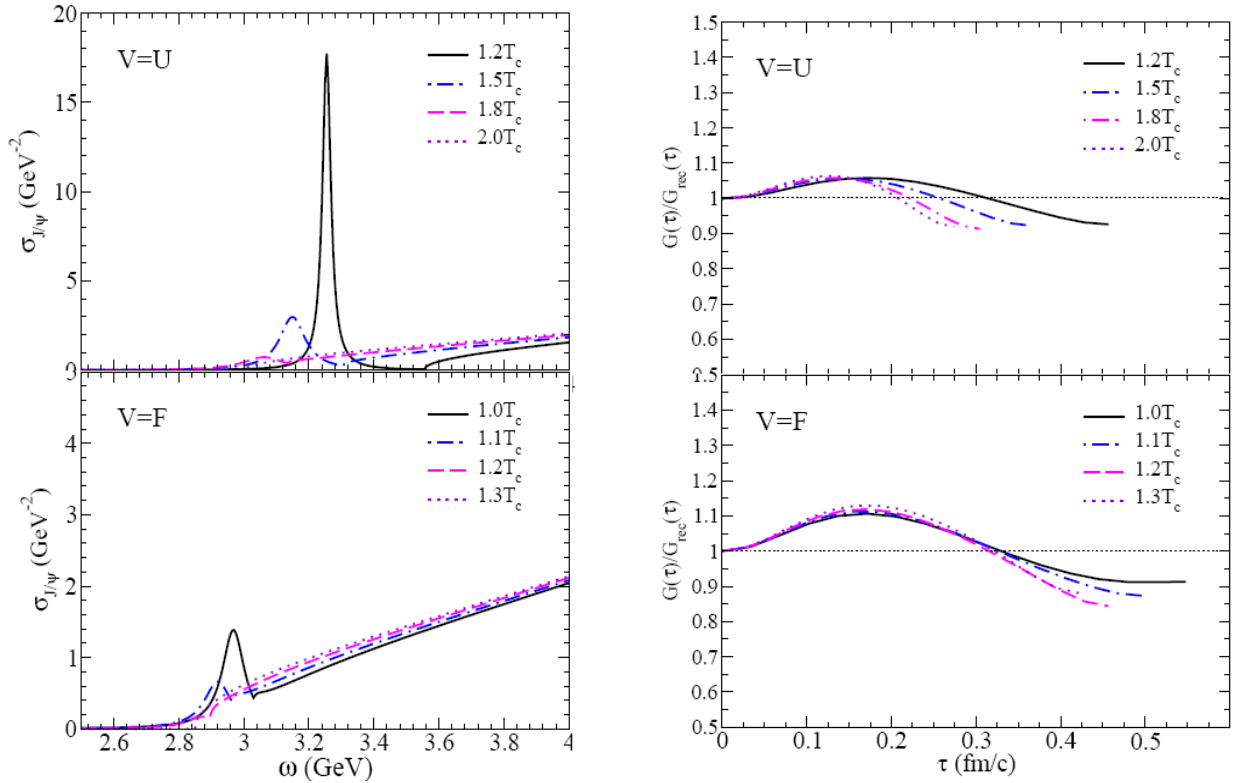
FIG. 1. Left panel: S-wave charmonium spectral functions in the strong (V=U) and weak (V=F) binding scenarios. Right panel: Corresponding correlation functions (normalized to the vacuum one) in euclidean time, τ. Current lattice QCD data suggest the ratio $(G(\tau)/ G_{rec}(\tau))$ to be close to 1 up to ~$3T_c$ [5].

fixed we calculate charmonium dissociation rates in "quasi-free" approximation [4].

Using the binding-energies, widths and charm-quark masses we calculate charmonium spectral functions and euclidean-time correlators (see Fig. 1). In both scenarios, the latter show variations at the 10% level, which is consistent with current lQCD computations.

Next we implement the binding energies, dissociation rates and quark masses into a thermal rate equation [1, 6] to calculate charmonium production in heavy-ion collisions. We also introduce a thermal relaxation time for charm quarks which controls the magnitude of the regeneration yield.
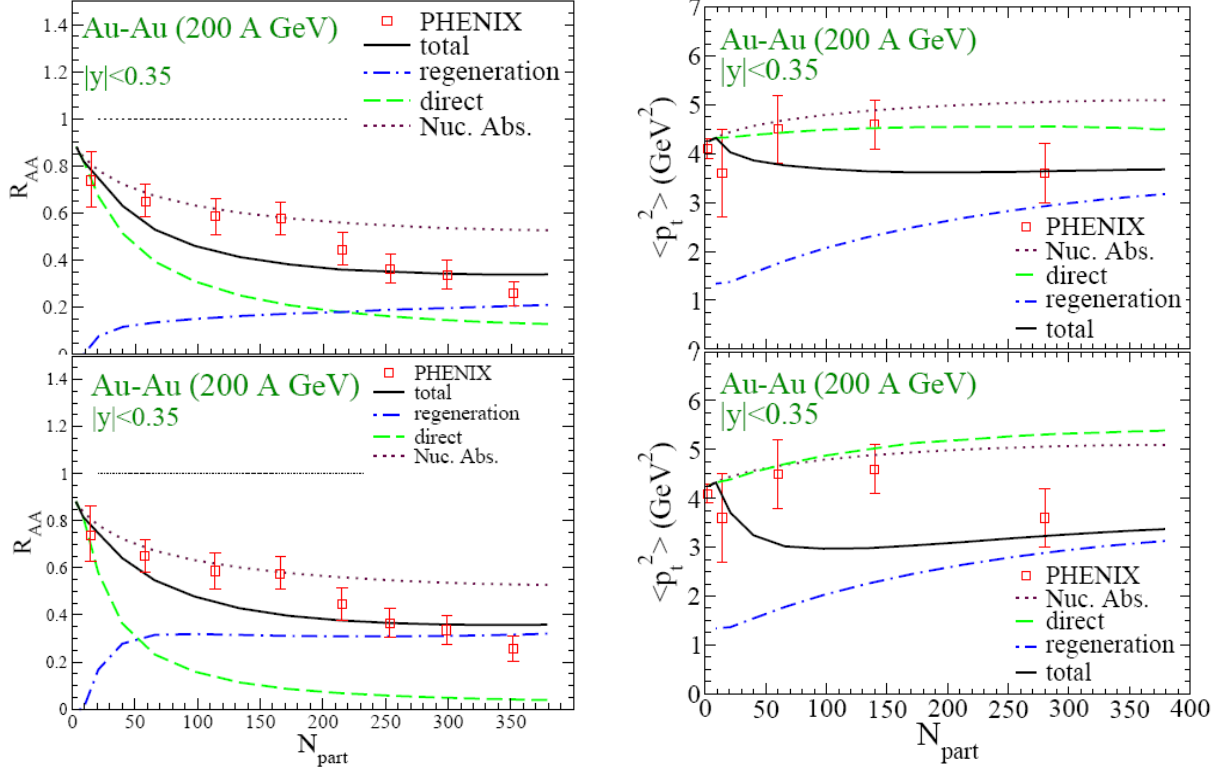
FIG. 2. Left panels: Centrality dependence of the nuclear modification factor (R_{AA}) for J/Ψ at RHIC compared to PHENIX data [7]. Right panels: Centrality dependence of $<p_t^2>$ of J/Ψ compared to PHENIX data [7]. Upper panels: strong binding scenario. Lower panels: weak binding scenario.

The numerical results at RHIC energy are compared to the experimental data in Fig. 2. We find that within the current uncertainty of charm-quark thermalization times, both strong- and weak-binding scenarios can reproduce the measured yields of J/Ψ's. However, the relative partition of direct and regeneration components is rather different in the two scenarios. For central Au-Au collisions, the strong-binding scenario predicts a sizable contribution of primordially produced charmonia while in the weak-binding scenario they are almost entirely suppressed. To better discriminate the two scenarios we calculate the transverse-momentum (p_t) spectra of J/Ψ, and plot their average $<p_t^2>$ in the right panels of Fig. 2. The regenerated J/Ψ's are characterized by softer spectra than the primordial ones. The strong-binding scenario, with a larger direct component, tends to reproduce the data better than the weak-binding scenario. The current uncertainty in the experimental data prevents definitive conclusions but our

calculations show that p_t spectra are of crucial importance to disentangle in-medium production mechanisms of charmonia in heavy-ion collisions, and thus to extract properties of the Quark-Gluon Plasma.

[1] L. Grandchamp, G.E. Brown and R. Rapp, Phys. Rev. Lett. **92**, 212301 (2004).

[2] X. Zhao and R. Rapp, in preparation.

[3] F. Riek and R. Rapp, arXiv:1005.0769.

[4] L. Grandchamp and R. Rapp, Phys. Lett. B **523**, 60 (2001).

[5] S. Datta *et al.,* Phys. Rev. D **69**, 094507 (2004).

[6] X. Zhao and R. Rapp, Phys. Lett. B **664**, 253 (2008).

[7] A. Adare *et al.* (PHENIX Collaboration), Phys. Rev. Lett. **98**, 232301 (2007).

Medium modifications of the ρ meson in nuclear photoproduction

F. Riek, R. Rapp, Y. Oh, and T.-S. H. Lee

The restoration of the spontaneously broken chiral symmetry in QCD implies that the spectral functions of hadrons are modified at high temperatures and density, especially when approaching the chiral phase transition [1]. Precursor effects are expected to occur already in more dilute hadronic matter. Dilepton decays of vector mesons are particularly suitable observables since the leptons do not suffer strong final-state interaction and thus carry the invariant-mass information of the parent particle at its moment of decay to the detector. The CLAS collaboration at Jefferson Lab has recently measured dilepton spectra in photoproduction off nuclear targets [2], reporting a moderate broadening of the ρ-meson spectral function for iron targets relative to deuterium. In Ref. [3] we conducted an initial analysis of these data by combining a model for the ρ production amplitude on the nucleon [4] with an in-medium ρ spectral function which has been successfully used in the interpretation of dilepton spectra in heavy-ion collisions [1]. With a simplified (average) treatment of the nuclear density profile, a reasonable agreement with the experimental dilepton invariant-mass spectra emerged. Here [5], we have improved and expanded on this work in several respects, by (a) folding the ρ-decay distribution over a realistic nuclear density profile (rather than using an average density), (b) accounting for the 3-momentum and density dependence of the decay rate, and (c) evaluating additional observables to better discriminate medium effects, including low-momentum cuts, the nuclear-mass (A) dependence and the so-called nuclear transparency ratio. It turns out that item (a) further improves the description of the measured mass spectra, reducing, e.g., the χ^2/N value for Fe targets from 1.29 in Ref. [3] to 1.05. The dependence of the mass spectra on the dilepton 3-momentum, q, is illustrated in Fig. 1 for uranium targets, indicating an appreciable increase in medium

FIG. 1. 3-momentum dependence of dilepton invariant-mass spectra from decays of ρ mesons produced in photoproduction off uranium.

effects at low q: slow ρ mesons stay longer in the nuclear volume (enhancing the fraction of in-medium decays) and the medium effects in the ρ spectral function increase at small q. The width increase of the ρ in the medium implies stronger absorption on nuclear targets relative to a single free nucleon, which is quantified in terms of the nuclear transparency ratio, T_A, in Fig. 2. We predict a 40% reduction in the dilepton yield from ρ -mesons for heavy target nuclei.

FIG. 2. Nuclear transparency ratio for $\rho \to e^- e^+$ decays, characterizing the survival probability relative to the production on a free nucleon.

[1] R. Rapp, J. Wambach and H. van Hees, Landolt Börnstein, New Series I/23-A (2010), in press.

[2] M.H. Wood *et al.* (CLAS Collaboration), Phys. Rev. C **78**, 015201 (2008).

[3] F. Riek, R. Rapp, T.-S.H. Lee, and Y. Oh, Phys. Lett. B **677**, 116 (2009).

[4] Y. Oh and T.-S.H. Lee, Phys. Rev. C **69**, 025201 (2004).

[5] F. Riek, R. Rapp, Y. Oh and T.-S.H. Lee, LANL arXiv:1003.0910 [nucl-th]; Phys. Rev. C (submitted).

Nonperturbative heavy-quark interactions in the QGP

F. Riek and R. Rapp

The properties of heavy quarkonia (charmonium and bottomonium) have long been recognized as a useful messenger of quark deconfinement in the Quark-Gluon Plasma (QGP) [1]. More recently, open heavy-flavor particles are utilized to extract transport properties of the QGP by computing their diffusion coefficient [1]. Both phenomena may be closely related [2,3]. The key connection is the large heavy-quark mass, m_Q, implying that for both quarkonia and individual heavy quarks the interactions are dominantly elastic with 3-momentum transfer dominating over energy transfer. This suggests that a potential-type picture is valid, at least for not too large temperatures and densities of the heat bath, T, μ_q $<< m_Q$. If so, formidable simplifications in the theoretical description arise, allowing for more accurate predictions.

In the present work [2,3], we start from a relativistic Bethe-Salpeter equation which can be simplified into a 3-dimensional Lippmann-Schwinger equation by reducing the energy-transfer variable. A partial-wave expansion yields a 1-D integral equation for the thermodynamic T-matrix, $T = V + VG_2T$, where the input consists of the driving kernel (potential), V, and the intermediate 2-particle propagator, G_2, in the medium. Model-independent guidance for the in-medium potential can be extracted from finite-temperature lattice QCD (lQCD) calculations where the free energy of a heavy quark-antiquark pair is computed with good precision. In the vacuum this quantity coincides with the well-established phenomenological Cornell potential. As a first application of our approach, we use this potential to compute the vacuum spectrum [3]. Fixing the bare heavy-quark mass at $m^0_{c,b} \sim 1.3, 4.7$ GeV and the constituent light-quark mass at $m_q = 0.45$ GeV, the empirical quarkonium and heavy-light meson spectra can be reproduced within an accuracy of ~0.1 GeV, which is comparable to the neglected hyperfine splittings (spin-spin interactions). In the medium a currently unresolved ambiguity arises as to whether the free (F) or internal energy (U) should be used as potential ($F=U-TS$; S: entropy). In Fig. 1 we
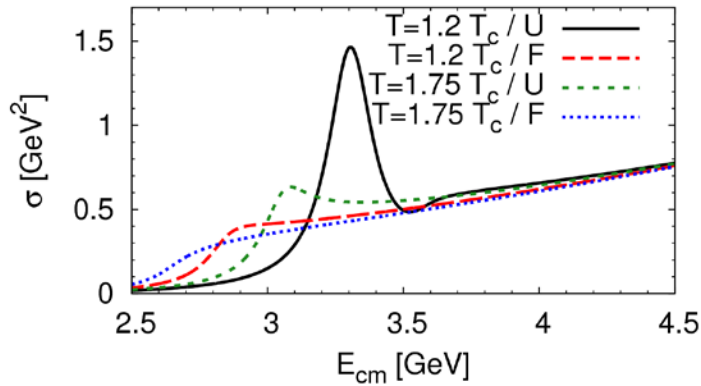
FIG. 1. Charmonium spectral functions calculated using either the internal (U) or the free energy (F).

summarize our results for the in-medium quarkonium spectral functions [3] for both choices and a quark width of 100 MeV (figuring into G_2). The spectral functions turn out to be quite different for the 2 potentials: for F, the ground-state charmonium dissolves at a temperature of ~1.2 T_c (T_c ~190MeV: critical temperature), compared to ~1.7 T_c for U. The results can be checked by calculating the corresponding correlator ratios in euclidean time and comparing them to lQCD results. For the latter only small variations around one (ca. 10 % at $T=2T_c$) have been found [4,5]. Surprisingly, this behavior is consistent with both our calculations, i.e. using U or F as potential (see Fig. 2): the rapid melting occurring for F is balanced by a smaller in-medium charm-quark mass. Within the same T-matrix approach, we can calculate heavy-quark transport properties. It turns out that the stronger interaction provided by U leads to a factor of ~2-3 faster thermalization time than for F.
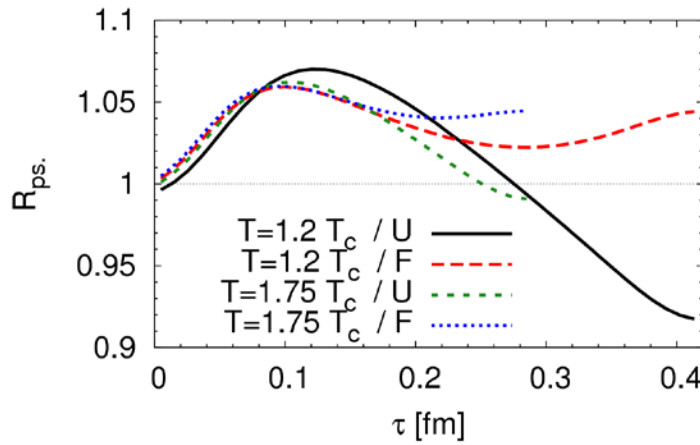
FIG. 2. Euclidian correlator ratios corresponding to the spectral functions shown in Fig. 1.

[1] R. Rapp and H. van Hees, in *Quark-Gluon Plasma 4*, edited by R.C. Hwa and X.N. Wang, (World Scientific, Singapore, 2010), p. 111.

[2] R. Rapp, F. Riek, H. van Hees, V. Greco and M. Mannarelli, Nucl. Phys. **A830**, 861c (2009).

[3] F. Riek and R. Rapp, LANL eprint arXiv:1005.0769 [hep-ph].

[4] A. Jakovac *et al.*, Phys. Rev. D **75**, 014506 (2007).

[5] G. Aarts *et al.*, Phys. Rev. D **76**, 094513 (2007).

Precision studies of dilepton spectra in heavy-ion collisions

R. Rapp

The spontaneous breaking of chiral symmetry (SBCS) in the QCD vacuum is believed to be at the origin of more than 95% of the visible mass in the Universe. The underlying mechanism is intimately related to the formation of zero-temperature condensates. Unlike the Higgs condensate in electroweak interactions, the QCD condensates are composites of quark and gluons, most notably the scalar quark-antiquark condensate. However, the condensates themselves are not physical observables, and thus information about the ground-state structure has to be deduced from its excitations. In the present context the latter are nothing but the hadronic spectrum. In particular, chiral multiplets (e.g. $\pi(140)$-$\sigma(500)$, $\rho(770)$-a1(1260) or N(940)-N*(1535)) exhibit a massive ($\Delta M{\sim}0.5$GeV) splitting corroborating the notion of SBCS. At finite temperatures and baryon densities the condensates are expected to melt giving rise to a chiral phase transition in hot/dense QCD matter. Clearly, such phase changes must be accompanied by a major reshaping (chiral restoration) of the hadron spectrum as we know it in the vacuum.

Three decades of high-energy heavy-ion collision experiments have demonstrated that hot and dense QCD matter close to equilibrium can be created and studied in these reactions. Dilepton invariant-mass spectra are the only known observable to directly extract information on the spectral modifications of hadrons, specifically vector mesons through their exclusive decays $V \to e^{+}e^{-}$ ($V=\rho,\omega,\phi$) [1]. The ρ meson is of particular interest since it dominates the dilepton emission rate in thermal equilibrium. Its vacuum line shape has been predicted to undergo a strong broadening in hot and dense hadronic matter [2], leading to a "melting" of the resonance ($\Gamma_\rho \to m_\rho$) close to the expected phase transition temperature of $T_c \sim 180$MeV, cf. left panel of Fig. 1. These predictions can now be tested quantitatively with the
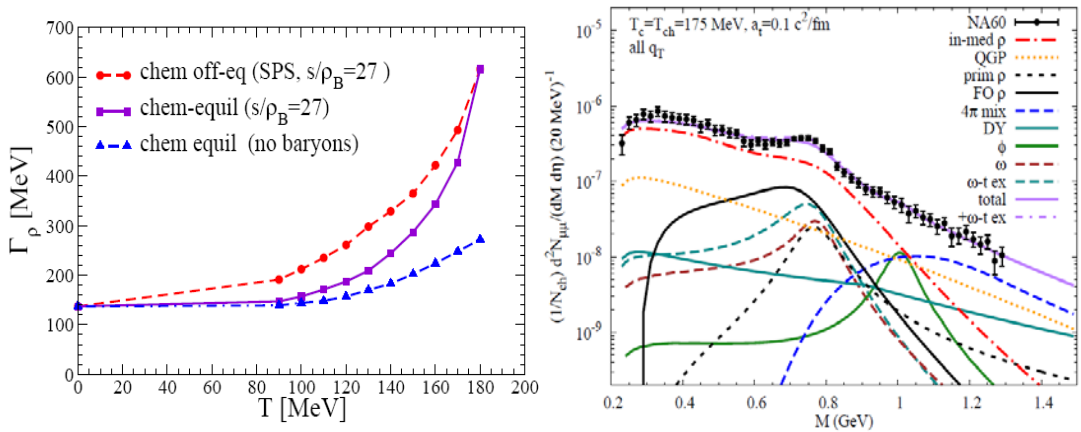
FIG. 1. Left panel: In-medium ρ-meson width as a function of temperature under CERN-SPS conditions (i.e., the baryon density increases with T as well) [1,2]. Right panel: Predictions for dilepton emission from a thermal fireball (plus "non-thermal" sources) [4], compared to fully acceptance-corrected NA60 dimuon data [3] in semi-central 158 AGeV In-In collisions.

newest fully acceptance-corrected dimuon spectra measured by NA60 in In-In collisions at the CERN-SPS [3], cf. right panel of Fig. 1. Note that since the mass spectra are invariant, details of the modeling of the medium expansion in the heavy-ion reaction do not matter. Therefore, the shape of the data directly reflects the theoretical thermal emission rate at the input level (which is basically given by the thermal Bose factor times the in-medium ρ spectral function). The quantitative agreement of the theory predictions [1,4] with the NA60 data allows to extract a (time-) average in-medium ρ width of $\Gamma_\rho = 350$-400 MeV, realized at an average temperature of about T~150-160MeV (with a baryon density close to that of normal nuclear matter). This necessarily implies contributions from higher temperatures and densities where the ρ width is indeed approaching its mass. The behavior of the ρ-width toward "T_c" may be closely related to the well-known Hagedorn limit of the hadron resonance gas which was one of the first arguments for the existence of a phase transition in hot hadronic matter. Schematically, the ρ-width may be written as $\Gamma_\rho^{med} \sim \Sigma_h \, \sigma_{\rho h} \, n_h \, v_{rel}$, where the summation is over all hadrons, h, with their respective densities in the medium. If the ρ-h cross section is finite, a divergence of the total hadron density (Hagedorn catastrophe) implies the divergence of the in-medium ρ width [1].

The theory comparisons to NA60 data enable further insights into the medium produced in heavy-ion collisions.The combined analysis of invariant-mass and transverse-momentum (q_t) spectra in the mass region of the narrow vector resonances ω and ϕ reveals a sequential freezeout pattern. The relatively soft q_t spectra of the ϕ require its kinetic decoupling close to the critical temperature which, in turn, is consistent with the (near) absence of an in-medium ϕ contribution in the dimuon excess spectra (right panel of Fig. 1 around M~1.02 GeV). The ω is inferred to decouple somewhat later, at a temperature of about 150MeV. On the contrary, the main emission yield driven by the in-medium ρ decays requires a significantly lower freezeout at about T~130MeV. This, in turn, enables a determination of the total lifetime of the interacting fireball in In-In collision at unprecedented accuracy, $\tau_{FB} = 6.5 \pm 1$fm/c.

Current applications of this framework to (less accurate) dilepton data at RHIC indicate marked discrepancies for central Au-Au collision in the mass region around 0.3GeV. Whether this requires a new production mechanisms (e.g. a disoriented chiral condensate due to supercooling through the chiral phase transition) is one of the exciting open question at this point.

[1] R. Rapp, J. Wambach and H. van Hees, Landolt-Börnstein, New Series I/23-A, 4-1 (2010).

[2] R. Rapp and J. Wambach, Eur. Phys. J. A **6**, 415 (1999).

[3] R. Arnaldi *et al.* (NA60 Collaboration) Phys. Rev. Lett. **100**, 022302 (2008); Eur. Phys. J. C **61**, 711 (2009).

[4] H. van Hees and R. Rapp, Nucl. Phys. **A806**, 339 (2008).

The initial state of high energy nuclear collisions

R. J. Fries and G. Chen

The initial state of nuclear collisions at very high energies is thought to be a phase of QCD called the Color Glass Condensate (CGC). A key problem in our understanding of relativistic heavy ion collisions is the question how this color glass evolves into a thermalized plasma of quarks and gluons (QGP).

We have continued our work on the evolution of the energy momentum tensor at early times in a heavy ion collisions. Previously, we had derived an expansion of the classical gluon field around the time of collision (t=0) in the color glass condensate model for fixed color sources ρ_i in the colliding nuclei. In order to compare with observables one needs to calculate the expectation value of those results under variations of the sources ρ_i. This comes about because the nuclei are on average color neutral even locally, $<\rho_i>=0$. However, during the collision, which happens on time scales much faster than the time needed to reorder degrees of freedom inside the nucleus, the actual sources are "snapshots" of fluctuations frozen during the very short time of interaction.

The expectation values can be reduced to evaluations of n-point correlation functions of gluon fields and covariant derivatives inside a single nucleus, $<A(x)A(y)...>$ etc., within the McLerran-Venugopalan framework. We have computed a hierarchy of correlation functions which allows us to express the energy momentum tensor at early times in a simple series which only depends on the coupling constant and the saturation scales of the two nuclei. This energy momentum tensor can be used as input for a further hydrodynamic evolution of the fireball.

Multiple scattering in nuclear matter

R. J. Fries and R. Rodriguez

The larger goal of this project is the description of multiple scattering in nuclei by means of perturbative quantum chromodynamics (QCD). This is strictly possible only for some simple processes, like deep-inelastic scattering on nuclei, the Drell-Yan process in nuclei, etc. On the other hand many results of hard probes in nucleus-nucleus collisions at the Relativistic Heavy Ion Collider (RHIC), lie beyond a strict perturbative description, even though they involve large momentum transfer. They can only be explained by modeling certain aspects of the collision. Hard probes in nuclear collisions at high energies, i.e. hadrons or jets with energies of several GeV and above, are important probes for the quark gluon plasma phase created in these collisions, and a better understanding of their propagation through hot nuclear matter is of great importance.

In the past year we have worked on a phenomenological front end to simulate hard probes in nuclear collisions at high energy. This software package propagates either single quarks and gluons or correlated pairs of quarks, gluons and photons through a background fireball, which is treated as a flexible input to the simulation. Several models of energy loss and several options for fragmenting quarks and gluons into hadrons have been implemented so far. Modules to calculate standard observables in heavy ion physics, e.g. single and di-hadron nuclear suppression factors, di-hadron correlation functions, azimuthal asymmetry coefficients v_2, etc., have been included.

This software package will be used for systematic studies of hard probes, some of which are reported on elsewhere. We are particularly interested in comparisons between different energy loss models, consistency checks between them, and systematic studies of how we can learn about the underlying fireball by using hard probes.

Event-by-event jet quenching

R. J. Fries, R. Rodriguez, and E. Ramirez

We investigate the role that realistic fluctuations and inhomogeneities of the fireball in nuclear collisions have on hard probes. State of the art calculations of jet quenching usually use parameterizations of an expected "average", smooth fireball. However, we know that in reality fluctuations of the positions of the nucleons inside the nuclei and fluctuations of the nucleon-nucleon cross section can lead to very inhomogeneous fireballs.

In this study we used the recently developed jet quenching software package, reported on elsewhere here. We compare observables for single hadron suppression, di-hadron correlation functions and elliptic flow for two different scenarios. In the first scenario we propagate quarks and gluons through a smooth fireball, which is created by averaging over 500,000 events created by GLISSANDO, a simulation of initial nucleus-nucleus interactions using Glauber scattering [1]. In the second scenario we propagate the hard probes through individual Glissando events and then take an average over events afterwards, which is a better reflection of the situation in heavy-ion experiments. We use several different energy loss models for this study.

We find that comparison of data to calculations from smooth fireballs lead us to overestimate the average value of the transport coefficient qhat by as much 50%. In other words, if we take the point of view that we do not want to bias the results by choosing a particular size for the fluctuations, this introduces an additional 50% uncertainty on the extraction of qhat from data.

We find that after readjusting qhat we can easily fit the momentum and centrality dependence of single hadron suppression data from the Relativistic Heavy Ion Collider (RHIC). However, a residual deviation remains for both elliptic flow and hadron correlations, opening the possibility to distinguish different fluctuations strengths and therefore to conduct something close to a true spatial tomography of the fireball.

[1] W. Broniowski, M. Rybczynski, and P. Bozek, Comp. Phys. Comm. **180**, 69 (2009).

SECTION IV

ATOMIC, MOLECULAR
AND MATERIALS SCIENCE

A system for 3D momentum imaging of molecular dissociation induced by fast, heavy-ion collisions

R. L. Watson and V. Horvat

The development of detector systems with both fast timing and two-dimensional position determination capabilities has generated new interest in the excitation of molecules by photons, electrons and ions. In experimental investigations of dissociation processes leading to the formation of charged product ions, it is now possible to measure the three-dimensional vector momentum of each ion with high resolution and efficiency. This is accomplished by coupling together large diameter microchannel plate detectors with multi-array delay-line anodes [1].

During the past year, we have designed and constructed a system for recoil-ion momentum spectroscopy of molecular dissociation induced by fast heavy-ion collisions. A schematic diagram of this system is shown in Fig. 1.
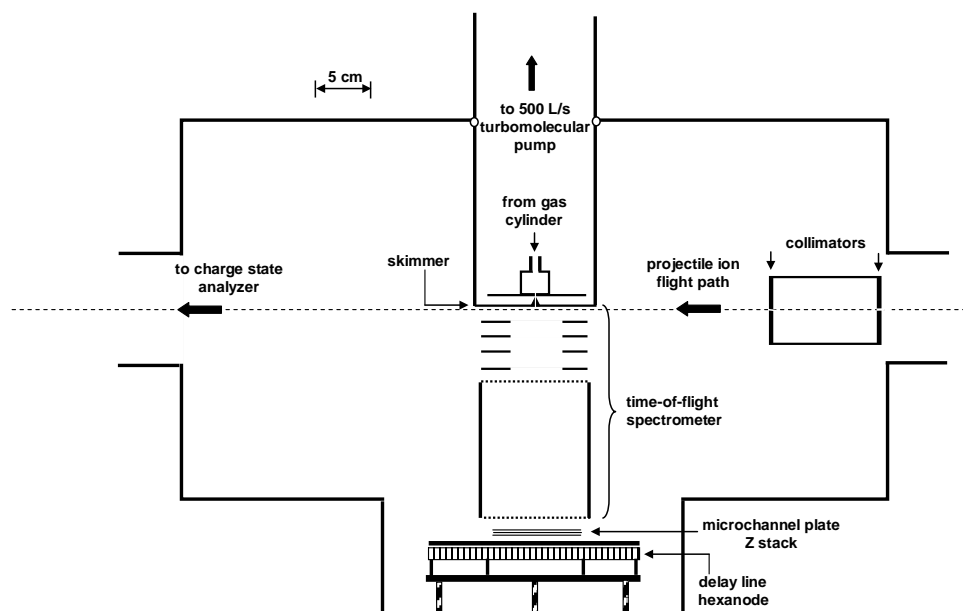
FIG. 1. A schematic diagram of the system for recoil-ion momentum spectroscopy of molecular dissociation induced by heavy-ion collisions.

A target gas jet is crossed with the heavy-ion beam in the interaction region. Charged fragments produced in collisions between heavy ions and gas molecules are accelerated by a uniform electric field into a time-of-flight (TOF) spectrometer and impact the surface of a triple set (Z-stack) of resistance-matched, 80 mm diameter, microchannel plates generating fast timing signals for the TOF measurements. The localized electron jets emerging from the back of the Z-stack are projected onto three overlapping arrays of delay lines comprising the anode. Each delay-line array consists of a signal and reference wire pair. Hence, an ion impact generates six anode signals, and based on their relative timing, the two impact position coordinates of the ion (x and y) can be determined. The redundancy of position signals enables reliable analysis of simultaneous multi-hit events.

Target gas is fed through a small microchannel plate collimator having 10 μm diameter parallel channels onto a 0.89 mm diameter skimmer producing a gas jet of approximately 2 mm diameter in the interaction region. A 500 L/s turbomolecular pump maintains the vacuum in the gas chamber at 4×10^{-4} torr, while the main chamber is maintained at 1×10^{-6} torr by two 2400 L/s diffusion pumps. The acceleration region is formed by five parallel aluminum rings interconnected by 10.0 MΩ resistors that step the voltage on the top plate down to ground potential at the flight tube in equal increments. The length of the acceleration region is 61 mm and the length of the flight tube is 122 mm. These dimensions satisfy the Wiley-McLaren space focusing condition.

The heavy-ion beam is directed through a 250 μg/cm^2 Al stripper foil and the desired charge state is selected by means of a bending magnet. The charge-selected beam then passes through two 1 mm diameter collimators before interacting with the gas jet. It then passes on through a post-collision charge state analyzing magnet into a one-dimensional position sensitive microchannel plate detector or alternatively into a plastic scintillation detector, either of which provide fast timing signals for the TOF measurements.

Signals from the projectile detector, the Z-stack, and the anode lines proceed through fast amplifiers and constant fraction discriminators to an eight-channel, multi-hit time-to-digital converter (TDC) interfaced to a personal computer. The timing signal from the projectile detector provides the trigger for the TDC. The TDC measures the time relative to the trigger for all signals that arrive within a fixed time interval, which in the test run described below extended from 500 ns before the trigger to 6000 ns after the trigger. The event is stored if at least one Z-stack signal is present.

The system was tested by examining the dissociation of carbon monoxide molecular ions produced in collisions with 2.5 MeV/amu Xe^{35+} projectiles. In these measurements, the acceleration field was set to 24 V/mm and up to three charged molecular fragment hits per event were recorded. A two-dimensional TOF map for coincident ion pairs is shown in Fig. 2. The various islands in this figure contain coincident events for specific charge division pathways. For example, the most intense island near the top right corner of the figure contains events for the dissociation reaction $CO^{2+} \rightarrow C^+ + O^+$, and the island near the center of the figure contains events for the dissociation reaction $CO^{4+} \rightarrow C^{2+} + O^{2+}$. Analyzable data was obtained for molecular ion charges as high as 9+.
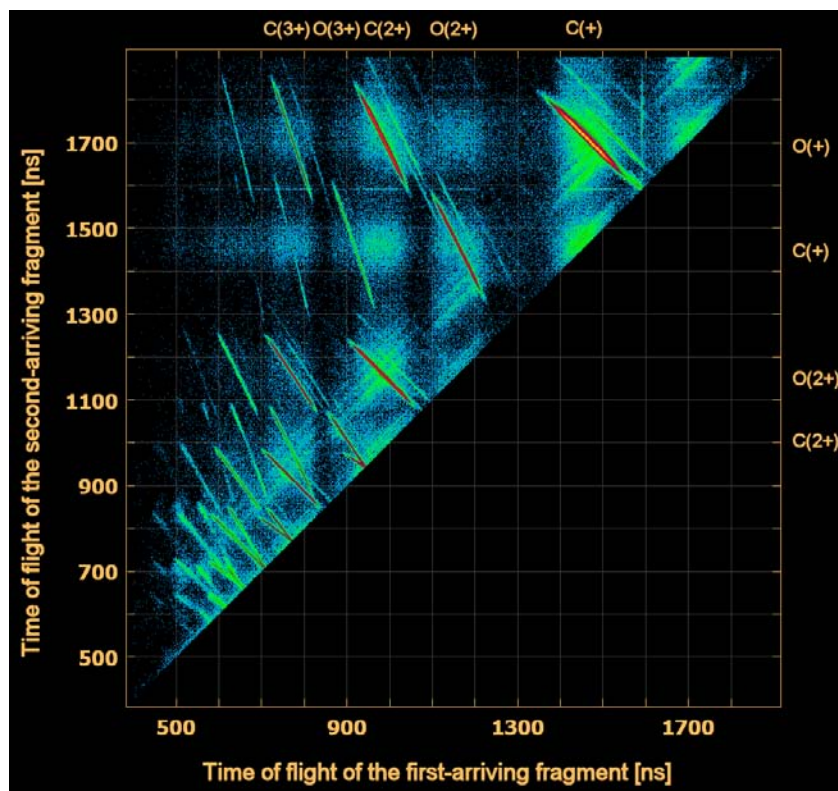
FIG. 2. Two-dimensional TOF map for the dissociation of CO molecular ions.
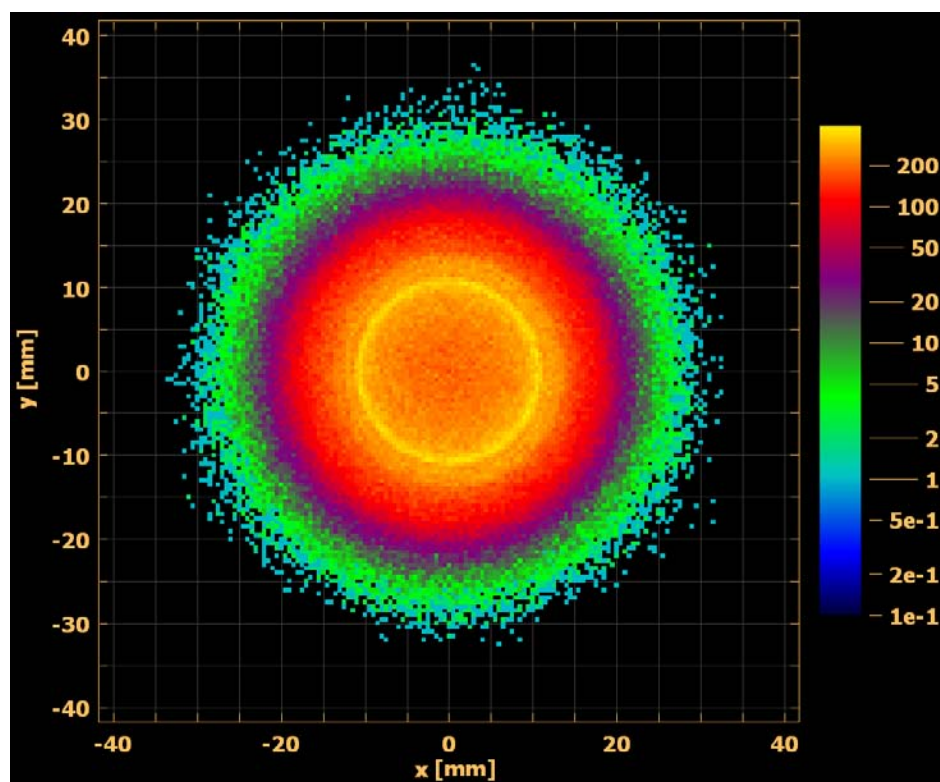
FIG. 3. Position distribution of O^+ ions in coincidence with C^+ ions.

The xy position distribution of O^+ ions detected in coincidence with C^+ ions is shown in Fig. 3. The position bin size is 0.5 mm $\times$ 0.5 mm and the coordinates are measured relative to the center of mass of the parent molecular ion. The rings that appear in this figure are caused by structure in the distribution of oxygen ion kinetic energies. Results of these measurements are presented in the report that follows this one.

[1] J. Ulrich, R. Moshammer, A. Dorn, R. Dorner, L. Schmidt, and H. Scmidt-Bocking, Rep. Prog. Phys. **66** (2003) 1463.

[2] http://www.roentdek.com

Momentum imaging of CO fragmentation products

V. Horvat and R. L. Watson

The breakup of CO molecular ions following multiple electron removal by 2.5 MeV/u Xe^{34+} ions has been studied by means of recoil-ion momentum spectroscopy (RIMS). At 2.5 MeV/u the projectiles travel the approximate length of a CO molecule (3 Angstroms) in only 14 attoseconds, which is much less than the typical time period for molecular rotations and vibrations. Consequently, the molecule remains essentially frozen in space during the interaction with the projectile. Since the interaction time is also much shorter than the typical fragmentation times of the ionized molecules (around 10 fs), the combined final kinetic energy of the molecular fragments formed in a specific breakup channel follows a distribution that reflects the range and relaxation patterns of molecular states excited in the collisions. The relative abundance of the events in each fragmentation channel provides information about the electronic rearrangement during molecular breakup and the total cross sections for multiple ionization of the molecule. The differential cross sections can be obtained from the distributions of molecular orientations at the time of collision.

RIMS is a powerful tool that provides the means for measuring all the quantities described above. They can be derived from the velocity vector components of every charged fragment created in the molecular dissociation event. These velocity components are, in turn, determined from the times of flight of the fragments and the positions of the fragments at the time they hit the detector. The complete set of variables for each ion is measured directly using a multi-hit, two-dimensional, delay-line detector equipped with a hexanode.

Charged fragment pairs originating from parent molecular ions with charge up to 9+ were identified and analyzed. Compared to previous measurements, the current data are significantly improved in terms of accuracy, resolution and overall counting statistics. Some preliminary results are illustrated in Figures 1-5.
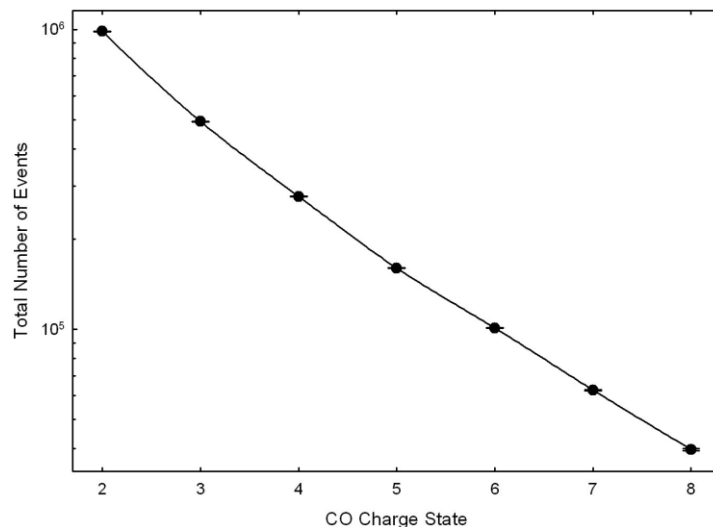
FIG. 1. Total measured number of CO molecular dissociation events as a function of the parent molecule's charge.

As shown in Fig. 1, the total measured number of CO molecular dissociation events is a monotonically decreasing function of the parent molecule's charge. A similar charge dependence was also found for the ionization of noble gas atoms, which indicates that collisions occur predominantly at large impact parameters, where the shape of the molecule and its charge distribution are not important. This is consistent with the direct ionization mechanism, which is expected (and experimentally verified) to be the dominant ionization process.
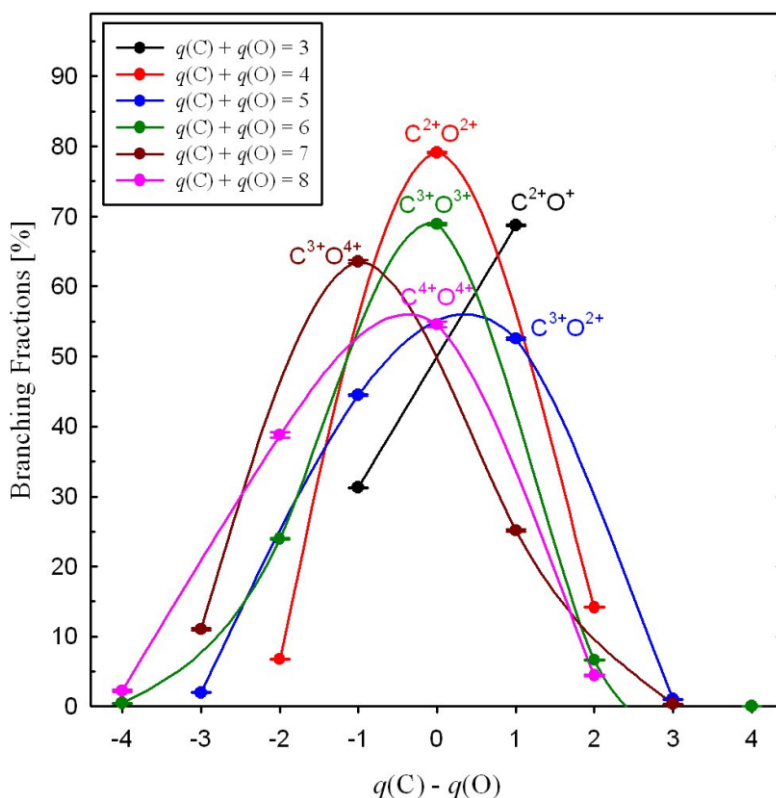
FIG. 2. Measured fractions of events in the dissociation channels originating from parent molecules having a given charge. The lines are drawn to guide the eye.

Fig. 2 shows the measured fractions of events in the dissociation channels originating from parent molecules having a given charge. It is evident that a symmetric division of charge between carbon and oxygen ions is preferred. On the other hand, for the closest dissociation channels with asymmetric charge division, it is found that carbon ions are more likely to have the higher charge when the parent molecule's charge is less than or equal to 5. The opposite is true when the parent molecule's charge is greater than 5. This effect is correlated with the total ionization energy of the molecular fragments in their final ground state. Namely, for the given combined charge of 4, 6, and 8, the total ionization energy is lowest when the fragments have equal charges. Also, the total ionization energy is lower for $C^{2+}O^+$, $C^{3+}O^+$, and $C^{3+}O^{2+}$, than for to C^+O^{2+}, C^+O^{3+}, and $C^{2+}O^{3+}$, respectively. For these combinations, the lower total ionization energy corresponds to the higher branching fraction. The same observation holds true for

some of the remaining dissociation channels ($C^{5+}O^+$ vs. C^+O^{5+}, $C^{5+}O^{2+}$ vs. $C^{2+}O^{5+}$, $C^{5+}O^{3+}$ vs. $C^{3+}O^{5+}$), but not for others ($C^{4+}O^+$ vs. C^+O^{4+}, $C^{4+}O^{2+}$ vs. $C^{2+}O^{4+}$, $C^{4+}O^{3+}$ vs. $C^{3+}O^{4+}$). The former group involves charge equal to 5 on the higher-charged fragment while the latter group involves charge 4. One possible explanation is that the latter group may be more affected by interatomic electron rearrangement in the early stages of dissociation.

The total kinetic energy release (KER) spectrum is shown in Figure 3 for the $CO^{2+} \rightarrow C^+ + O^+$ and $CO^{3+} \rightarrow C^{2+} + O^+$ dissociation channels. In the former case, the three well-resolved narrow peaks (the most prominent features in the spectrum) correspond to excitations of known metastable bound states of the CO^{2+} molecular ion [1]. The prominent narrow peak in the latter KER spectrum is likely to correspond to some metastable bound state in the CO^{3+} ion.
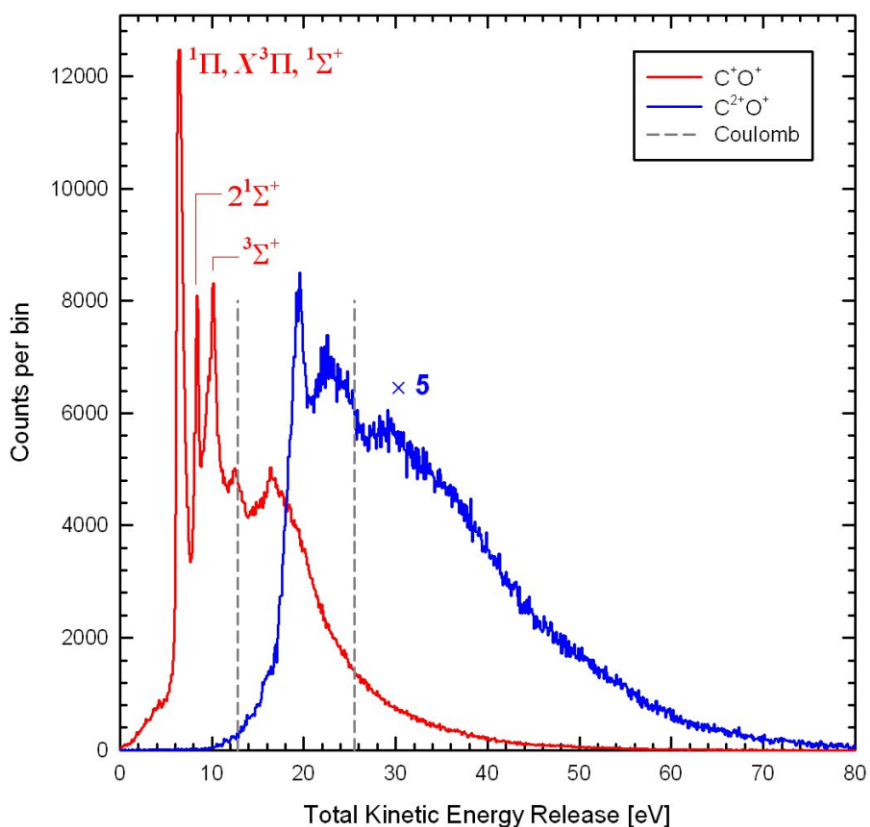
FIG. 3. Total kinetic energy release for C^+O^+ and $C^{2+}O^+$ pairs (red and blue lines, respectively). The vertical dashed gray lines indicate the KER's associated with pure Coulomb repulsion of the fragments initially separated by the CO equilibrium distance, assuming that they have non-overlapping spherical (or point-like) charge distributions.

The KER distributions for the breakup of the higher charged molecular ions, shown in Fig. 4, each display only a single broad asymmetric peak. A few of them also show additional partially
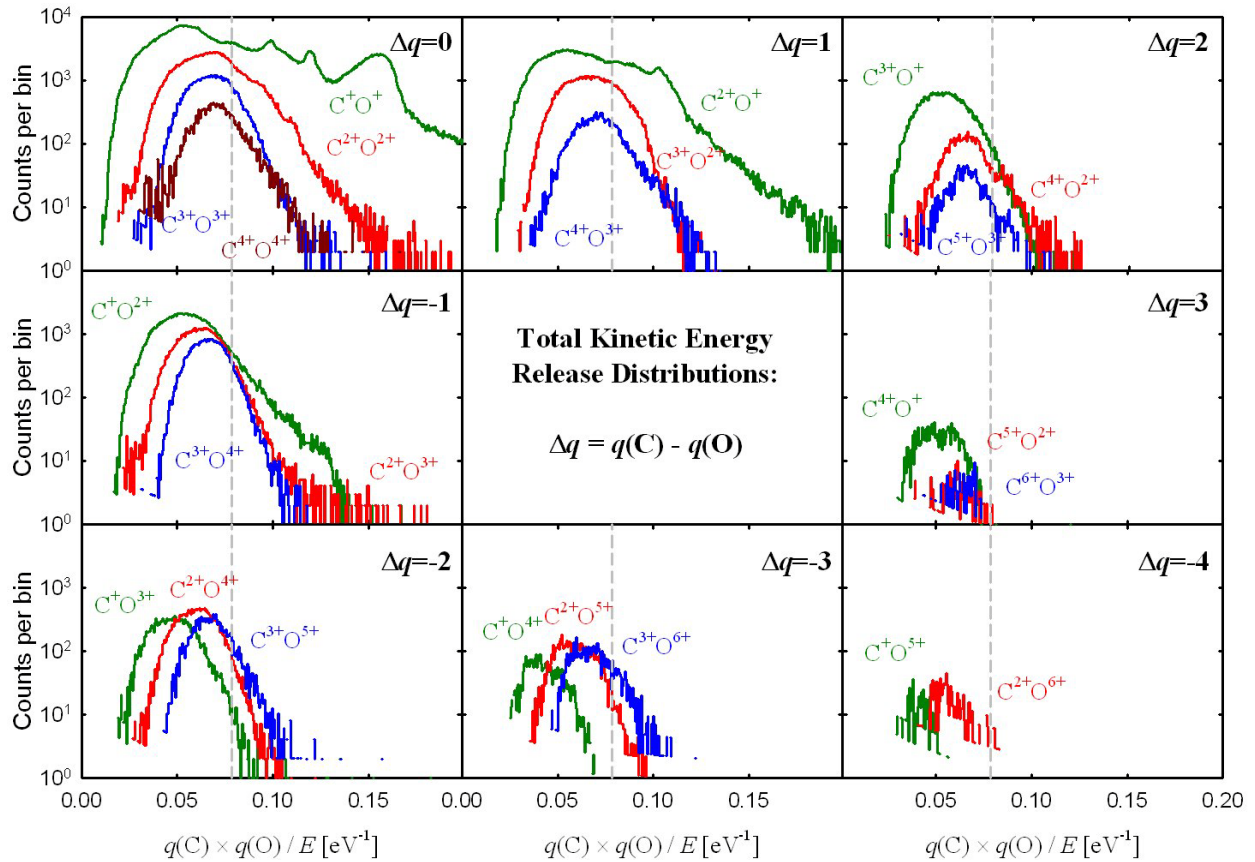
FIG. 4. Measured distributions of the total recoil-ion kinetic energy released (KER) in the breakup. The horizontal scale was chosen to condense the information to be conveyed and to provide a better match between the bin size and the counts per bin on one hand and the level of detail associated with the spectral features on the other hand. The vertical dashed gray line indicates the position of the point charge Coulomb explosion energy.

overlapping broader peaks. These broad peaks indicate the excitation of a wide range of repulsive states. It should be noted that all KER distributions were determined with a resolution of 1 eV (FWHM) or better.

The angular distributions, shown in Fig. 5, are essentially isotropic, except perhaps those for ion pairs originating from highly charged parent molecular ions, which tend to indicate a slight preference for emission perpendicular to the beam direction.
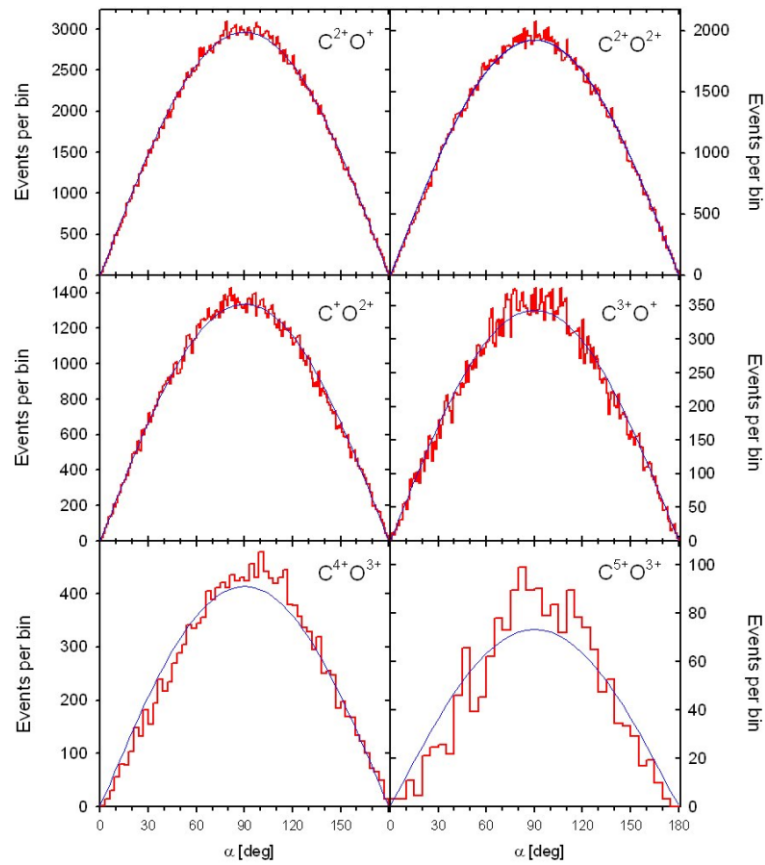
FIG. 5. Measured angular distributions for selected dissociation channels (red curve). α is the angle between the beam direction and the molecular axis at the time of collision. The thin blue line corresponds to an isotropic distribution.

[1] M. Lundqvist, P. Baltzer, D. Edvardsson, L. Karlsson, and B. Wannberg, Phys. Rev. Lett. **75**, 1058 (1995).

SECTION V

SUPERCONDUCTING CYCLOTRON, INSTRUMENTATION, AND RIB UPGRADE

K500 operations and development

D. P. May, G. J. Kim, H. L. Clark, and F. P. Abegglen

Introduction

During the 2009-2010 reporting period a total of 29 different beams, including 9 newly developed beams, were used for experiments, and there were a total of 43 beam tunings for these experiments. The SEE program will be treated separately.

Ion Sources

During the January shut-down ECR1 was opened for examination and cleaning. There had been no further deterioration in the damaged spot that had developed over a plasma flute on the aluminum wall. It had been noticed and compensated for in 2008.

Cyclotron Beams

New beams of ^{14}N at 18 AMeV, ^{24}Mg at 12 AMeV, ^{28}Si at 15 and 35 AmeV, ^{40}Ar at 5.4 and 5.6 AMeV, ^{52}Cr at 5 AMeV, and ^{58}Ni at 15 and 35 AMeV were developed.

Operations

For the period April 1, 2009 through March 31, 2010, the operational time is summarized in Table I, while Table II lists how the scheduled time was divided. While the unscheduled maintenance was much less than the last reporting period, there were several repairs that caused loss of beam-time. In November the coaxial line from the "B" final-stage rf amplifier was severely damaged because a signal-loss detector was accidentally disabled, resulting in two days of lost beam-time. In February a mistake was made in the reassembly of the E2 deflector high-voltage feed-through after the annual shut-down that resulted in a week of lost time to diagnose and repair. Finally, in March two days were lost to a failed rf coupler and an rf water-cooling leak.

TABLE I. 2009-2010 Operational Time

Time	Hrs.	%Time
Beam on target	6145.50	**80.7**
Tuning, optics, set-up	92.50	**1.2**
Beam development	1043.25	**13.7**
Scheduled maint.	17.50	**0.2**
Unscheduled maint.	321.25	**4.2**
Idle time	0.00	**0.0**
Total	**7620.00**	**100.0**

TABLE II. 2009-2010 Scheduled Beam Time.

Time	Hrs.	%Time
Nuclear physics	1894.25	**25.3**
Nuclear chemistry	893.50	**11.9**
Atomic physics	272.00	**3.6**
Outside collaboration	0.00	**0.0**
Outside users	3264.50	**43.3**
Beam development	1188.25	**15.9**
Total	**7494.50**	**100.0**

Texas A&M cyclotron radiation effects facility
April 1, 2009 – March 31, 2010

H. L. Clark, J. Brinkley, G. Chubarian, V. Horvat, B. Hyman, and G. Tabacaru

The activity of the Radiation Effects Facility (REF) decreased slightly over the previous reporting year. In this reporting period, the facility was used for 2,551.5 hours, which is a ~2% decrease over the 2,600 (record) hours used in the 2008-2009 reporting period. Users of the facility (and hours used) over the past year were: NASA GSFC (314), Xilinx Corporation (249.5), BAE Systems (210.5), Boeing Seattle (209.5), NAVSEA (150.75), NASA JPL (138.75), International Rectifier (130.75), Sandia National Laboratory (122), SEAKR (111), Aeroflex (103.25), Intersil (96), Ball Aerospace (91), Actel Corporation (51), Southwest Research Institute (48), General Dynamics (43.5), ASTRUM (40), University of Colorado (38), Silicon Space Technology (32), Micro RDC (29.5), Johns Hopkins University (29), Lockheed Martin Corporation (27.5), VPT Inc (23), Los Alamos National Laboratory (22), MDA Corporation (21.75), SOREQ (19), Cisco Systems (17.5), AMTEC Corporation (16), Data Devices (16), JD Instruments (16), Naval Research Laboratories (16), Star Vision (16), Sun Tronics (16), Vanderbilt University (12.75), Broadcom Communications (12), Northrop Grumman (12), ITT Communications (10), Harris Corporation (8), NASA JSC (8), Peregrine Semiconductor (8), Radiation Assured Devices (8) and University of Idaho (8). New users included Broadcom Communications, Data Devices and Star Vision.

Table I compares the facility usage by commercial and government customers. The ratio from this reporting year (66% to 34%) is similar to the trend seen in previous reporting periods and commercial hours still dominate. Commercial hours decreased by 7% and government hours increased by

TABLE I. Radiation Effects Facility usage by commercial and government customers for this and previous reporting years.

Reporting Year	Total Hours	Commercial Hours (%)	Government Hours (%)
2009-2010	2,551	1,692 (66%)	859 (34%)
2008-2009	2,600	1,828 (70%)	772 (30%)
2007-2008	2,373	1,482 (62%)	891 (38%)
2006-2007	2,498	1,608 (64%)	890 (36%)
2005-2006	2,314	1,314 (57%)	1,000 (43%)
2004-2005	2,012	1,421 (71%)	591 (29%)
2003-2004	1,474	785 (53%)	689 (47%)
2002-2003	1,851	1,242 (67%)	609 (33%)
2001-2002	1,327	757 (57%)	570 (43%)
2000-2001	1,500	941 (63%)	559 (37%)
1999-2000	548	418 (76%)	131 (24%)
1998-1999	389	171 (44%)	218 (56%)
1997-1998	434	210 (48%)	224 (52%)
1996-1997	560	276 (49%)	284 (51%)
1995-1996	141	58 (41%)	83 (59%)

11% over hours from 2008-2009. Much of the testing conducted at the facility continues to be for defense systems by both government and commercial agencies. It is expected that the facility will continue to be as active in future years.

Table II lists the beams used this year and the number of times each was requested. In total, 546 beams were run this year which is identical to the previous year. 15 and 25 MeV/u Kr and Xe were most utilized as well as 15 MeV/u Au. No new beams were added to SEELine users list.

TABLE II. Beams used and the number of times requested for this reporting year and previous years. 546 beams were run this year.

Particle Type	A MeV	2000-2001	2001-2002	2002-2003	2003-2004	2004-2005	2005-2006	2006-2007	2007-2008	2008-2009	2009-2010
^{4}He	15	N/A	N/A	N/A	N/A	N/A	N/A	N/A	N/A	1	3
^{14}N	"	N/A	N/A	N/A	N/A	N/A	N/A	N/A	N/A	0	4
^{20}Ne	"	1	13	19	15	23	36	39	37	41	39
^{40}Ar	"	4	24	43	46	51	56	60	57	63	60
^{63}Cu	"	N/A	N/A	5	14	22	23	25	24	19	22
^{84}Kr	"	6	26	55	47	49	75	81	77	63	73
^{109}Ag	"	N/A	N/A	6	18	15	26	28	28	34	30
^{129}Xe	"	5	18	43	51	50	78	84	84	48	72
^{141}Pr	"	N/A	N/A	2	2	1	4	4	4	4	4
^{165}Ho	"	3	11	17	7	8	22	24	24	13	20
^{181}Ta	"	4	5	4	3	5	3	3	3	3	3
^{197}Au	"	12	9	23	34	34	46	50	49	44	47
^{4}He	25	N/A	N/A	N/A	N/A	N/A	N/A	N/A	N/A	2	4
^{14}N	"	N/A	N/A	N/A	N/A	N/A	N/A	N/A	N/A	1	5
^{22}Ne	"	27	13	19	6	15	21	23	20	21	21
^{40}Ar	"	31	20	32	16	25	31	33	35	28	32
^{84}Kr	"	32	20	35	26	33	40	43	45	47	45
^{129}Xe	"	25	18	24	15	25	34	37	40	37	38
H-D	40	1	8	10	4	7	4	4	5	2	3
^{3}He	"	N/A	N/A	N/A	N/A	N/A	N/A	N/A	N/A	0	3
^{14}N	"	N/A	N/A	N/A	N/A	N/A	N/A	N/A	3	2	5
^{20}Ne	"	5	3	5	6	11	2	2	3	4	3
^{40}Ar	"	12	8	10	7	13	7	8	9	6	7
^{78}Kr	"	13	9	6	5	10	3	3	3	2	3
Total		192	207	360	324	399	511	552	550	485	546

Cyclotron computing

R. Burch and K. Hagel

To continue our mission of providing the Cyclotron Institute personnel the computational and network resources necessary to their research programs, we have increased the Institute's computing capacity and infrastructure over this past year by adding three additional computational servers, replacing our aging main firewall, adding a secondary firewall, and adding a pair of servers to virtualize several administrative services offered. We completed the migration of administrative servers from Scientific Linux, SL 4.x to SL 5.x and started the migration of these servers/services to Ubuntu LTS. We are pursuing the virtualization of administrative servers to allow us to better utilize server room rack space, power and cooling by reducing our physical machine count.

To increase productivity and reduce turn-around time we added three new computational servers, increasing our capacity by 24 late model processors or up to 48 concurrent jobs. One server was provisioned with 1GByte of RAM per processor thread allowing lab users to analyze the more memory intensive jobs quickly. To continue protecting the lab from external networking threats, we replaced our aging firewall server with a Dell PowerEdge R610 equipped with an energy efficient Quad Core Xeon E5505 processor running Ubuntu and also added a second, reprovisioned, mostly closed firewall running Ubuntu to isolate the data acquisition network from the lab network.

In an effort to reduce the number of administrative servers in the data center, and thereby reduce administrative server rack, power and cooling requirements, we added a Dell PowerEdge R610 server with two energy efficient Quad Core Xeon E5520 processors and reprovisioned the Dell PowerEdge R610 with the 12 SATA disk enclosure [1]. The motivation for these two servers is to free up physical computers running administrative services, one machine for each service; data, mail, web, database, ssh-gateway, authentication, wireless, and other services by hosting all these services on one physical server as VM's (Virtual Machine), one for each service. Two servers are required to minimize down time in the event that the primary VM host fails. Currently, a data fileserver VM is in production with four of the twelve drive slots populated with Terabyte drives. We also have a ssh-gateway VM provisioned awaiting its disaster recovery plan verification and a web server VM in development.

These changes and additions allow us to supply the Institute with the resources it needs to execute its mission by increasing our computational and data serving capacity, by providing more security with updated firewall services, by reducing physical machine footprint via migration of administrative servers to SL 5.x and Ubuntu in a VM infrastructure and by providing a path for further expansion in the coming years.

[1] R.Burch and K.Hagel, *Progress in Research*, Cyclotron Institute, Texas A&M University (2007-2008), p.V-5.

Cyclotron Institute upgrade project

H. L. Clark, F. Abegglen, G. Chubarian, G. Derrig, G. Kim, D. May, and G. Tabacaru

On January 3, 2005 the Cyclotron Institute Upgrade Project (CIUP) began with the approval of the CIUP management plan by the Department of Energy Nuclear Physics Office. The project will extend to the fourth quarter of calendar year 2011. When completed, the upgraded facility will provide high-quality re-accelerated secondary beams in a unique energy range in the world. Funding for the upgrade comes from several sources: the Department of Energy, matching support from TAMU, the Robert A. Welch Foundation and beam time sales for testing electronics components at the Cyclotron Institute.

The CIUP is divided into three major tasks: (1) Re-commission of the existing K150 (88") cyclotron and refurbish beam lines; (2) Construct light-ion and heavy-ion guides and produce 1+ radioactive ions; (3) Transport and charge boost radioactive ions and accelerate them in the K500 cyclotron.

As detailed in the Management Plan, effort made during this year on Task 1 included,

- Installation of equipment for the K150 high vacuum system,
- Installation and testing of the dee inserts for the central region of the cyclotron,
- Installation and testing of the negative ion source,
- Development of high intensity 30 MeV proton beams,
- Final assembly of K150 beam lines, and
- Procurement of the radiation monitoring system for the K150 cyclotron.

Progress was also made on Tasks 2 and 3. This included,

- Procurement of the radiation shielding for the ion guide cave,
- Construction of the Heavy Ion Guide gas cell and transport system,
- Installation and testing of the CB-ECR ion source, and
- Assembly and installation of the n+ transport system.

Below we report on a few of the accomplishments listed above.

Initial Results from Center Region Calculations with Batwings

The dee inserts (Berkeley batwings), see Fig. 1, were installed in October of 2009. These titanium inserts are electrically connected to the dee and dummy dee and narrow the dee gap both horizontally and vertically in the center region. The proper alignment of the batwings is very important, especially the vertical placement with respect to the median plane, and it took a lot of effort by our mechanical engineer and crew to install the batwings.

The dummy dee side batwing was installed first. It was accessible from the deflector side with the deflector table removed from the dee tank. Three transits set up along orthogonal axes were used to verify the alignment of the batwings: one at 0° looking along the dee (see Fig. 2a), one at 90°, and one looking up through the center hole on the lower yoke (with the inflector removed). The batwing was

mounted to the upper dummy dee support bracket, which already had two mounting holes drilled. (The dummy dee did not have to be removed from the cyclotron.) The vertical position of the batwing was

Dee Inserts - Batwings

Dee side

Dummy dee side
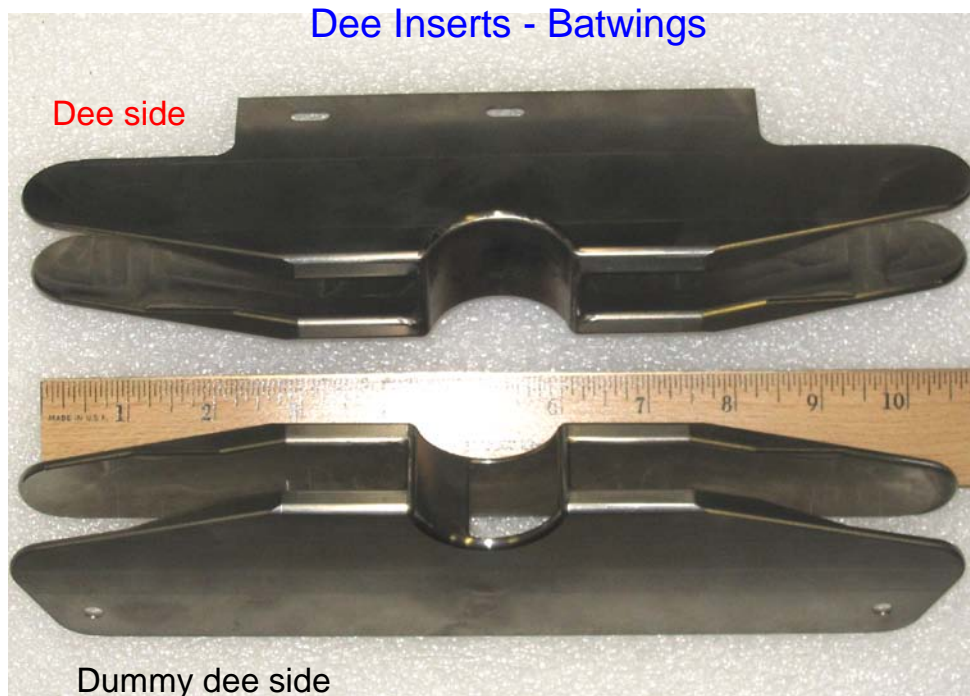
FIG. 1. Dee and dummy dee inserts.

adjusted by the height of spacers between the batwing and the mounting bracket. The batwing was mounted to the dummy dee bracket by passing two grooved posts, which were mounted on the top of the two spacers which in turns were fastened onto the batwing, through the mounting holes and capturing the posts with spring loaded clips from above (see Figs. 2b and 3). It took many iterations – mounting the batwing and checking for the alignment, and then taking it apart and adjusting the mounting mechanism - to install the batwing properly. Having to manipulate the batwing from 6 feet away in the 6 inch vertical gap of the cyclotron added to the difficulty of the task.

The dee side insert was installed by retracting the dee stem and moving the dee into the rf resonator tank. The insert was first mounted onto the end of a 10"x8"x0.25" copper plate, and then the insert and the copper plate were mounted onto the upper inside dee. The dee is lined with 10" wide graphite plates that run from the front to the back of the dee. The graphite plates are attached to the dee by regularly spaced screws and clamps along the seams. The graphite plates in the middle section of the dee had been removed years earlier and the clamps which remained were used to secure the copper plate along with the dee insert. Once again it took several iterations to mount and push the dee and the batwing into the position, and then to check the position of the batwing as well as the gap between the batwings.
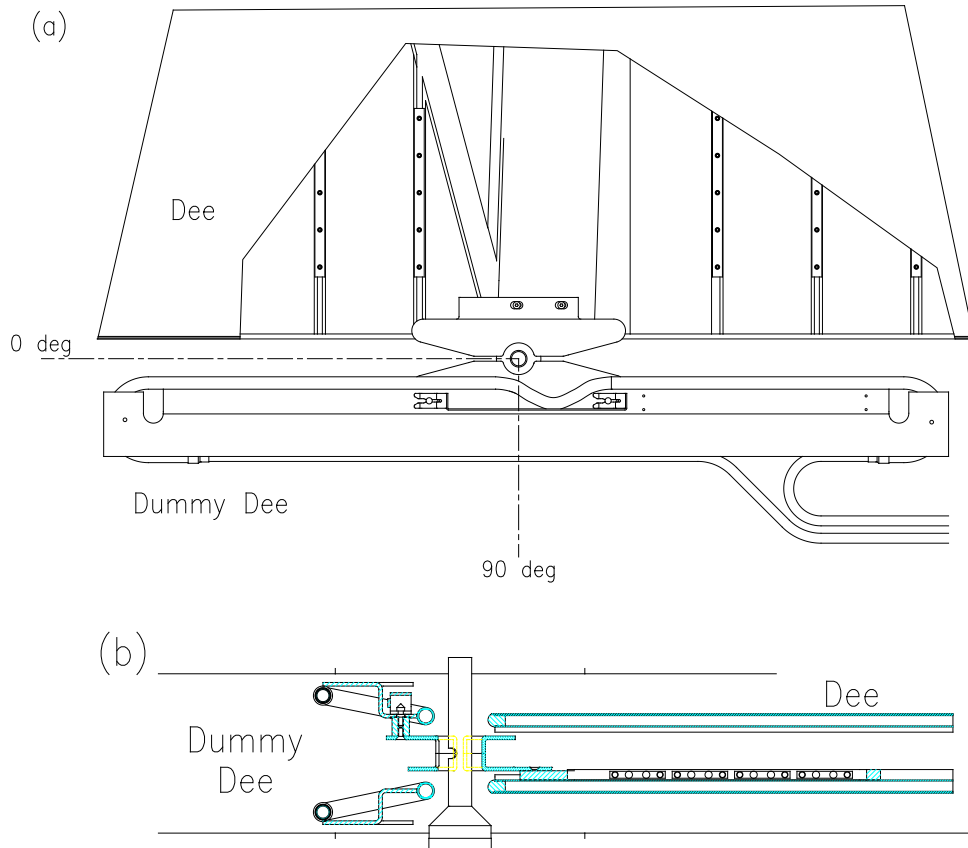
FIG. 2. (a) Top view and (b) side view of the dee and dummy dee and the batwings.

FIG. 3. Photo of the dummy dee side batwing after the installation.

After the dee inserts were installed, we were anxious to find out how the cyclotron would perform with the batwings. Just before the Christmas break, we got to look at several proton and oxygen beams with the batwings (Table I). Because we were mainly interested in the beam acceptance into the cyclotron and the internal transmission, all the Dec. 2009 beams were internal beams and were not extracted. The beam buncher was not operational and was not used. We used the CYDE calculations to set up the cyclotron (the main coil and 17 trim coils and the rf frequency) initially for beam tuning. During the beam tuning the trim coils were mostly left set to the CYDE values and only the main coil was adjusted. In order to test CYDE, we did run old run solutions for 20 MeV proton and 7.5 AMeV $^{16}O^{5+}$ beams, and we obtained very similar beam currents between the old run solutions and the CYDE solutions. The use of the CYDE calculations will allow faster beam tuning in the future, and at this early stages of running K150 we will perform more comparison studies with old run solutions to gain confidence in CYDE.

TABLE I. First look at beams with the batwings (Dec. 2009).

T/A (MeV/u)	Ion	Main Mag (A)	Vdee (kV)	ILC02* (µA)	Inflector (µA)	BP=10" (µA)	35" (µA)
20	protons (Oct./07)	612	73 (w/o batwings)			0.65	0.22
20	protons	613	45	29	10	0.33	0.32
25	protons	669	46	23	8	0.56	0.54
30	protons	742	52	25	9	0.40	0.37
7.5	16 O 5+	1262	53	89	35	3.1	1.9
10	16 O 6+	1186	56	132	62	3.9	3.5
12	16 O 6+	1367	65	130		5.0	4.7
14	16 O 6+	1606	65	110		3.4	2.9
14	16 O 7+	1199	65	22	12	0.74	0.67

The first beam on Table I, the 20 MeV proton, was the first beam accelerated (without the batwings) and extracted 2 years ago, and it is listed only as a comparison. Looking at the beam currents from Table I, the first thing that stands out is how much the internal transmission improved with the batwings. Two years ago it was only 33% from 10" to 35" on the beam probe for the 20 MeV proton beam. With the batwings we obtained 85% or better. The exception is the 7.5 AMeV oxygen beam which may be affected more severely by poor vacuum. Next, looking at the cyclotron acceptance as measured by the percentage of the beam current at 10" from the beam on the inflector, the proton beams averaged 5% and this is consistent with Berkeley, where they typically obtain 2.5 to 5% acceptance without beam bunching. The acceptance for the oxygen beams was slightly better. Lastly, it was observed that the rf dee voltage ran much lower with the batwings, 73 to 45 kV for 20 MeV proton beam, and even for the higher energy 25 and 30 MeV proton beams it ran under 52 kV. This is a good development, but this does not clarify how much higher the dee voltages will be for more energetic beams, such as 55 MeV proton beam. In the constant-geometry mode, the dee voltage scales with the beam energy (actually the total kinetic energy divided by the charge). From the observed dee voltages, namely 45, 46, and 52 kV for 20, 25, and 30 MeV proton beams, respectively, while it was not calibrated it does seem that the three proton beams did not follow the strict constant-geometry mode. And also, while the dee voltage depends mostly on the electromagnetic structure of the center region, the dee voltage does affect the beam extraction. Further beam studies are obviously needed to learn more about the dee voltage requirements.

In the meantime, the beam orbits in the center region were further investigated using the MSU program Z3CYCLONE, this is a continuation of the calculations which was described in the last year's progress report. This year the 3D electric map of the batwings and the grounded inflector housing was calculated with TOSCA, a 3D electro-magnetostatic solver. The magnetic field map was obtained from CYDE, however, because of its coarse polar map, $\Delta r=1'$ and $\Delta\theta=3°$, the averaged magnetic values (over angle) were used in the Z3CYCLONE calculations instead of the actual map. This should not matter for the first few turns as the flutter effect is small inside $5''$.

The beam tracking starts from the exit of the mirror inflector (mirror angle was assumed to be 45.7 degrees). With the opening of the inflector oriented toward the dummy dee side, as was the case for the Dec. 2009 beams, the beam emerges from the inflector into the dummy dee through the opening in the dummy dee batwing. The beam then bends around towards the active dee side to start the acceleration (Fig. 4). Two important parameters in the calculations are the rf dee voltage and the starting rf time. The dee voltage needs to be large enough so that the energy gain from the first gap-crossing allows for the beam to make it around the batwing collars. And the rf starting time must be properly synchronized so when the beam gets to the accelerating gap the rf would be correctly phased for acceleration. Additionally, in order to utilize the electric vertical focusing property, the beam needs to go through the RF electric field gap in the falling e-field, namely that the electric field experienced by the beam must be stronger in the first half of the gap crossing than that from the second half. Also, because the magnetic field is not isochronous at the center of cyclotron (it is about 3 to 5% larger than the isochronous value), the particle orbital period near the center is shorter than the rf period, and so it is necessary to start the beam late with respect to the rf and allow the beam to "catch up" with the rf after several turns. For the 20 MeV proton beam, see Fig. 4, using 20 to 40 kV on the dee produces well centered, reasonable looking orbits at the center region. (The 20 kV on the dee translates into about 500 turns inside the cyclotron to reach the maximum energy.) So, the Z3CYCLONE is useful in finding a range of acceptable dee voltages, but perhaps not the optimal dee voltage. The calculations do show that higher dee voltages lead to wider RF phase widths, which in turn lead to larger beam acceptance into the cyclotron.
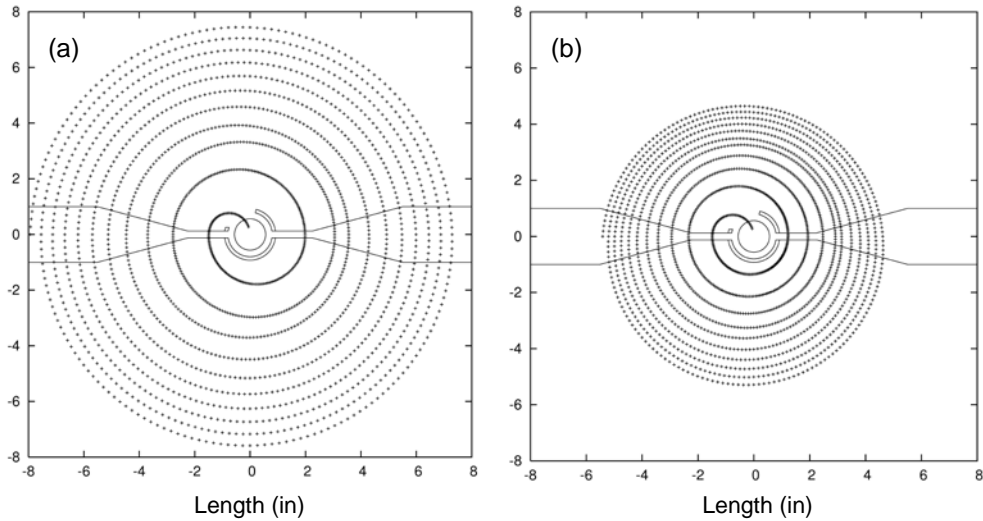
FIG. 4. Simulating 20 MeV proton beam with the dee at (a) 40 kV and (b) 20 kV.

The dee inserts (Berkeley batwings) were installed in Oct. 2009, and then in Dec. 2009 we tested them with several internal beams. The tests showed that the dee inserts work very well: the beam acceptance into cyclotron and the internal beam transmission were very good, and the dee inserts allowed the rf to run at lower dee voltages than two years ago.

H- Acceleration

One of the concerns for the project is the extraction efficiency of high intensity protons from the cyclotron. Poor extraction efficiency may cause radiation damage to and high activation of the cyclotron deflector. One solution is to accelerate H- ions and then strip to H+ near extraction. At other cyclotron labs this technique has shown to have extraction efficiencies of nearly 100% and greatly reduces interior activation problems. Ray tracing calculations show that such a system could physically fit into and operate within the vacuum space of the K150 cyclotron. With the deflector pulled back from the extraction channel (but not removed from the cyclotron), H- ions could be accelerated to 38" (extraction channel radius) and then stripped to H+. Upon exit, the trajectory of the H+ ions would then be steered along the normal beam line with a dipole magnet (Fig. 5).

The cyclotron laboratory in Jyväskylä, Finland (JYFL) has had great success with a multi-cusp negative ion source that was built by them with help from the TRIUMF lab in Vancouver, Canada. The experience of JYFL is that their source LIISA (Light-Ion Ion Source Apparatus) produces over 5 mA of H- at the 5.9 kV extraction voltage suitable for their fixed center region geometry for 30 MeV. This results in a proton beam out of the cyclotron of 60 eμA. The injection line has a vacuum in the region of mid 10^{-8} torr while the cyclotron has a vacuum in the low 10^{-7} torr region. This vacuum results in only

about 5% residual gas losses. The major loss seems to be from matching the beam from the source to the cyclotron inflector. The dose from lost beam in the JYFL cyclotron has decreased by a factor of 10 to 20 for 30 MeV protons over the case from running positive ions. Their LIISA source matches very well with our needs for an ion source.
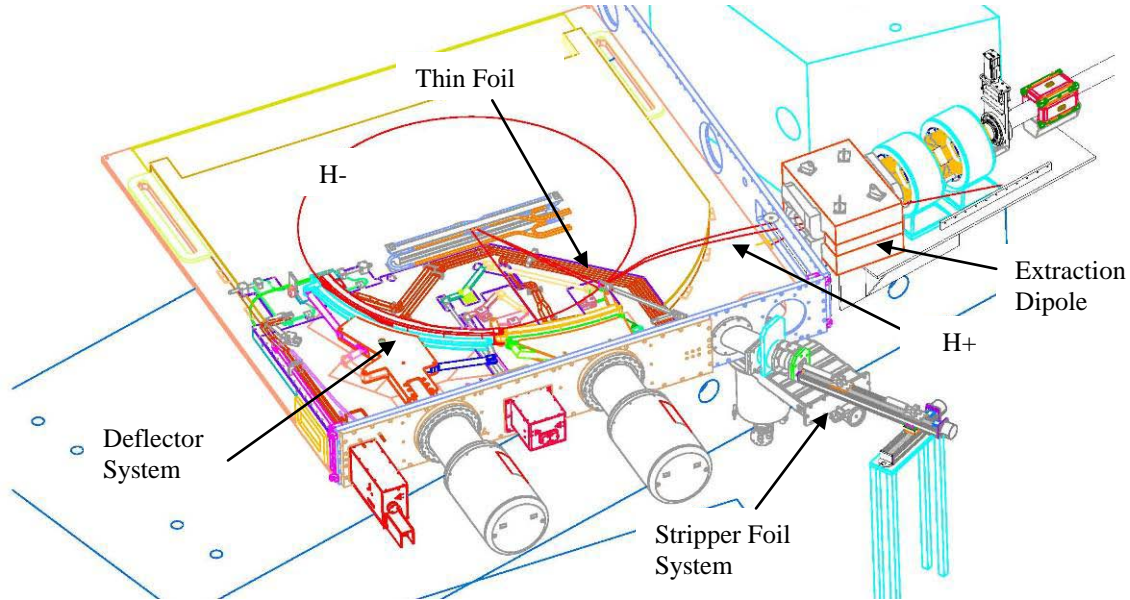
FIG. 5. Illustration of H- extraction from the K150 cyclotron. With the deflector pulled from the 38" extraction radius, H- ions would strip to H+ by a thin foil and then exit the cyclotron. A dipole magnet would then steer the beam along the normal beam line leading from the cyclotron.

In April 2009, Cyclotron staff traveled to JYFL to discuss H- cyclotron acceleration, operation and construction of a negative ion source for the K150 cyclotron. Discussions with them lead to the suggestion that we use their prototype (in storage) LIISA source to get started. Quick testing on a test stand showed that their prototype LIISA source could produce a sufficient amount of H- beam for our project. JYFL has offered their prototype LIISA source on loan and then they would sell it to us once it was proved to work on the cyclotron.

For the LIISA source to provide the intensity and emittance needed for the project, a new source extraction system was built by Texas A&M with design help from JYFL. In August, the new source extraction system was brought to JYFL and tested on the prototype LIISA source. Results showed that the ion source produced up to 1 mA of H- ions and with an emittance of less than 8π mm-mrad which is sufficient for our project. After additional testing in September and October, the source was shipped to Texas A&M in late November.

In order to receive the beam into the K150 cyclotron, the transport of H- ions was studied with the code SIMION (transport plus space charge effects). The results showed that a double Einzel lens system is needed to first, get the beam through the vertical beam tube of the ECR2 injection line 90° magnet and second, to refocus the beam to the Faraday cup at the mid-point of the vertical injection line. Fig. 6 shows the final layout of the H- ion source and double Einzel lens system. Fig. 7 shows the ray tracing results predicted by SIMION using a double Einzel lens system.

H- ion source →
Extractor/Filter system →

Einzel lens #1 →

…Beam from ECR2 through 90° magnet →

Einzel lens #2 →

Faraday cup →
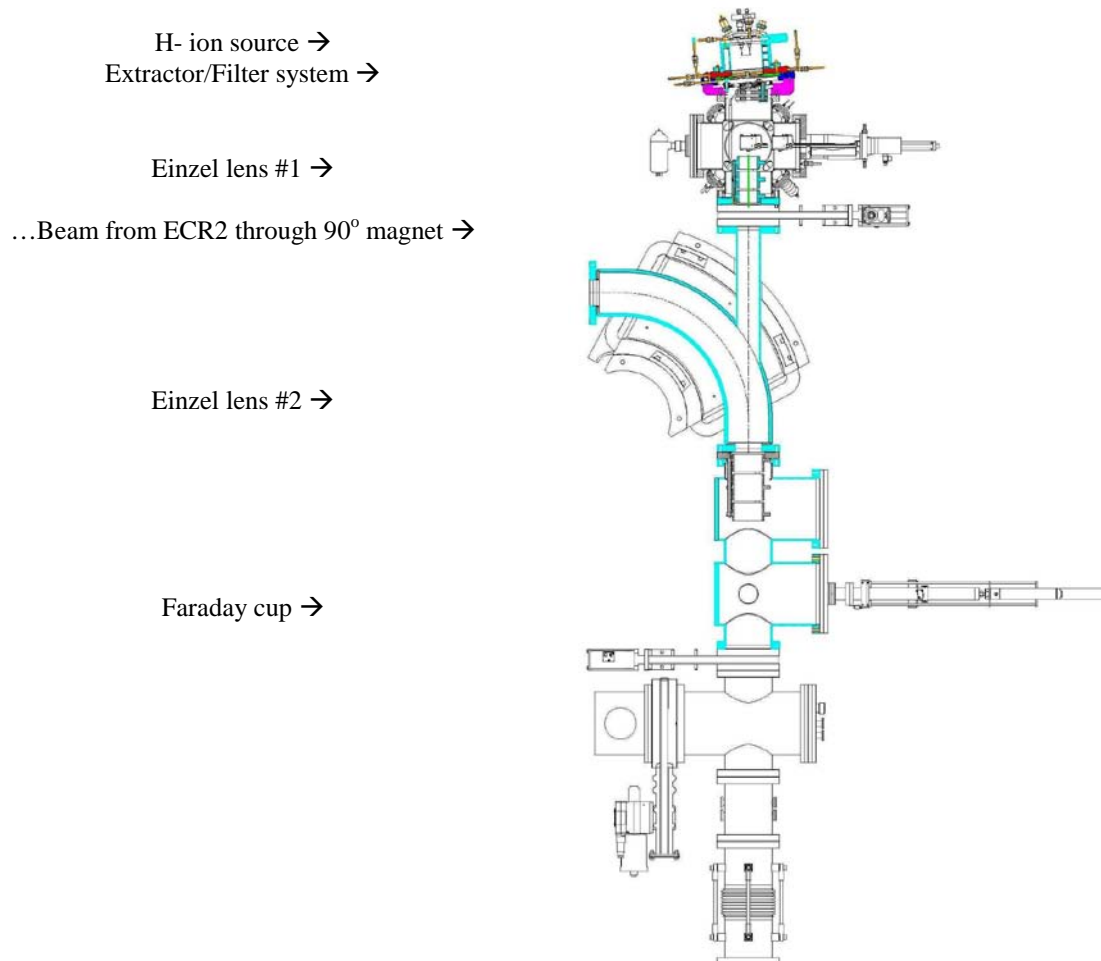
FIG. 6. Layout of the H- ion source and double Einzel lens system. The system fits above and below the ECR2 90° magnet and without any modifications.

During the installation of the dee inserts, the deflector positioning system was modified so that the deflector electrode and shoe could be pulled out to 41". This allows unobstructed extraction of the H- beam with the foil stripper system at 38". Equipment for the foil stripper system was installed by mid March. The exit magnet acquired from surplus was refurbished and installed in February. The pole tips were reshaped and extra steel was added to the yoke in order to produce the magnetic fields for the highest energy H- and D- beams that can be accelerated. The power supply for the exit dipole magnet was installed in January.

Except for Einzel lens #2, the source and all its equipment were fully installed by early February. Two experts from the JYFL lab came to TAMU in February to help with start-up, and optimize the ion source and beam transport system. Testing showed that the ion source and transport system worked properly. A beam current of ~1.5 mA of H- ions was measured at the H- Faraday cup, and ~0.5 mA was measured at the ECR2 Faraday cup.   Einzel lens #3 was installed in March and improved the transmission between the two Faraday cups from 30% to 60-70% as expected.
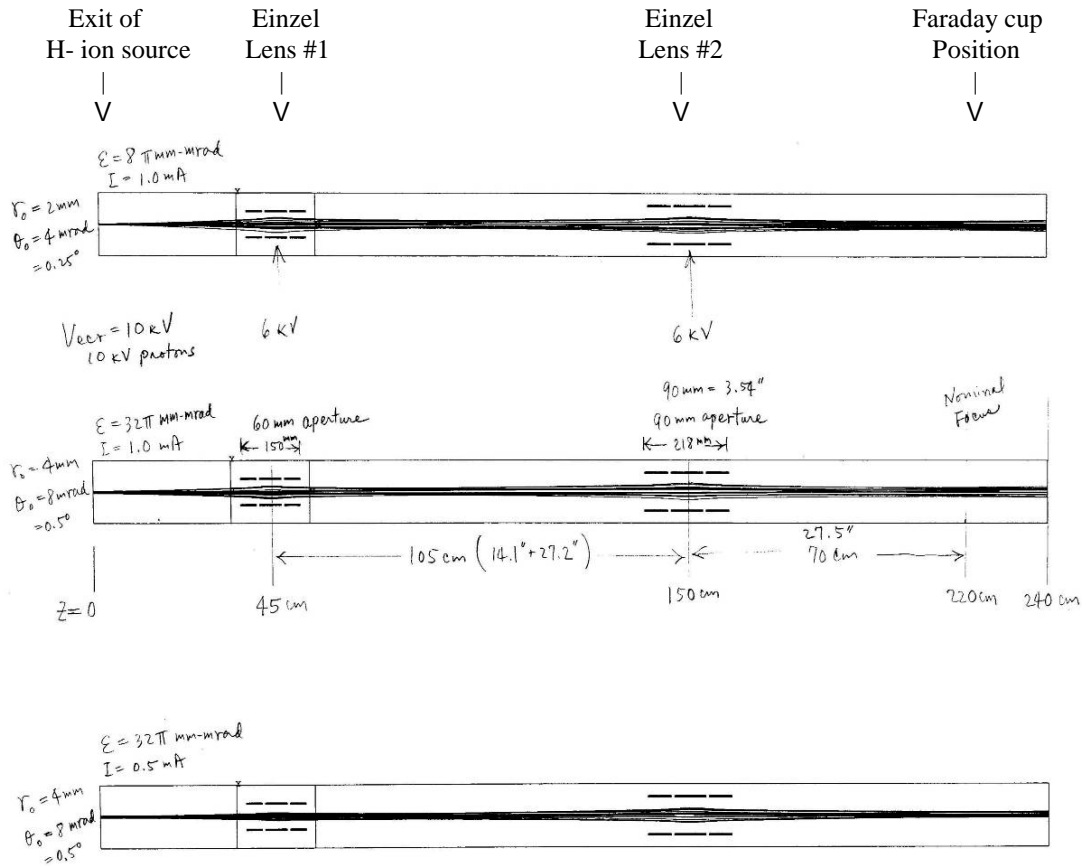
FIG. 7. Simion calculations for various assumptions for the emittance and current of the H- ion source. The diagrams show the position for the double Einzel lens system.

In order to deflect H- ions into the center region of K150 cyclotron, the inflector power supply had to be replaced with a negative high voltage supply. The main magnetic field of the cyclotron was reversed by crossing over the buss bar leads from the main supply to the cyclotron coils. The "crossing buss bar" was installed and tested in late March 2010. The magnetic fields from the trim and valley coils are also reversed, in order to accelerate H- ions. However these supplies can switch between positive and negative potential so no modifications were needed.

With the ion source set at -10 kV, H- acceleration at 20 MeV was tried as a first test. The main, trim and valley coil power supply voltages were reversed and set to the current values from the 20 MeV proton run in December 2009. After several hours of optimization, beams of ~10 μA of H- were stripped and extracted from the cyclotron on to the Faraday cup after the exit dipole. This first test showed that the H- acceleration system was working properly.

Lower proton energy was tried first to allow time for the RF system to condition and to keep the secondary radiation level as low as possible in the cyclotron vault. After the RF system had time to condition, 30 MeV H- ions were then accelerated. As with the 20 MeV tune, the starting currents for the main, trim and valley coils were set to the 30 MeV proton values from the test run in December 2009, but with the power supply voltages reversed to reverse the cyclotron magnetic field. After a couple days of optimization, steady beams of 14 μA of H- were extracted and measured on the exit Faraday cup. Fig. 8

shows the reading on the current meter for the exit Faraday cup. The optimized parameters for the H- ion source are shown in Table II.

FIG. 8. Beam current of 14 µA of 30 MeV protons measured at the Faraday cup at the exit of the K150 cyclotron. H- ions accelerated to 30 MeV were stripped to protons at the extraction radius.

TABLE II. Optimized parameters for the H- ion source for 30 MeV H- acceleration.

BM1:	0.94 A @ 0.32 V
Puller:	+8.82 kV @ 56 mA
Plasma Electrode:	+4.03 V @ 2.18 A
ARC:	79.9 V @ 21.70 A
Filament:	3.99 V @ 146.1 A
Source Bias:	-10.0 kV @ 0 A
Einzel #1:	-7.49 kV @ 0 A
Einzel #2:	-6.28 kV @ 0 A
Einzel #3:	-4.18 kV @ 0 A
Ion Source Vacuum:	1.3 E-5 Torr
Injection line Vacuum:	9.2 E-7 Torr

Leak valve @ 3 full turns open, pressure on regulator set at ~37 psi

While the beam was stopped on the exit Faraday cup of the K150 cyclotron, secondary radiation levels from neutrons were measured in the cyclotron vault and at the injection line above the K150 cyclotron. Levels of ~1 Rem/hr were measured in the vault and 2 – 3 mRem/hr were measured at the injection line. These are very low values with regard to the safety of the staff working around cyclotron facility. Fig. 9 shows the reading by the RAM system at the injection line.

FIG. 9. Secondary radiation levels of 2 – 3 mRem/hr were measured at the injection line above the K150 cyclotron while 14 µA of 30 MeV protons were stopped on the exit Faraday cup of the K150 cyclotron. H- ions accelerated to 30 MeV were stripped to protons at the extraction radius .

Charge Breeding ECR Ion Source

The CB-ECRIS was delivered in September 2007 and was assembled by Wayne Cornelius of Scientific Solutions of San Diego in October 2007. All of the equipment needed to complete the CB-ECRIS has been procured and installed including both coil power supplies, the turbo pumping systems, microwave transmitters and control equipment. CB-ECRIS was installed completely and turned on for a short period of time first, with the TWT transmitter and plasma was created successfully. During Q4 FY09, a section of n+ transport system following the CB-ECR ion source was installed and allowed analysis of the beams produced by the CB-ECR ion source. With 100 watts of RF power from the 14.4 GHz transmitter and an extraction voltage at 10 KV, first results of the CB-ECR ion source were obtained.

One of the milestones in the upgrade project is the commissioning of the CB-ECRIS This ion source will be used to further ionize low charge-state (1^+ mainly) radioactive ions to higher charge-states (charge-breeding) for acceleration by the superconducting K500 cyclotron. The frequency used to ignite the plasma was 14.5 GHz and the extraction voltage varied between 7 kV to 10 kV. The source was initially tested as a conventional ECR ion source by injecting neutral gases: oxygen and argon. After running for few weeks the source became unstable and was inoperable due to the appearance of a large and oscillating drain current. It was found that the insulator between the plasma chamber and the steel from the injection side coil had developed significant damage from a sparking track. After the insulator was removed and examined, it was replaced with one redesigned to have a longer path from high-voltage to ground. The source has since operated in a more stable fashion. Fig. 10 shows a scan for high charge-states for argon with low microwave power. To test the charge-breeding capability of the CB-ECRIS we chose to inject a beam of stable 1^+ ions into the plasma chamber from a commercial ion gun made by HeatWave Labs and capable of producing 1 µA of 1+ current from the alkali elements, Li, Na, K, Rb and

FIG. 10. Plot representing the extracted current (μA) from the CB-ECRIS with argon versus Q/M. The peaks are labeled with the corresponding charge-states.

Cs. Details of the ion gun can be found on the company website. The critical feature for high efficiency charge-breeding is the capture of the injected ions by the plasma. For this to happen the injected ions should be within a few volts of zero velocity as they encounter the plasma. Since the potential ΔV of the plasma with respect to the plasma chamber is on the order of a few volts and indeterminate, the extraction voltages V_{ext} of the ion gun and of the CB-ECRIS were tied together through a single high-voltage supply with ΔV applied to the ion gun via a low-voltage, remotely adjustable supply floating at V_{ext}. Fig. 11 illustrates the injection system. The ion gun is mounted on the left-hand flange in the figure.

We conducted ion transport simulations using the SIMION code, a software package designed to calculate the trajectories of ions moving through electric and magnetic fields. The code was used to visualize the trajectories of the ions at the entrance in the plasma chamber as well as to estimate voltages to be applied to the Einzels A and B. The solenoid magnetic field from the injection side coil was considered during the simulations, and we could observe that it does provide extra focusing to the injected beam. In Fig. 12 we present a comparison for Rb^+ injected beam with the solenoid turned on and turned off. ΔV used in this simulation was 40 V.

In tests of detecting the Rb^+ beam on the extraction side of the CB-ECRIS, without the ECR plasma ignited, it was found that the voltages used for the Einzels A and B differ from the SIMION simulations within ±10 %. Einzel A has a narrow range of voltages whereas voltages for Einzel B span a larger range for the 1^+ beam at the extraction side to still be detectable. When the microwave transmitter

is turned on, the Einzel A voltage must be decreased in order to detect the Rb$^+$ beam again. Higher charge states of Rb have not yet been observed, and further investigations and tests are underway. For the next series of experiments we will inject a Na 1$^+$ beam, Einzel A will be eliminated from the injection scheme.
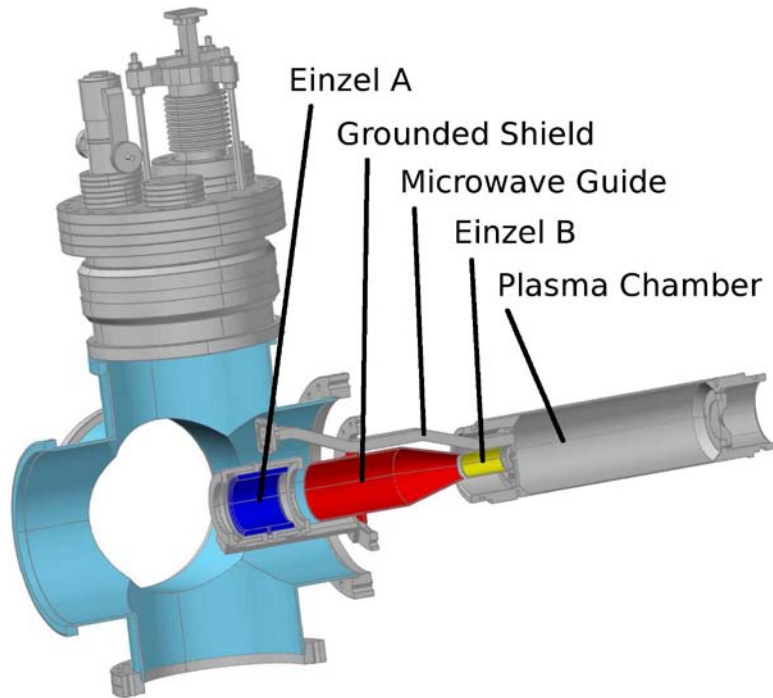
FIG. 11. The injection system of the CB-ECR. Einzel A, grounded shield, and biased tube are respectively highlighted blue, red, and yellow. The microwave guide and the plasma chamber are shown in gray.
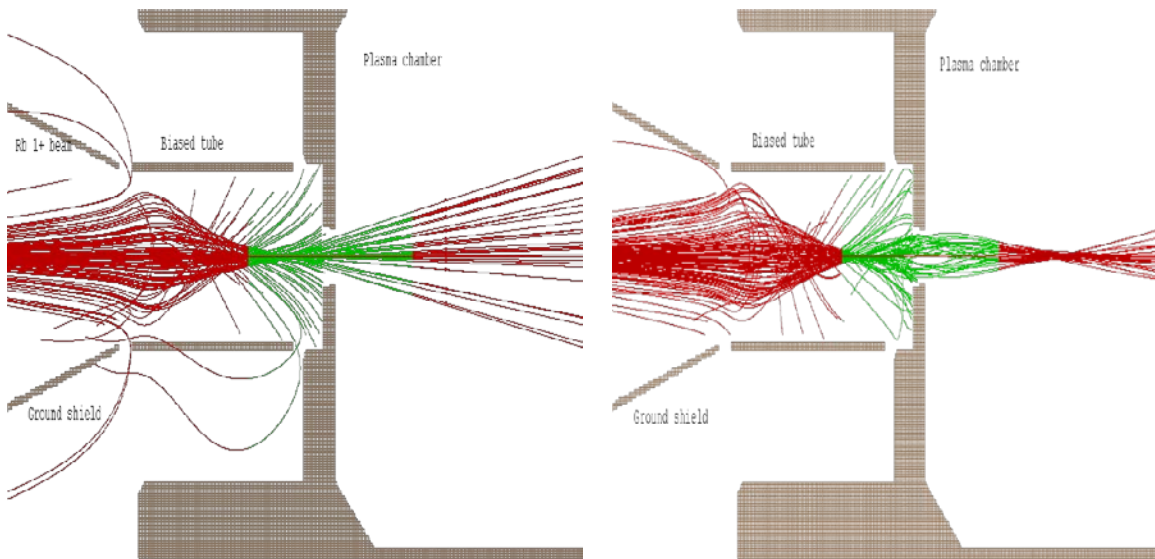
FIG. 12. SIMION simulations for the Rb$^+$ beam. In the left panel the magnetic field was turned off and in the right panel the magnetic field was turned on.

Testing the injection of ions in the CB-ECRIS* at the Cyclotron Institute

G. Tabacaru, D. P. May, and J. Saathoff

One of the milestones in the upgrade project is the commissioning of the CB-ECRIS*. This ion source will be used to further ionize low charge-state (1^+ mainly) radioactive ions to higher charge-states (charge-breeding) for acceleration by the superconducting K500 cyclotron. The details about the CB-ECRIS can be found in the last progress report and in Ref. [1]. The frequency used to ignite the plasma was 14.5 GHz and the extraction voltage varied between 7 kV to 10 kV. The source was initially tested as a conventional ECR ion source by injecting neutral gases: oxygen and argon. After running for few weeks the source became unstable and was inoperable due to the appearance of a large and oscillating drain current. It was found that the insulator between the plasma chamber and the steel from the injection side coil had developed significant damage from a sparking track. After the insulator was removed and examined, it was replaced with one redesigned to have a longer path from high-voltage to ground. The source has since operated in a more stable fashion. Fig. 1 shows a scan for high charge-states for argon with low microwave power.
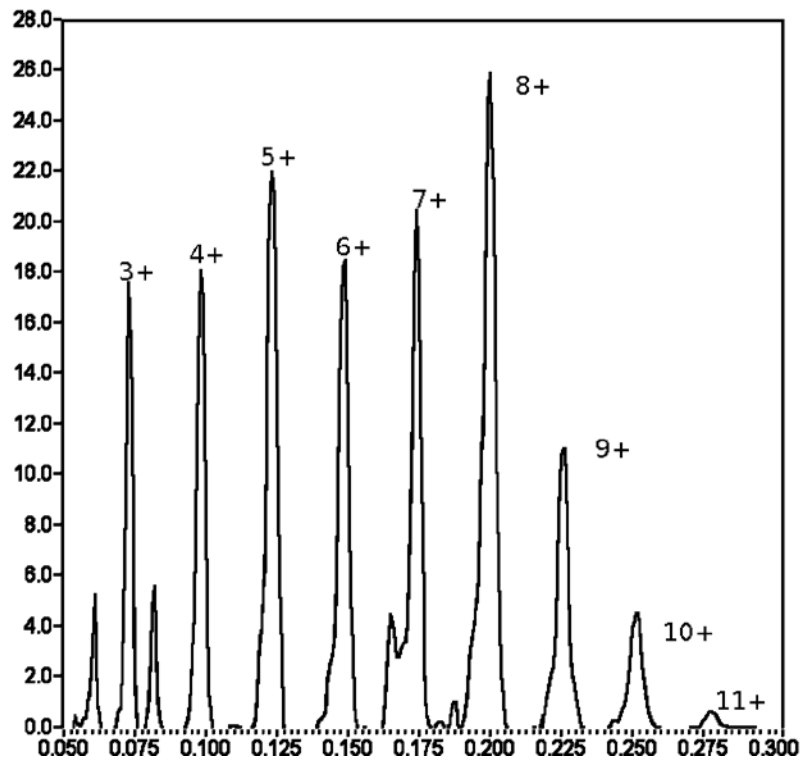
FIG. 1. Plot representing the extracted current (µA) from the CB-ECRIS with argon versus Q/M. The peaks are labeled with the corresponding charge-states.

To test the charge-breeding capability of the CB-ECRIS we chose to inject a beam of stable 1^+ ions into the plasma chamber from a commercial ion gun made by HeatWave Labs and capable of producing 1 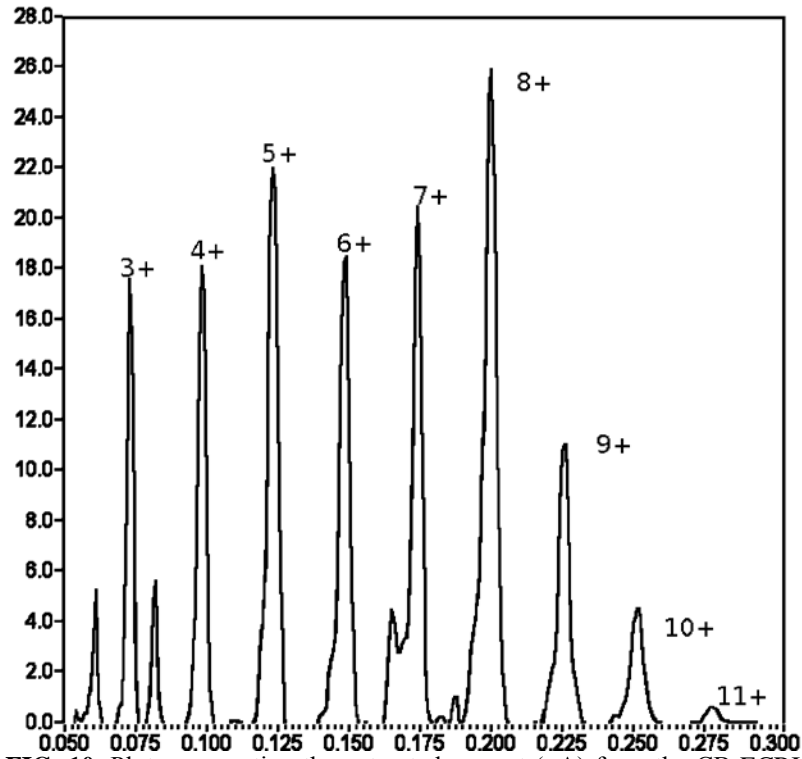μA of 1+ current from the alkali elements, Li, Na, K, Rb and Cs. Details of the ion gun can be found on the company website. The critical feature for high efficiency charge-breeding is the capture of the injected ions by the plasma. For this to happen the injected ions should be within a few volts of zero velocity as they encounter the plasma. Since the potential ΔV of the plasma with respect to the plasma chamber is on the order of a few volts and indeterminate, the extraction voltages V_{ext} of the ion gun and of the CB-ECRIS were tied together through a single high-voltage supply with ΔV applied to the ion gun via a low-voltage, remotely adjustable supply floating at V_{ext}. Fig. 2 illustrates the injection system. The ion gun is mounted on the left-hand flange in the figure.
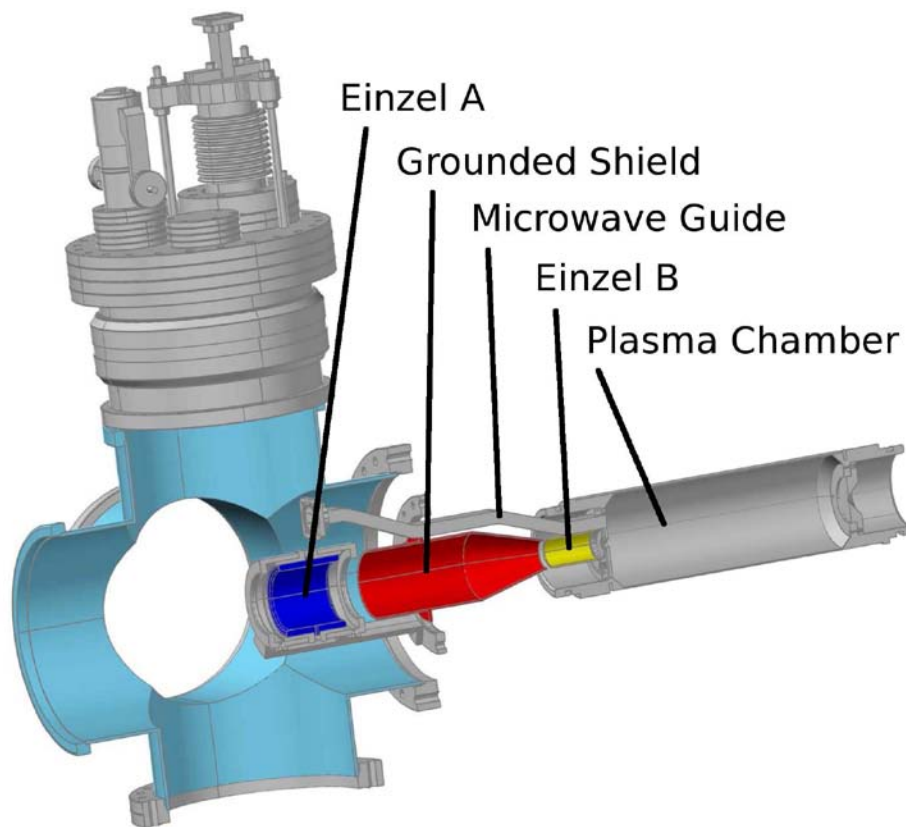
FIG. 2. The injection system of the CB-ECR. Einzel A, grounded shield, and biased tube are respectively highlighted blue, red, and yellow. The microwave guide and the plasma chamber are shown in gray.

We conducted ion transport simulations using the SIMION code, a software package designed to calculate the trajectories of ions moving through electric and magnetic fields [2]. The code was used to visualize the trajectories of the ions at the entrance in the plasma chamber as well as to estimate voltages to be applied to the Einzels A and B. The solenoid magnetic field from the injection side coil was

considered during the simulations, and we could observe that it does provide extra focusing to the injected beam. In Fig. 3 we present a comparison for Rb$^+$ injected beam with the solenoid turned on and off. ΔV used in this simulation was 40 V.
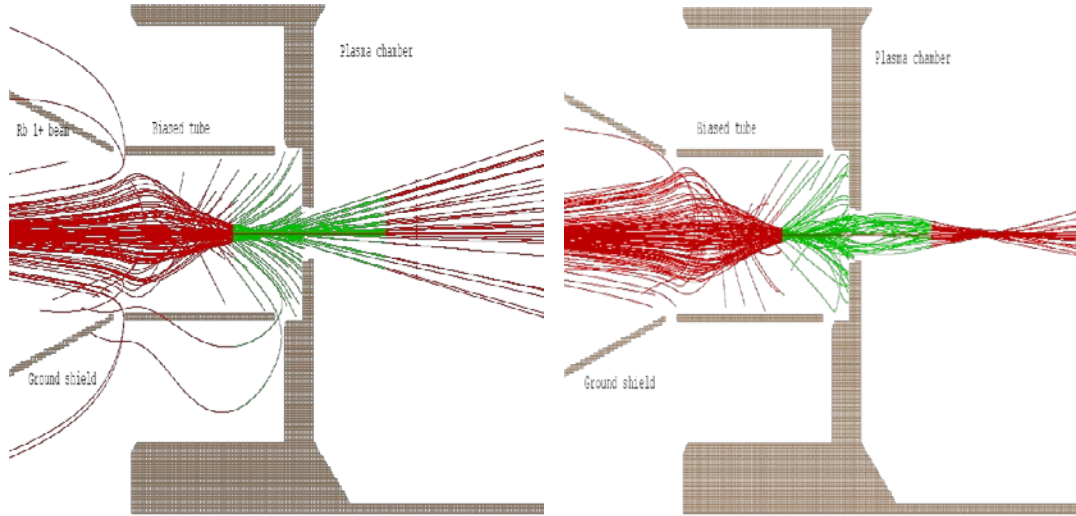
FIG. 3. SIMION simulations for the Rb$^+$ beam. In the left panel the magnetic field was turned off and in the right panel the magnetic field was turned on.

In tests of detecting the Rb$^+$ beam on the extraction side of the CB-ECRIS, without the ECR plasma ignited, it was found that the voltages used for the Einzels A and B differ from the SIMION simulations within ±10 %. Einzel A has a narrow range of voltages whereas voltages for Einzel B span a larger range for the 1$^+$ beam at the extraction side to still be detectable. When the microwave transmitter is turned on, the Einzel A voltage must be decreased in order to detect the Rb$^+$ beam again. Higher charge states of Rb have not yet been observed, and further investigations and tests are underway. For the next series of experiments we will inject a Na$^+$ beam, Einzel A will be eliminated from the injection scheme.

[1] W.D. Cornelius, ECRIS 2008, 18th International Workshop on ECR Ion Sources, Chicago, Illinois USA; http://accelconf.web.cern.ch/AccelConf/ecris08/papers/weco-b01.pdf
[2] http://www.simion.com and references therein.

Digital signal processing for improved half-life measurements

L. Chen and J. C. Hardy

We are exploring new methods for processing our 4π β-detector signals with a view to improving the precision with which we can make half-life measurements of superallowed β emitters. Elsewhere in this report [1] we describe a TDC-based data-acquisition system we have developed; here we describe another system based on digital signal processing.

Our present β-counting system takes signals from our gas proportional counter and passes them to a preamplifier followed by an amplifier, a discriminator, a gate-and-delay generator (to establish a single dominant dead-time) and a multichannel scaler. The main limitations of this kind of system are a relatively long dead time (> 3 µs) and the inability to completely exclude noise and spurious signals. Nowadays, digital signal-processing devices make it possible to perform a more subtle analysis of the detector signals than a traditional data-acquisition system allows. The essential idea of our new counting system is to use a high speed digitizer (NI PCI 5154; see Ref. [2]) to record pulses from the detector with a minimum dead time (~1µs) and then perform detailed analysis of the saved waveforms. After only one stage of amplification by a fast preamplifier (ORTEC VT120C) the detector signals are digitized at 1 GHz, and a 300-ns-long time window is saved, bracketing each signal.

Off-line we have done a detailed pulse analysis using a ^{90}Sr-^{90}Y β source. Based on an analysis of the pulse shapes (width, amplitude and integral) we were able to distinguish real β events from noise. Figure 1 shows the width distribution of pulses which we obtained at three different detector biases.
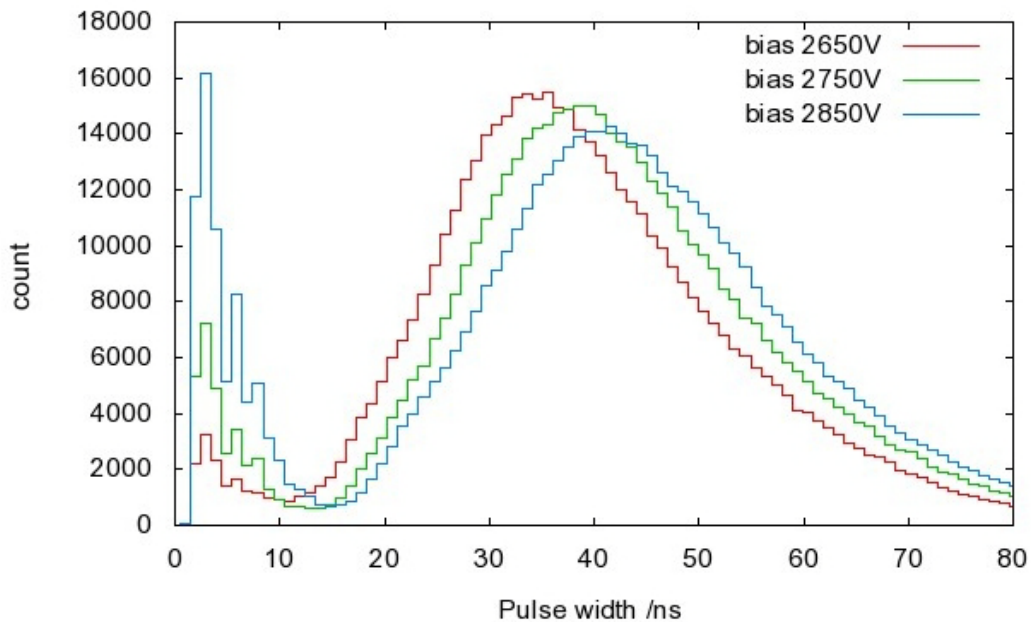
FIG. 1. The pulse-width distribution measured with three different different detector biases. The noise (pulses less than ~13 ns in width) and real β events are clearly separated by their width.

Because of their very different width distribution we can easily separate the real β events from the noise. Similar separation occurs for the amplitude and integral distributions but the width distribution shown in the figure is the most definitive. Once noise signals have been filtered out, the remaining signals – real β events – can be analyzed and compared with results obtained with our current experimental arrangement. Figure 2 shows a measurement of the total number of counts recorded from the ^{90}Sr-^{90}Y β source as a function of detector bias. Without noise discrimination, the plateau region, where count-rate is nearly independent of bias, is very limited. This is approximately what we encounter with our current system. With the implementation of noise filtering, a very flat plateau appears from 2600 V to 2950 V, showing that the digital system yields a big improvement.
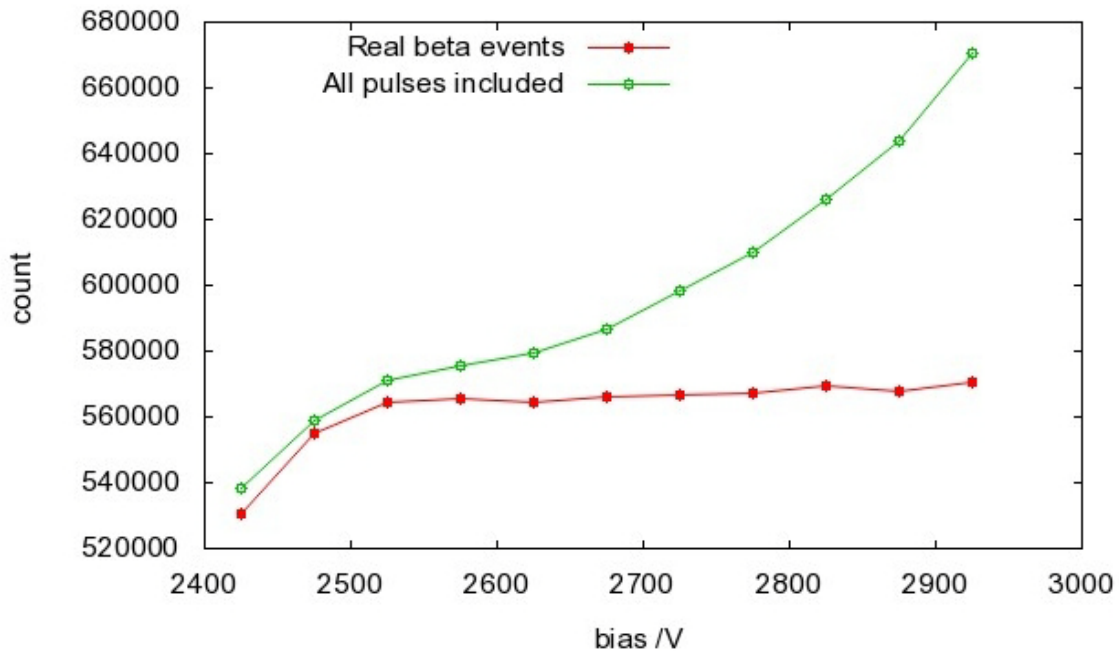
FIG. 2. Plateau measured using a high speed digitizer. Noise was removed by filtering the pulses according to their width, amplitude and integral.

With this arrangement, we expect to be able to reduce the system dead-time and increase the maximum count-rate that we can accept, thus improving the precision of our half-life results by at least a factor of two.

[1] V. Horvat and J.C. Hardy, *Progress in Research*, Cyclotron Institute, Texas A&M University (2009-2010) p. V-24.
[2] NI 5154 high speed digitizer: www.ni.com/digitizers

A new TDC-based data acquisition system for half-life measurements

V. Horvat and J. C. Hardy

For accurate high-precision measurements of β-decay half-lives, two new data acquisition systems are being tested as possible alternatives to the one that is currently in use. One of these systems is described elsewhere in this report [1]. The other is described here, where its capabilities are compared with the system currently being used.

While both systems utilize Nuclear Instrumentation Module (NIM) electronics to convert analog signals from the beta detector to logic pulses, the current system processes those logic pulses using Computer Automated Measurement and Control (CAMAC) electronics interfaced with a personal computer (PC) running the Windows NT$^©$ operating system. In contrast, the new system processes the logic pulses using a single multi-channel time-to-digital converter (TDC) plugged directly into a Peripheral Component Interconnect (PCI) expansion bus slot of a personal computer (PC) running the Microsoft Windows XP$^©$ or Windows Vista$^©$ operating system. Consequently, it is a lot simpler, and far less expensive, than the old system. It eliminates the need for CAMAC electronics and a CAMAC-to-PC interface, as well as the dependency on the Microsoft Windows NT operating system, which is now considered obsolete and is no longer supported by the manufacturer.

Since a PC running the Windows NT operating system does not have adequate protection against cyber attacks, we are not allowed to connect it to the Institute's network. Furthermore, Windows NT does not support Universal Serial Bus (USB) ports, which precludes the use of convenient portable mass-storage devices. Therefore, the transfer of data files from an NT-based computer to another computer is inconvenient at best.

While the data-acquisition software for the new system (CoboldPC$^©$) is written specifically for the TDC, it can be fully customized and used for data organization, visualization and analysis, since its data-acquisition and data-analysis modules (in the form of dynamic link libraries) can be reprogrammed using Microsoft Visual Studio C++ 2008$^©$ tools. For comparison, the current system is based on KmaxNT$^©$ software. It is more versatile, since it can also be used to program the graphics user interface, but it requires the use of a specific, not commonly known, programming language.

Apart from its technical advantages, the new system also has a better duty cycle. The data acquisition and buffering is done locally on-board the TDC, while transfer of the buffered data to the computer's mass-storage device runs concurrently. This means that there is no acquisition down time. The CAMAC-based system requires a brief pause in the data acquisition while the data are being transferred from the crate controller to the PC.

The main advantage of the new system is related to its mode of data acquisition. It stores each event (*i.e.* the arrival of a logic pulse) in a raw format, by recording the corresponding TDC channel and the time since acquisition start (within 16 ps). The latter is normally based on the on-board clock (having precision of 0.3 ppm), but the use of an external clock is also supported. This way a histogram of the time between consecutive events can be constructed and used to determine the system's dead time. If warranted, the dead time can also be artificially increased in the analysis until the optimum setting is

found. This eliminates the need for repeated measurements with different pre-set dominant dead times, which has been a standard practice with the old system.

The current CAMAC-based system is set to pre-process the events by assigning them to pre-set time-spectrum channels. It then records the collected time spectra rather than individual events. While this reduces the amount of data transferred between the CAMAC controller and the PC, it also results in the loss of detailed information on the time sequence of events. Having the time sequence of events, which is provided by the new system, may prove to be useful in detecting and handling anomalies in the data stream such as sudden bursts of spurious pulses. Furthermore, with the new system, it is possible to select and adjust the number of channels in the decay time spectrum (*i.e.* the channel width) at the time of data analysis. This may be helpful in the case of two-component decays or if impurities contribute significantly to the time spectrum.
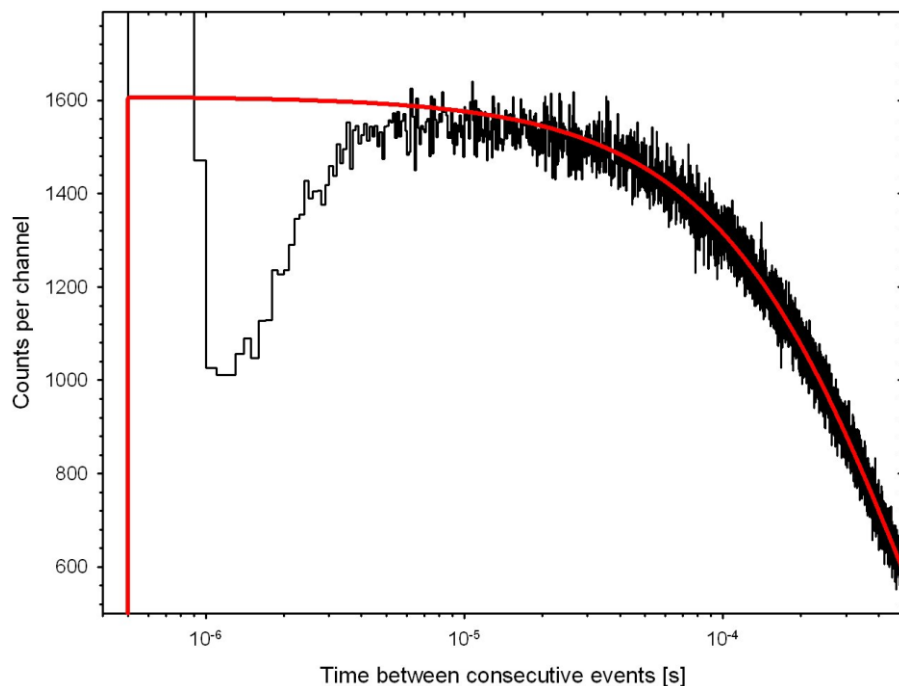
FIG. 1. Measured histogram of the time between consecutive pulses from a detector recording beta particles emitted from a ^{90}Sr-^{90}Y source (black line). The red line shows the expected trend. The cutoff at 0.5 μs is due to the imposed dominant dead time. Excessive counts between 0.5 μs and 0.9 μs are due to multiple pulsing. The dip between 0.9 μs and 10 μs is explained in the text. Note that the vertical scale is linear, while the horizontal scale is logarithmic.

A simplified version of the new data acquisition system was used to record the pulses due to beta particles emitted from a radioactive source (^{90}Sr-^{90}Y). Since the duration of the measurement was much shorter than the source half-life, the histogram of the time between consecutive events was expected to follow an exponential decay curve (with the decay constant equal to the event rate), featuring a sharp cutoff due to the dominant dead time imposed by the NIM gate-and-delay generator and the software. However, the measured histogram showed a smaller-than-expected number of events close to the dead-

time cutoff, as illustrated by Fig. 1. This effect was found to be related to the shape of the analog pulses from the fast filter amplifier, which were subsequently converted to logic pulses by the discriminator: The negative pulses from the fast filter amplifier typically became slightly positive before returning to the base line. Consequently, a pulse that arrived between the crossover time of the previous pulse and its return to the base line was piled up and had a reduced chance of crossing the discriminator threshold, thus decreasing the chance of it being converted to a logical pulse and counted.

[1] L. Chen and J.C. Hardy, *Progress in Research,* Cyclotron Institute, Texas A&M University (2009-2010) p. V-29.

Determination of beam impurities by means of x-ray spectroscopy

V. Horvat and J. C. Hardy

Accurate high-precision measurements of nuclear half-lives require high-purity samples. Consequently, if the samples are prepared by implantation of a radioactive beam of the nuclide of interest, it is important (a) to ensure that the beam is as pure as possible and (b) to have an independent means of assessing quantitatively the actual contributions from contaminants.

For our half-life measurements of superallowed β emitters, we produce radioactive beams by directing a suitable primary heavy-ion beam at a hydrogen target and selecting the desired nuclide from the projectile-like reaction products using the Momentum Achromat Recoil Separator (MARS). However, if another reaction product has a charge-to-mass ratio similar to that of the desired nuclide, it may end up contributing to the secondary beam as an impurity. Currently we assess the contribution from impurities using a position-sensitive detector inserted at the focal plane of MARS. However, this process obviously interrupts the secondary beam, so it is only used on a periodic basis, at the beginning and end of the run, and at most once a day during the run.

Additional purification of the secondary beam is achieved because of the different ranges of the various ions in matter. The secondary beam passes through the MARS exit window, a plastic scintillator, and a series of suitably chosen degraders before reaching the 76-µm-thick tape in which the nuclides of interest are implanted. Because of their different ranges, some impurities are stopped before reaching the tape, while some others pass entirely through the tape.

In order to investigate the feasibility of using x-ray spectroscopy to continuously monitor and
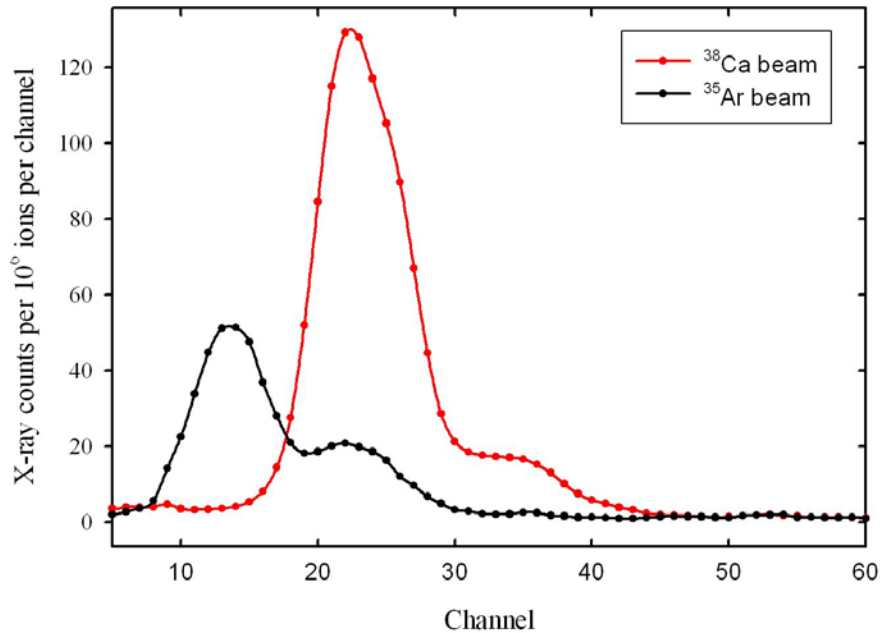
FIG. 1. X-ray spectra collected in the measurements with secondary beams of ^{38}Ca (red circles connected by red line) and ^{35}Ar (black circles connected by black line).

record the amount of impurities in the secondary beam based on their different atomic numbers, a PIN-diode detector was mounted behind the tape and positioned so that, for the most part, it accepts only those x rays that originate from the region near the intersection of the secondary beam and the tape. An example of the x-ray spectrum collected during measurements with a secondary beams of ^{38}Ca (the beam of interest) and ^{35}Ar (a potential impurity) is given in Fig. 1. The primary beam was 30 MeV/u ^{39}K in both cases. The most prominent features in each spectrum are two peaks due mostly to the K_α and K_β x-ray transitions. Note, though, that these transitions originate from atoms with a large variety of electronic configurations and velocities, so that the peak shapes, their centroids and their relative intensities may differ significantly from those observed from single-vacancy ions.

Based on the measured number of secondary-beam particles corresponding to each spectrum in Fig. 1, it was possible to construct a hypothetical background-subtracted spectrum of x rays simulating a secondary beam containing 95% of ^{38}Ca ions and 5% of ^{35}Ar ions. (Actual impurity levels are typically <1%.) The result is shown in Figure 2 (green circles connected with green line). Also shown in Fig. 2 are the separate contributions from each nuclide (red and black line, respectively). While the effect of the impurity on the total x-ray spectrum is relatively small, its contribution can, in principle, be assessed. The precision of the result will depend mostly on the amount of data collected.
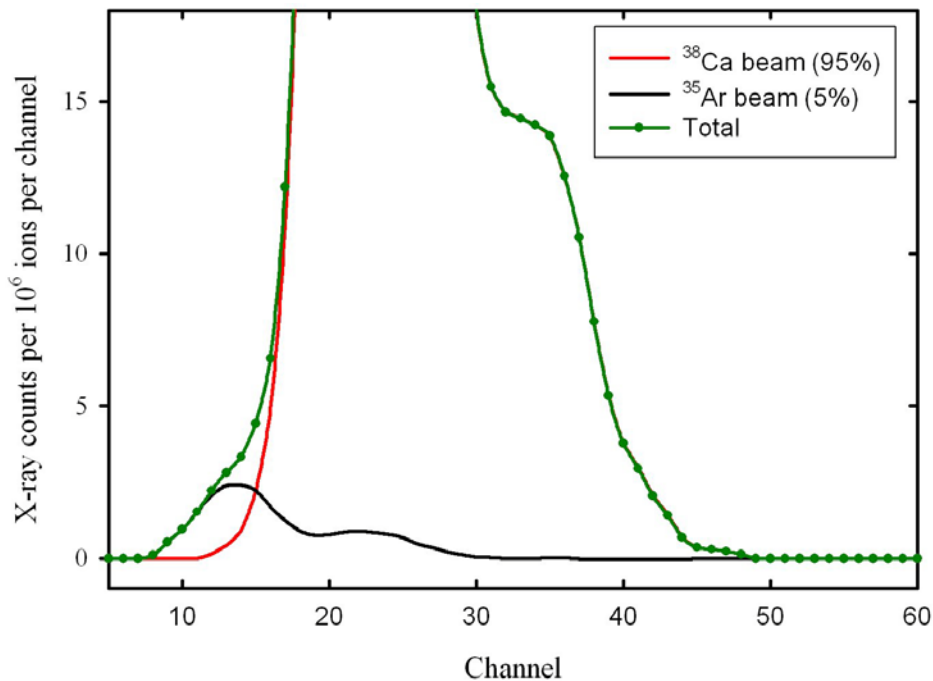
FIG. 2. A hypothetical background-subtracted spectrum of x rays due to a secondary beam containing 95% ^{38}Ca ions and 5% ^{35}Ar ions (green circles connected with green line). Also shown are the separate contributions from each nuclide (red and black line, respectively).

Improved laser determination of source-detector distance for superallowed branching-ratio measurements

L. Chen and J. C. Hardy

The precision of branching ratios extracted from simultaneous measurements of β-γ coincidences and β singles is ultimately limited by how well the absolute efficiency of the γ-ray detector is known. For the decay scheme of a superallowed β emitter with $(T, T_Z) = (1, -1)$, in which each excited level populated in the β-decay daughter subsequently γ decays to the ground state, the branching ratio can be expressed to a first approximation as

$$BR_\gamma = \frac{N_{\beta-\gamma}}{N_\beta \times \varepsilon_\gamma} \qquad (1)$$

where $N_{\beta-\gamma}$ and N_β are the total numbers of observed β-γ coincidences and β singles respectively, and ε_γ is the absolute efficiency for detection of the γ ray. We have already calibrated the absolute efficiency of our HPGe detector to a precision of 0.2% in the energy range 50 keV to 1800 keV and 0.5% up to 3.5 MeV using long-lived sources [1]. However, in the calibration measurements the source-to-detector distance could be controlled to ±0.1 mm, while in a real experiment the source is implanted in a mylar tape, which is positioned in front of the β- and γ-ray detectors by our fast tape-transport system. Being a mechanical system, the tape-transport positions the activity to a lower accuracy. To overcome this limitation, several years ago [2] we upgraded our measurement system by adding a laser-based position sensor, *AccuRange 600-4*, which was, in principal, capable of determining the distance to ± 0.1 mm for distances in the range from 9 to 19 cm. With the distance recorded for each counting cycle, the β-γ coincidence data could then be corrected off-line after the experiment was over.

Unfortunately the laser proved to be quite temperature dependent and its precision was only barely adequate for our branching-ratio measurements. Consequently, we have now installed an improved high-precision laser sensor, an *AccuRange 700* [3], which has 5-μm resolution. This laser sensor has a temperature dependence of only 10 μm per degree Celsius, but nonetheless we now also monitor and record the temperature with a resolution of 0.1 $^{\circ}$C in the cave where the device is located. The laser sensor and temperature monitor are both connected to a PC via an RS232 interface, and during an experiment the position and temperature data can both be taken automatically for each tape cycle. Taking into account the mounting uncertainties and the temperature correction, a precision of 10 μm should be achievable for the tape-detector distance

[1] J.C. Hardy, *et al.*, Int. J. Appl. Radiat. Isot. **56**, 65 (2002), R.G. Helmer, *et al.*, Nucl. Instrum. Methods Phys. Res. **A511**, 360 (2003). R.G. Helmer, *et al.*, Int. J. Appl. Radiat. Isot. **60**, 173 (2004).
[2] V.E. Iacob, V.V. Golovko and J.C. Hardy, *Progress in Research*, Cyclotron Institute, Texas A&M University (2007-2008), p. V-19.
[3] www.acuitylaser.com/AR700

Testing of time of flight diamond detectors at TAMU cyclotron:
31st March - 2nd April 2010

M. A. Bentley,[1] L. Scruton,[1] S. P. Fox,[1] B. S. Nara Singh,[1] F. Schirru,[2] A. Lohstroh,[2] A. Banu,[2]
M. McCleskey, B. R. Roeder, E. Simmons, A. A. Alharbi, and L. Trache

[1]*Department of Physics, University of York, Heslington, York, YO10 5DD, United Kingdom*
[2]*Department of Physics, University of Surrey, Guildford, GU2 7XH, United Kingdom*

A project is under way in the UK, led by the Universities of York and Surrey, to develop diamond detectors for time of flight measurements as part of the LYCCA array (Lund-York-Cologne-Calorimeter), designed to identify and track the many fragments to be generated in the Super FRS at GSI. This array will form part of the NuSTAR project at FAIR, and in particular the HISPEC project which will concentrate on in-beam gamma-ray spectroscopy of exotic fragments at 100 – 200 MeV/u [1].

A commissioning run for the prototype of the LYCCA array, LYCCA-0, is planned to take place toward the end of June 2010 in which diamond detectors (used as start time of flight) shall be tested. In order to be able to distinguish between fragments with mass differences of only 1 u, the timing resolution of the diamond detectors must be less than 100 ps, and preferably close to 50 ps for a flight path of only 3.4 m [2].

Up until the beam time at Texas A&M University (TAMU) cyclotron institute, timing resolutions of, at best, ~300 ps per diamond detector had been attained. This was primarily due to a lack of understanding of how the electronic setup (CFD/leading edge thresholds, bias, PCB's, cables etc.) affected the resolution, as well as the fact that tests could only be made with 20-30 MeV deposited in the detectors in the UK.

The beam time at the cyclotron institute enabled us to take measurements with energy deposits of around 500 MeV in the front detector and 800 MeV in the back detector, which was essential to create pulses with a good signal to noise ratio and is far more like the energies that shall be deposited in the detectors during the HISPEC project. Beam time prior to the commissioning run was vital in order to understand and optimise the electronics associated with fast timing. Diamond detectors have been used as timing detectors before, but never with a surface area as large as that of the LYCCA-0 diamond detectors. It was therefore important to change and test variables in a systematic way so that the principles of their operation could be well understood.

Experimental Setup

Two polycrystalline diamond wafers with dimensions 20 mm x 20 mm x 0.3 mm were placed one above the other onto an impedance-controlled PCB, one wafer having an Aluminium contact, the other a Gold contact. The front contacts of the wafers were divided into four strips of 20 mm x 5 mm, each strip acting as an individual timing detector. An identical PCB with identical diamond wafers and contacts was placed 15 mm behind the first PCB in transmission geometry, inside a vacuum chamber at the end of

the MARS separator. This provided sixteen channels of timing signals which could be used for coincidence measurements between front and back PCBs.

DBA-IV preamplifiers, specially designed for use with diamond, were used to shape and amplify the current pulse from the diamond detectors. This pulse was then sent through a variety of conventional electronic modules, including either leading edge or constant fraction discriminators, before the data was acquired using Caen V1290 TDC.

The detectors were placed in a secondary beam consisting mainly of 35 MeV/u ^{40}Ar and the first front detector pulses, viewed on an oscilloscope outside the cave, looked extremely encouraging. The pulses were large, ~ 2 V, well above the noise which was found to be around 40 mV, and pulse heights varied far less than expected. Pulses from the back detectors did not look quite as high-quality, but a few of the strips were more than good enough to make worth-while coincident measurements between.

Optimum settings were found by systematically increasing the bias on the detectors and lowering the thresholds of the leading edge discriminators and CFD's, something that we have never been able to do before. From initial data analysis, a total timing resolution of 124 ± 12 ps has been measured (Fig. 1), from which, assuming equal contributions, a resolution of 88 ± 11 ps for each detector results. This is far better than any previous tests with these diamond detectors, and is less than 100 ps as desired.
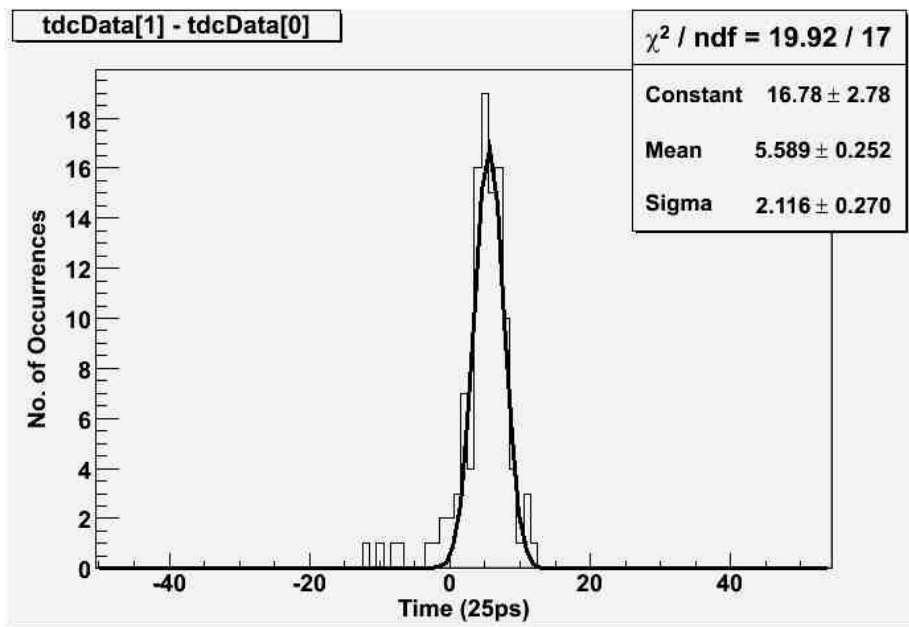
FIG. 1. Histogram of best timing resolution of sigma=2.116, which corresponds to 88 ps for each detector.

The primary beam was then changed to 25 MeV/u ^{20}Ne in order to observe how decreasing the energy deposited in the detectors affects the timing resolution. The data acquired for the first few runs with this beam showed two peaks in the time resolution histogram, separated by ~6 channels, which corresponds to 150 ps (25 ps per channel). It was suggested that this second peak may be caused by the

presence of ^{16}O in the secondary beam. To verify this, MARS settings were changed to eliminate any ^{16}O in the beam, and as expected, the second peak in the time resolution histogram disappeared, suggesting that we were in fact viewing two different species in the beam.

For further confirmation, the beam was adjusted to its original settings and an extra spacer was inserted between the front and back PCB's, increasing the distance from 14.5 mm to 29.5 mm. This should cause the peaks in the time resolution histogram to shift and increase the distance between them by an approximate factor of two. As can be seen in Figs 2(a) and (b), this is exactly what happened. Fig. 2(a) shows the peaks with a 14.5 mm gap between PCB's, and 2(b) shows the peaks with a gap of 29.5
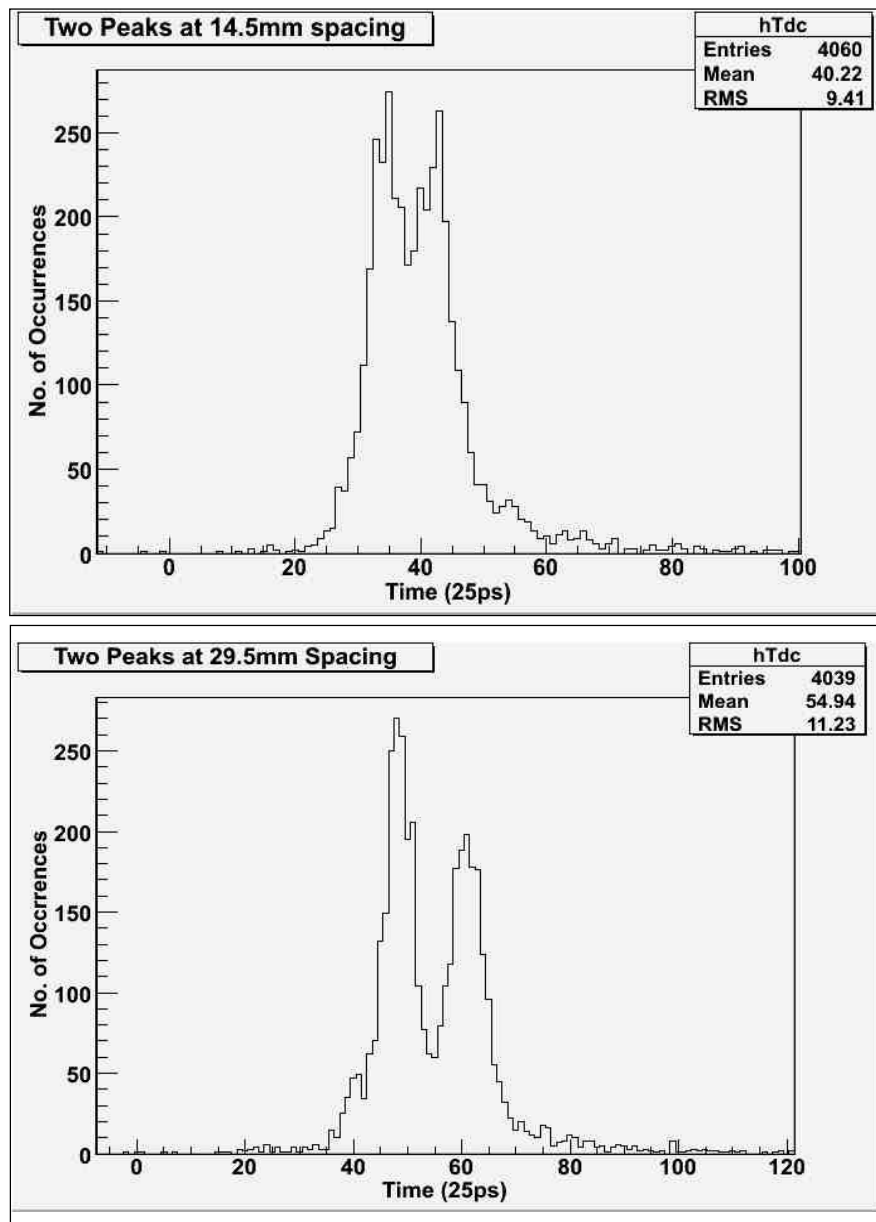
FIG. 2. Timing histograms before and after addition of spacer. (a) Two peaks of O-16 and Ne-20 at 14.5mm spacing. Peaks ~6 channels apart. (b) Same two peaks at 29.5mm spacing. Peaks now ~12 channels apart.

mm. The two peaks clearly separate further in Fig. 2(b), and the distance between these peaks are now found to be ~12 channels (300 ps), which is a factor of two increase as expected.

With proof that the diamond detectors could distinguish between different species within the beam, consideration then had to be made to the fact that both ^{39}Ar and ^{40}Ar were present in the first ^{40}Ar beam. Physical calculations found that the time difference between the two Ar species over a flight path of 14.5 mm would be around 14ps, which wouldn't be distinguishable on the timing histograms, but would certainly cause a widening of the timing peak. It is therefore possible that the timing resolution of the diamond detectors may, in fact, be better than initial analysis indicates.

In conclusion, the beam time at Texas A&M cyclotron institute not only allowed optimum electronic settings to be found and understood, but we were also able to measure sub 100 ps timing resolutions with the diamond detectors (88 ± 11 ps), something we have never been able to obtain prior to these runs. This proves that the diamond detectors will certainly provide a good solution to large area time of flight measurements, which is a major step forward in the project. The detectors were also able to distinguish between ^{20}Ne and ^{16}O over only a 14.5 mm flight path. This is in fact the very first use of time of flight measurements for particle identification using large-area diamond detectors.

[1] D. Rudolph *et al*, *LYCCA – the Lund-York-Cologne-Calorimeter: Identification of reaction products in HISPEC_DESPEC@NuSTAR,* Technical Report V1.2, (June 2009).
[2] M.A. Bentley *et al, Commissioning of the LYCCA Spectrometer: Preparation for exotic nuclear spectroscopy at HISPEC,* GSI Experimental Proposal, (2009).

The Texas-Edinburgh-Catania silicon array (TECSA): a status report

M. McCleskey, B. T. Roeder, L. Trache, A. Banu, S. Cherubini,[1] T. Davinson,[2] V. Goldberg,
C. Spitaleri,[2] R. E. Tribble, and P. J. Woods[2]

[1]*INFN Laboratori Nazionali del Sud & DMFCI Università di Catania, 95123 Catania, Italy.*

[2]*School of Physics and Astronomy, University of Edinburgh, Edinburgh EH9 3JZ, United Kingdom.*

The Texas A&M-Edinburgh-Catania Silicon detector Array (TECSA) is a collaborative effort to build a high-efficiency detector array for reactions involving radioactive ion beams produced in MARS or by the facility upgrade at Texas A&M. The array consists of up to 16 Micron Semiconductor YY1-300 detectors with 8 detectors being used to measure position and energy loss and the other 8 behind in close geometry to measure the residual energy. Each detector has 16 annular ring sectors and is about 300 um thick. TECSA will be useful for measuring reactions of interest for nuclear astrophysics.

In the last year much progress has been made in preparation for the commissioning run with TECSA on MARS, scheduled for May 2010. Two new chambers have been built, one to house the target (henceforth to be referred to as the "TECSA target chamber") and a second for the detector array itself (the "detector chamber"). The new chambers are designed such that they may be bolted to the existing MARS target chamber in either a backwards scattering or forward scattering configuration. The targets are on a holder with a rotating, six position wheel to allow for up to five targets and one target detector. The target detector is a four corner [1] position sensitive detector from Micron, which allows for good position and energy resolution whilst minimizing the number of signals that must be processed. This target detector is in addition to the usual MARS target detector on which initial beam identification and tuning will be performed and will allow precise focusing of the secondary (radioactive) beam so as to minimize the beam spot size at the target and the associated degradation of the angular resolution. The target holder is on a precision linear motion track mounted to a plate in the detector chamber to allow reproducible control of the z-axis position of the target relative to the detector-as well as fixing the x and y position-and thus the angular range of the array.

The current MARS target chamber (Fig. 1) is electrically isolated from the beamline and is grounded to the clean power ground, which is shared by the electronics. The TECSA chambers are on this same ground and are in electrical contact with the MARS target chamber. Each of the detectors used for position and energy (the front 8) is connected to its preamplifier by a standard flat 34 conductor cable. Two 34 pin electrical vacuum feedthrough flanges are mounted on each of the four 6" diameter CF flanges on the detector chamber. Mounting each of the 34 pin feedthroughs on its own flange allows for easy swapping in the event of a vacuum leak in one of the connectors. The preamplifier boxes are mounted directly to these 34 pin feedthrough flanges to that the unamplified signals never have to pass outside shielding and thus to minimize noise pickup and so as to keep the length of the cables from the detectors to the preamplifiers as short as possible. Also on each of the 6" CF flanges on the detector chamber are four Lemo 00 coaxial feedthroughs to be used for the residual energy detectors, the TECSA target position detector and for any other electrical connections that are in the future desired such as, for instance, a thermistor for monitoring detector cooling. A provision for detector cooling has been made-

though not yet implemented- that consists of a set of extended copper detector mounts. A ¼" diameter copper tube may be soldered to these mounts, through which chilled water could be run. A QF25 flange is provided for the supply and return connections.

The electronics arrived from Edinburgh in May 2009. They have since been tested using a pulser and with sources. The setup is basically as follows: They consist of RAL-108 16 channel preamplifiers (one for each YY1-300 detector) whose output goes into RAL-109 shaper-amplifiers [2]. The RAL shaper-amplifiers have both an analog output which is converted by Mesytec VME ADCs and an ECL timing signal output. The ECL output is split between CAEN VME TDCs and an OR module which gives a NIM logic signal for an event in any of the detector strips. This OR signal is sent to a Phillips 756 logic unit where an OR condition is made for all of the strips in all of the detectors. This final OR is used in the master trigger and for the ADC gates. The ADC, TDC and scaler outputs are read using our in-house data acquisition system.

The first test run for TECSA is scheduled for May 2010 and will use a ^{14}C beam at 12MeV/nucleon on a CD_2 target to measure ^{14}C(d,p)^{15}C in inverse kinematics which will be analyzed to extract the ANC for ^{15}C$_{gs}$ which is also being extracted from neutron transfer with heavy ions.
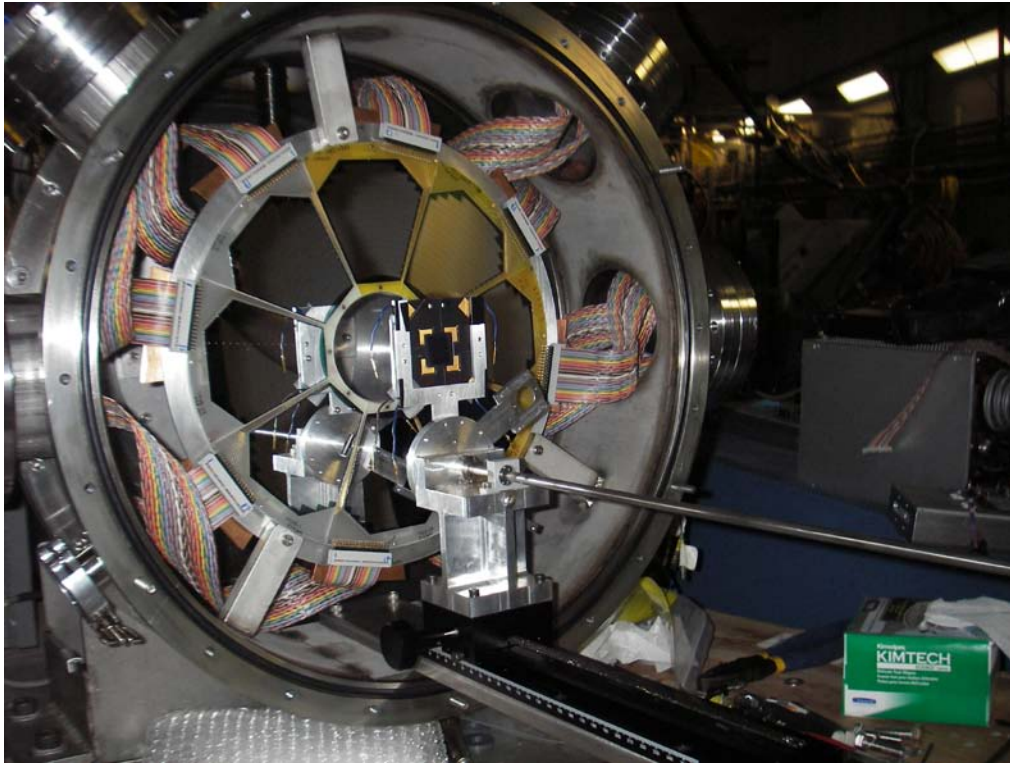
FIG. 1. TECSA with target chamber removed.

[1] A. Banu *et al.*, Nucl. Instrum. Methods Phys. Res. **A593**, 399 (2008).
[2] S.L. Thomas *et al.*, Nucl. Instrum. Methods Phys. Res. **A288**, 212 (1990).

Medical radioisotopes production research program at the Cyclotron Institute, Texas A&M University

A. A. Alharbi, [*] M. McCleskey, A. Spiridon, B. Roeder, E. Simmons, A. Banu, G. Akabani,[1]
V. Bhakta,[1] A. Azzam,[2] L. Trache and R. E. Tribble

[1]*Department of Nuclear Engineering, Texas A&M University, College Station, Texas*
[2]*Faculty of Sciences, Physics Department, Princess Nora Bint Abdulrahman University,*
Riyadh, Saudi Arabia.

Introduction

One of the important applications of cyclotrons is the production of radioisotopes for use in biomedical procedures such as diagnostic imaging and/or therapeutic treatments. An advantage of using the accelerators for medical radioisotope production is the potential of high specific activities. Since the targets and the products are different chemical elements it is possible to find suitable chemical or physical means for separation [1].

Experimental work and setup

At the Cyclotron Institute, Texas A&M University a research program for the study of medical radioisotope production has been started in 2009. Beams of protons and alpha particles extracted from the K500 superconducting cyclotron have been used for the irradiation of metallic targets. The activation
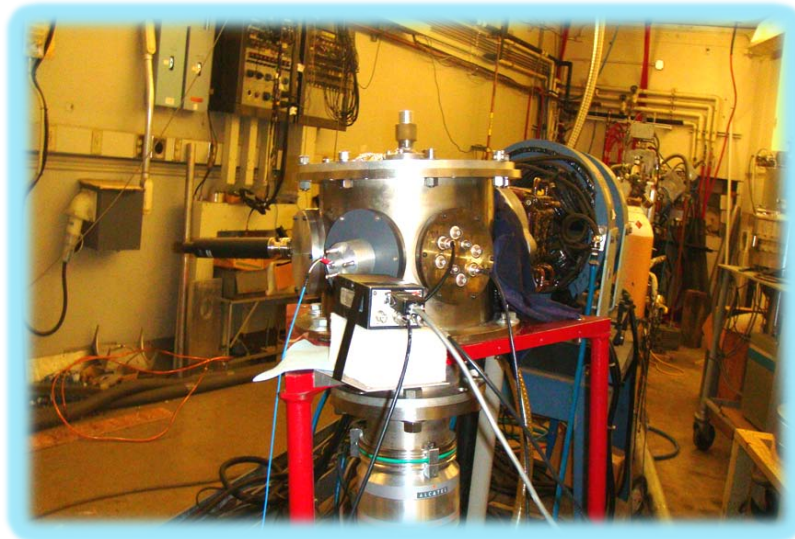
FIG. 1. Experimental setup.

technique has been used for cross-section measurements of the nuclear reactions: $^{nat}Mo(p,x)^{95}Nb$, ^{96}Tc ,^{99}Mo, ^{99m}Tc, $^{nat}Ag(p,x)^{111}In$, and $^{nat}V(\alpha,x)^{51,52}Mn$ which lead to the production of some important medical radioisotopes for diagnostic studies via emission tomography, viz. single photon emission computed tomography (SPECT) and positron emission tomography (PET). Two experiments were carried out to study the alpha emitter radioisotope ^{211}At for therapeutic use (in collaboration with the Nuclear Engineering Department). Table I lists the experiments that we have done to study the production of medical radioisotopes used for imaging, diagnostic as well as therapeutic proposes along with the importance of the studied radioisotope. The irradiations were made using a reaction chamber, which was adapted for the activation purpose (Fig. 1).

TABLE I. The studied nuclear reactions leading to the production of medical radioisotopes that can be used for diagnostic or therapeutic purposes for tumors and some other diseases.

Experiment No.	Projectile	Beam condition	Target	Aim of the work	Medical application
Exp. 1	Protons	@40MeV/u – 40 nA	^{nat}Mo	A study of the yield and the excitation functions for the longer lived medical radioisotopes and the attendant impurities for the production of the 99Mo.	^{96}Tc which is used for animal studies with Tc-99m.
Exp. 2	Alpha particles	@25MeV/u – 100 nA	^{nat}Ag	A detailed study of the yield and the excitation functions for the production of ^{111}In along with the attendant impurities.	^{111}In-Detection of heart transplant rejection, imaging of abdominal infections, antibody labeling, white blood cell imaging, cellular dosimetery, imaging tumors.
Exp. 3	Protons	@40MeV/u – 50 nA	^{nat}Mo	A study for the production of the important diagnostic medical radioisotope ^{99}Tc (relatively short lived) and ^{99}Mo (the generator system) along with some attendant impurities.	^{99}Mo is the parent for ^{99m}Tc generator used for brain, liver, lungs, bones, thyroid, kidney, antibodies, red blood cells and heart imaging.
Exp. 4+5	Alpha particles	@25MeV/u – 150 nA	^{209}Bi	Study the production of the therapeutically medical radioisotope ^{211}At.	^{211}At is used for monoclonal antibody attachment used for cancer treatment (RIT), used with ^{18}F for in vivo studies.
Exp. 6	Alpha particles	@25MeV/u – 50 nA	^{nat}V	A detailed study of the production of the important diagnostic medical radioisotopes ^{51}Mn and ^{52}Mn along with some attendant impurities to identify the optimum condition for the production.	^{51}Mn is used in myocardial localizing agent. ^{52}Mn is used PET scanning.

An aluminum target holder was designed to hold the targets and to act as Faraday cup to measure the beam intensity. We irradiated a stack of several groups of targets along with some monitor foils, which also served as beam degraders (Fig. 2).
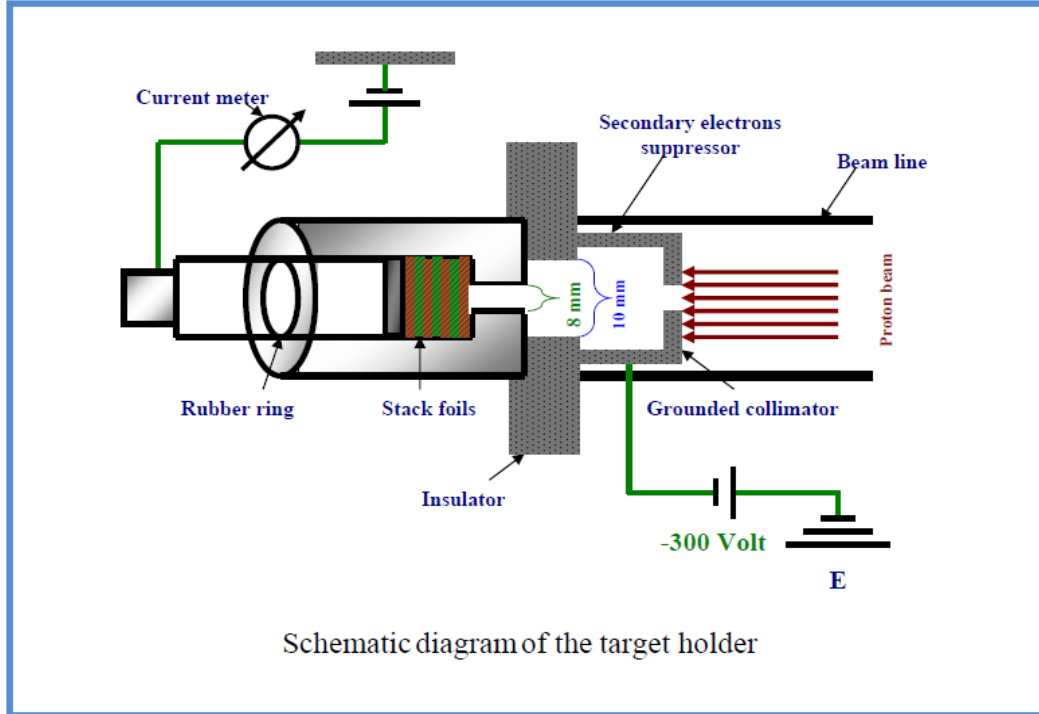
FIG. 2. Schematic diagram of the target holder setup and the faraday cup.

The monitor foils were inserted into each stack simultaneously with the main targets and were analyzed with the same gamma ray spectrometer in a comparable geometry as the targets to confirm the beam intensity and energy. Table II shows the different monitor reactions such as: $^{27}Al(p,x)^{22,24}Na$, $^{nat}Cu(p,x)^{62,63,65}Zn$, $^{nat}Ti(p,x)^{48}V$, $^{nat}Ni(p,x)57Ni$, $^{nat}Ti(\alpha,x)^{51}Cr$, $^{27}Al(\alpha,x)^{22,24}Na$, and $^{nat}Cu(\alpha,x)^{66,67}Ga$, ^{65}Zn that were studied to measure the excitation functions [2].

The chosen irradiation geometry allows the beam to pass through every foil. The secondary effect of the background neutrons on each target was checked by foils placed in the stack far beyond the range of the fully stopped proton beam [3].

The radioactivity of the residual nuclei in the activated foils was measured using one HPGe γ-ray detector (70% relative efficiency). Each foil was recounted after different cooling times to avoid disturbance by overlapping γ-lines from undesired sources and in order to accurately evaluate cross-sections for cumulative formation of the corresponding longer-lived daughter radionuclide. The detector-source distance was kept large enough to keep the dead time below 5% and to assure the same geometry.

From the decay rates of the radioactive products and the measured beam current, the cross sections for the nuclear reactions were determined.

TABLE II. The used monitor reactions.

	Projectile	Targets	Main studied reactions	Energy range (MeV)
Monitor reaction	Protons	^{nat}Ti	^{nat}Ti(p,x)^{48}V	40-5
	Protons	^{nat}Cu	^{nat}Cu(p,x)^{62}Zn	40-12
			^{nat}Cu(p,x)^{63}Zn	40-4
			^{nat}Cu(p,x)^{65}Zn	40-2
	Protons	^{nat}Al	^{27}Al(p,x)^{22}Na	40-25
			^{27}Al(p,x)^{24}Na	40-25
	Protons	^{nat}Ni	^{nat}Ni(p,x)^{57}Ni	40-12
	Alpha particles	^{nat}Ti	^{nat}Ti(α,x)^{51}Cr	100-5
	Alpha particles	^{nat}Al	^{27}Al(α,x)^{22}Na	100-30
			^{27}Al(α,x)^{24}Na	100-30
	Alpha particles	^{nat}Cu	^{nat}Cu(α,x)^{66}Ga	100-8
			^{nat}Cu(α,x)^{67}Ga	100-11
			^{nat}Cu(α,x)^{65}Zn	100-11

The excitation functions of the studied reactions were constructed using the well known staked foil technique [4]. Then the determined excitation functions will be compared with the simulated calculations using TALYS and ALICE-IPPE codes and with the available previous published research [5]. The thick target yields for the production of the required isotopes as well as their impurities will be estimated from the cross section data.

The data analyses for the studied reactions are progressing. We will continue the program with further irradiations for different targets using 32 MeV/u ^{3}He particles.

[1] S. M. Qaim, *Use of cyclotron in medicine*, Rad. Phys. and Chem. **71**, 917 (2004).
[2] F. Tarkany *et al.*, *Beam Monitor Reactions*, IAEA-TECDOC-1211, (IAEA, Vienna, 2001) p. 49.
[3] J.F. Ziegler *et al.*, SRIM 2003 code, the stopping and Range of Ions in Solids (Pergamon, New York, 2003).
[4] F. Helus, Lelio G. Colombetti, *Radionuclides Production*, CRC Press Inc., (Boca Raton, Florida, 1980)
[5] K. Gul *et al.*, IAEA-TECDOC-1211, IAEA, Vienna, Austria (2001).

Production of the alpha particle emitting radionuclide [211]At for targeted radionuclide therapy

G. Akabani,[1] A. A. Alharbi,[*] V. Bhakta,[1] C. M. Folden III, A. Spiridon, and R. E. Tribble

[1]*Department of Nuclear Engineering, Texas A&M University, College Station, Texas*

Alpha particle radioimmunotherapy is considered to be a potentially powerful strategy to eradicate disseminated tumor cells and small clusters of metastases. Whereas solid tumors and large metastases can be treated with surgery and external beam radiation, radioimmunotherapy holds the promise to treat the infiltrating tumor and metastatic microclusters [1,2]. The promising results so far observed for the treatment of lymphoma tumors provide a reasonably expectation that radionuclide therapy, and specifically alpha particle emitting radioimmunotherapy, will be an effective strategy for the treatment of disseminated disease from solid tumors, including clinically indiscernible micro-metastases [3-6]. The beta particle emitting radionuclides ^{131}I and ^{90}Y have been used preferentially for their commercial availability and distribution and easy radiolabeling methods. However, beta particle emitting radionuclides generate low LET particles (~ 0.3 keV/µm for electrons) and their corresponding radiobiological effectiveness depends upon cumulated activity concentration, total absorbed dose and dose rate. On the other hand, alpha particle emitting radionuclides have significant radiobiological advantages. Alpha particles have a high LET (~ 100 keV/µm), the range of these alpha particles is less than 100 µm in tissue, which allows for a highly localized dose to tumors while sparing normal tissues [7,8]. Furthermore, the radiobiological effect of alpha particles is dose rate independent. Thus, the use of alpha particle emitting radionuclides carries a significant therapeutic potential for the treatment of minimal residual disease and metastatic micro-clusters.

The production of alpha particle emitting radionuclides remains difficult and dependent upon the availability of either generators or proximity to a cyclotron for direct production. Among all alpha particle emitting radionuclides, At-211 is one of the most promising for use in radionuclide therapy [9]. It has a high carrier free specific activity of 76 GBq/µg with a favorable decay scheme and a half-life of 7.214 h, which is sufficient for labeling, dispensing and administering the radiolabeled compound. The radionuclide [211]At has a α-branching of 41.80% decaying into [207]Bi and the remaining 58.20%, although decaying by EC, leads to the ultra-short-lived α-emitter Po-211g with a half-life of 516 ms and a α-branching of 100%. Therefore, the overall α-branching of [211]At/[211g]Po is 100%. The range alpha particle energies produced by the decay of [211]At are less than 70 µm in water (see Table I) with a nominal LET between 100 and 130 keV/µm, which is about the maximum relative biological effectiveness (RBE) for heavy ions. In this report we present the production methods and results for the alpha particle emitting radionuclide [211]At via the [209]Bi(α,2n) reaction.

---

[*]Fulbright Fellow 2009, On leave from Physics Department, Faculty of Sciences, Princess Nora Bint Abdulahman University, Riyadh, Saudi Arabia

TABLE I. Alpha particle energies and intensities emitted by the decay of At-211.

Alpha Particle Energy (MeV)	Intensity (%)	Range in Water (μm)	Approximate # of Cell Diameters
5.87	41.94	47.98	3.2
6.57	0.337	57.26	3.8
6.89	0.325	61.78	4.1
7.45	57.4	69.92	4.7

Experimental Design and Data Evaluation

The reaction ^{209}Bi(α,x) carries multiple open channels as a function of alpha particle energy (see Table II) and, therefore, the alpha particle beam energy produced by the K500 cyclotron required to be

TABLE II. Open channels of an alpha particle beam on a bismuth target (Bi-209, 99.995+ % purity).

Reaction product	Half-life, $T_{1/2}$	Open Channel	Q (MeV)
^{207}At	1.8 h	^{209}Bi(α,6n)	-51.02
^{208}At	1.63 h	^{209}Bi(α,5n)	-43.7
^{209}At	5.41 h	^{209}Bi(α,4n)	-35.29
^{210}At	8.1 h	^{209}Bi(α,3n)	-28.07
^{211}At	7.214 h	^{209}Bi(α,2n)	-20.33
^{212g}At	0.3124 s	^{209}Bi(α,n)	-15.29
^{212m}At	0.119 s	^{209}Bi(α,n)	-15.51
^{210}Po	138.37 d	^{209}Bi(α,p2n)	-23.31

degraded from its initial energy of 80 MeV to energies below 30 MeV using nine foils in order to avoid the production of unwanted radionuclides (see Fig. 1). The beam energy of 80 MeV was selected in order to obtain the maximum intensity of the beam. The order of the foils, their corresponding thicknesses, and energy degradation were estimated using the computer code Lise++ (see Table III). A final 500-µm thick metallic ^{209}Bi foil was used, and the particle currents used in both experiments were approximately 165 and 96 nA, respectively, which did not pose a problem in heat dissipation as higher currents can melt the ^{209}Bi target. Moreover, the cupper foils were used to monitor the beam intensity and energy.
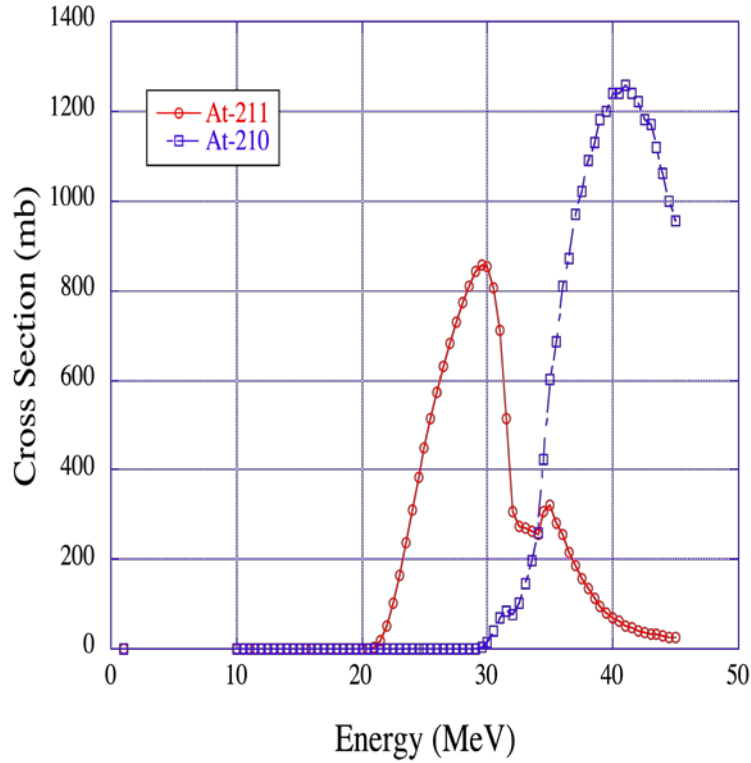
FIG. 1. Evaluated cross section for the reactions $^{209}Bi(\alpha,3n)^{210}At$ and $^{209}Bi(\alpha,2n)^{211}At$ as a function of alpha particle energy. The cross sections were evaluated using the program Talys.

TABLE III. Implemented stack foil order used for energy degradation and monitoring. The initial energy of the alpha particle beam was 80 MeV and it was degraded to a final energy of approximately 28.1 and 25.7 MeV for the two experiments, respectively. The residual energy of the alpha particle beam was estimated using the computer code Lise++.

Number	Foil	Thickness (μm)	E_{in} (MeV)	E_{out} (MeV)	E_{loss} (MeV)	Thickness (μm)	E_{in} (MeV)	E_{out} (MeV)	E_{loss} (MeV)
1	Cu	100.0	80.0	74.1	5.9	100.0	80.0	74.1	5.9
2	Cu	100.0	74.1	67.7	6.3	100.0	74.1	67.7	6.3
3	Cu	100.0	67.7	61.0	6.8	100.0	67.7	61.0	6.8
4	Cu	100.0	61.0	53.6	7.4	100.0	61.0	53.6	7.4
5	Cu	100.0	53.6	45.3	8.2	100.0	53.6	45.3	8.2
6	Cu	100.0	45.3	35.8	9.5	100.0	45.3	35.8	9.5
7	Al	127.0	35.8	30.4	5.3	127.0	35.8	30.4	5.3
8	Al	50.0	30.4	28.1	2.3	127.0	30.4	25.7	4.8
9	Bi	500.0	28.1	0.0	28.1	500.0	25.7	0.0	25.7

Results

The initial experimental run using a degraded nominal energy of 28 MeV resulted in the substantial production of the contaminant [210]At, even though our calculations predicted that the production of [210]At should be minimal or negligible. The average yield of [210]At was 0.83 MBq/μA-h. This can be attributed to the broad energy spectrum of the alpha particle beam, with an initial energy of 80 MeV, which could spread about ± 4 MeV after degradation. This effect was corroborated when our second experiment was carried out using a lower nominal energy of 25 MeV. In this experiment, the production of [210]At was not observed. The estimated [211]At production yields from both experiments were 34.5 and 12.9 MBq/μA-h, which are in accordance to those results published in the open literature of around 30 MBq/μA-h.

Conclusions

Based on these initial experiments we successfully produced [211]At with no major impurities using a high purity Bismuth target (99.995%). There were neither physical deformation nor melting of the bismuth foil at the beam currents used in these experiments, which will allow us to proceed to activate bismuth nanoparticles for further studies in radioimmunotherapy.

[1] W.A. Volkert and T.J. Hoffman, Chem. Rev. **99**, 2269 (1999).

[2] M.T. Ercan and M. Caglar, Curr. Pharm. Des. **6**, 1085 (2000).

[3] A.V. Rao, G. Akabani *et al.*, Clin. Med. Res. **3** ,157 (2005).

[4] R.L. Wahl, J. Nucl. Med. **46** Suppl. 1, 128S (2005).

[5] H.A. Jacene, R. Filice *et al.*, J. Nucl. Med. **48**, 1767 (2007).

[6] H. Song, Y. Du *et al.*, J. Nucl. Med. **48**, 150(2007).

[7] G. Akabani, S. Carlin *et al.*, Nucl. Med. Biol. **33**, 333 (2006).

[8] M.R. Zalutsky, D. A. Reardon *et al.*, J. Nucl. Med. **49**, 30 (2008).

[9] G. Henriksen, S. Messelt, *et al.*, Appl. Radiat. Isot. **54**, 839 (2001).

SECTION VI

PUBLICATIONS

PAPERS PUBLISHED
April 1, 2009 – March 31, 2010

Elastic and inelastic scattering to low-lying states of ^{58}Ni and ^{90}Zr using 240 MeV ^{6}Li, Krishichayan, X. Chen, Y.-W. Lui, Y. Tokimoto, J. Button, and D.H. Youngblood, Phys. Rev. C **81**, 014603 (2010).

Isoscalar giant resonance strength in ^{24}Mg, D.H. Youngblood, Y.-W. Lui, X.F. Chen, and H.L. Clark, Phys Rev C **80**, 064318 (2009).

Giant resonance in ^{24}Mg and ^{28}Si from 240 MeV ^{6}Li scattering, X. Chen, Y.-W. Lui, H.L. Clark, Y. Tokimoto, and D.H. Youngblood, Phys. Rev. C **80**, 014312 (2009).

Stellar reaction rate for ^{22}Mg+$p \rightarrow$ ^{23}Al from the asymptotic normalization coefficient in the mirror nuclear system ^{22}Ne+$n \rightarrow$ ^{23}Ne, T. Al-Abdullah, X. Chen, H.L. Clark, C. Fu, C.A. Gagliardi, Y.-W. Lui, A. Mukhamedzhanov, G. Tabacaru, Y. Tokimoto, L. Trache, and R.E. Tribble, Phys. Rev. C **81**, 035802 (2010).

A novel approach to measure the cross section of the ^{18}O(p,α)^{15}N resonant reaction in the 0-200 keV energy range, M. La Cognata, C. Spitaleri, A. Mukhamedzhanov, A. Banu, S. Cherubini, A. Coc, V. Crucilla, V. Goldberg, S. Romano, M.L. Sergi, G. Tabacaru, L. Trache, R.E. Tribble, W. Trzaska, and A. Tumino, Astrophys. J. **708**, 796 (2010).

Improved determination of the astrophysical S(0) factor of the ^{15}N(p,α)^{12}C reaction, M.La Cognata, V.Z. Goldberg, A.M. Mukhamedzhanov, C. Spitaleri, R.E. Tribble, Phys. Rev C **80**, 012801(R) (2009).

Complete correlation studies of two-proton decays: ^{6}Be and ^{45}Fe, L.V. Grigorenko, T.D. Wiser, K. Miernik, R.J. Charity, M. Pfützner, A. Banu, C.R. Bingham, M. Cwiok, I.G. Darby, W. Dominik, J.M. Elson, T. Gintner, R. Grzywacz, Z. Janas, M. Karny, A. Korgul, S.N. Liddick, K. Mercurio, M. Rajabali, K. Rykaczewski, R. Shane, L.G. Sobotka, A. Stolz, L. Trache, R.E. Tribble, A. Wuosmaa, M.V. Zhukov, Phys. Lett. B **677**, 30 (2009).

Continuum spectroscopy with a ^{10}C beam: cluster structure and three-body decay, R.J. Charity, T.D. Wiser, K. Mercurio, R. Shane, L.G. Sobotka, A.H. Wousmaa, A. Banu, L. Trache, R.E. Tribble, Phys. Rev. C **80**, 024306 (2009).

Three-body decay of ^{6}Be, L.V. Grigorenko, T.D. Wiser, K. Mercurio, R.J. Charity, R. Shane, L.G. Sobotka, J.M. Elson, A.H. Wuosmaa, A. Banu, M. McCleskey, L. Trache, R.E. Tribble, M.V. Zhukov, Phys. Rev. C **80**, 034602 (2009).

Astrophysical S factor for the radiative capture ^{12}N(p,γ)^{13}O determined from the ^{14}N(^{12}N,^{13}O)^{13}C proton transfer reaction, A. Banu, T. Al-Abdullah, C. Fu, C.A. Gagliardi, R.E. Tribble, Y. Zhai, F. Carstoiu, V. Burjan, and V. Kroha, Phys Rev C **79**, 025805 (2009).

Extreme α-clustering in the ^{18}O nucleus, E.D. Johnson, G.V. Rogachev, V.Z. Goldberg, S. Brown, D. Robson, A.M. Crisp, P.D. Cottle, C. Fu, J. Giles, B.W. Green, K.W. Kemper, K. Lee, B.T. Roeder, and R.E. Tribble, Eur. Phys. J. A **42**, 10887 (2009).

Probing the standard model with superallowed nuclear beta decay, J.C. Hardy and I.S. Towner in *Karlsruher Nuklidkarte: Commemoration of the 50th Anniversary*, ed: G. Pfennig, C. Normand, J. Magill and T. Fanghanel (Publications of the European Communities, Luxembourg, 2008) pg. 116.

New calculations of the isospin-symmetry-breaking correction to superallowed Fermi beta decay, I.S. Towner and J.C. Hardy in *Rare Isotopes and Fundamental Symmetries*, Proceedings from the Institute for Nuclear Theory – Vol. 16, (World Scientific, 2009) pg. 51.

Superallowed nuclear beta decay: recent results and their impact on V$_{ud}$, J.C. Hardy and I.S. Towner in *Rare Isotopes and Fundamental Symmetries*, Proceedings from the Institute for Nuclear Theory – Vol. 16, (World Scientific, 2009) pg. 41.

Superallowed beta decay: the role of nuclear structure in standard-model tests, J.C. Hardy and I.S. Towner, Acta Physica Polonica B **40**, 675 (2009).

Superallowed $0^+ \rightarrow 0^+$ nuclear β Decays: a new survey with precision tests of the conserved vector current hypothesis and the standard model, J.C. Hardy and I.S. Towner, Phys. Rev. C **79**, 055502 (2009).

Half-life of the electron-capture decay of ^{97}Ru: precision measurement shows no temperature dependence, J.R. Goodwin, V.V. Golovko, V.E. Iacob and J.C. Hardy, Phys. Rev. **C 80**, 045501 (2009).

Further test of internal conversion theory with measurement in ^{197}Pt, N. Nica, J.C. Hardy, V.E. Iacob, J. Goodwin, C. Balonec, M. Hernberg and J. Nolan, Phys. Rev. C **80**, 064314 (2009).

Q$_{ec}$ values of the superallowed β emitters ^{34}Cl And ^{38}K^{m}, T. Eronen, V.-V. Elomaa, J. Hakala, J.C. Hardy, A. Jokinen, I.D. Moore, M. Reponen, J. Rissanen, A. Saastamoinen, C. Weber and J. Aysto, Phys. Rev. Lett. **103**, 252501 (2009).

The Status of V$_{ud}$, J.C. Hardy and I.S. Towner in *10th International Conference on the Intersections of Particle and Nuclear Physics*, edited by M.L. Marshak, AIP Conference Proceedings **1182**, 352 (2009).

The evaluation of V_{ud} and its impact on the unitarity of the Cabibbo-Kobayashi-Maskawa quark-mixing matrix, I.S. Towner and J.C. Hardy, Rep. Prog. Phys **73**, 046301 (2010).

β-delayed proton decay of proton-rich nuclei ^{23}Al and ^{31}Cl and explosive H-burning in classical novae, L. Trache, A. Banu, J.C. Hardy, V.E. Iacob, M. McClesky, E. Simmons, G. Tabacaru, R.E. Tribble, J. Aysto, A. Jokinen, A. Saastamoinen, M.A. Bently, D. Jenkins, T. Davinson, P.J. Woods, N.L. Achouri and B, Roeder in Proceedings of *10th Symposium on Nuclei in the Cosmos*, PoS(NiC X)163 (2009).

Nuclear data sheets for A=84, Daniel Abriola, Melih Bostan, Sefa Erturk, Manssour Fadil, Monica Galan, Sakari Juutinen, Tibor Kibédi, Filip Kondev, Aurelian Luca, Alexandru Negret, Ninel Nica, Bernd Pfeiffer, Balraj Singh, Alejandro Sonzogni, Janos Timar, Jagdish Tuli, Tsanka Venkova and Kazimierz Zuber, Nuclear Data Sheets **110,** 2815 (2009).

Nuclear data sheets for A=147, N. Nica, Nuclear Data Sheets **110**, 749 (2009).

Nuclear data sheets for A = 97, N. Nica, Nuclear Data Sheets **111**, 525 (2010).

Schottky mass measurement of the ^{208}Hg isotope: implication for the proton-neutron interaction strength around doubly-magic ^{208}Pb, L. Chen *et al.*, Phys. Rev. Lett. **102**, 122503 (2009).

New high-precision measurement of the reaction rate of the O-18(p, alpha)N-15 reaction via THM, M. La Cognata, C. Spitaleri, A.M. Mukhamedzhanov, B. Irgaziev, R.E. Tribble, A. Banu, S. Cherubini, A. Coc, V. Crucilla, V.Z. Goldberg, M. Gulino, G.G. Kiss, L. Lamia, Chengbo Fu, J. Mrazek, R.G. Pizzone, S.M.R. Puglia, G.G. Rapisarda, S. Romano, M.L. Sergi, G. Tabacaru, L. Trache, W. Trzaska, A. Tumino, Pub. Astron. Soc. Australia **26**, 237 (2009).

Nuclear physics for astrophysics with radioactive beams: indirect methods, L. Trache, in Proceeding of *2nd International Conference on Current Problems in Nuclear Physics and Atomic Energy,* Kyiv, Ukraine (June 2008), pg. 21.

Breakup of proton-rich nuclei ^{24}Si, ^{23}Al, ^{22}Mg, ^{21}Na at intermediate energies for reaction rates in explosive H-burning in novae. A. Banu, L. Trache, R.E. Tribble, F. Carstoiu, F. Negoita, F. Rotaru, N. Orr, L. Achouri, B. Laurent, B. Roeder, M. Chartier, B. Fernandez-Dominguez, S. Paschalis, B. Pietras, P. Roussel-Chomaz, L. Gaudefroy, R. Lemmon, M. Labiche, W. Catford, N. Patterson, J. Thomas, M. Freer, M. Horoi, A. Bonaccorso in Proceeding of *10th Symposium on Nuclei in the Cosmos,* PoS (NIC X) 052 (2009).

Mass of ^{23}Al for testing the isobaric multiplet mass equation, A. Saastamoinen, T. Eronen, A. Jokinen, V.-V. Elomaa, J. Hakala, A. Kankainen, I.D. Moore, S. Rahaman, J. Rissanen, C. Weber, J. Aysto, L. Trache, Phys. Rev. **C** 80, 044330 (2009).

Lifetime effects for high-resolution gamma-ray spectroscopy at relativistic energies and their implications for the RISING spectrometer, P. Doornenbal, P. Reiter, H. Grawe, T. Saito, A. Al-Khatib, A. Banu *et al.*, Nucl. Instrum. Methods Phys. Res. **A613**, 218 (2010).

Photoneutron cross sections for ^{96}Zr: a systematic experimental study of photoneutron and radiative neutron capture cross sections for zicronium isotopes, H. Utsunomiya, S. Goriely, H. Akimune, H. Harada, F. Kitatani, S. Goko, H. Toyokawa, K. Yamada, T. Kondo, O. Itoh, M. Kamata, T. Yamagata, Y.-W. Lui, S. Hilaire, and A.J. Koning, Phys. Rev. C **81**, 035801 (2010).

γ-ray strength function for ^{116,117}Sn with the pygmy dipole resonance balanced in the photoneutron and neutron capture channels, H. Utsunomiya, S. Goriely, M. Kamata, T. Kondo, O. Itoh, H. Akimune, T. Yamagata, H. Toyokawa, T. Kaihori, A. Makinaga, S. Goko, H. Akimune, T. Yamagata, H. Toyokawa, Y.-W. Lui, S. Hilaire, and A.J. Koning, Phys. Rev. C **80**, 055806 (2009).

Precision test of the isobaric multiplet mass equation for the A=32, T=2 qunitet, A.A. Kwiatkowski, B.R. Barquest, G. Bollen, C.M. Campbell, D.L. Lincoln, D.J. Morrissey, G.K. Pang, A.M. Prinkle, J. Savory, S. Schwarz, C.M. Folden III, D. Melconian, S.K.L. Sjue, and M. Block, Phys. Rev. C **80**, 051302(R) (2009).

Lineshape Analysis of Doppler-Broadened γ-lines following the β-decay of ^{11}Li, C.M. Mattoon, F. Sarazin, C. Andreyev, R.A.E. Austin, G.C. Ball, R.S. Chakrawarthy, D. Cross, E.S. Cunningham, J. Daoud, P.E. Garrett, G.F. Grinyer, G. Hackman, D. Melconian, C. Morton, C. Pearson, J.J. Ressler, J. Schwarzenberg, M.B. Smith, and C.E. Svensson, Phys. Rev. C **80**, 034318 (2009).

Characterization of thin-foil ultracold neutron detectors, B.A.L. Sallaska, S. Hoedl, A. Garcia, D. Melconian, A.R. Young, P. Geltenbort, S.K.L. Sjue, and A.T. Holley, Nucl. Instrum. Methods Phys. Res. **A603**, 421 (2009).

β–decay correlation studies using very cold, highly polarized sources, D. Melconian, Rev. Mex. Fis. **55**, 81 (2009).

A dual axis dual lateral position sensitive detector for charged particle detection, S.N. Soisson, B.C. Stein, L.W. May, R.Q. Dienhoffer, M. Jandel, G.A. Souliotis, D.V. Shetty, S. Galanopolous, A.L. Keksis, S. Wuenschel, Z. Kohley, S.J. Yennello, M.A. Bullough, N.M. Greenwood, S.M. Walsh, and C.D. Wilburn. Nucl. Instrum. Methods Phys. Res. **A613**, 240 (2010).

Isoscaling for Z=1-17 in reconstructed quasi-projectiles, S. Wuenschel, R. Dienhoffer, G.A. Souliotis, S. Galanopoulos, Z. Kohley, K. Hagel, D.V. Shetty, K. Huseman, L.W. May, S.N. Soisson, B.C. Stein, A.L. Caraley, and S.J. Yennello, Phys. Rev. C **79**, 061602 (R) (2009).

Isoscaling of mass A~40 reconstructed quasiprojectiles from collisions in the Fermi energy regime, S. Galanopoulos, G.A. Souliotis, A.L. Keksis, M. Veselsky, Z. Kohley, L.W. May, D.V. Shetty, S.N. Soisson, B.C. Stein, S. Wuenschel, S.J. Yennello, Nucl. Phys. **A837**, 145 (2010).

Statistical and dynamical aspects in the decay of hot neutron-rich nuclei, M. Veselsky, G.A. Souliotis, A.L. Keksis, M. Jandel, D.V. Shetty, S.J. Yennello, K. Wang, Y.G. Ma, Nucl. Phys. **A837**, 163 (2010).

NIMROD-ISiS, A versatile tool for studying the Isotopic Degree of Freedom in Heavy Ion Collisions, S. Wuenschel, K. Hagel, R. Wada, J.B. Natowitz, S.J. Yennello, Z. Kohley, C. Bottosso, L. W. May, W.B. Smith, D.V. Shetty, B.C. Stein, S.N. Soisson, Nucl. Instrum. Methods Phys. Res. **A604**, 578 (2009).

Laboratory studies of low density matter, L. Qin, J.B. Natowitz, G. Roepke, K. Hagel, R. Wada, Z. Chen, M. Hung, S. Kowalski, C. Bottosso, S. Shlomo, M. Barbui, A. Bonasera, M. Rodriques, D. Fabris, M. Lunardon, S. Moretto, G. Nebbia, S. Pesente, V. Rizzi, G. Viesti, M. Cinausero, G. Pete, T. Keutgen, Y. El Marsi, and Z. Majka, Nucl. Phys. **A834**, 521c (2010).

Electron screening effects on alpha-decay, A. Musumarra, F. Farinon, C. Nociforo, ..A. Bonasera *et al*., International Conference on Nuclear Structure and Dynamics '09, AIP Conference Proceedings **1165**, 415 (2009).

Energy loss of energetic Ar-40, Kr-84, Au-197 and U-238 ions in mylar, aluminum and isobutane, M. Barbui, D. Fabris, M. Lunardon *et al.*, Nucl. Instrum. Methods Phys. Res. **B268**, 20 (2010).

New experimental: approach for heavy and super-heavy element production, M. Barbu, T. Materna, P. Sahu *et al.*, International J. Mod. Phys. E **18**, 1036 (2009).

Elemental analysis of light constituents in thin plastic films, Y. El Masri, C. Heitz, T. Keutgen *et al.*, Nucl. Instrum. Methods Phys. Res. **B267**, 1158 (2009).

Asymptotic normalization coefficient and important astrophysical process ^{15}N(p,γ)^{16}O, A.M. Mukhamedzhanov, A. Banu, P. Bem, V. Burjan, C.A. Gagliardi, V.Z. Goldberg, Z. Hons, V. Kroha , M. La Cognata, S. Piskor, R.G. Pizzone, S. Romano, E. Simeckova, C. Spitaleri, L. Trache, and R.E. Tribble, J. Phys. Conf. Series (Nuclear Physics in Astrophysics IV) **202**, 012017 (2010).

Indirect measurement of ^{17}O(p,α)^{14}N cross section at ultra-low energies, A.M. Mukhamedzhanov, A. Banu, P. Bem, V. Burjan, C.A. Gagliardi, V.Z. Goldberg, Z. Hons, V. Kroha , M. La Cognata, S. Piskor, R.G. Pizzone, S. Romano, E. Simeckova, C. Spitaleri, L.Trache, and R.E. Tribble, J. Phys. Conf. Series (Nuclear Physics in Astrophysics IV) **202**, 012021 (2010).

First measurement of the $^{18}O(p,\alpha)^{15}N$ cross section at astrophysical energies, M. La Cognata, C. Spitaleri, A.M. Mukhamedzhanov, R.E. Tribble, T. Al-Abdullah, A. Banu, S. Cherubini, A. Coc, V. Crucillμa, V.Z. Goldberg, M. Gulino, B. Irgaziev, G.G. Kiss, L. Lamia, J. Mrazek, R.G. Pizzone, S.M.R. Puglia, G.G. Rapisarda, S. Romano, M.L. Sergi, G. Tabacaru, L. Trache, W. Trzaska, S. Tudisco, and A. Tumino, J. Phys. Conf. Series (Nuclear Physics in Astrophysics IV) **202**, 012019 (2010).

The inhomogeneous Schrödinger equation for the off_shell wave function, B.F. Irgaziev, A.M. Mukhamedzhanov, and Yu.V. Orlov, Bulletin of the Russian Academy of Sciences: Physics, **73**, 773 (2009) [Izvestiya Rossiiskoi Akademii Nauk. Seriya Fizicheskaya, **73**, 814. (2009), in Russian].

Generalisation of scattering theory to charged particles, S. Kadyrov, I. Bray, A.M. Mukhamedzhanov, and A.T. Stelbovics, J. Phys. Conf. Series **185**, 0120179 (2009).

Unified theory of scattering for arbitrary potentials, S. Kadyrov, I. Bray, A. M. Mukhamedzhanov, and A.T. Stelbovics in *Few-body problems in Physics*, Proc. of the 3rd Asia-Pacific Conf. (World Scientific, 2009) pg. 283.

Surface-integral formulation of scattering theory, A.S. Kadyrov, I. Bray, A.M. Mukhamedzhanov, A.T. Stelbovics, Ann. Phys. **324**, 1516 (2009).

Surface-integral approach to the Coulomb few-body scattering problem, A.S. Kadyrov, I. Bray, A.M. Mukhamedzhanov, A.T. Stelbovics, Eur. Phys. J. Web of Conf. **3**, 04014 (2010).

Scattering theory with the Coulomb potential, A.S. Kadyrov, I. Bray, A.M. Mukhamedzhanov, A.T. Stelbovics, J. Phys. Conf. Ser. **194**, 012017 (2009).

Generalisation of scattering theory to charged particles, A.S. Kadyrov, I. Bray, A.M. Mukhamedzhanov, A.T. Stelbovics, J. Phys. Conf. Ser. **185**, 012017 (2009).

Effects of distortion of the intercluster motion in ^2H, ^3He, ^3H, ^6Li, and ^9Be on Trojan horse applications, R.G. Pizzone, C. Spitaleri, A.M. Mukhamedzhanov, L.D. Blokhintsev, C.A. Bertulani, B. F. Irgaziev, M. La Cognata, L. Lamia, and S. Romano, Phys. Rev. C **80**, 025807 (2009).

Surface-integral excitation of compound states in the subsystems as indirect tool in nuclear astrophysics, formulation of scattering theory, A.M. Mukhamedzhanov, M. La Cognata, C. Spitaleri, and R.E. Tribble, Eur. J. Phys. Web of Conf. **2**, 13001 (2010).

η/s ratio in finite nuclei, N. Auerbach and S. Shlomo, Phys. Rev. Lett. **103**, 172501 (2009).

Determining a modern energy density functional using the simulating annealing method, S. Shlomo, Application of Mathematics in Technical and Natural Sciences, AIP Conference Proceeding **1186**, 93 (2009).

Effect of medium dependent binding energies on inferring the temperatures and freeze-out density of disassembling hot nuclear matter from cluster yields, S. Shlomo, G. Ropke, J.B. Natowitz *et al.*, Phys. Rev. C **79**, 034604 (2009).

Nuclear modification factor of nonphotonic electrons in heavy-ion collisions, and the heavy-flavor baryon to meson ratio, Y. Oh and C.M. Ko, Phys. Rev. C **79**, 067902 (2009).

Higher-order effects on the incompressibility of isospin asymmetric nuclear matter, L.W. Chen, B.J. Cai, C.M. Ko, B.A. Li, C. Shen, and J. Xu, Phys. Rev. C **80**, 014322 (2009).

Deuteron production and elliptic flow in relativistic heavy ion, Y. Oh, Z.W. Lin, and C.M. Ko, Phys. Rev. C **80**, 064902 (2009).

Isospin-dependent pion in-medium effects on the charged-pion ratio in heavy ion collisions, J. Xu, C.M. Ko, and Y. Oh, Phys. Rev. C **81**, 024910 (2010).

Transport model study of deuteron production in relativistic heavy ion collisions, C.M. Ko, Z.W. Lin, and Y. Oh Nucl. Phys. **A834**, 253c (2010).

Quasi-particles and effective mean field in strongly interacting matter, P. Levai and C.M. Ko, Nucl. Phys. **A834**, 285c (2010).

Constraining the EOS of neutron-rich matter and properties of neutron stars with heavy ion collisions, B.A. Li, L.W. Chen, C.M. Ko, P.G. Krastev, D.H. Wen, A. Worley, Z. Xiao, J. Xu, G.C. Yang and M. Zhang, Proceedings of 5th ANL/MSU/JINA/INT FRIB Workshop: Bulk Nuclear Properties, East Lansing, Michigan, November 19-22, 2008, edited by P. Danielewicz, AIP Conference Proceeding **1128**, 131 (2009).

Transport model study of the baryon-rich quark-gluon plasma formed in heavy ion collisions, L.W. Chen, C.M. Ko, W. Liu, and B.W. Zhang, Proceedings of 5th International Workshop on Critical Point and Onset Of Deconfinement, Brookhaven National Laboratory, Upton, New York, June 8-12, 2009, edited by P. Sorenson, Proceedings of Science, 034 (2009).

Resonance recombination model and quark distribution functions in the quark-gluon plasma, L. Ravagli, H. van Hees,and R. Rapp, Phys. Rev. C **79**, 064902 (2009).

T-matrix approach to heavy-quark diffusion in the QGP, H. van Hees, M. Mannarelli, V. Greco, and R. Rapp, Eur. Phys. J. C **61**, 799 (2009).

Forward and midrapidity charmonium production at RHIC, X. Zhao and R. Rapp, Eur. Phys. J. C **62**, 109 (2009).

Medium effects in rho-meson photoproduction, F. Riek, R. Rapp, T.-S.H. Lee, and Y. Oh, Phys. Lett. B **677**, 116 (2209).

Theory and phenomenology of heavy flavor at RHIC, R. Rapp, J. Phys. G **36**, 064014 (2009).

Dileptons in heavy-ion collisions, H. van Hees and R. Rapp, Nucl. Phys. **A827**, 341c (2009).

Nonperturbative heavy-quark interactions in the QGP, R. Rapp, F. Riek, H. van Hees, V. Greco and M. Mannarelli, Nucl. Phys. **A830**, 861c (2009).

Charm and charmonium at finite temperature and chemical potential, R. Rapp, Proc. of Science (CPOD 2009) **040**, (2009).

The chiral restoration transition of QCD and low mass dileptons, R. Rapp, J. Wambach, and H. van Hees, Landolt-Börnstein (Springer), New Series **I/23A**, 1 (2010).

Heavy quarks in the quark-gluon plasma, R. Rapp and H. van Hees in *Quark-Gluon Plasma 4*, (World Scientific, 2010) pg. 111.

High p_T Physics with identified particles, R.J. Fries and W. Liu, Nucl. Phys. **A830**, 693c (2009).

From 0 to 5000 in 2×10^{24} seconds: Entropy production in relativistic heavy-ion collisions, R.J. Fries, T. Kunihiro, B. Muller, A. Ohnishi, and A. Schafer, Nucl. Phys. **A830**, 519c (2009).

The QCD confinement transition: Hardon formation, F. Becattini and R.J. Fries, Landolt-Boernstein, New Series **1**, Vol. **23** (2010).

Enhanced production of direct photons in Au+Au collisions at$\sqrt{\ } s_{NN}$=200 *GeV* and implications for the initial temperature, A. Adare *et al.* (PHENIX Collaboration), Phys. Rev. Lett. 104, 132301 (2010).

Observation of an antimatter hypernucleus, B.I. Abelev *et al*. (STAR Collaboration), Science **328**, 58 (2010).

Azimuthal charged-particle correlations and possible local strong parity violation, B.I. Abelev *et al.* (STAR Collaboration), Phys. Rev. Lett. **103**, 251601 (2009).

System size dependence of associated yields in hadron-triggered jets, B.I. Abelev *et al.* (STAR Collaboration), Phys. Lett. B **683**, 123 (2010).

Longitudinal double-spin asymmetry and cross section for inclusive neutral pion production at midrapidity in polarized proton collisions at $\sqrt{s}_{NN} = $ **200 GeV**, B.I. Abelev *et al.* (STAR Collaboration), Phys. Rev. D **80**, 111108 (2009).

Long range rapidity correlations and jet production in high energy nuclear collisions, B.I. Abelev *et al.* (STAR Collaboration), Phys. Rev. C **80**, 064912 (2009).

Center of mass energy and system-size dependence of photon production at forward rapidity at RHIC, B.I. Abelev *et al.* (STAR Collaboration), Nucl. Phys. **A832**, 134 (2009).

Azimuthal charged-particle correlations and possible local strong parity violation, B.I. Abelev *et al.* (STAR Collaboration), Phys. Rev. Lett. **103**, 251601 (2009).

Longitudinal spin transfer to λ and $\overline{\lambda}$ hyperons in polarized proton-proton collisions at at $\sqrt{s}_{NN} = $ **200 GeV,** B.I. Abelev *et al.* (STAR Collaboration), Phys. Rev. D **80**, 111102 (2009).

Growth of long range forward-backward multiplicity correlations with centrality in Au+Au collisions at $\sqrt{s}_{NN} = $ **200 GeV**, B.I. Abelev *et al.* (STAR Collaboration), Phys. Rev. Lett. **103**, 172301 (2009).

Neutral pion production in Au + Au collisions at $\sqrt{s}_{NN} = $ **200 GeV**, B.I. Abelev *et al.* (STAR Collaboration), Phys. Rev. C **80**, 044905 (2009).

J/Ψ production at high transverse momenta in $p + p$ **and Cu + Cu collisions at** $\sqrt{s}_{NN} = $ **200 GeV,** B.I. Abelev *et al.* (STAR Collaboration), Phys. Rev. C **80**, 041902 (2009).

Decay of negative muons bound in ^{27}**Al**, A. Grossheim, R. Bayes, J.F. Bueno, P. Depommier, W. Faszer, M.C. Fujiwara, C.A. Gagliardi, D.R. Gill, P. Gumplinger, M.D. Hasinoff, R.S. Henderson, A. Hillairet, J. Hu, D.D. Koetke, G.M. Marshall, E.L. Mathie, R.E. Mischke, K. Olchanski, A. Olin, R. Openshaw, J.-M. Poutissou, R. Poutissou, V. Selivanov, G. Sheffer, B. Shin, T.D.S. Stanislaus, R. Tacik, R.E. Tribble, Phys. Rev. D **80**, 052012 (2009).

Measurements of φ meson production in relativistic heavy-ion collisions at RHIC, B.I. Abelev *et al.* (STAR Collaboration), Phys. Rev. C **79**, 064903 (2009).

K/π fluctuations at relativistic energies, B.I. Abelev *et al*. (STAR Collaboration), Phys. Rev. Lett. **103**, 092301 (2009).

Pion interferometry in Au+Au and Cu+Cu collisions at $\sqrt{s_{NN}} = 62.4$ and 200 GeV, B.I. Abelev, *et al*. (STAR Collaboration), Phys. Rev. C **80**, 024905 (2009).

Measurement of D^* mesons in jets from $p + p$ collisions at $\sqrt{s_{NN}} = 200$ GeV, B.I. Abelev *et al*. (STAR Collaboration), Phys. Rev. D **79**, 112006 (2009).

Measurement of angular distributions of Drell-Yan dimuons in $p + p$ interactions at 800 GeV/c, L.Y. Zhu, J.C. Peng, P.E. Reimer, T.C. Awes, M.L. Brooks, C.N. Brown, J.D. Bush, T.A. Carey, T.H. Chang, W.E. Cooper, C.A. Gagliardi, G.T. Garvey, D.F. Geesaman, E.A. Hawker, X.C. He, L.D. Isenhower, D.M. Kaplan, S.B. Kaufman, S.A. Klinksiek, D.D. Koetke, D.M. Lee, W.M. Lee, M.J. Leitch, N. Makins, P.L. McGaughey, J.M. Moss, B.A. Mueller, P.M. Nord, V. Papavassiliou, B.K. Park, G. Petitt, M.E. Sadler, W.E. Sondheim, P.W. Stankus, T.N. Thompson, R.S. Towell, R.E. Tribble, M.A. Vasiliev, J.C. Webb, J.L. Willis, D.K. Wise, G.R. Young (FNAL E866/NuSea Collaboration), Phys. Rev. Lett. **102**, 182001 (2009).

Energy and system size dependence of φ meson production in Cu+Cu and Au+Au collisions, B.I. Abelev *et al*. (STAR Collaboration), Phys. Lett. B **673**, 183 (2009).

Identified particle production, azimuthal anisotropy, and interferometry measurements in Au+Au collisions at $\sqrt{s_{NN}} = 9.2$ GeV, B.I. Abelev *et al*. (STAR Collaboration), Phys. Rev. C **81**, 024911 (2010).

Detailed measurement of the $e^+ e^-$ pair continuum in p+p and Au+Au collisions at $\sqrt{(s_{NN})} = 200$-GeV and implications for direct photon production, A. Adare *et al.* (PHENIX Collaboration), Phys. Rev. C **81**, 034911 (2010).

Double helicity dependence of jet properties from dihadrons in longitudinally polarized p+p collisions at $\sqrt{(s_{NN})} = 200$-GeV, A. Adare *et al.* (PHENIX Collaboration), Phys. Rev. D **81,** 012002 (2010).

Longitudinal double-spin asymmetry and cross section for inclusive neutral pion production at midrapidity in polarized proton collisions at $\sqrt{(s_{NN})} = 200$ GeV, B.I. Abelev *et al.* (STAR Collaboration), Phys. Rev. D **80,** 111108 (2009).

High-pT π^o production with respect to the reaction plane in Au + Au collisions at $\sqrt{(s_{NN})} = 200$-GeV, S. Afanasiev *et al.* (PHENIX Collaboration), Phys. Rev. C **80**, 054907 (2009).

Kaon interferometric probes of space-time evolution in Au+Au collisions at $\sqrt{(s_{NN})} = 200$-GeV, S. Afanasiev *et al.* (PHENIX Collaboration), Phys. Rev. Lett. **103**, 142301 (2009).

Measurement of bottom versus charm as a function of transverse Mmomentum with electron-hadron correlations in p+p collisions at $\sqrt{(s_{NN})}$=200 GeV, A. Adare *et al.* (PHENIX Collaboration), Phys. Rev. Lett. **103**, 082002 (2009).

Systematic studies of elliptic flow measurements in Au+Au collisions at $\sqrt{(s_{NN})}$ = 200-GeV, S. Afanasiev *et al.* (PHENIX Collaboration), Phys. Rev. C **80**, 024909 (2009).

Photon-hadron jet correlations in p+p and Au+Au collisions at $\sqrt{(s_{NN})}$= 200-GeV, A. Adare *et al.* (PHENIX Collaboration), Phys. Rev. C **80**, 024908 (2009).

Photoproduction of J/psi and of high mass $e^{+}e^{-}$ in ultra-peripheral Au+Au collisions at $\sqrt{(s_{NN})}$ = 200-GeV, S. Afanasiev *et al.* (PHENIX Collaboration), Phys. Lett. B **679**, 321, (2009).

Nuclear stopping and rapidity loss in Au+Au collisions at $\sqrt{s}$ = 62.4 GeV, I.C. Arsene, I.G. Bearden, D. Beavis, S. Bekele, C. Besliu, B. Budick, H. Boggild, C. Chasman, C.H. Christensen, P. Christiansen, H.H. Dalsgaard, R. Debbe, J.J. Gaardhoje, K. Hagel, H. Ito, A. Jipa, E.B. Johnson, C.E. Jorgensen, R. Karabowicz, N. Katrynska, E.J. Kim, T.M. Larsen, J.H. Lee, G. Lovhoiden, Z. Majka, M.J. Murray, J.B. Natowitz, B.S. Nielsen, C. Nygaard, D. Pal, A. Qviller, F. Rami, C. Ristea, O. Ristea, D. Rohrich, S.J. Sanders, P. Staszel, T.S. Tveter, F. Videbaek, R. Wada, H. Yang, Z. Yin, I.S. Zgura, Phys. Lett. B **677**, 267 (2009).

Rapidity dependence of proton-to-pion ratio in Au+Au and p+p at $\sqrt{s}$ = 62.4 and 200 GeV, I. G. Arsene, I. G. Bearden, D. Beavis, S. Bekele, C. Besliu, B. Budick, H. Bøggild, C. Chasman, C. H. Christensen, P. Christiansen, H. H. Dalsgaard, R. Debbe, J. J. Gaardhøje, K. Hagel, H. Ito, A. Jipa, E. B. Johnson, C. E. Jørgensen, R. Karabowicz, N. Katry´nska, E. J. Kim, T. M. Larsen, J. H. Lee, G. Løvhøiden, Z. Majka, A. Marcinek, M. J. Murray, J. Natowitz, B. S. Nielsen, C. Nygaard, D. Pali, A. Oviller, R. Płaneta, F. Rami, C. Ristea, O. Ristea, D. R¨ohrich, S. J. Sanders, P. Staszel, T. S. Tveter, F. Videbæk, R. Wada, H. Yang, Z. Yin, and I. S. Zgura, Phys. Lett., B **684**, 22 (2010).

A FORTRAN program equipped with a Windows graphics user interface that calculates ECPSSR cross sections for the removal of atomic electrons, V. Horvat, Comput. Phys. Commun. **180**, 995 (2009).

Using Monte Carlo simulations and experimental measurements to calibrate an HPGE Gamma detector precisely, Y.J. Zhai, L. Trache, R.E. Tribble *et al.*, Am. J. Clinical Oncology-Cancer Clinical Trials **32**, 105 (2009).

Measurement and calculation of characteristic prompt gamma ray spectra emitted during proton irradiation, J.C. Polf, S. Peterson, M. McCleskey, B.T. Roeder, A. Spiridon, S. Beddar, L. Trache, Physics in Medicine and Biology **54**, N519 (2009).

SECTION VII

APPENDIX

The U. S. Nuclear Physics Program, **R.E. Tribble**, **Invited Talk**, St. Petersburg University, St. Petersburg, Russia (June 2009).

Nuclear Astrophysics Underground, **R.E. Tribble**, **Invited Talk**, International Union of Pure and Applied Physics Working Group 9 Meeting, Bonn, Germany (August, 2009).

The U. S. Nuclear Physics/Nuclear Astrophysics Program into the Next Decade, **R.E. Tribble**, **Invited Talk**, Public Lecture as part of the European Nuclear Astrophysics Summer School, Cantania, Italy (September 2009).

Science and Technology to Strengthen National, **R.E. Tribble**, **Invited Talk**, 10th Anniversary Symposium for the Korea Research Council on Fundamental Science and Technology, Seoul, south Korea (October 2009).

Development of New Techniques to Determine Neutron Induced Reaction Rates, **R.E. Tribble**, **Invited Talk**, 2010 Stewardship Science Academic Alliances Symposium, Washington, D.C. (January 2010).

Recent Results on Astrophysical Reaction Rates, **R.E. Tribble**, **Invited Talk**, Niidata2010, Niigata, Japan (March 2010).

Astrophysical Reaction Rates by Indirect Techniques, **R.E. Tribble**, **Invited Talk**, Osaka, Japan (March 2010).

The Status of V_{ud}, **J.C. Hardy, Invited Talk**, 10th Conference on the Intersections of Particle and Nuclear Physics, CIPANP 2009, La Jolla, California (May 2009).

Superallowed Nuclear β Decay: Symmetry Breaking, CVC and CKM Unitarity, **J.C. Hardy, Invited Talk**, 4th International Symposium on Symmetries in Subatomic Physics, Taipei, Taiwan (June 2009).

Testing CVC and CKM Unitarity via Superallowed Nuclear Beta Decay, **J.C. Hardy, Invited Talk**, WE-Heraeus-Seminar on "Precision experiments at lowest energies for fundamental tests and constants," Bad Honnef, Germany (June 2009).

Superallowed Nuclear β Decay: Precision Measurements for Basic Physics, **J.C. Hardy, Invited Talk**, Nuclear Physics Summer School, Michigan State University (June, July 2009).

Tests of Nuclear Half-Lives as a Function of the Host Temperature: Refutation of Recent Claims, **J.C. Hardy, Invited Talk**, 17th International Conference on Radionuclide Metrology and its Applications (ICRM 2009), Bratislava, Slovakia (September 2009).

New Precision Internal Conversion Measurements as Tests of Internal Conversion Theory: $^{197}Pt^m$ case, **N.Nica, Invited Talk**, 18th meeting of the International Network of Nuclear Structure and Decay Data Evaluators (NSDD), IAEA Headquarters, Vienna, Austria (March 2009).

Evaluation Codes : GTOL, **N. Nica, Invited Talk**, Workshop for Nuclear Structure and Decay Data Evaluators ENSDF-2009, Bucharest-Magurele, Romania (March, April 2009).

Beta-Decay of Proton-Rich ^{31}Cl and its Relevance for Explosive H-Burning, **L. Trache**, A. Banu, J.C. Hardy, V.E. Iacob, M. McCleskey, B. Roeder, E. Simmons, G. Tabaracu, R.E. Tribble, T. Davinson, G. Lotay, P.J. Woods, A. Saastamoinen, A. Jokinen and J. Aysto, APS Meeting, Waikoloa, Hawaii (October 2009).

Very Low Energy Protons from β-Delayed p-Decay of Proton-Rich Nuclei for Nuclear Astrophysics, **E. Simmons**, L. Trache, A. Banu, J.C. Hardy, V.E. Iacob, M. McCleskey, B. Roeder, A. Spiridon, R.E. Tribble, T. Davinson, G. Lotay, P.J. Woods, A. Saastamoinen, and J. Aysto, APS Meeting, Waikoloa, Hawaii (October 2009).

Confirmation of the Precise Half Life of ^{26}Si, **V.E. Iacob**, V.V. Golovko, J. Goodwin, J.C. Hardy, N. Nica, H.I. Park, L. Trache, R.E. Tribble, APS Meeting, Waikoloa, Hawaii (October 2009).

Superallowed $0^+ \rightarrow 0^+$ Beta Decay and CKM Unitarity: A New Overview and Improved Precision, **J.C. Hardy**, Colloquium, Physics Department, University of Jyvaskyla, Finland (March 2009).

Superallowed Nuclear β Decay: A Window on the Weak Interaction, **J.C. Hardy**, Colloquium, Physics Department, National Central University, Chungli, Taiwan (June 2009).

High Precision Half-Life Measurement of ^{38}Ca, **H.I. Park**, J.C. Hardy, V.E. Iacob, L. Chen, J. Goodwin, V. Horvat, N. Nica, L. Trache and R.E. Tribble, 2010 APS Meeting, Washington, D.C (February 2010).

New Results from Mass and Lifetime Measurements of Stored Exotic Nuclei at the FRS-ESR Facility, **L. Chen**, 8th International Conference on Radioactive Beams (RNB8), Grand Rapids, Michigan (May 2009).

Final Results on Muon Decay from TWIST, **C.A. Gagliardi** (for the TWIST Collaboration), **Invited Talk**, 2010 APS Meeting, Washington, D.C. (February 2010).

STAR Spin: Recent Results, Future Directions, **C.A. Gagliardi** (for the STAR Collaboration), **Invited Seminar**, Berkeley Summer Program on Nucleon Spin, Berkeley, California (June 2009).

STAR Spin: Recent Highlights and Results, **C.A. Gagliardi** (for the STAR Collaboration), **Invited Talk**, 2009 RHIC & AGS Annual Users' Meeting, Brookhaven National Laboratory, Upton, New York (June 2009).

Nuclear Reaction Rates for H-burning from Experiments with Rare Nuclear Beams: Indirect Methods, **L. Trache**, **Invited Talk**, Defining the Neutron Star Crust 2009, Santa Fe, New Mexico (May 2009).

Single Nucleon Transfer between p-shell Nuclei around 10 MeV/u – for Nuclear Astrophysics, **L. Trache**, ATLAS Workshop 2009, UG Meeting, Argonne, Illinois (August 2009).

Indirect Studies for Nuclear Astrophysics with Radioactive Nuclear Beam, **L. Trache**, 2009 ACS Meeting, Washington, D.C. (August 2009).

Indirect Methods for Nuclear Astrophysics with Radioactive Nuclear beams, **L. Trache**, **Invited Lecture**, 5th European Summer School in Experimental Nuclear Astrophysics, St. Tecla, Sicily, Italy (September 2009).

Decay Spectroscopy for H-burning Reactions in Novae and XRB, **L. Trache**, **Invited Talk**, Department of Physics, University of Notre Dame, South Bend, Indiana (February 2010).

Nuclear Physics for Astrophysics with RNBs from 10 to 50 MeV/u, **A. Banu**, **Invited Talk**, Nuclear Chemistry Gordon Conference, Colby-Sawyer College, New London, New Hampshire (June 2009).

Breakup of Proton-rich Nuclei ^{24}Si, ^{23}Al at Intermediate Energies for Reaction Rates in Explosive H-burning in Novae and X-ray Bursts, **A. Banu**, APS Meeting, Waikoloa, Hawaii (October 2009).

Reaction Rates for Hydrogen Burning in Novae and X-ray Bursts from Proton Breakup at Intermediate Energies and Decay Spectroscopy, **A. Banu**, TUNL, Durham, North Carolina (October 2009).

Breakup of Proton-rich Nuclei ^{24}Si, ^{23}Al at Intermediate Energies for Reaction Rates in Explosive H-burning in Novae and X-ray Bursts, **A. Banu**, Direct Reaction with Exotic Beams (DREB09), Tallahassee, Florida (December 2009).

Quasimolecular States in N≠Z Light Nuclei, **V.Z. Goldberg**, **Invited Talk**, International Conference on Fundamental Problems and Applications of Nuclear Physics: From Space to Nanotechnologies, Cheboksary, Russia (June 2009).

Aims and Methods in Resonance Reaction Studies Using Exotic Beams, **V.Z. Goldberg**, Lomonosov Moscow State University, Moscow, Russia (July 2009).

New Nuclide, ^{14}F, **V.Z. Goldberg**, International Workshop on Direct Reaction with Exotic Beams (DREB 2009), Tallahassee, Florida (December 2009).

Unique Double Folding Optical Parameters for 240 MeV ^{6}Li, **Krishichayan**, X. Chen, Y.-W. Lui, Y. Tokimoto, J. Button, and D.H. Youngblood, 3rd Joint Meeting of the APS DNP and the Physical Society of Japan, Waikoloa, Hawaii (October 2009).

Probing Fundamental Properties of the Weak Interaction: Atomic Meets Nuclear Meets High-Energy Physics, Values, **D. Melconian,** **Invited Seminar**, Joint Complex Quantum Systems and Nonlinear Dynamics Seminar, University of Texas, Austin, Texas (October 2009).

Probing High-Temperature QCD Matter at the Relativistic Heavy-Ion Collider with High Transverse Momentum Particles, **Saskia Mioduszewski**, **Invited Talk**, 2009 APS Meeting, Denver, Colorado (May 2009).

Heavy Flavor from STAR, **Saskia Mioduszewski**, **Invited Talk (Selected by STAR Collaboration)**, 10th Conference on the Intersections of Particle and Nuclear Physics (CIPANP 2009), San Diego, Calfornia (May 2009).

Probing High-Temperature Nuclear Matter at the Relativistic Heavy-Ion Collider, **Saskia Mioduszewski**, **Invited Talk**, Colloquium for the Physics Department, Trinity University, San Antonio, Texas (November 2009).

Upsilon Production at STAR, **Ahmed Hamed, Invited Talk**, Lake Louise Winter Institute 2010, Lake Louise, Canada (February 2010).

Gamma-Jet Measurements in Au+Au Collisions with the Solenoidal Tracker At RHIC (STAR), **Martin Codrington**, 2009 Texas Section APS Meeting, San Marcos, Texas (October 2009).

γ-Hadron Correlations with STAR, **Martin Codrington**, 37th National Organization for the Professional Advancement of Black Chemists and Chemical Engineers, NOBCChE, Atlanta, Georgia (March 2010).

Upsilon + Hadron correlations at the Relativistic Heavy-Ion Collider, **Matthew Cervantes**, 2010 APS Meeting, Washington, D. C. (February 2010).

Laboratory Studies of Low Density Nucleonic Matter, **J.B. Natowitz**, **Invited Talk**, Nucleus-Nucleus 2009, Beijing, China (August 2009).

Low Density Nuclear Matter in Fermi Energy Collisions, **J.B. Natowitz**, **Invited Talk**, International workshop on Nuclear Dynamics, Shanghai, China (August 2009).

Nuclear Science in the 21st Century, **J.B. Natowitz**, **Invited Talk**, Mexican Academy of Sciences, Mexico City, Mexico (November 2009).

Nascent Fireballs and Low Density Nuclear Matter in Near Fermi Energy Collisions, **J.B. Natowitz**, **Invited Talk**, American Chemical Society National Meeting, San Francisco, California (March 2010).

Quantum Nature of a Nuclear-Phase Transition, **A. Bonasera**, International Conference in Honor of M. Di Toro 70th Birthday, Cantania, Italy (September 2009).

Measuring the Astrophysical s-Factor in Plasmas, **A. Bonasera**, Colloquium, Scalay, France (February 2010).

Quantum Nature of a Nuclear-Phase Transition, **A. Bonasera**, Colloquium, GANIL, Caen, Cedex, France (February 2010).

Nuclear Reactions, **S.J. Yennello**, **Invited Talk**, National Nuclear Physics Summer School, East Lansing, (June 2009).

Facility Upgrade for Texas A&M University for Accelerated RIBS, **S.J. Yennello**, **Talk**, Radioactive Nuclear Beams Conference, Grand Rapids, Michigan (May 2009).

Isoscaling in Projectile Fragmentation Reactions: A Way to Elucidate the Density Dependence of the Symmetry Energy, **S.J. Yennello**, **Invited Talk**, 2nd International Conference on Nuclear Fragmentation: from Basic Research to Applications (NUFRA), Antalya, Turkey (September 2009).

Isoscaling of Fragments from Reconstructed Quasiprojectiles, **S.J. Yennello**, **Invited Talk**, International Workshop on Multifragmantation, Catania, Italy (November 2009).

Can LeChatlier's Principle be Used to Maintain Equilibrium? **S.J. Yennello**, **Invited Talk**, Michigan State University, East Lansing, Michigan (March 2009).

How Undergraduate Research Experiences Prepare Students for Graduate School, **S.J. Yennello, Invited Talk,** AAPT, Ann Arbor, Michigan (July 2009).

Impact Parameter Characterization, Reaction Plane Determination, and Flow Analysis of 35 MeV/u $^{70}Zn+^{70}Zn, ^{64}Zn+^{64}Zn, ^{64}Ni+^{64}Ni, **Z. Kohley,** L. May, S. Wuenschel, B.C. Stein, R. Tripathi, S.N. Soisson,

G.A. Souliotis, and S.J. Yennello (NIMROD Collaboration), 2010 APS Meeting, Washington, D.C. (February 2010).

Improving Climate and Gender Equity in Physics Departments, **S.J. Yennello**, **Invited Talk**, 2010 APS Meeting, Washington, D.C. (February 2010).

The Effect of N/Z on Caloric Curves, **S. Wuenschel,** S.J. Yennello, Z. Kohley, L.W. May, G.A. Souliotis, D.V. Shetty, K. Hagel, B.C. Stein, S.N. Soisson, and S. Galanopoulos, 2009 APS Meeting, Denver, Colorado (May 2009).

Isoscaling of Z=1 to 17 fragments from the reaction of ^{86,78}Kr with ^{64,58}Ni targets at 35MeV/nucleon, **R.Q. Dienhoffer**, S. Wuenschel, S.J. Yennello, G. Souliotis, Z.W. Kohley, A.L. Caraley, S. Galanopoulos, K. Hagel, L.W. May, D.V. Shetty, S.N. Soisson, B.C. Stein, 2009 APS Meeting, Denver, Colorado (May 2009).

A Quadrupole Momentum Thermometer for Heavy- Ion Reaction, **L.W. May,** Aldo Bonasera, S. Wuenschel, and S.J. Yennello, 3rd Joint Meeting of the APS DNP and the Physical Society of Japan, Waikoloa, Hawaii (October 2009).

Probing densities of hot nuclei, **R. Tripathi,** S. Wuenschel, G.A. Souliotis, S. Galanopoulos, Z. Kohley, K. Hagel, D.V. Shetty, K. Huseman, L.W. May, S.N. Soisson, B. C. Stein, and S.J. Yennello, 2010 APS Meeting, Washington, D.C. (February 2010).

Studies of the Nuclear Landscape and the Nuclear Equation of State Using Peripheral Collisions Near the Fermi Energy, **G. Souliotis**, **Invited Talk**, 18th Symposium of the Hellenic Nuclear Physics Society, INP/NCSR "Demokritos" (May 2009).

Studies of the Nuclear Landscape and the Nuclear Equation of State Using Peripheral Collisions Near the Fermi Energy, **G. Souliotis**, **Invited Lecture**, XVIII International School of Nuclear Physics, Varna, Bulgaria (September 2009).

Studies of Heavy Residues from Peripheral Collisions Near the Fermi Energy and the Nuclear Equation of State, **G. Souliotis**, **Invited Talk**, 2nd International Conference on Nuclear Fragmentation: from Basic Research to Applications (NUFRA), Antalya, Turkey (September 2009).

Studies of the Nuclear Landscape and the Nuclear Equation of State (EOS) using Peripheral Heavy-Ion Collisions at Fermi Energies, **G. Souliotis**, **Invited Seminar**, Department of Physics, Aristotle University of Thessaloniki, Thessaloniki, Greece (October 2009).

Modern Energy Density Functional for Nuclei and the Nuclear Matter Equation of State, **S. Shlomo**, **Invited Talk**, Department of Physics, Argonne National Laboratory, Argonne, Illinois (April 2009).

Modern Energy Density Functional for Properties of Nuclei and Nuclear, **S. Shlomo**, **Invited Talk**, 2009 APS Meeting, Denver, Colorado April 2009).

Liquid-Gas Phase Transition in Heavy-Ion Collisions, **S. Shlomo**, **Invited Talk**, Joint Nuclear/Hadronic Seminar, Department of Physics, Hebrew University of Jerusalem, Jerusalem, Israel (May 2009).

Liquid-Gas Phase Transition in Heavy-Ion Collisions, **S. Shlomo**, **Invited Talk**, Department of Physics, Ben-Gurion University, Bee-Sheva, Israel (June 2009).

Modern Energy Density Functional for Properties of Nuclei and the Nuclear Matter Equation of State, **S. Shlomo**, **Invited Talk**, International Conference on Fundamental Problems and Applications of Nuclear Physics: From Space to Nanotechnologies, NUCLEUS-2009, Cheboksary, Russia (Junel 2009).

Determining a Modern Energy Density Functional Using the Simulating Annealing Method, **S. Shlomo**, **Invited Talk**, The 1st Conference for Promoting the Application of Mathematics in Technical and Natural Sciences, AMiTaNS, Sozopol, (June 2009).

Freeze-Out Temperature and Density in Heavy Ion Collisions at Liquid-Gas Phase Transition, **S. Shlomo**, **Invited Talk**, 8th Latin American Symposium on Nuclear Physics and Applications, Santago, Chile (December 2009).

Giant Resonances and the Nuclear Equation of State, **S. Shlomo**, **Invited Talk**, Department of Physics, Ben-Gurion University, Bee-Sheva, Israel (January 2010).

Determining a Modern Energy Density Functional for Nuclei Using the Simulating Annealing Method, **S. Shlomo**, **Invited Talk**, Joint Nuclear/Hadronic Seminar, Department of Physics, Hebrew University of Jerusalem, Jerusalem, Israel (January 2010).

Asymptotic Normalization Coefficients and Important Astrophysical Processes, **A.M. Mukhamedzhanov**, **Invited Talk**, Nuclear Physics in Astrophysics IV, Frascatti, Italy (June 2009).

Nuclear Reactions and Indirect Methods in Nuclear Astrophysics, **A.M. Mukhamedzhanov**, **Invited Lecture**, European School on Experimental Nuclear Astrophysics V, Santa Tecla, Italy (September 2009).

Absorption of Nucleons by Mini Black Holes, **A.M. Mukhamedzhanov**, **Invited Talk**, Institute of Nuclear Physics, Orsay, Paris, France (October 2009).

Excitation of Compound State in the Subsystems as Indirect Tool in Nuclear Astrophysics, **A.M. Mukhamedzhanov**, **Invited Talk**, Workshop in Compound Nuclear Reactions 2009 (CNR09), Bordeaus, France (October 2009).

Trojan Horse as Indirect Technique in Nuclear Astrophysics, **A.M. Mukhamedzhanov**, **Invited Talk**, Lawrence Livermore National Laboratory, Livermore, California (March 2010).

Charms in Heavy Ion Collisions, **C.M. Ko**, **Invited Talk**, ECT* Workshop on Heavy-Quarkonium Production in Heavy-Ion Collisions, Trento, Italy (May 2009).

Transport Model Studies of the Baryon-Rich Quark-Gluon Plasma Formed in Heavy Ion Collisions, **C.M. Ko**, **Invited Talk**, 5th International Workshop on Critical Point and Onset Of Deconfinement, Brookhaven National Laboratory, Upton, New York (June 2009).

Charms in Heavy Ion Collisions, **C.M. Ko**, **Invited Talk**, XXVI Max Born Symposium on Strong Interactions, Wroclaw, Poland (July 2009).

Probing QCD Phase Diagram in Relativistic Heavy Ion Collisions, **C.M. Ko**, **Invited Talk**, International Seminars on Strong Interaction Physics, Seoul, Korea (July 2009).

Recent Progress in Isospin Physics and the Nuclear Symmetry Energy, **C.M. Ko**, **Invited Talk**, International Seminars on Strong Interaction Physics, Seoul, Korea (July 2009).

Particle Production in Heavy Ion Collisions, **C.M. Ko**, **Invited Talk**, Workshop on Relativistic Heavy Physics, Wei Hai, Hepei, China (August 2009).

Transport model Study of Deuteron Production in Relativistic Heavy Ion Collisions, **C.M. Ko**, **Invited Talk**, International Conference on Nucleus-Nucleus Collisions, Beijing, China (August 2009).

Isospin-Dependent Pion In-Medium Effects on Charged Pion Ratio in Heavy ion Collisions, **C.M. Ko**, **Invited Talk**, International Workshop on Isospin Dynamics and Nuclear Symmetry Energy", Shanghai, China (August 2009).

Particle Production and Nucleon Stopping in AMPT Model, **C.M. Ko**, **Invited Talk**, Symposium on Proton-Proton Interactions, Frankfurt, Germany (February 2010).

Nonperturbative Quark Interactions in the Quark-Gluon Plasma, **R. Rapp**, 21st International Conference of Ultrarelativistic Nucleus Nucleus Collisions (Quark Matter 2009) Knoxville, Tennessee (April 2009).

Heavy Quark Interactions in the Quark-Gluon Plasma, **Felix Riek**, **Invited Talk**, International ECT* Workshop on Heavy Quarkonium Production in Heavy-Ion Collisions, Trento, Italy (May 2009).

In-Medium Charmonium Production, **Xingbo Zhao**, **Invited Talk**, International ECT* Workshop on Heavy Quarkonium Production in Heavy-Ion Collisions, Trento, Italy (May 2009).

Dileptons, Charm and Charmonium at Finite Temperature and Chemical Potential, **R. Rapp**, **Invited Plenary Talk**, 5th International Workshop on Critical Point and Onset of Deconfinement, Brookhaven National Laboratory, Upton, New York (June 2009).

Quarkonia in Medium: From Spectral Functions to Observables, **Ralf Rapp**, **Invited Talk**, Joint CATHIE-INT Mini-Program on Quarkonia in Hot Medium: From QCD to Experiment, Institute for Nuclear Theory, University of Washington, Seattle, Washington (June 2009).

Bremsstrahlung and Dalitz Decays from in-Medium Electromagnetic Spectral Functions, **Ralf Rapp**, **Invited Talk**, Extreme Matter Institute Workshop on Virtual Bremsstrahlung and HADES, Frankfurt University, Frankfurt, Germany (August 2009).

Dileptons in Heavy-Ion Collisions, **Ralf Rapp**, **Invited Lecture**, HIC4FAIR Workshop on Dense Matter in Heavy-Ion Collisions and Supenovae, Prerow, Germany (October 2009).

Heavy-Flavor Probes of Quark-Gluon Plasma and RHIC, **R. Rapp**, **Invited Colloquium**, CATHIE/TECHQM Workshop, Brookhaven National Laboratory, Upton, New York (December 2009).

Theory Update on Electromagnetic Probes II, **R. Rapp**, **Invited PlenaryTalk**, CATHIE/TECHQM Workshop, Brookhaven National Laboratory, Upton, New York (December 2009).

Quarkonium Spectral Functions in Potential Models, **Felix Riek**, **Invited Talk**, CATHIE/TECHQM Workshop, Brookhaven National Laboratory, Upton, New York (December 2009).

Resonances in Medium, **R. Rapp**, **Invited Talk**, STAR Collaboration Analysis Meeting, Austin, Texas (January 2010).

Medium Effects in Rho-Meson Photoproduction at Jefferson Lab, **R. Rapp**, Theory Seminar GSI Darmstadt, Germany (June 2009).

Electromagnetic Probes and the Quest for Chiral Symmetry Restoration, **R.Rapp**, Graduiertenkolleg's colloquium, University of Giessen, Germany (June 2009).

Hot and Dense QCD Matter and Heavy-Ion Collisions, **R. Rapp**, Mayer-Leibniz Laboratory colloquium, Technical University Munich, Munich, Germany (October 2009).

Vector Mesons in Medium and Dileptons in Heavy-Ion Collisions, **Ralf Rapp**, Strong Interaction seminar, Technical University Munich, Munich, Germany (October 2009).

Heavy Quarks and Quarkonia in the Quark-Gluon Plasma, **Ralf Rapp,** Seminar, Technical University Darmstadt, Germany (November 2009).

Quarkonia in Medium and in Heavy-Ion Collisions, **R. Rapp**, Brookhaven National Laboratory, Upton, New York (February 2009).

Charmonium Production in Heavy-Ion Collisions – Revisited, **X. Zhao**, 2009 Texas Section of APS, San Marcos, Texas (October 2009).

A Phenomenological Study of Charmonium Dissociation Temperatures in Heavy-Ion Collisions, **X. Zhao**, Los Alamos National Laboratory, Los Alamos, New Mexico (December 2009).

Charmonium Production in Heavy-Ion Collisions, **X. Zhao**, Lawrence Berkeley National Laboratory, Berkeley, California (January 2010).

The Origin of the Visible Mass in the Universe, **R. Rapp**, Cyclotron/High Energy Research Experience for Undergraduates (REU) program, Cyclotron Institute, Texas A&M University, College Station (July 2009).

Investigating the Primordial Quark-Gluon Liquid, **R. Rapp**, Special Seminar, Texas A&M University, College Station (October 2009).

The Primordial Liquid and a Rubber Band at a Trillion Degrees, **Felix Riek**, 2010 Saturday Morning Physics program for high-school students, Texas A&M University, College Station (February 2010).

High -P_T Physics with Identified Particles, **R.J. Fries**, XXI International Conference on Ultrarelativistic Nucleus-Nucleus Collisions (Quark Matter 2009), Knoxville, Tennessee (April 2009).

High -P_T Physics with Identified Particles, **R.J. Fries**, **Invited Talk**, Conference on the Intersections of Particle and Nuclear Physics (CIPANP) 2009, San Diego, California (May 2009).

Hadro-Chemistry with High-P_T Particles in Nuclear Collisions, **R.J. Fries**, **Invited Talk**, 2009 APS Division of Particles and Fields (DPF) Meeting, Detroit, Michigan (July 2009).

High Energy Collisions: Probing Hot Nuclear Matter, **R.J. Fries**, Department of Physics, Nagoya University, Nagoya, Japan (October 2009).

Hard Probes in Heavy Ion Collisions: Jet Chemistry and Tomography, **R.J. Fries**, University of Tokyo, Komaba Campus, Komaba, Meguroku, Tokyo, Japan (November 2009).

Hard Probes in Heavy Ion Collisions: Jet Chemistry and Tomography, **R.J. Fries**, Yukawa Institute, Kyoto University, Kyoto, Japan (November 2009).

Direct Photons and Jet Conversions in Heavy Ion Collisions, **R.J. Fries**, **Invited Talk**, 7th Heavy Ion Pub, Osaka University, Osaka, Japan (November 2009).

High Energy Nuclear Collisions: Theory Overviews, **R.J. Fries**, **Invited Talk**, International Symposium on Nuclear Physics (ISNP) 2009, Bhabha Institute, Munbai, India (December 2009).

Collisions of Nuclei: New Ideas for Hard Probes, **R.J. Fries**, Tata Institute for Fundamental Research, Mumbai, India (December 2009).

Recombination of Quarks, **R.J. Fries**, **Invited Talk**, STAR Collaboration Meeting, University of Texas, Austin, Texas (January 2010).

Collisions of Nuclei: Some Ideas for Hard Probes, **R.J. Fries**, Department of Physics, Duke University, Durham, North Carlina (February 2010).

Effect of Fluctuations in the Fireball on Jet Quenching Observables at RHIC, **Ricardo Rodrizues**, 2010 APS Meeting, Washington, D. C. (February 2010).

RESEARCH PERSONNEL AND ENGINEERING STAFF

April 1, 2009 - March 31, 2010

Faculty and Research Group Leaders

Aldo Bonasera, Research Scientist – From 4/16/09
Charles M. Folden III, Assist. Prof. of Nuclear
   Chemistry
Rainer Fries, Assist. Professor of Physics
Carl A. Gagliardi, Professor of Physics
John C. Hardy, Professor of Physics
Che Ming Ko, Professor of Physics
Dan Melconian, Assist. Professor of Physics
Saskia Mioduszewski, Assist. Prof. of Physics
J. B. Natowitz, Professor of Chemistry, Bright Chair
Ralf Rapp Associate Professor of Physics
Shalom Shlomo, Senior Scientist
Robert E. Tribble, Professor of Physics, Director
Rand L. Watson, Professor of Chemistry
Sherry J. Yennello, Professor of Chemistry
Dave H. Youngblood, Professor of Physics
Akram M. Zhanov, Senior Scientist

Research Staff

Henry Clark, Accelerator Physicist (50%)
Grigor Chubaryan, Research Scientist
John C. Hagel, Research Scientist (50%)
Vladimir Horvat, Research Scientist (50%)
Victor Iacob, Associate Research Scientist
Yiu-Wing Lui, Research Scientist
Ninel Nica, Assist. Research Scientist
George Souliotis, Associate Research Scientist
Livius Trache, Research Scientist
Ryoichi Wada, Research Scientist

Visiting Scientists

Vladilen Goldberg
Taesoo Song – From 1/1/2010
Ian Towner – From 6/19/09 To 8/31/09

Accelerator Physics and Radiation Line Staff

Joseph Brinkley, Research Associate
Henry Clark, Accelerator Physicist (50%)
Vladimir Horvat, Research Scientist (50%)
Bruce Hyman, Research Associate

George Kim, Accelerator Physicist
Don May, Accelerator Physicist
Gabriel Tabacaru, Accelerator Physicist

Computer Systems Staff

Robert Burch, Jr., Sr. Microcomputer/LAN
   Administrator
John C. Hagel, Research Scientist (50%)

Engineering Staff

Greg Derrig, Senior Mechanical Engineer
Robert Olsen, Senior Mechanical Engineer

Postdoctoral Research Associates

Tariq Al-Abdullah – From 7/1/09 To 9/30/09
Abeer Alharbi – From 10/1/09
Adriana Banu
Marina Barbui – From 3/18/09
Lixin Chen – From 1/23/09
Rory Clarke – To 7/16/09
Pibero Djawotho
Ahmed Hamed
Min He – From 9/11/09
Sachie Kimura – From 5/15/2009 To 11/15/09
Krishichayan
Paola Marini – From 1/4/10
Yong S. Oh – To 7/31/09
Felix Riek
Marcia Rodrigues – From 5/13/09
Ricardo Rodriguez
Brian Roeder
Praveen Shidling – From 3/1/10
Rahul Tripathi – From 5/14/09
Jun Xu

STUDENTS

April 1, 2009 - March 31, 2010

Graduate Students

Marisa Alfonso
Richard Spence Behling
Jonathan Button
Matthew Cervantes
Guangyao Chen – From 6/1/09
Martin Codrington
James Drachenberg
David Carson Fuls
John Goodwin
Kyong Choi Han – From 9/1/09
Liaoyuan Huo
Zach Kohley
Larry May
Demitri Mayorov – From 11/1/09
Matthew McCleskey
Hyo-In Park
Andrew Raphelt – From 11/1/09
Kevin Resil – From 6/10/09
John Saathoff – From 6/1/09
Ellen Simmons
Sarah Soisson
Alexandra Spiridon
Brian Stein
Sara Wuenschel – To 6/30/09
Xingbo Zhao
Hua Zheng – From 9/1/09

Undergraduates and Student Technicians

Chibueze Vincent Amanchukwu – From 9/1/09
Giacoma Bonasera – From 9/1/09
Michael Dachowski – From 6/4/09 To 11/1/09
Todd Hammer – From 6/15/09
Sarah Loupot – From 6/8/09
Thomas Merket – To 4/22/09
Ashley Noack
Taylor Olsen – From 7/6/09 To 1/22/10
Robert Polis
Wade Ben Smith – To 9/1/09
Amanda Spaw

ORGANIZATIONAL CHART - CYCLOTRON INSTITUTE

DIRECTOR
Tribble

SEE Line
Proj. Manager
H. Clark

Brinkley
Chubaryan
Horvat
Hyman

Senior ME
Derrig

Sr.
Mechanical
Engineer
Olsen

Designer II
Molitor

Machine Shop
Supervisor
Norris

Bielamowicz
A. Clark
Raines
Udovicic
Whiteley

Operations Chief
Abegglen

Electrical Shop
Cowden
Eisenmann
Ford
Gathings
LaPoint
Law
Morgan
O'Berski
Peeler
Russell
Sherman
Yendrey
Zajicek

Building
Maint.
Gallegos
Kingsbury
Mynar
Piolet

Senior Accelerator
Physicist
May

Accelerator
Physicists
Kim
H. Clark
Tabacaru

Computer
Systems
Hagel
Burch

Administration/
Accounting
Jeske

Anderson
Deason
Speikes
Student Worker

Research
Group Leaders

Research
Scientists

Research
Associates

Graduate
Students

STUDENTS WHO RECEIVED GRADUATE DEGREES
FROM THESIS WORK CONDUCTED
AT
THE CYCLOTRON INSTITUTE

April 1, 2009 – March 31, 2010

Name	Year	Thesis Title	Advisor	Present Position
Sara Wuenschel	2009	*Temperature and Scaling Studies from Projectile Fragmentation of $^{86,78}Kr + {}^{64,58}Ni$ at 35MeV/A*	S. J. Yennello	Post Doc., Department of Radiation Oncology, School of Medicine, University of Washington, St. Louis, Missouri

2009

April 17	Professor Jian-Wei Qiu, Department of Physics and Astronomy, Iowa State University, Ames, Iowa and Brookhaven National Laboratory, Upton, New York	*QCD and High Energy Nuclear Collisions*
April 21	Dr. Peter Levai, KFKI Research Institute for Particle and Nuclear Physics, Budapest, Hungary	*Can We Find Quark-Gluon Plasma in pp Collision at LHC?*
April 28	Professor Wolfgang Mittig, NSCL, Michigan State University, East Lansing, Michigan	*Nuclear Power and Global Energy Problems*
April 30	Dr. A. S. Botvina, Institute for Nuclear Research, Russian Academy of Sciences, Moscow, Russia	*Stellar Matter in Supernova Explosions and Nuclear Multifragmentation*
May 19	Mr. J. Savory, NSCL, Michigan State University, East Lansing, Michigan	*The rp Process and Mass Measurement of N=Z=34 Nuclei*
July 28	Dr. A. A. Alharbi, Faculty of Sciences, Physics Department, Princess Nora Bint Abdul Rahman University, Riyadh, Saudi Arabia and Cyclotron Institute, Texas A&M University, College Station, Texas	*Application of Radioisotopes in Nuclear Medicine: Experimental Study of Proton Induced Nuclear Reactions on ^{Nat}Tl*
August 5	Dr. Adriana Banu, Cyclotron Institute, Texas A&M University, College Station, Texas	*Nuclear Physics for Astrophysics with RNBs from 10 to 50 MeV/nucleon*
September 1	Professor Gerd Roepke, Institute of Physics, University of Rostock, Rostock, Germany	*Light Clusters in Nuclear Matter*
September 9	Dr. M. Mazzocco, Dipartimento di Fisica and INFN-Sezione di Padova, Padova, Italy	*RIB's for Reaction Studies at Near-Barrier Enegies: the Project EXOTIC at LNL*
October 3	Dr. Min He, Cyclotron Institute, Texas A&M University, College Station, Texas	*Susceptibilites and QCD Chiral Phase Transition*

October 13	Professor M. Urin, Moscow Engineering Physics Institute, Moscow, Russia	*Giant-Resonance Damping:Semi-Microscopic Description (Methods, Results, Perspectives)*
November 10	Professor Gamal Akabani, Department of Nuclear Engineering, Texas A&M University, College Station, Texas	*Alpha Particle Targeted Radionuclide Tumor Therapy – Physical and Biological Aspects*
November 16	Dr. Tommi Ropponen, Department of Physics, University of Jyväskylä, Jyväskylä, Finland	*Ion Source Related R&D at the University of Jyväskylä*
November 18	Dr. H. Esbensen, Physics Division, Argonne National Laboratory, Argonne, Illinois	*Coulomb Dissociation of ^{15}C and the Radiative Neutron Capture on ^{14}C*
November 24	Professor Peter McIntyre, Mitchell-Heep Chair in Experimental Physics, Department of Physics, Texas A&M Univeristy, College Station, Texas	*Amazing Accelerators: Petavolt collider and Gigawatt Fission Power*
December 1	Dr. Rahul Tripathi, Cyclotron Institute, Texas A&M Univeristy, College Station, Texas	*Recent Heavy Ion Reaction Studies at Radiochemistry Division (RCD), Bhabha Atomic Research Center (BARC), Mumbai, India*
December 9	Dr. Professor Michael Golovkov, Flerov Laboratory of Nuclear reactions, Joint Institute for Nuclear Research, Dubna,	*Correlation Study of Light Neutron Rich Nuclei*
December 10	Dr. Alexandre Obertelli, Service de Physique Nucléaire, CEA/Saclay, DSM/IRFU/SPhN, France	*New Developments for Knockout Reactions at Intermediate Energies*
December 11	Dr. Emanuel Pollacco, Service de Physique Nucléaire, CEA/Saclay, DSM/IRFU/SPhN, France	*Particle Spectroscopy with Radioactive Beams*

2010

February 9	Professor Ulrich Mosel, Institute for Theoretical Physics, University of Giessen, Giessen, Germany	*Neutrino-Long-Baseline Experiments: Where Nuclear Physics is Needed*
February 18	Dr. Michel Gonin, Ecole Polytechnique, France	*The Tokai to Kamioka Long Baseline Neutrino Oscillation Experiment*

February 23	Dr. Thomas Davinson, Department of Physics and Astronomy, University of Edinburgh, Edinburgh, United Kingdom	*Decay Spectroscopy at FAIR Using the Advanced Implantation Detector Array (AIDA)*
February 26	Dr. Taesoo Song, Cyclotron Institute, Texas A&M University, College Station, Texas	*R_{AA} of J/Ψ Near Mid-Rapidity in Heavy-Ion Collisions at $\sqrt{s} = 200$ GeV*
March 2	Dr. Gavin Lotay, Department of Physics and Astronomy, University of Edinburgh, Edinburgh, United Kingdom	*Determining the Steller Origin of the Cosmic γ-ray Emitting Nucleus ^{26}Al*
March 9	Professor Fridolin Weber, Department of Physics, San Diego State University, San Diego, California	*Neutron Stars as Astrophysical Laboratories for Nuclear and Particle Physics*
March 23	Mr. Alan McIntosh, Department of Chemistry and Indiana University Cyclotron Facility, Indiana University, Bloomington, Indiana	*Binary and Ternary Break-up of Excited Projectile-like Fragments Produced in ^{124}Xe + ^{112,124}Sn Reactions at E/A = 50 MeV*
March 30	Professor Michael A. Bentley, Department of Physics, University of York, York, United Kingdom	*Nuclear Structure, Astrophysics and Reactions at FAIR*